Human-Robot Interaction using a Behavioural Control Strategy

by

Paramin Neranon

Thesis submitted in fulfilment of the requirements
for the Degree of Doctor of Philosophy

Department of Mechanical and Systems Engineering
Newcastle University
United Kingdom

2014

ABSTRACT

A topical and important aspect of robotics research is in the area of human-robot interaction (HRI), which addresses the issue of cooperation between a human and a robot to allow tasks to be shared in a safe and reliable manner. This thesis focuses on the design and development of an appropriate set of behaviour strategies for human-robot interactive control by first understanding how an equivalent human-human interaction (HHI) can be used to establish a framework for a robotic behaviour-based approach. To achieve the above goal, two preliminary HHI experimental investigations were initiated in this study. The first of which was designed to evaluate the human dynamic response using a one degree-of-freedom (DOF) HHI rectilinear test where the *handler* passes a compliant object to the *receiver* along a constrained horizontal path. The human dynamic response while executing the HHI rectilinear task has been investigated using a Box-Behnken design of experiments [Box and Hunter, 1957] and was based on the McRuer crossover model [McRuer et al. 1995].

To mimic a real-world human-human object handover task where the handler is able to pass an object to the receiver in a 3D workspace, a second more substantive one DOF HHI baton handover task has been developed. The HHI object handover tests were designed to understand the dynamic behavioural characteristics of the human participants, in which the *handler* was required to dexterously pass an object to the *receiver* in a timely and natural manner. The profiles of interactive forces between the *handler* and *receiver* were measured as a function of time, and how they are modulated whilst performing the tasks, was evaluated. Three key parameters were used to identify the physical characteristics of the human participants, including: peak interactive force (f_{max}), transfer time (T_{trf}), and work done (W). These variables were subsequently used to design and develop an appropriate set of force and velocity control strategies for a six DOF Stäubli robot manipulator arm (TX60) working in a human-robot interactive environment. The optimal design of the software and hardware controller implementation for the robot system has been successfully established in keeping with a behaviour-based approach. External force control based on proportional plus integral (PI) and fuzzy logic control (FLC) algorithms were adopted to control the robot end effector velocity and interactive force in real-time.

The results of interactive experiments with human-to-robot and robot-to-human handover tasks allowed a comparison of the PI and FLC control strategies. It can be concluded that the quantitative measurement of the performance of robot velocity and force control can be considered acceptable for human-robot interaction. These can provide effective performance during the robot-human object handover tasks, where the robot was able to successfully pass the object from/to the human in a safe, reliable and timely manner. However, after careful analysis with regard to human-robot handover test results, the FLC scheme was shown to be superior to PI control by actively compensating for the dynamics in the non-linear system and demonstrated better overall performance and stability. The FLC also shows superior performance in terms of improved sensitivity to small error changes compared to PI control, which is an advantage in establishing effective robot force control. The results of survey responses from the participants were in agreement with the parallel test outcomes, demonstrating significant satisfaction with the overall performance of the human-robot interactive system, as measured by an average rating of 4.06 on a five point scale.

In brief, this research has contributed the foundations for long-term research, particularly in the development of an interactive real-time robot-force control system, which enables the robot manipulator arm to cooperate with a human to facilitate the dextrous transfer of objects in a safe and speedy manner.

KEYWORDS: Human-human interaction, Human-robot interaction, Object handover task, Real-time system, Proportional integral control and Fuzzy logic control

PUBLICATIONS:

Neranon, P. and Bicker, R. 'Human-human interaction using a behavioural control strategy', *Technologies for Practical Robot Applications (TePRA), 2013 IEEE International Conference*, 22-23 April 2013. pp. 1-6.

Neranon, P. and Bicker, R. 'A behavioural control strategy of human-human interaction in an object transfer task', *Technologies for Practical Robot Applications (TePRA), 2014 IEEE International Conference*, 14-15 April 2014. pp. 1-6.

Neranon, P. and Bicker, R. 'Design of Force/Position Controller of Robotic System in Human-Robot Handover Task' *Technologies for Practical Robot Applications (TePRA), 2015 IEEE International Conference (Submitted).*

Neranon, P. and Bicker, R. Human-Robot interaction using a behavioural control strategy' *Journal of Human-Robot Interaction (In preparation).*

ACKNOWLEDGEMENTS

First of all, I would like to express my sincere gratitude to my supervisor, Dr R. Bicker, for all his help, support, encouragement, advice, motivation, enthusiasm, immense knowledge and guidance given throughout the research. I would like to thank my second supervisor, Dr J. Hedley, for his support, advice and direction in this research. I would also like to thank all technicians and staff at the School of Mechanical and Systems Engineering at Newcastle University.

I am truly grateful to the Thai government and Prince of Songkla University (PSU) for financial support throughout my PhD study at Newcastle University, and I promise that I will subsequently use all my knowledge acquired to advance mechatronics know-how at PSU and across educational institutions in Thailand.

I am especially grateful to my dearest parents, my wife, my sister and my wife's family for their continuous love, understanding, support and encouragement every day. Finally, I would like to thank my test participants: Arisara Romyen, Bhathrapol Dhanasobhon, Phatthanawan Chanrattanayothin, Simon Ignance Marandu, Ababukar Surajo Imam, Charuwan Manmee, Ahmad Alsaab, Wan Nurshazwani, Mehmet Serdar Guzel, Kanida Sinmai, Prattana Phuekvilai, Jaya Bhanu Rao, Alaa Jaber, Erwin Wern-Juin Choy, Napaporn Tangtinthai, Kanungnid Busarakam, Patchanok Kitikanan and Nuatip Sumkaew for their assistance in interactive tests.

LIST OF ABBREVIATIONS AND SYSBOLS

Abbreviations:

A/D	Analog-to-digital converter
$ALTER_{trsf}$	ALTER transformation matrix
ANOVA	Analysis of variance
ANSI	America National Standard Institute
ARMAX	Auto Regressive Moving Average with Exogenous Input
DOF	Degree of freedom
E_RMS	Root mean square error
FFT	Fast Fourier transform
FIFO	First in first out
FLC	Fuzzy logic control
H_0 and H_1	Hypothesis and alternative hypothesis of the test
HHI	Human-human interaction
HRI	Human-robot interaction
HRI with PI	Human-robot interaction based on proportional control
HRI with FLC	Human-robot interaction based on fuzzy logic control
IFPS	Interface power supply
LabVIEW	Laboratory Virtual Instrument Engineering Workbench
MCP	Manual control panel
NI-DAQ	National Instruments data acquisition
NL	Negative large
NM	Negative medium
NS	Negative small
PEM	Prediction error method
PI	Proportional integral control
PID	Proportional plus integral and derivative control
PL	Positive large
PM	Positive medium
PS	Positive small
RSM	Response surface methodology

RT Linux OS	Real-time Linux operating system
SD	Standard deviation
Sig.	Significance value
TCP/IP	Transmit control protocol and internet protocol
Ze	Zero

Following notation is used for robot-to-human tasks

Phase A	Sending posture
Phase B	Transfer posture
Phases B_1 and B_2	Actual interaction time between the robot and human and the time delay of the robot gripper' operational process
Phase C	Receiving posture

Following notation is used for human-to-robot tasks

Phase A	Object velocity tracking phase
Phase B	Sending posture
Phases B_1, B_2 and B_3	The movement of the robot end effector is maintained acceleration, constant movement and the robot gripper' operational process
Phase C	Transfer posture
Phase D	Receiving posture

Matrix and Vector Symbols:

Symbols	Description
B_d	(6×6) Designed damping matrix (N.s/m)
f	(6×1) Cartesian force and moment vector (N and N.m)
f_d	(6×1) Designed Cartesian force and moment vector (N and N.m)
f_e	(6×1) Cartesian force and moment error vector (N and N.m)
J	(6×6) Manipulator Jacobian matrix
K	(6×6) Cartesian stiffness matrix (N/m)
K_d	(6×6) Designed stiffness matrix (N/m)
M_d	(6×6) Designed inertia matrix (kg.m^2)
S	(6×6) Diagonal matrix with the elements being either a one for position control or zero for no position control

X	(6×1) Cartesian position and orientation vector (m and rad)
X_d	(6×1) Designed Cartesian position and orientation vector (m and rad)
X_e	(6×1) Cartesian position and orientation error vector (m and rad)

Parameter Symbols:

Symbols	Description
A	Actual hand moving distance or amplitude (m)
a and b	Two constants relating to the task and the person (s/bit)
α	Significance level
β_0	Mean of overall experimental responses
β_i	Coefficient effecting to the variable x_i
c	damping factor (N.s/m)
de	Change in error (e) (N)
df	Sample degrees of freedom
df_{demon}	Demonstrator degrees of freedom
δ	An incremental angle of the robot end effector (degree)
$e(t)$	Difference between $y_{de}(t)$ and $y(t)$ (N)
ε	Error observed in estimated human force response (N)
f and F	Human applied force (N)
F_1 and F_2	Frictional forces produced by the right- and left- hand electromagnetic clutches respectively (N)
F_c	Frictional force added to a one DOF HHI system (N)
f_c	Force of dashpot (N)
f_d	Desired force which was initially defined as 0 (N)
f_{int}	Interactive force (N)
f_k	Force of spring (N)
$F_{left\ handle}$ and $F_{right\ handle}$	Forces applied to the left/right handles (N)
f_{max}	Maximum magnitude of interactive forces (N)
F_R	Radial force (N)

f_{res1} and f_{res2}	Frictional forces at masses m_1 and m_2 (N)
f_s	Actual force (measured by the ATI force sensor) (N)
f_s and f_r	External force applied by the *handler* and *receiver*(N)
F_T	Tangential force (N)
F_x, F_y and F_z	Force values recorded along the x, y and z axes (N)
F^E	External variable force (N)
F_c^E	External frictional force (N)
F_{net}^E	External net force (N)
F_r^E	External *receiver* force (N)
F_s^E	External *handler* force (N)
F^I	Internal interactive force (N)
$G_H(s)$	Human transfer function as a linear feedback controller
$G_p(s)$	Machine or plant transfer function
$H(s)$	Sensory feedback transfer function
i, j	Process orders
ID	Index of difficulty (bits)
k	Spring stiffness (N/m)
K	Spring stiffness used in a one DOF HHI system (N/m)
K_D	Derivative gain and
K_H	Human muscle gain
K_I	Integral gain
K_P	Proportional gain
m	Mass (kg)
M	Mass added to a one DOF HHI system (kg)
m_1 and m_2	Two set of masses (kg)
m_r, k_r and c_r	Impedance parameters of the human *receiver* arm (kg, N/m and N.s/m)
m_s, k_s and c_s	Impedance parameters of the human *handler* arm (kg, N/m and N.s/m)
MT	Performance time (s)
N	Number of participants (People)
$n_1$and n_2	Total numbers of sample participants of the first and second groups (People)
r	Radius of a circle (m)

s	Object displacement (m)
$s_1$and s_2	Standard deviations of task completion times of the first and second groups (s)
S'	The number of sample participants (People)
T	Transfer displacement (m)
t	Continuous time (s)
T_{trf}	Transfer time in object handover tasks (s)
T_z and T_p	Lead and lag coefficients respectively (s)
τ	Sampling time period (s)
τ_d	Reaction time delay of the human (s)
$U(t)$	PID incremental displacement control output (m)
θ	Angle of the 'crank' based on the world coordinates (degree)
$\sigma^2_{S/A}$	Population variance
$\emptyset_A$	A value used in determining power quantity
$\Delta u(k)$	Incremental PI robot displacement control output (m)
v	Object velocity (m/s)
v_d	Desired velocity (m/s)
$V_{left\ handle}$ and $V_{right\ handle}$	Output voltages of the left/right handles (V)
v_s	Actual velocity (m/s)
W	Work done by the handler and receiver (J or N.m)
ω_C	Crossover frequency (Hz)
x	Human arm's displacement (m)
x_0	Position at time t_0 (m)
x_1 and x_2	Object displacements of masses m_1 and m_2 (m)
x_1, x_2, x_3, and x_4	Input variables of a second order RSM model: (x_1:N/m), (x_2:kg), (x_3:N), and (x_4: m)
x_f	Position at time t_f (m)
$\dot{x}$	Human arm's velocity (m/s)
$\dot{x}_1$ and $\dot{x}_2$	Corresponding velocity of masses m_1 and m_2 (m/s)
$\ddot{x}_1$ and $\ddot{x}_2$	Corresponding acceleration of masses m_1 and m_2 (m/s^2)
$\overline{x}_1$ and $\overline{x}_2$ or μ_1 and μ_2	The means of task completion times the first and second groups respectively (s)

(x_0, y_0)	The world coordinates of the home position (m)
(x_{cur}, y_{cur})	The world coordinates of the current position of the robot end effector based on (x_0, y_0) (m)
(x_{new}, y_{new})	The world coordinates of the updated position of the robot end effector (m)
y	Estimated human force output of a second order RSM model (N)
$y_{de}(t)$	Desired force output (N)
$y(t)$	Actual force output (N)

CHAPTER I

INTRODUCTION

Robots are poised to fill a growing number of roles in today's society; these include applications in automated factories, and medical and other facilities. Robots continue to be successfully employed in industry to improve productivity, quality, accuracy, and reliability, carrying out spray painting, welding, grinding and assembly. Industrial robots are used particularly in static environments, using only minimal feedback signals for position and joint torque, and are normally isolated from humans for safety; however, the next generation of intelligent robots will be expected to have a larger operating range and to offer increased flexibility, as well as sharing the workspace with humans in order to further improve productivity. To achieve successful collaboration, robots are required to collaborate with humans in a safe and natural manner.

Human-robot interaction (HRI) is the scientific study of the dynamics of interaction between humans and robots, in an attempt to maximise the benefits of collaboration between a human and a robot to successfully accomplish a specific set of interactive tasks in a shared workspace [Heyer et al., 2010]. Consider the car assembly process of installing the front windshield. This task requires two semi–skilled operators to manipulate and position the front windshield, which is supported on a passive compensator as shown in Figure 1.1. A more cost effective solution would be to use a robot arm to replace one of the semi–skilled workers and utilize an interactive human-robot strategy.

Figure 1.1 Installing the front windshield
[http://www.assemblymag.com/articles/human-robot-collaboration]

With regard to both human and robot capabilities, human-robot interaction provides several benefits. Burghart et al [2007] suggested that, in the near future, human-robot interaction will be significantly developed and implemented, with robots used as assistants to industrial workers, tour guides, teachers, receptionists, or as household aids or assistive devices for the elderly. Dong et al. [2009] stated that interest in HRI has increased considerably and that industrial robots can collaborate with human operators through physical interaction in the same workspace. Furthermore, the direct teaching technology of human-robot cooperation enables operators with no experience to work together with robots in completing processes.

Safety is a crucial issue in haptic human-robot interaction, and so intelligent robots should be developed to facilitate safe and effective collaboration with human partners in shared workspaces, and the timing of any interaction is a crucial aspect in enhancing system efficiency, safety and acceptability. In addition, in order to increase confidence in predicting handover actions in time and space, it was recommended that the kinematics and dynamics of both position and movement parameters between humans and humans and robots should be comprehensively studied [Glasuer et al., 2010]. A control scheme which can compute and perform grasping movements whilst reaching targets has been proposed and scientifically developed by investigating the kinematics and dynamics of object grasping by robots and understanding the behavioural characteristics [Smeets et al., 1995].

Researchers have studied and developed a variety of different HRI control strategies. Nevertheless, in human-robot interactive applications, robots are usually controlled to cope with various uncertainties in the behaviour carried out by human partners. Therefore, this challenge is further complicated by the dynamic nature of the human-robot environment, which by its nature necessitates very careful design of the control strategy and its implementation in order to protect the human operator from the risk of harm or injury by the robot, particularly if the sensing system becomes occluded by the pose of the robot or any object within its workspace.

1.1 Motivation and Aim of the Research

Reed et al. [2007; 2008] stated that understanding the principle of human haptic interaction when two humans work together in a joint effort to complete a shared task is crucial in designing an effective human-robot interactive system. This body of work highlights the development of human-robot interaction in which an 'intelligent' robot manipulator has been configured with the capability of generating natural and synchronized responses with a human partner to facilitate safe and effective collaboration in a shared workspace. To achieve a conceptual guideline for a robotic human-like control strategy, human behavioural characteristics in human-human interaction were investigated.

To achieve the above goal two preliminary experimental investigations were initiated. The first was designed to evaluate the human dynamic response using a one degree-of-freedom (DOF) human-human interactive rectilinear test in which the *handler* passes a compliant object to the *receiver* by sliding it along a constrained horizontal path. To mimic a real-world human-human object handover task where the handler is able to pass an object to the receiver in a 3D workspace, a second more substantive handover task in which the *handler* transfers a baton type object to the *receiver* has been undertaken.

This preliminary work formed the basis for further research and postulated the research question of whether a behavioural control strategy can be developed for use in Human-Robot Interaction by understanding the dynamics of a human-human object handover task. Furthermore, is it possible feasible to utilize fuzzy logic control (FLC) techniques in the robot control strategy to improve the effectiveness and reliability of the human-robot object handover procedure in terms of force and velocity-control?

The scope of this research was focused on developing a robot behavioural control strategy which would allow a robot manipulator to safely and effectively perform object handover tasks with a human. To achieve this, the behavioural and dynamic characteristics of both a *handler* and *receiver* in human-human object handover tasks were first investigated, and used to establish the behavioural control strategy for robot force and velocity control to enable the robot to successfully transfer an object from/to a human in a safe and reliable manner. Finally, the robot's performance whilst performing the handover task with the human will be compared with the outcomes of the HHI tests in order to assess the robot control system. The outline of the sequence of key experiments in this study is illustrated in Figure 1.2.

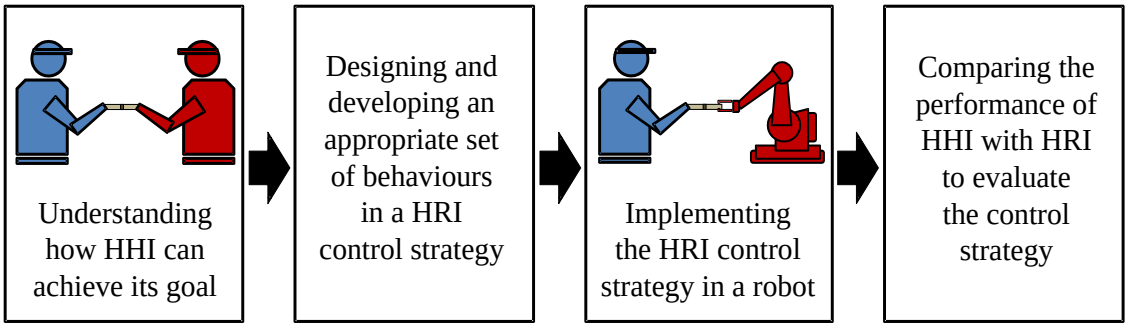

Figure 1.2 Outline of the sequence of key experiments

To satisfy the aim of this project, the following objectives have been defined:

- To determine an appropriate set of trials, based on a number of participants and sequence of physical tasks, to satisfy a preliminary one DOF HHI rectilinear task.
- To investigate the human dynamic response based on the McRuer cross-over model [McRuer et al. 1995] while performing compliant object handover in the preliminary one DOF HHI rectilinear experiment designed using a Box-Behnken statistical technique [Box and Hunter, 1957].
- To evaluate human physical characteristics in using a one DOF human-human object handover task in order to successfully design and develop an appropriate set of behaviours in a human-robot interactive control strategy which permits a robot manipulator arm to effectively transfer an object from/to a human.
- To validate the quantitative performance of the implemented robot system based on both conventional proportional plus integral (PI) control and 'intelligent' fuzzy logic control (FLC) implementation in human-to-robot and robot-to-human object handover tasks, and which can be compared to that of the human-human handover tests, and
- To evaluate the stability of robot control in human-robot interaction based on its acceptability to the humans involved using a survey questionnaire.

1.2 Layout of the Thesis

The work presented in this thesis addresses issues related to the design and development of an appropriate set of behaviours in a human-robot interaction (HRI) control strategy by studying the kinematics and dynamics of human behaviour in an effective human-human interactive (HHI) task. The effectiveness of robot control schemes have been established based on human-to-robot and robot-to-human handover tasks which were specifically designed for this investigation. Chapter 2 critically reviews the relevant recent and contemporary research in the area of interactive behaviour-based robots, human-robot interaction technologies, human-human interaction strategy and the conceptual frameworks of HHI and HRI control strategies.

Chapter 3 presents a one DOF human-human interactive study, which introduces two preliminary HHI tests. The first is a one DOF human-human interactive rectilinear task in which an appropriate set of trials, number of participants and sequence of the physical test were statistically carried out by a pilot study. In addition, the experiment has been designed using a Box-Behnken methodology [Box and Hunter, 1957] to evaluate the human dynamic response based on the McRuer crossover model [McRuer et al. 1995] while performing compliant object handover. Nevertheless, the sliding test does not mimic a real-world human-human object handover task; therefore, a substantive human-human object handover task, in which the *handler* is able to transfers an object to the *receiver* in a 3D shared workspace, has also been undertaken. Physical dynamic responses in the interactive tasks have been investigated to establish an appropriate set of behaviours in a human-robot interactive control strategy. Furthermore, all of the HHI tests were arranged based on the recommendations arising from the one DOF pilot study, as proposed in the first preliminary test.

Chapter 4 describes the design of external force and velocity control systems, which was strategically developed in order to ascertain its capability in HRI task execution, where the performance evaluations of an ATI multi-axis force/torque sensor and an ALTER real-time robotic control path were applied to quantify the effectiveness of the robot control system as explained in Appendix D. Optimized proportional plus integral control is typically used to complete an effective task with satisfactorily stable performance in a specific environment, and also has some disadvantages such as high starting overshoot, sensitivity to controller gains and steady-state error [Khuntia et al. 2009]. According to the complicated dynamic nature of human behaviour, fuzzy logic control (FLC), which has higher capability in dealing with non-linear dynamic applications, was therefore adopted. Fuzzy logic control was appropriately designed and developed based on understanding of the kinematics and dynamics of human behaviour in a one DOF human-human handover task.

Safety issues are crucial aspects in the design of human-robot interaction, and were addressed using control software and stand-alone emergency stop buttons available in the robot manual control panel and external control box. Furthermore, the robot control modelling was conducted using the active compliant motion control method suggested by De Schutter [1987], and it includes simple models of the robot, an ATI force/ torque sensor, a gripper and workpiece components.

The results, discussion and evaluation of the overall human-to-robot and robot-to-human handover tasks using the proportional integral and fuzzy logic control schemes are fully explained in Chapter 5. The test programme was carried out to evaluate the comparative performance of human-robot and human-human interaction at the various required velocities in terms of the human force profile, maximum interactive force, transfer time and work done. Finally, Chapter 6 provides the conclusions drawn from the human-robot interactive study and offers recommendations for future work based on the current research findings.

CHAPTER II

LITERATURE REVIEW

Industrial robots are typically programmed by operators to execute a sequence of predefined functions. Although early industrial robots were not developed to interact with humans directly, the next generation of smart robots will be designed to further increase flexibility and to share their workspaces with humans in aiming for product improvement. There are two key issues which should be addressed to facilitate successful human-robot interaction. Firstly, robots should be able to physically interact and work naturally with humans in a safe and reliable way. Secondly, the robots themselves should be able to decide their task priority or action levels that can allow them to interact with humans in a timely and speedy manner.

Human-robot interaction (HRI) has become the crucial aspect when robots have been used for collaboration with humans in industrial applications, due to the requirements of technological feasibility and productivity improvements in terms of quality, accuracy reliability and flexibility. Interest in human-robot interaction has tended to increase significantly. Consequently, various human-robot cooperative technologies, which are used to enable unskilled workers to be able to directly teach intelligent robots, have been developed. For example, when a human operator gives instructions about task trajectory to a manipulator, the trajectory ordered can be automatically created by the robot instead of requiring offline programming [Dong et al 2009]. Human-robot interaction has been investigated significantly since 1994 [Fong et al. 2003], and interactive control methods were previously applied in basic on-off control systems or manipulator joint control systems by using analog joysticks. Human-robot collaborative technology has since developed so as to be more intelligent, smooth, natural, and safe, as in human-human interactive relationships. Human-robot interaction (HRI) has also defined as ‘the study of humans, robots, and the ways they influence each other’ [Fong et al. 2003]. Additionally, the essential factors of self-awareness, self-reliance, capacity for dialogue and adaptive systems, must be taken into account to provide an effective control system.

There has been much research in safe and effective Human-Robot Interaction (HRI) particularly with respect to robot design and control algorithms. Chanhun [2010] designed and developed a control strategy for industrial robot manipulators which allows easy and safe human–robot collaboration by directly teaching a robot high speed and high precision movements. Arai et al. [2000] demonstrated a human-robot master control method for moving an object in the horizontal plane, where the operator coordinates the action with the assistance of the robot. In order to support human-robot interaction in cellular manufacturing the human-human interactive task analysis, investigation and safety issues, were addressed by Tan et al. [2010]. Huber et al [2008] studied a simple physical human-robot interactive handover task and compared the results of human-human handover coordination with the same task completed by a human-robot combination. Their results illustrate a shorter reaction time for minimum-jerk profiles and provide a background for joint action strategies in humanoid robot systems.

Haddadin et al [2009] developed robot capabilities in the areas of sensor and actuator systems. The aim of the study was to design a robot to mimic human behaviour and to develop a prototype of a co-worker scenario. Various researchers [Ikeura et al, 1997; 2002; Daesik et al, 1998; Tsumugiwa et al, 2002; Aggarwal, 2007] have developed designs of robot control strategies for human-robot collaboration while moving an object to different targets, and it has been suggested that intelligent control systems designed for smart robots should be developed by imitating human behaviour.

Cakmak and his colleagues [2011] studied human handover configurations, which are an essential aspect of applications involving an assistive robot, and the most significant of human preferences whilst performing an object handover task were identified and evaluated. The observation of human-human handover interaction was conducted before implementing the handover structure on human- robot interaction. *Handlers* and *receivers* were evaluated in terms of gestures when approaching, carrying, reaching and transferring [Strabala et al., 2013]. Other researchers, who also investigated different issues to improve human-robot handover interactive tasks, have studied how a human applies grip force during an object transfer task [Mason and MacKenzie, 2005; Wesley et al., 2012].

2.1 Conceptual Framework for Human-Human Interaction (HHI)

As human-robot interaction has developed, industrial robots have been used increasingly in more complex structured tasks and activities. Human-robot interactive design attempts to maximize the benefits of collaboration between a human and a robot to successfully accomplish a specific set of tasks in a shared workspace. It can be postulated that the understanding of the kinematics and dynamics of human-human interaction (HHI) during two humans working together in a joint effort to complete a smooth and efficient task is fundamental in designing an effective human-robot interactive system. Breazeal et al. [2005] stated that the robot applications involved in human-robot interaction, which include industrial robots, robots working in hazardous environments, service or transportation robots or those assisting the elderly, have to be able to recognize the other teammate's actions in order to accomplish effectively coordinated goals. For instance, both partners should realize that they have to appropriately apply their forces based on interactive force feedback.

There are several studies that have examined the cooperation between two human subjects in a shared workspace in order to help in implementing human-robot interaction more efficiently. Raman et al [2000a; 2000b; 2002], investigated the control characteristics of two humans in a cooperative task, and designed control systems for cooperative robots to work with other partners by imitating human-based behaviour strategies. Firstly, control characteristics such as impedance analysis based on a biomechanical model of two humans working together were analysed. A cooperative task was then modelled by evaluating the system parameters. Finally, the results of the impedance characteristics from the proposed model were implemented in a robot to mimic the same interactive tasks with a human partner.

A single degree of freedom linear horizontal movement in a human-human cooperative task was investigated, as shown in Figure 2.1. Two types of cooperation were analysed: master-master and master-slave. The two subjects were required to grasp each handle of an object and rapidly move it to a target whilst acceleration and force were measured and analysed. A linear motor served as an actuator to drive the linear slider, and the system was implemented to simulate the collaborative task with one human. In master-slave cooperation, the master moves the object while the slave grasps the handle and performs passive movements.

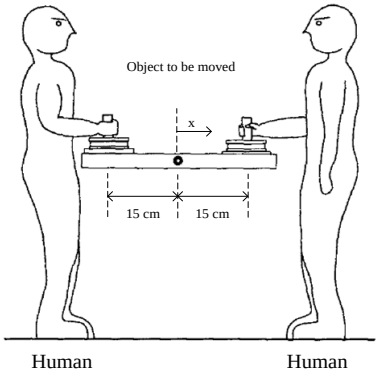

Figure 2.1 Human-human interactive task with
an object in horizontal motion [Raman et al. 2002]

As proposed by Raman et al. [2002], the human muscle can be mechanically represented in the system as a spring and damper, as shown in Figure 2.2. The dynamic model of the arm can be described by the second-order equation shown in Equation 2.1 based on an equivalent of the arm's mass, stiffness and damping factors. The key abbreviations of *m*, *c* and *k* represent human arm impedance parameters for the mass, damping factor and stiffness respectively, and f and *x* represent the force that acts on the arm and its displacement, respectively.

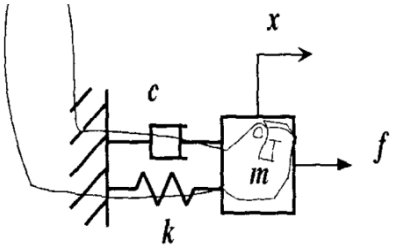

Figure 2.2 Human arm impedance model [Raman et al 2002]

$$f(t) = m(t)\ddot{x} + c(t)\dot{x} + k(t)x(t) \tag{2.1}$$

$$\dot{x}(t) = \left[\frac{x(t)-x(t-1)}{T}\right] \tag{2.2}$$

$$\ddot{x}(t) = \left[\frac{\dot{x}(t)-\dot{x}(t-1)}{T}\right] \tag{2.3}$$

Substituting Equations 2.2 and 2.3 into Equation 2.1 gives:

$$f(t) = a_1 x(t) - a_2 x(t-1) + a_3 x(t-2) \tag{2.4}$$

where,

$$a_1 = \left[\frac{m+cT+kT^2}{T^2}\right], a_2 = \left[\frac{-(2m+cT)}{T^2}\right] \; and \; a_3 = \left[\frac{m}{T^2}\right]$$

Studies by Reed et al. [2007; 2008] have demonstrated that understanding the kinematics of how humans physically collaborate with each other is a major goal of human-robot research as shown in Figure 2.3 to investigate this interaction. The experiment requires a single DOF crank with a projector to simulate targets and two randomly selected participants attempting to turn the crank to the targets with a curtain between them. The tasks consisted of a human working individually, two human individuals working together and a human working with a motorized partner, where one of the participants was replaced by a robot to perform an interactive task.

Figure 2.3 Experimental set-up of human-human interactive task
with two-handled crank [Reed et al., 2007; 2008]

Both human subjects were commanded to turn the rigid handles as quickly as they could to a set of targets which appeared randomly. The interactive force profile of each human subject was tracked. After the analysis and understanding of the human-human haptic communication, Reed et al. [2007; 2008] implemented a robot which simulated the human behaviour strategies used to enable the robot to perform the same cooperative tasks as a human. The experimental results demonstrated that the performance time for achieving the targets by two humans working together is significantly faster than the average time of a human working individually. Furthermore, the results shown that the completion times of human-robot interactive tasks in both cases, where the human participants may or may not have known that the resistant force belonged to a robotic partner, scarcely differed.

In order to provide appropriate human-robot interaction, Ikeura et al. [1995; 1997; 2002] studied human behavioural characteristics based on a physical human-human interactive task. The characteristics of two humans carrying an object were investigated in order to provide a suitable control property for a robot. One of the two human subjects was instructed to move the object in a desired curve while the other person had no knowledge of the object's trajectory. The human characteristics were approximated based on an impedance model using the least-square method, and the experimental results demonstrated that the damping value was large in quick movement and low in slow movement. A behavioural control strategy was subsequently implemented in the robot for HRI execution.

It is reasonable to learn from human performance in safe and efficient collaboration in order to enable robots to cooperate directly with humans. Erlhagen et al. [2006] have developed high-level joint action strategies for HHI, and these techniques were transferred to competitive robot control. In addition, Huber et al. [2008] postulated that an important research area was to understand the joint action of humans working together and then the behaviour patterns could be transferred directly to HRI. The timing characteristics of physical coordination in transferring an object from a robot to a human have been investigated and compared to the performance of HHI and HRI tasks.

The human behavioural characteristics in HHI when moving an object have been investigated and implemented in a robot to ensure that the robot collaborates with a human as smoothly as possible [Bakar et al., 2006; 2009; 2010]. Completing interactive tasks naturally and smoothly allows both participants to communicate using audiovisual and tactile means. The experimental devices involve 3D position sensors and force sensors. Two human subjects were selected to work together in the tasks, where one of them performed as a leader (master) and another acted as a follower (slave) as illustrated in Figure 2.4. Additionally, in investigating human characteristics whilst performing the interactive task of moving an object together, behaviour can be described using the minimum jerk trajectory (MJT) model developed by Flash and Hogan [1985].

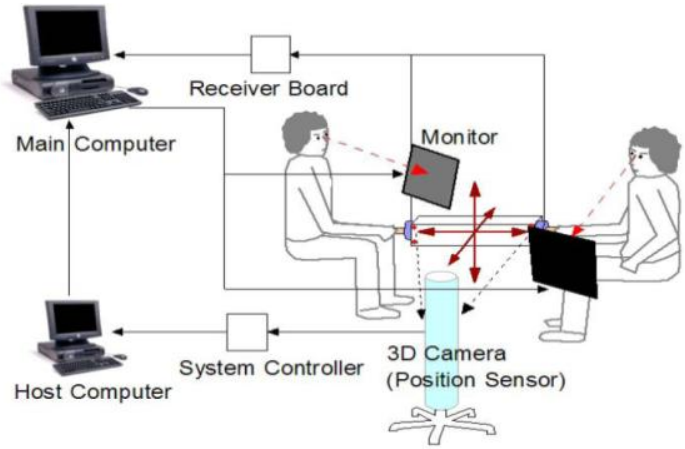

Figure 2.4 Human-human interactive experimental set-up [Bakar et al., 2010]

Miossec and Kheddar [2008] have also studied the physical interactive tasks between humans. Their person-object-person experiment was arranged to allow human subjects (individually and cooperatively) to move a handle-shaped object into a circular area. The observed characteristics of human performance show that the minimum jerk trajectory model [Flash and Hogan, 1985] was not the most advantageous measure to use in this set of experiments. Flash and Hogan formulated a mathematical model used to predict the qualitative features and details of human arm movements. Additionally, the integrated time of the square of jerk was proposed as a measure to determine the best performance of the arm movements of human participants. However, their results could be characterized explicitly by using a solver for local optimization (SOLVOPT) to achieve movement prediction, and this technique proved more accurate than the minimum jerk trajectory method.

2.2 Object Grasping

Humans can perform a rich diversity of manipulation strategies which are suitable for the robot manipulator in mimicking the tool acquisition and manipulation dexterity. Although the robot manipulator can be programmed or re-programmed to complete a desired task of grasping an object in a fixed environment, human subjects adapt their manipulation and behavioural strategies more easily given novel interactive task conditions. In the observation of human grasping actions, it has been found that human participants rarely grasp a given object directly without adjustments to the object configuration [Chang et al. 2008]. For example, a human may pull a mug handle to bring it closer to the body before lifting; or when a person attempts to grasp a pencil on a table, it could be quickly rotated to the writing position before lifting it.

The word (grasp) can be defined as the actions of a robot or a human hand to firmly hold an object so as to prevent its movement. Two factors should be taken into consideration in terms of stability of the grasp. These are form closure, which relates to the capability of a hand to prevent the object's motion, and force closure which involves the ability of the stable grasp to resist external disturbances [Bicchi, 2000; Xiangyang and Jun, 2003]. A grasp can be classified into various groups based on the shapes of the objects involved [Rezzoug and Gorce 2003]. The categories suggested by Napier [1956] are defined by the properties of the grip, which generally relate to the patterns of the human palm and the precision of the grip.

The observation of human behaviour allows robotics researchers to understand the principles of a human hand as they relate to an object manipulation task. Understanding human motions in HHI tasks gives significant information which can be used to enhance the capability of robotic hand movements when a robot helps a human to manipulate or keep hold of an object in a gentle manner [Bicchi, 2000]. Typically, the study of the motor control of robotics hand movements tends to concentrate on simple actions, such as elbow flexion or finger tapping, before applying those to the more complex movements that require several motions in various joints [Rotman et al. 2004]. Several studies have investigated improvements in the area of robot grasping capability. For example, the aims of a study by Raphael [2011] were to increase the understanding of object grasping, and the outcome was a significantly descriptive model of the grasp, consisting of the following elements:

i. A defined goal, which includes the factors causing a grasp to be initiated.
ii. Human-object relationships or feelings during grasping; for example, a person tends to pick up a used paper towel with a pinching grasp if it does not belong to them.
iii. Differences in the characteristics of human hand anatomy while grasping an object, such as hand size or finger size.
iv. The setting, which includes factors relating to the environment where the grasp takes place; for example, an object is pulled out of a crate or picked from a shelf.
v. The properties of the object, which are factors intrinsic to the object such as its surface, size, shape or weight.

In the task of humans lifting or holding objects with different properties, such as the shape, weight and density, it is important to perform the tasks as smoothly as possible. For instance, passing a glass of water without jerky movements requires gentle grasping and transfer. Human subjects can rapidly change their performance of grasping and manipulating a variety of unknown objects after a few experiences with the objects and this learning has been carefully analysed [Gordon et al. 1993]. In this study, humans generally estimated the weights of objects based on their knowledge of similar objects and then generated appropriate power amplitudes before lifting each object.

Johansson [1998] investigated human characteristics in picking up unknown objects which can unexpectedly vary in weight. The subjects could not estimate the exact object weight; for example, if a box is lighter than anticipated, it will be lifted more quickly than a heavier one. Through experiments, the objects are identified and the relevant models conveyed by using virtual or haptic information. Before executing the tasks, these model formations are then adapted to give motor commands along with simultaneous updating of the object's properties. Therefore, the objects, where weights can be varied, can be gripped and transferred by increasing or decreasing the gripping force in order to ensure that the objects do not slip.

Unlike the studies of Gordon et al. [1993] and Johansson [1998] which considered human-human interaction with passive objects by updating models generated from the subjects' existing knowledge, Scheidt et al. [2001] examined how humans learn to act given unpredictable disturbances. Twenty participants were chosen and each was instructed to hold a handle connected to a two-DOF robotic manipulator, which provided viscous force to randomly disturb the movements. The human subjects were commanded to complete the tasks by moving the mechanism to an ordered target within half a second. The results suggested that only a single piece of past information was necessary to anticipate performance i.e. only human short-term memory is required for the neural structures concerned to be modified during motor adjustment.

When a human makes an attempt to perform the task of grasping, he/she cannot immediately achieve the exact positioning of a movable object through the manipulation interaction because of its complexity. To achieve an effective grasp, pre-grasp interaction is therefore required to update the information about the object. Chang et al. [2009] stated that pre-grasp action strategies which can adjust object orientation were

used while the object was moving. This was used to identify the location of objects before adopting a hand formation, and a taxonomy was developed to classify pre-grasp interactive primitives. In the experiment, video filming was selected to capture the richness of reach-to-grasp interactive behaviour. The ten activities which related to both individual working and group participation were studied, such as food preparation, basic mechanical repairs, housekeeping and office work.

The key step in manipulation movements is object acquisition. The use of vision based on 2D images for the robotic grasping of novel objects has been studied by developing learning algorithms in order to identify object location and predict how to perform an efficient grasp. A learning algorithm for robot implementation was successful in providing effective robotic execution in grasping several objects such as screwdrivers, plates, jugs, pens, or tape rolls. The proposed algorithm was successfully applied in unloading dishes from a dishwasher machine [Saxena, et al. 2008]. Yoshikawa et al. [2008; 2009] and Romero et al. [2001] established a shape recognition technique of unknown objects in order to achieve effective positions for robotic grasping with soft fingers by utilizing differences in vision systems and grasp quality criteria. Huebner et al. [2008a; 2008b], and Geidenstam et al. [2009] developed a method to classify object properties by fitting and splitting the 3D data points of objects such as mugs, models, phones or notebooks into minimum volume bounding boxes.

Virtual reality technology provides objects to be grasped and transferred by creating and interacting with virtual objects [Boud et al. 1999]. However, the object localization and reorganization based on visual methods is not sufficient to capture certain types of data such as the weight or surface friction of the objects. This restriction was emphasized by Earnshaw et al. [1993]. Burdea [1996] postulated that when users are allowed to touch and explore objects, their performance can markedly improve. Lederman and Klatzky [2001] studied the haptic system, which is a perceptual system for the collection of desired inputs from mechanoreceptors embedded in human skin, muscles and joints. Touching objects enables humans to recognize their shapes, weights and forms. Tactile sensations include the vibrations and surface textures of the objects which are measured by the receptors. Typically, humans can detect frequency of force up to 30Hz and can perform exercise movements up to around 30Hz. The tactile receptors on a fingertip can sense vibration inputs of a maximum of 400Hz, whilst dextrous robot manipulator can measure up to 10kHz [Burdea, 1996].

2.3 Human Perception and Cognition

One of the key aspects in improving human-robot interaction is to develop the cognitive system for the control of the robot's behaviour in real-time. The cognitive system is chiefly used in the detection of human states and object properties in order to perform the appropriate responses and to optimize human-robot interactive tasks, and should be able to recognize and identify notable actions signifying human anxiety or stress in order for the interactive performance and smoothness to be improved. These cognition reorganizations would lead to benefits for the robot control architecture [Rani et al. 2004; Kulic and Croft, 2005].

The development of human-robot interactive cognition is an interesting area of robotics research. The responses of robots whilst appropriately interacting with humans as co-workers and the investigation of how reliable recognition and perception systems can be constructed are significant areas of concern. The main goal of a cognitive system is to develop intelligent robots with human-like cognition given the complexity of conditions involved in decision making, planning and reasoning [Begum and Karray, 2001]. The cognitive robotics engine (CRE) was implemented so that robots could identify callers and to follow callers in a real environment with various other noises. The experimental results revealed that the robot's capabilities were improved in terms of their dependability and stability [Sukhan et al. 2006a; 2006b].

Qining et al. [2006] mentioned that the human brain often involves the integration of object recognition and visual experiences. In the human cognitive process, object recognition is not only used to sense the surroundings in real time, but also the recognition of the surroundings is applied to take account of unnecessary features. To mimic human behaviour in the cognitive system, robots should be designed to automatically achieve localization. The use of vision-based self-localization robots to extract the features of the dynamic environment has been realized by Rofer and Jungel [2003]. In addition, a vision-based state estimation method applied to robot localization has been proposed by Schmitt et al. [2002].

The need to improve the capacities of robots to coordinate with humans in constrained environments has led to the investigation of the human's visual, haptic, proprioceptive, and motor systems and their relationships [Garcia et al., 2000]. The term 'attention' has been defined as the robot's ability to notice an interesting phenomenon from which useful information might be extracting. The principal challenges identified by Garcia and his colleagues are as follows: firstly, to construct an effective mechanism which can adapt itself to enhance attention focus; secondly, to construct the pattern categorization and attention control which are used to achieve efficient interaction between the robot and its environment; thirdly, to understand the characteristics of objects; and finally, to the attention map carried out.

The cognitive info-communication channels proposed by Soros et al. [2009], have been applied to human-machine interaction in order to enable unskilled operators to teach robots. These studies divided the information and communication technologies into three major sections, consisting of: the media used to create and store information, such as databases; secondly, videos and music, where communication is used to transfer information with high efficiency, security and reliability; and finally, informatics or information processing tools.

The basic anatomy of human perception and cognition is modelled in Figure 2.5, consisting of vision, hearing, and sensation systems, learning memory, and problem solving as well as operation and evaluation capacities. In the model, each 'sense' has an individual processor accompanied by a short term memory which is able to store images (visual short term memory), sound (audio short term memory) and object shapes (short term memory for sensation). Memory contexts are analysed by the sensory processor before the information is transferred to the central cognitive short term memory and cognitive processor in order to identify the input. These shorter memory contexts are still in the form of abstract information, and their meanings are constructed once they are conveyed to the central cognitive short term memory processor [Sutcliffe, 1988], whose purpose is to identify meanings by using the information from past experience that is fetched from the sensory processors or the long term memory. All of the cognition results may be stored in short term memory or long term memory, or may be transferred to the motor processor for the control of muscle movement based on human responses and human behaviour [Sutcliffe, 1988].

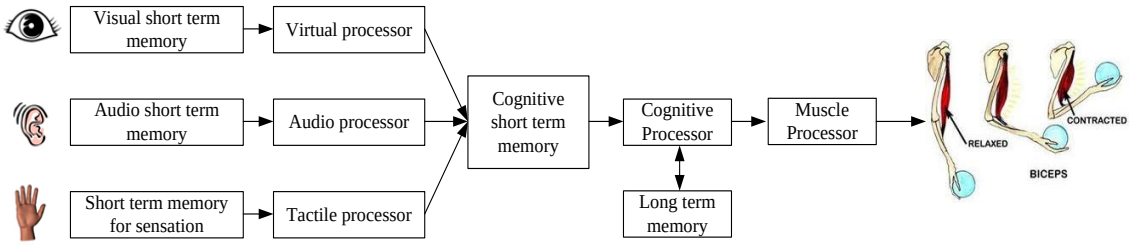

Figure 2.5 Information processing model of human perception and cognition [Sutcliffe, 1988]

Much of the relevant human operator modelling research has been extensively reviewed. For instance Zhihao et al. [2007], Trujillo et al. [2011], and Gagne and Lloyd [Fitt, 1954] have considered human abilities such as successful flying skills aimed at developing pilot tests to enhance training effectiveness. In the 1960s, the studies of McRuer et al. [1967; 1995] evaluated a human characteristics model based on dynamic responses in human-machine interaction. The general perceptual control architecture of the major human pathways are described as precognitive, pursuit and compensatory modes. The McRuer crossover model was based on a combination of sensing, computation and actuating systems, whereas the human operator model was defined as a set of linear differential equations. Nevertheless, a noise term, namely the remnant, is also added to the crossover function in order to take into account variations in the performance of individual humans.

2.4 Conceptual Framework for Human-Robot Interaction (HRI)

Since new technology has developed so rapidly, robotics innovations have become useful in various applications. One of the major motivations for improvements in robotics technology was to replace humans working in hazardous jobs or environments. Recently, as a result of the need for improvements in technological feasibility and productivity, robots have been required to function in a friendly manner with humans as co-workers to achieve complex collaborative tasks. The number of research projects in the field of human-robot coordination has steadily increased in order to enhance system development, such as in discussing and proposing their new conceptual designs, methods, model algorithms, safety, behaviour-based strategies or system performance evaluation.

According to Gini et al [2002], the classification of human-robot interaction in terms of the perception of a robot and the interpretation of humans was investigated. There are two general key categories of human-robot interaction as shown in Figure 2.6. Here cooperation in the interactive class without an object can be divided into two types called *leading* such as when a human operator teaches a robot manipulator arm, and *restriction* such as when an operator constrains the robot's movement by stopping the robot as a safety mechanism. When, an object is directly involved in human-robot interaction, cooperation can be divided into two schemes: firstly, *a handing over* scheme such as a direct handover, where an object transferred hand-to-hand using a medium; and secondly, *a manipulation* scheme. The latter may be a symmetrical object manipulation where a robot and a human carry or push or pull an object together, or anti-symmetric object manipulation where a robot force and a human force are generated against each other such as when opening a screw plug, and independent object manipulation with a human taking an object held by a robot.

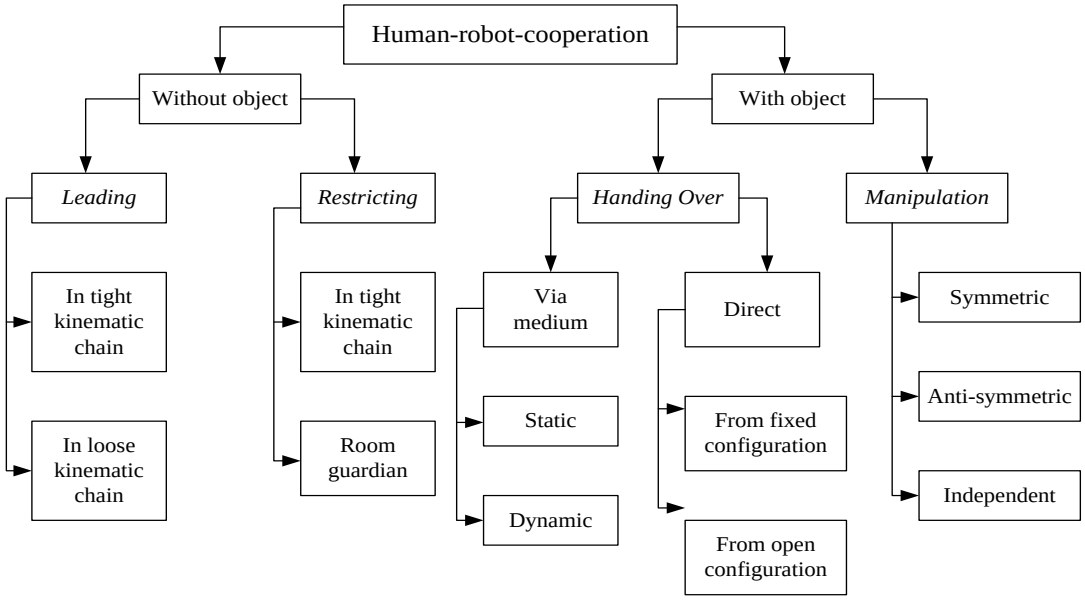

Figure 2.6 Possible classification of human-robot cooperation [Gini et al 2002]

Yanco and Drury [2004a] discussed the different combinations of humans and robots that can collaborate with individuals or in teams. Their classification was based on the number of humans giving commands to one or more robots resulting in eight categories as shown in Figure 2.7 in which a human is represented by H and a robot by R. The double arrow-headed connections indicate bilateral commands which flow between humans and robots, and vice versa.

The simplest case, as shown in Figure 2.7(a), represents an operator providing a set of commands to one robot which can transmit information back. Consider for example an operator directing a robot manipulator arm handling radioactive materials in a nuclear fuel reprocessing plant. In this situation, the operator needs a sufficient level of human-robot situational awareness to understand the positions, identities, activities, or surroundings of the robot. Furthermore, the robot needs a similar level of robot-human interactive awareness of its activities and human-delineated constraints that may require command non-compliance or a modified course of actions. Figures 2.7(f) through (h) illustrate multiple humans controlling multiple robots, and Figure 2.7(h) demonstrates individual operators controlling a team of robots using different commands. The robots have to prioritize all instructions before performing tasks. For example, a cluster of industrial robots are required by individual humans to accomplish parts of an assembly.

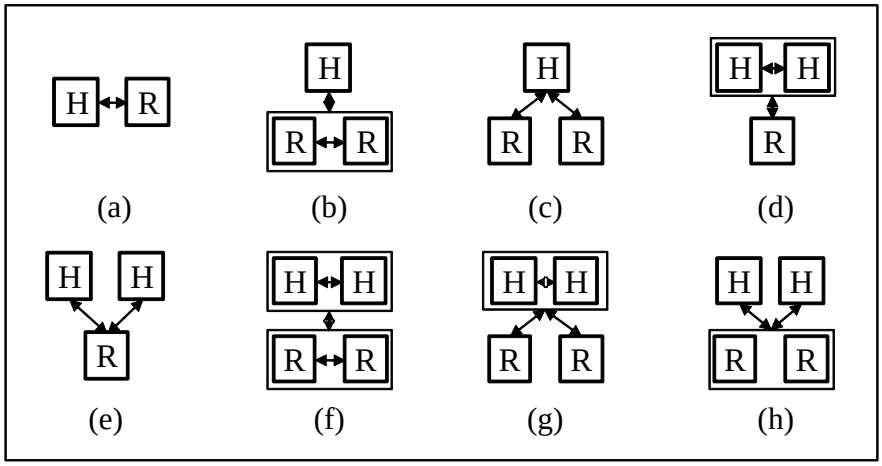

Figure 2.7 Possible combinations of single or multiple humans and robots, acting as individuals or in teams [Yanco and Drury, 2004a]

In order to efficiently establish human-robot interactive behaviour strategies for advanced intelligent robots, a set of principles are required to make interaction efficient, such as neglect time, interaction time, robot attention demand, free time, and fan out. Goodrich and Olsem [2003] proposed the seven principles for efficient human-robot interaction, consisting of: implicitly switching modes, using natural cues, directly manipulating the world coordinates, manipulating the robot-world relationship where information is meant to be manipulated, externalizing memory, and supporting attention management. However, these seven principles of efficient interaction still need to be validated due to the presence of unknown factors and new experience gained while

developing efficient human-robot interactive interfaces. Kleinehagenbrock et al. [2004] introduced the conceptual design of an agent-based architecture for human-robot coordination, whereas Fritsch et al [2005] argued that the proposed system infrastructures for robot companion learning and evolution (SIRCLE) can be used to enable human-robot interaction to be stable, powerful and more natural.

Previously, the physical interaction of humans and robots has largely been based on a master-slave strategy, in which a human operator teleoperates or programs all instructions off-line; moreover, the workspaces are strictly separated to ensure safety. The current trend is for human-robot interaction to be improved by enhancing the capabilities of robots to work with humans as partners and to combine the advantages of workers and robot manipulators. Lawitzky et al. [2010] investigated and evaluated load sharing policies, as shown in Figure 2.8, from the perception of a task's geometric, dynamic and environmental properties in a restricted environment.

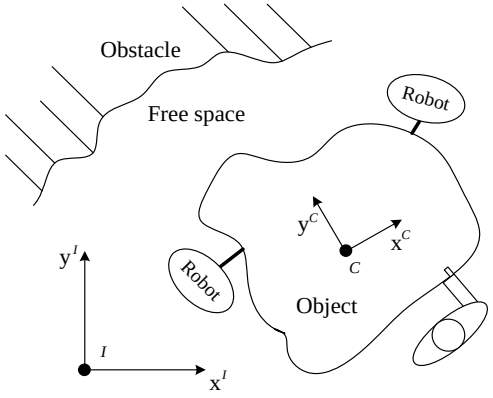

Figure 2.8 Manipulation of a bulky object by multi-agents [Lawitzky et al., 2010]

The problem of multiple humans and robots carrying a rigid bulky object has been defined using the following conditions:

i. One or more human operators collaborate with one or more robots,
ii. All participants know the common goal, such as a human and a robot physically manipulating an object to a desired target,
iii. All participants gently grasp the object whose shape and dynamics are known,
iv. The haptic interaction between a human and a robot via the object is the key factor of interest.

Lenz et al. [2008] designed the concept of a smart working system between humans and industrial robots in order to assemble industrial products using the model of the architecture of joint action for humans and industrial robots (JAHIR), as shown in Figure 2.9. The main purpose of the system is to authorize peer to peer collaboration by dealing with data from multiple input modalities and a cognitive system. The capability for interaction between industrial robots and human workers is crucial in physical interactive tasks, which require both participants to create a perceptual common ground in order to share the work [Sebanz et al 2006; Lenz et al, 2008].

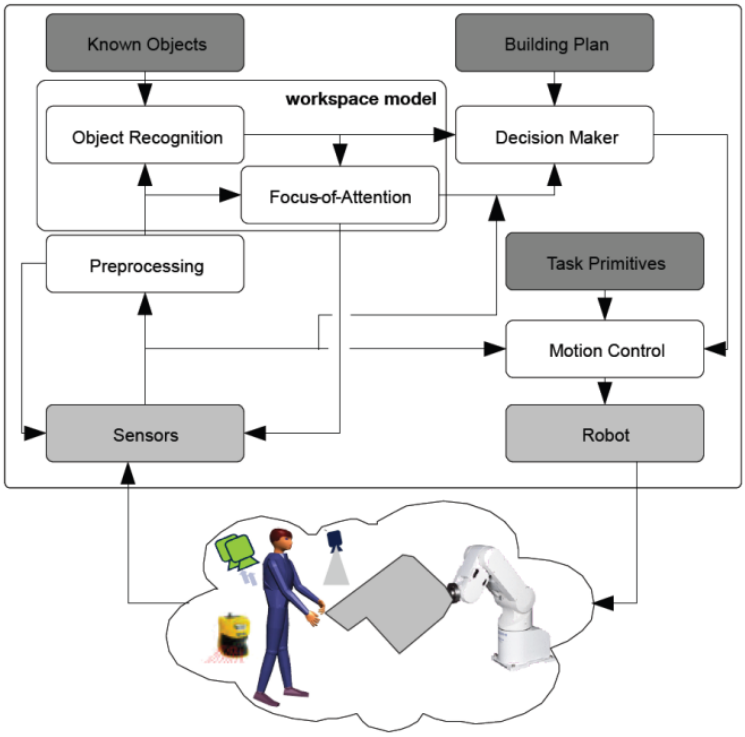

Figure 2.9 The modules of architecture of joint action for humans and industrial robots [Lenz et al, 2008]

According to Figure 2.9, the focus of attention is to be extracted by virtual devices and then stored in a database as a known object. For a production process, human skills are needed to manage a predefined goal in product assembly; hence the allocation of both partners should be dynamically adapted throughout the process. The workspace model is drafted by the sensor information, including elements such as the inventory and the assembly line. The decision maker is crucial in deciding the next action according to sensory information and task knowledge from the building plan module. The motion control module is necessary to authorize the robot's movements since the robot cannot be programmed off-line during human-robot interaction for safety reasons.

Takubo et al. [2002] presented a robot assistant to help a human to lift or manipulate a large bulky object in which they would find it difficult to perform alone. A virtual nonholonomic constraint method based on impedance control was proposed in order to demonstrate an industrial robot collaborating with a human by dealing with a simple tool. The schematic control of impedance control in 2D motion and the free rotation of the robot wrist was also examined. The experimental results revealed that the operator and the robot could suitably carry and transport the object to the desired locations and orientation. All participants could share the gravitational load equally by using "skills similar to steering a wheelbarrow". This study was then extended to object transfer in 3D space by combining virtual nonholonomic constraints in vertical and horizontal motion. The control method for human-robot interactive manipulation can be described as follows: if the operator wants to move an object directly down to a desired configuration, the human subject should drop his/her end and pull down the object before the robot trajectory will be finally adjusted to the same height.

Robot manipulator's arms are mainly used to replicate the human capacities to complete complex tasks. The key to human-robot collaborative control is to build robot abilities in order to perform efficient actions and help humans in interactive tasks by learning from human behaviour strategies and imitating human actions [Becker et al. 1999; Acosta-Calderon and Hu, 2005]. Studies by Breazeal and Scassellati [2002] presented a taxonomy of social learning in robotics, which can be described by the following set of definitions as shown in Table 2.1.

Table 2.1 Taxonomies of social learning [Breazeal and Scassellati, 2002]

Behavioural terms	**Definitions**
Imitation:	A robot can learn and observe behaviour from human performance.
Goal emulation:	After learning the human's actions, the robot can perform the same task as the human.
Stimulus enhancement:	Robot is instructed to move to an object location as a result of human actions.
Social support:	Robot is more likely to learn from human behaviour, since human actions generate the same motivational state in the robot.
Exposure:	Both operators perform comparable environments; therefore they adopt comparable actions.
Social facilitation	Previous behaviour is replaced in a robot due to human performance.

Wolper et al. [2003] suggest that a robot observes human performance to set-up a predictive framework, which enables the robot to be able to simultaneously imply the human state and predict incoming actions in order to effectively perform a coordinative task. Shibata et al. [2003] have studied the movement coordination between humans and robots in a scenario of human-robot interactive movement. The motions involved were described in terms of the timing of interpersonal collaboration, which reveals that both participants delay their actions during the overlapping space of the coordinated working area. In the long term, the human-human interactive parameters are extracted in order to implement the results with robots so as to execute interactive tasks with humans.

To achieve effective human-robot interaction, a robot working as a mimicking partner has to be able to understand and recognize the structural congruence between the imitator and the demonstrator [Meltzoff and Brooks, 2001]. A robot can work together with a human in common tasks by mimicking the human's movements; however, there are situations where this cannot be accomplished due to the physical differences between the demonstrator's and imitator's bodies. This is called the correspondence problem [Dautenhahn and Nehaniv, 2002; 2004]. Experiments completed by Calderon and Hu [2004] successfully solved this issue by proposing a representation of the demonstrator's body and providing a relevant method.

Luh and Shuyi [1998] stated that when a robot and a human jointly move an object, it is important to assign the human to the decision making with the robot being strategically trained to achieve the task trajectory. A set of learning strategies for the robot manipulator has been considered along with the analysis of human action models in interactive tasks using a fuzzy model. In Luh and Shuyi's experiment, the calculations of robotic dynamics and kinematics were not necessary, since force sensors, encoders and a microcontroller were used for robotic trajectory control. This system can be sufficiently fast to accomplish the force control, and is illustrated schematically in Figure 2.10.

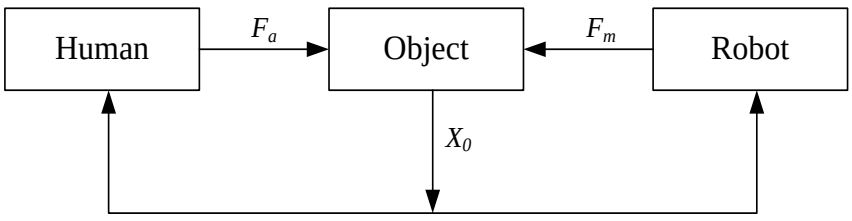

Figure 2.10 Block diagram control of HRI [Luh and Shuyi, 1998]

Behaviour-based robotics systems have become one of the most attractive approaches to human-robot interaction, and are made up of four key principles, as follows: providing rule collections; secondly, collecting the required information from input sensors or other behavioural strategies which relate to the system; thirdly, computing and analyzing the information received; and finally, transferring the output signals to the system effectors for effective robot performance. Although, behaviour-based robotics systems have been increasingly applied to robots and are successful in several applications, they have not often been used for more complex problems such as the control of hierarchical tasks [Monica and Maja, 2002]

The three key methods in designing and constructing behaviour-based robotics systems, are expressing, encoding and coordinating behaviour methods. In addition, the robotics architectures which include software systems, a robotics language and tool specifications are also crucial in developing suitable behaviour-based systems for robots [Ronald, 1998]. Behaviour-based architecture is required to clarify the problem in the robotics control system in order to enable a robot to appropriately solve a problem in the right way to achieve a goal. A reactive control architecture based on behaviour is illustrated in Figure 2.11, where each sensor used collects suitable input information and then distributes it to reactive behaviour modules. Action selection controls individual interactive actions by either choosing one of the various behaviour modules using an arbitration method, or combining all relevant behavioural modules so as to generate an appropriate output behaviour which is called the common fusion method, as shown in Figure 2.12(a) and (b) respectively [Mataric, 2007].

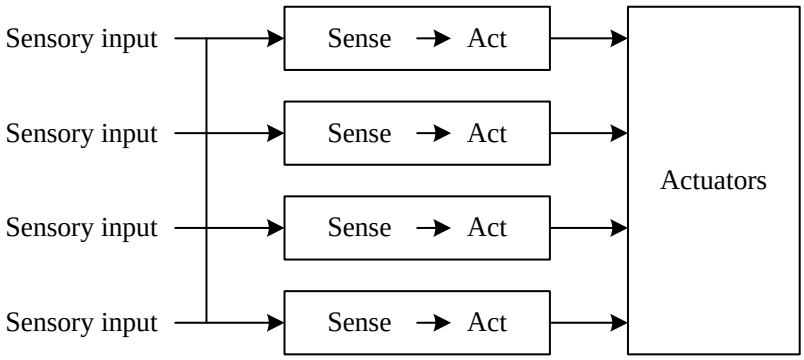

Figure 2.11 Parallel reactive architecture together
with task achievment modules [Mataric, 2007]

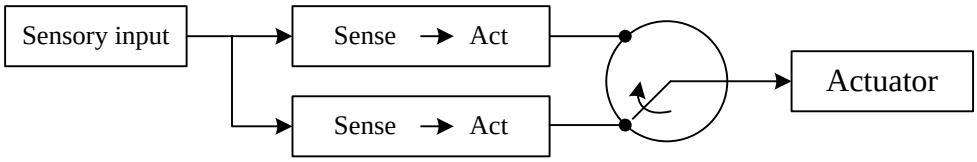

(a) Common arbitration

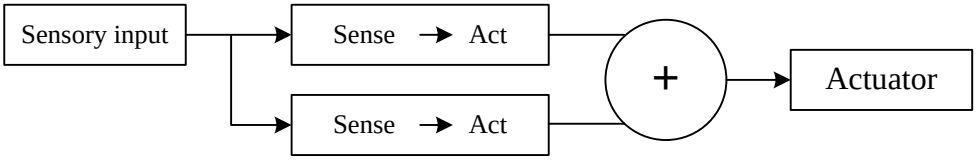

(b) Common fusion

Figure 2.12 Types of the action-selection mechanism [Mataric, 2007]

2.5 Force Control in Robotic Systems

Robot force control is a fundamental requirement in the achievement of the control of the robot's real-time path in any physical robot interaction task. It has been developed in the past three decades, using for example force, torque and visual feedback to operate robots to participate in unstructured environments. The compliant behavioural motion control of robots can be categorized as: passive and active compliant motion. Passive compliance is where the robot end effector position is modified by the contact force because of the inherent compliance of the robot, whereas active compliance facilitates a programmable robot reaction using a force feedback signal, for which purpose the robot control system has been designed [Siciliano et al. 2008]. Typically, this contact force and torque feedback signals are measured by a multi-axis force/torque sensor before being transferred to the robot controller in order to generate an updated trajectory of the robot end effector.

Raibert and Craig [1981] proposed a new method for robot force control, in which two control schemes, consisting of position and force, are combined into one control scheme termed hybrid position/force control. The advantage of this control is that the position and force data are analysed independently and synchronously, and then combined in the final process before being converted to joint torques [Volpe and Khosla, 1998]. Figure 2.13 shows the explicit force control scheme which can be separated into two control loops each of which has an individual sensor system, one to detect the force applied to the robot end effector and the other the position of the robot joints [Vukobratovic et al.

2008]. The X and F are 6×1 vectors represented Cartesian position and orientation and Cartesian force and moment respectively. The S is a 6×6 diagonal selection matrix, where each element becomes a one for position control or zero for no position control, and $S^{\perp}$ is I – S.

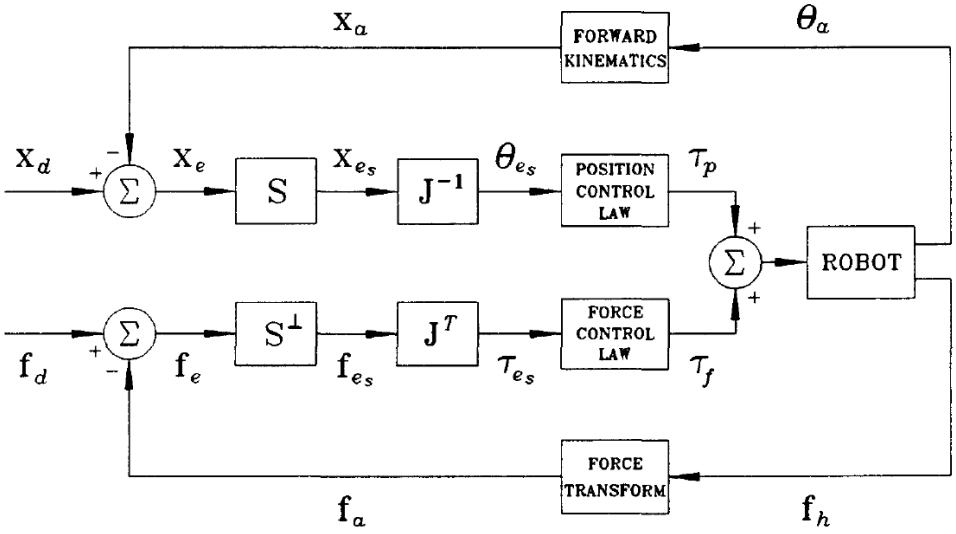

Figure 2.13 Hybrid position/force control [Fisher and Mujtaba, 1991]

From an extensive review of research into control technique for explicit force control, it can be found that proportional (P), proportional integral (PI) or proportional derivative (PD) types of control are most often used for the purpose of system simplicity and effectiveness [Komati et al. 2013]. Perdereau and Drouin [1993] stated that some difficulties are encountered with this hybrid position/force control technique during implementation; for example, the set points of position and force information have to be elaborated during movement since the constrained frame moves along with the robot end effector. In this technique, noise might be often modified in the system because each control scheme could behave as an external disturbance of another.

Salisbury [1980] developed a control method for active compliant motion based on the apparent stiffness of a robot manipulator using three translational and three rotational stiffness components. This technique considers the rate of force and torque signals detected by a force/torque sensor, and controls the behaviour of the robot end effector based on the linear spring relationship as follows:

$$F = K.\delta X \tag{2.5}$$

where, δX is the Cartesian displacement from a commanded Cartesian position X_0,

K is the Cartesian stiffness matrix, and

$\delta\theta$ is the joint angle displacements from a commanded joint angle θ_0.

The Jacobian matrix (J) used to calculate δX according to the joint angle displacements represented by $\delta\theta$ can be given by:

$$\delta X = J.\delta\theta \tag{2.6}$$

By assuming that both dynamic and static forces are small and thus can be neglected, the relationship between the joint torque (τ) and applied force (F) can be expressed as:

$$\tau = J^T.F \tag{2.7}$$

By substituting Equations 2.6 and 2.7 into 2.5, the joint torque for six dimensions can be therefore expressed as follows:

$$\tau = J^T.K.J.\delta\theta \tag{2.8}$$

Impedance control, developed by Hogan [1984], provides the motion control of a robot end effector based on a second-order differential equation defined as a mass-spring-damper system, where the interactive force is controlled based on system error, i.e. the error between the desired and actual positions of the robot end effector. The impedance control formula can be presented as follows:

$$M_d\left(\ddot{X} - \ddot{X}_d\right) + B_d\left(\dot{X} - \dot{X}_d\right) + K_d(X - X_d) = -F \tag{2.9}$$

By assuming the real-time trajectory of the robot end effector can be controlled by acceleration, the new transformation equation is as follows:

$$\ddot{X}_r = \ddot{X}_d + {M_d}^{-1}[-F + B_d\left(\dot{X} - \dot{X}_d\right) + K_d(X - X_d)] \tag{2.10}$$

where, M_d is a designed inertia matrix,

B_d is a designed damping matrix,

K_d is a designed stiffness matrix,

X, X_d are vectors of the actual and desired positions of the robot end effector,

$\dot{X}, \dot{X}_d, \ddot{X}, \ddot{X}_d$ are the corresponding velocity and acceleration of the actual and desired positions of the robot end effector respectively,

$\ddot{X}_r$ is a reference acceleration, and

F is the force exerted on the robot end effector.

Equation 2.10 can be illustrated in Figure 2.14, in which $G_c(s)$ is a transfer function representing the non-ideal behaviour of the acceleration control loop

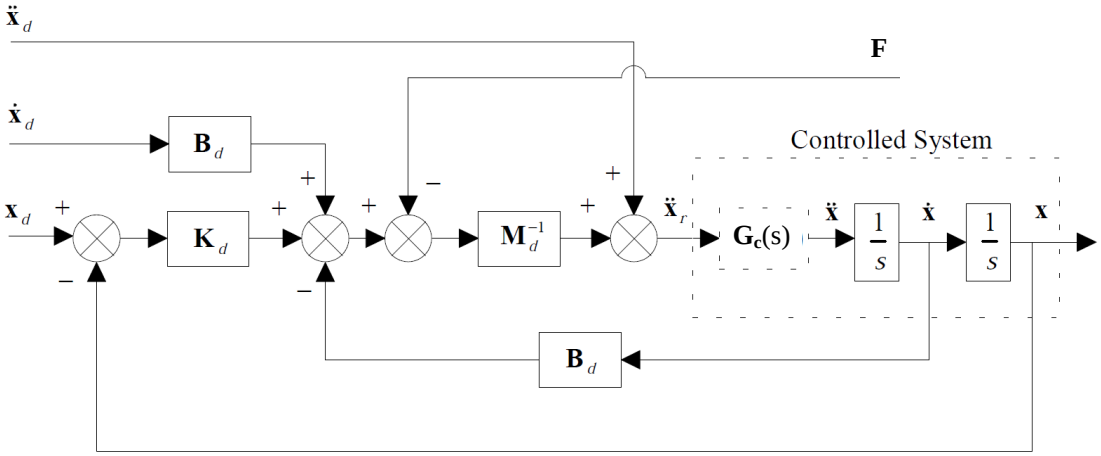

Figure 2.14 Block diagram of impedance control scheme [Almeida et al. 1999]

In practice, it may not be possible to appropriately control commercial robot manipulators using explicit hybrid position/force control or force-based impedance control because the commercial robots are developed as positioning devices. However, by using implicit or position-based force control (external force control), the force control rule functions to respond to the environment, track the desired forces, and compensate for variations in robot positioning at the contact surface [Vukobratovic et al. 2008]. The key features of this technique provide reliability and stability because switching between position and force loops is avoided. Both position and force control are handled in the same Cartesian direction. This implicit position-based force control is able to be appropriately associated with simple control schemes such as robust PI or PID control, and it is also easily implemented on various types of robot controllers [Farid and Redouane, 2009].

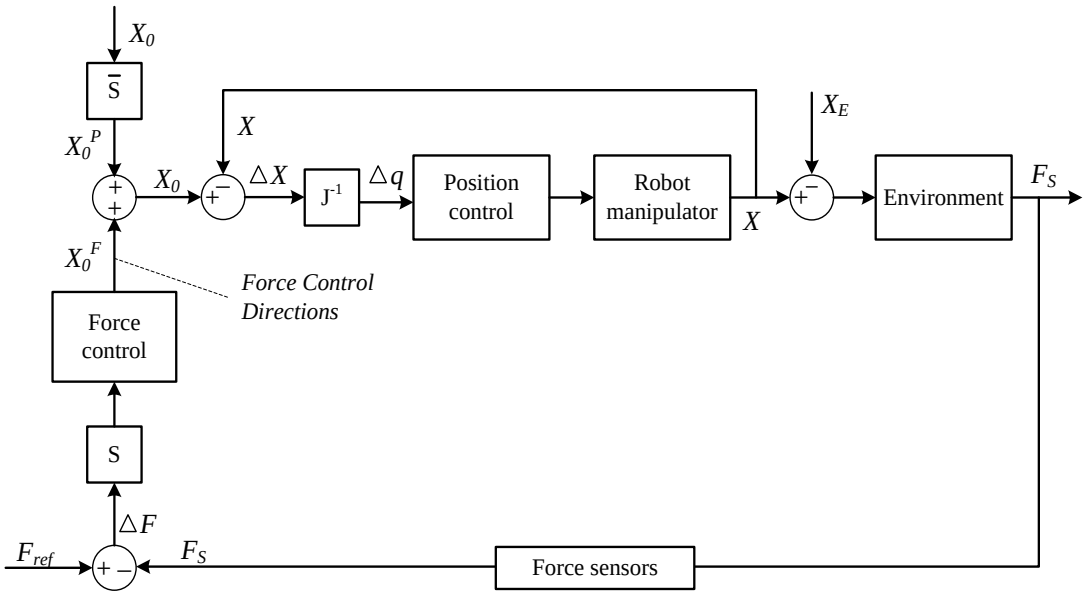

Figure 2.15 Position-based implicit force control or external force control [Farid and Redouane, 2009].

Typically, there are two important control loops in a position-based force control system, in which the inner and outer loops refer to force control and position control respectively. Figure 2.15 shows a schematic of the implicit position-based force control or external force control. In this control method, the input of the force control loop is the error between desired and actual force values. An output of the control system provides an equivalent position, which is directly modified by an input reference position. Cartesian coordinates are conveyed by the position control and then transferred directly to the robot to modify its trajectory.

2.6 Performance Evaluation of HHI and HRI

The overall qualitative performance of human-human or human-robot interaction is the key aspect in system development. A large amount of research has considered the development of performance metrics to obtain the necessary information in designing more effective human-robot interaction [Aaron et al. 2006]. A motion quality metric which is useful in evaluating human-robot interaction has been proposed by Yanco and his colleagues [2004b]. Olsen and Goodrich [2003] established a number of metrics to evaluate the performance of human-robot interaction. However, because of the complexity of human behaviour, it is difficult to establish the effective measurement of

human qualitative performance. Based upon Shannon and Weaver's research [Shannon, 2001] and applied to human-human performance are the Fitts and Hick-Hyman laws. However, a review of recent human-computer interactive literature shows that the Hick-Hyman law cannot be completed in human-computer interaction, whereas Fitts's law has received significant attention [Seow, 2005]. Fitts' law [Fitts, 1954] can be used to explain a model of human movement in human–computer interaction and estimate the time taken when a human moves an object to a target in different distance and size of the target, as expressed in Equations 2.11 and 2.12.

$$MT = a + \left[b \times log_2\left(\frac{2A}{W}\right)\right] \tag{2.11}$$

or

$$MT = a + [b \times ID] \tag{2.12}$$

where,

	MT (s)	is the performance time,
	A (m)	is the actual hand moving distance or amplitude,
	W (m)	is the target size,
	ID (bits)	is the index of difficulty, and
	a and b (s/bit)	are the two constants relating to the task and the person respectively.

Fitts' law has been developed and it has been shown that the rule can be applied to complex robots or machines. Cannon [1990] studied the target-threshold model, which is a fundamental theory used to predict response speed or movement time in the parameter design of a human-machine system using Fitts' law as a predictive design tool. Studies by Reed et al. [2007; 2008] investigated human-human interactive behaviour in turning a crank and then provided the human imitating control framework for a robot to physically complete a human-robot interactive task. Furthermore, Reed and his colleagues investigated whether or not Fitts' law can support two people working together in crank turning tasks.

Some robotics researchers have used different techniques to assess the system qualitative performance. Raman and his colleagues [2000; 2002; 2009] evaluated the velocity trajectories measured in experiments, which were similar to results calculated by using the minimum jerk trajectory (MJT) method proposed by Flash and Hogan

[1985]. A mathematical model of point-to-point human arm movement was formulated

which can estimate the multi-joint arm movement quality of experimental features and details. The best performance of each trajectory can be directly calculated using dynamic optimization theory. The fifth order polynomial equation for the minimum jerk trajectory (MJT) function is as follows:

$$J = \int_0^{t_f} \left[\left(\frac{d^3x}{dt^3} \right)^2 \right] dt \tag{2.13}$$

The criterion function can be determined from the point-to-point trajectory by assuming that the velocities and accelerations of the start and end points are zero. The hand trajectory can therefore be expressed as in Equation 2.14:

Then, $$x(t) = x_0 + (x_f - x_0)(6\tau^5 - 15\tau^4 + 10\tau^3) \tag{2.14}$$

where, $\tau = \frac{t}{t_f}$, x_0 is the position at time t_0, and x_f is the position at time t_f.

Bicker [1989] and Burn [1993] implemented a circle-tracking test to assess the system performance of the tracking capacity of position/force control applied in a telemanipulation task. The test determined the ability of the slave arm to follow the movement of the hand controller along a circular path of 100mm in diameter, in which radial and tangential force components were analysed. The performance of the control system was measured by the root-mean-square of the radial force.

The error in a human-robot interactive system can be divided into two main categories: static and dynamic error. Static error may arise from several causes; for instance, incorrect viewing parameters and optical distortion errors which could happen such as when the captured straight line may appear as a curve. Tracking system errors may arise from the sensor system and this is the most serious problem because such errors can hardly be detected or eliminated. Mechanical misalignment errors could also occur, such as when proposed model values and actual experimental results are unequal. Dynamic errors involve delays in the system achieving the positions and orientations from captured images. These include frame rate delays, lags in the detection systems and delays in communication interfaces [Azuma 1997].

2.7 Safety in Physical Human-Robot Interaction

Conventional robots can provide fast and accurate motion without using external sensors to detect their environment, and can therefore pose a significant risk to operators working within their vicinity. Human-robot interactive strategies are required to guarantee that humans who share physical movements with robots in the same workspace remain safe at all times. Giuliani et al [2010] postulated when humans coordinate with industrial robots, there is one essential limitation. This is the protection of human operators from the risk of harm or injury by the robots. Therefore three imperative principles applied to robot architectures have been proposed to increase safety in human-robot interaction: robustness, fast reaction time, and context awareness.

Mitka et al. [2012] have reviewed standards and safety features in design of robots from the point of view of safe performance, which relate to requirements for robots in terms of electrical safety, software robustness, emergency stops, sensory devices, measuring static and dynamic performance and operation stages. Safety requirement standards for industrial robots are addressed by ISO 12100:2003 – Basic concept general principles for design, ISO 13482:2014 – safety requirements for robots in personal care, ISO 13849:1999 – Safety related parts of control systems, ISO 13855 – positioning of protective equipment with respect to the approach speeds of parts of the human body and ISO 10218:1992 – safety standard for robots which was revised and published in 2006 and the salient changes of this revision are as follows [Alami et al. 2006]:

- *New modes of operation*: the standard permits the introduction in the workplace of advanced robots such as simultaneous control of robot manipulators in collaborative operation in which the designed robots work in direct cooperation with a human operator in a workspace,
- *Control reliability*: the revision allows safety-rated, soft-axis and space-limiting control circuitry to use state-of-the-art software, hardwired electromechanical components and network-based technology, and
- *Safeguarding and clearance*: this revised one can be evaluated based on the assessment of fixed safeguard zone, stop time, distance to be provided in various loads, maximum statistic load at a robot end effector and maximum velocity.

The present landscape for robotics safety standards proposed by the America National Standard Institute (ANSI) has established the following key components [Bicchi et al., 2008]:

- Risk assessment: it is advised to identify and reduce risks in proportion to their seriousness and probability,
- Safety critical software: it is designed for the shutdown of the system in a safe state and the prevention of subsequent automatic operation,
- Dynamic limits: the physical limits of human operators taken into account,
- Emergency stop: it is used to allow external devices to initiate context-based safety stops, and
- Man-machine interface: few key modes are provided to avoid misunderstanding and cause of safety problems.

Although, human-robot interaction has a potentially wide field of application, the coexistence between humans and robots brings a significant risk of dangerous situations. If a robot is not appropriately designed with safety intrinsic, it could harm a human partner during an interactive task. Therefore, safety and reliability are the primary concern for the technical challenges in the design of human-like robot control operating in the human environments. The control strategy also allows robot motions to be comfortable and natural for the humans in cooperative tasks and any risk of injury to humans must be eliminated [Bicchi et al., 2008]. Safety is an important benchmark for HRI which must be properly evaluated in order to minimize of the inherent safety risk associated with physical contact and protect a robot itself and a human partner Haddadin et al. [2008]. Heinzmann and Zelinsky [2003] expressed important safety requirements for human-friendly robots which are as follows:

- A human-friendly robot must be controlled in such a way that a person has to be able to safely share a common workspace with a robot;
- The bandwidth of interactive operations by a human-friendly robot must be limited in order to fully understand and predict the motion of the robot; and
- The collision of a human-friendly robot with a stationary human operator must not result in any serious injury to the human.

Additionally, Heinzmann and Zelinsky [1999] proposed that the appropriate characteristics of human-friendly robots, which are used to ensure safety during human-robot interaction in real-time, are as follows:

- The humans should be able to easily control robots;
- The robots should have sufficient autonomy to facilitate their use;
- The overall autonomous behaviour of the robot should be predictable and understandable to the human operators; and
- The robot's autonomous actions must pose no threat to humans.

Safety in human-robot interaction can be improved by developing robots able to identify all hazards, and then to plan to prevent those risks from occurring in advance. Another safety improvement strategy is to generate a safeguarding zone, which is applied to industrial robots in human environments. If human operators are detected entering the safeguarded zone, a controller is then executed which immediately triggers an emergency stop. Yamada et al. [1997] proposed another technique to combine the concepts of mechanical measurement and safeguarding zone together to facilitate an effective human detection system and an emergency stop system in a fail-safe mode. Human operators are normally able to make higher-level problem-solving decisions, whereas robots can achieve the best manipulation performance. Safety for humans and robots jointly working together is addressed by the person responsible for the command of the robots using the effective instructions in order to allow the robots to work with the humans in a safe manner [Heinzmann and Zelinsky, 2003].

Many robotics researchers have proposed innovative solutions to the problem of ensuring safety in human-robot interactive performance. Some groups have focused on reactive control, danger evaluation or planning to guarantee safety. Others have concentrated on human or visual monitoring to ensure safety. Human-robot interaction has to be maintained in a safety mode of operation by reducing the impact force generated from human-robot contact [Heinzmann and Zelinsky, 2003].

To develop the evaluation of human-robot interaction, Weiss et al. [2009] investigated a framework of usability, social acceptance, user experience, and societal impact (USUS) based on a model of multi-level indicators. The proposed method focuses on four key items. Usability relates to effectiveness, flexibility and robustness, and user experience relates to performance and effort expectancy and self-efficacy. Social acceptance relates to embodiment, emotion, security and perception, and finally social impact relates to quality of life, working conditions and employment and education. A danger index was established as human-robot relative factors, which can be useful in the comparison of mechanical system designs. Factors include *relative displacement index, relative velocity index, robot inertia index* and *robot stiffness index*. The robot's actions can be adjusted based on the localization and monitoring of humans during interactive tasks by applying a danger evaluation technique to the robots [Ikuta et al. 2003].

Table 2.2 Classification of safety strategies [Ikuta et al. 2003].

		Control strategy	Design strategy
Before collision	Avoid collision	Distance	
	Minimize impact force	Speed Moment of inertia	Weight
After collision	Attenuation diffusion	Stiffness Posture	Cover Joint compliance Surface Shape

Additionally Ikuta and his colleagues presented a classification of safety strategies as shown in Table 2.2. This classification can be divided into two key components: pre-contact safety strategies, which reduce the risk in injuries to humans before collision; and post-contact safety strategies which minimize injuries to humans after collision. Two categories of human-robot interactive safety strategies have been identified: safety design and safety control strategies. To ensure safety in real-time-human-robot interaction, Kulic and Croft [2005] proposed a danger index formulation to explicitly identify surrounding obstacle levels. A six-degree-of-freedom manipulator was implemented and performed the robotics movement tasks while minimizing the danger index in real time.

Lew et.al [2000] established a fundamental motion planning strategy based on a feedback control system for human-robot coordination in the same workspace. To guarantee safety during interaction, three algorithms are used which consist of inertia reduction, passivity and parametric path planning. The inertia reduction method can provide a virtual force to decrease the effect of the robots. Simulation results have shown that the proposed algorithm method creates less contract force when the robot interfaces with its human environment, and that the robot could be manipulated using small external forces, leading to a safer environment for the human operator.

Compared with control-based methods, motion planning in a suitable collision avoidance strategy has been important in minimizing the safety hazards of robots in environments with obstacles. Jerk-bounded trajectory planning for robot manipulators has been studied and demonstrated by Macfarlane and Croft [2003]. This technique was implemented with a six DOF robot manipulator, and successful and smooth point-to-point movement was achieved with limited jerks in real-time application. Erkorkmaz and Altintas [2001] developed a trajectory generation algorithm which can construct a continuous kinematic profile including position, velocity and acceleration profiles. In addition, the algorithms generated can also be easily implemented with a three-axis milling machine in real time tasks.

Although human-robot interactive systems have been currently applied in various applications, the conceptual principles remain similar. For instance, safety in physical human-robot collaboration can be enhanced via the user monitoring in order to detect emotional expression, voice or gestures from the humans [Bien et al. 2002]. In human-robot interactive tasks, human monitoring can supply the beneficial information to develop safety in the interactive system. System monitoring is also realized to examine the human communication signals using visual or physical monitoring. Traver et al. [2000] proposed a visual feedback signal which could be applied in robotics planning and control strategies in order to enhance safety in human-robot interaction. Bicchi et al. [2001; 2004] have investigated the use of a compliant joint to achieve safe systems. Human monitoring is also practiced in human-human interactive tasks in which non-verbal communication between participants is used [Reed et al. 2007; 2008].

Visual servoing techniques involved the use of cameras to track the features of human operator and then the data received are analyzed to guide human-robot interaction, and this has been applied to a wheelchair based on KARES II, a conventional Cartesian robot. It provided autonomous operations by collecting virtual feedback. Additionally, the effective intention reading was also implemented to the robot to recognize the meaning of a human by detecting the person's facial expressions, while log-polar mapped methods were applied to the stereo camera to detect and track the robot's features using virtual information processing [Won-Kyung et al. 2001]. These techniques were successfully applied to the Cartesian robot to feed beverages to an operator.

Head tracking is a key challenge not only in human-robot interaction (HRI) and human-human interaction HHI, but also in the human-computer interface (HCI). Morimoto and Flickner [2002] have studied a multi-face detection technique to capture the pupils of the eyes which are identified using heuristic rules. Unlike Stiefelhagen and his colleagues [2002], they have evaluated a method of gaze direction tracking of the human's virtual attention. In this technique, the head position of human participants is simultaneously detected instead of the eyes. The person's focus of attention can be estimated by using neural network control and a probabilistic model to predict the human's targets. The concept of a gaze-aware robot has been successfully applied to a humanoid robot prototype system, and additionally the proposed technique provides the enhanced safety in the human-robot coordination [Stiefelhagen et al, 2002].

The development of safety human-robot coordinative systems depends on the analysis of hazard characteristics in the system, environmental conditions, other specific requirements and human error. Many essential factors of human-robot interaction should be taken into account, such as emergency stops, load limitation, motor monitoring and working space limitations. Various features can be implemented such as system power supply being cut-off automatically when a robot performs a dangerous movement. Furthermore, robotics links are provided with overload protection detectors to warn of or switch off the power supply if an overload occurs. The robotics motors or actuators can be protected by overload or temperature protection detectors, and additionally the robotics workspace sensors will give warning when non-permitted actions occur in the restricted area.

2.8 Summary

This chapter has reviewed the relevant research in human-robot and human-human interaction. The conceptual frameworks of HHI and HRI control strategies are introduced. Human perception and cognition systems are explained as a basic model of anatomical structure; additionally, the McRuer crossover model used to determine a human behavioral characteristics model based on dynamic responses is explained. The observations of human grasping actions, which are suitable for imitation by robotics manipulators to smoothly and efficiently perform the cooperative tasks, have been carried out. In addition, the evaluation of the overall qualitative performance of the system and safety issues in human-robot interaction, which are key aspects, has been presented. Robot force control is detailed and categorized into several techniques, such as stiffness, impedance, hybrid position/force and implicit position-based force control or external force control. However, commercial robot manipulators are typically designed as positioning devices, and here explicit hybrid position/force control or force-based impedance control may not be appropriate for implementation. Therefore, in this project, external force control has been adopted for human-robot interactive tasks, which has the key advantage of provide reliability and stability because switching between a position loop and a force loop is avoided. Moreover, this external force control is able to be appropriately associated with simple control methods such as robust PI or PID control [Farid and Redouane, 2009].

Human-robot interaction (HRI) is the study of the collaborative dynamics between robots and humans who work as partners. The key issue in this project is to understand and parameterize the characteristics of human-human interaction, when humans jointly coordinate to realize a goal in order to assure a smooth and efficient workflow. This is achieved by studying simple physical collaboration in order to set-up and develop the framework for human-robot interaction. The robot must have the capability to predict its actions and goals as well as to understand the interactive context, which should not require training and adaptation from humans. The development of an appropriate set of behaviour strategies will allow a robot manipulator arm to interact safely with a human to facilitate the dextrous and speedy transfer of objects in a timely manner. An intelligent collision avoidance strategy will be an essential requirement to enable the robot manipulator arm to safely interact with a human within its workspace, and to facilitate transfer of objects between the robot and human and vice-versa.

CHAPTER III

ONE DEGREE OF FREEDOM HUMAN-HUMAN INTERACTIVE PILOT STUDY

In haptic HRI, a human and a robot attempt to jointly manipulate and dexterously transfer an object along a common trajectory, in a natural, safe and timely manner. One of the fundamental control issues for the robot manipulator arm concerns the interactive force applied by the human throughout the course of the interactive task in such a way as to allow safe and effective HRI [Kosuge and Hirata, 2004]. As discussed in Chapter II, understanding of HHI behaviour is a fundamental requirement in developing a framework for functional HRI, and to facilitate natural HRI in a shared workspace, it is important to understand the kinematics and dynamics of the behaviour and to design and develop an appropriate set of strategies for robust, behaviour-based, human-robot interaction [Reed et al., 2004]. A study of a one DOF human dynamic model has been carried out, and modelled to predict human response under different conditions whilst performing interactive tasks. The optimization of the model in a range of tasks of a highly adaptive nature cannot be easily estimated without using high-level numerical computation software, such as Matlab [Aslan and Cebeci, 2007].

This chapter introduces two preliminary HHI tests; the first test is a one DOF human-human interactive rectilinear task in which the *handler* has to transfer a compliant object to the receiver along a constrained horizontal path to a random transfer target position. This experiment has been designed using a Box-Behnken methodology [Box and Hunter, 1957] to evaluate human dynamic response based on the McRuer crossover model [McRuer et al. 1967; 1995], where the appropriate full-scale set of tests were statistically examined by a pilot study.

However, the sliding task does not mimic a real-world human-human object handover task where the handler is able to pass an object to the receiver in a 3D workspace. To this end a substantive human-human object handover task, in which the *handler* transfers a baton type object to the *receiver*, has been undertaken. Physical responses in the handover tasks have been studied to establish an appropriate set of behaviours in a human-robot interactive control strategy. In addition, the human-human object handover tests have been arranged based on the recommendations of the one DOF pilot study, as proposed in the first preliminary HHI test.

3.1 Force Analysis of Human-Human Interaction

This section describes the basic concepts used in the force analysis of single DOF human-human physical interaction and how the applied external forces applied to a compliant object are classified, where the external force was measured using two parallel full bridge-thin-beam load cells. Assuming that F_c, F_s and F_r are the frictional force and applied forces from the *handler* and *receiver* respectively, 'net force' (F_{net}) is initially defined as the sum of the forces, and is similar to a single participant's force profile during the individual performance of a task.

Figure 3.1 schematically shows grasping sequences during the one DOF HHI task, which include three distinct states consisting of the sending, transfer and receiving phases. In the sending phase, the *handler* dispatches the object to a transfer target, by applying a force (F_s) which is the same as the direction of movement of the object. The transfer phase is where the object is transferred to the *receiver*, where the direction of the net force (F_{net}) depends on the sum of F_c, F_s and F_r; at this point. Finally, the object is manipulated to the final position by the *receiver* during the receiving phase.

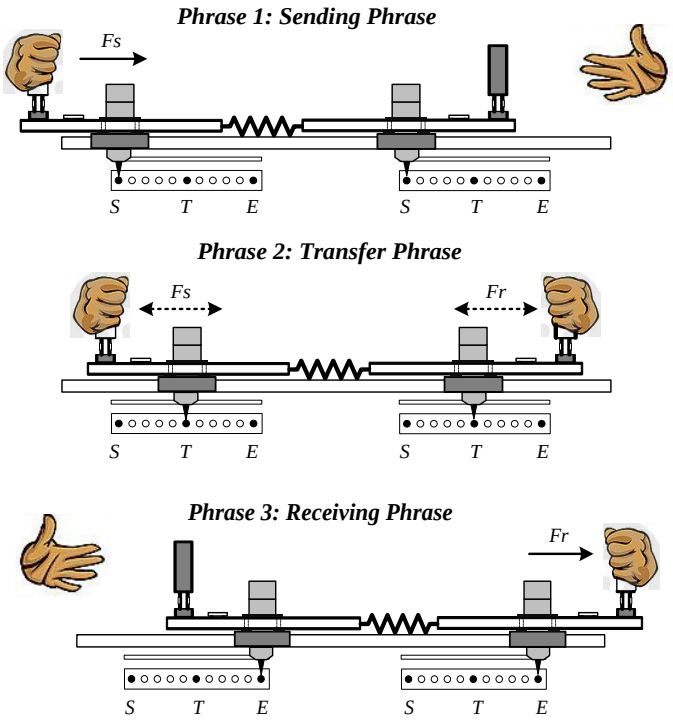

Figure 3.1 Sequence involved in the real human-human interactive slider task

The mechanical model shown in Figure 3.2 presents the simplest form of the one DOF human-human haptic interaction, and the model is similar to that of two masses coupled by a spring with two frictional forces acting against its motion. The key abbreviations of the relevant parameters are as follows:

Spring stiffness:	k		
Two sets of masses:	m_1	and	m_2
Object displacements:	x_1	and	x_2
Object velocities:	$\dot{x}_1$	and	$\dot{x}_2$
Object accelerations:	$\ddot{x}_1$	and	$\ddot{x}_2$
External force applied by a *handler* and a *receiver*:	f_s	and	f_r
Frictional forces:	f_{res1}	and	f_{res2}

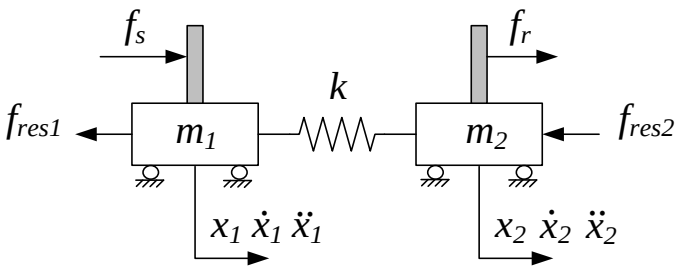

Figure 3.2 The mechanical model of the human-human interactive slider test rig

In the studies by Peng et al. [2005] and Groten et al. [2009], a human-human haptic interaction in a rigid object manipulating task was considered for use as a basic controller design in haptic human-robot interaction. According to Feth et al. [2009], "haptic interaction is considered as the negotiation of the positional trajectory of interactive force via object between two partners". The force applied in the interactive haptic application is classified into two different types, which are internal interactive force (F^I) and external variable force (F^E).

Therefore the forces applied by the *handler* (F_s) and *receiver* (F_r) are:

$$F_s = F_s^E + F_s^I \tag{3.1}$$

$$F_r = F_r^E + F_r^I \tag{3.2}$$

The movement of the object is caused by the external net force, which can be calculated from the external *handler* (F_s^E) and *receiver* (F_r^E) forces and frictional force (F_c^E), as follows:

$$F_{net}^E = F_s^E + F_r^E + F_c^E \tag{3.3}$$

The mathematical models of the *handler* and *receiver* forces are conveyed in their simplest forms using the mechanical modelling diagram shown in Figure 3.3. It assumes that the haptic interactive behaviour is based on the movement of the compliant object. In the proposed free body diagram, the following notation is used: two human forces (f_s and f_r), two masses (m_1 and m_2), two frictional forces (f_{res1} and f_{res2}), object displacements (x_1 and x_2), and spring stiffness (k).

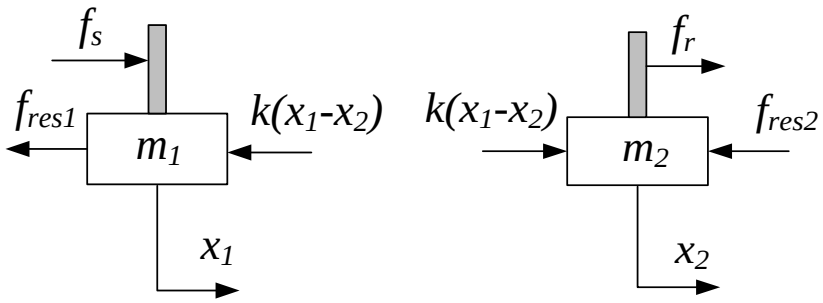

(a) Free body diagram of mass m_1 (b) Free body diagram of mass m_2

Figure 3.3 Free body diagrams of the two masses in human-human interactive tests

The *handler*'s continuous-time equation based on the free body diagram Figure 3.3(a) can be calculated using Newton's second law of motion as follows:

$$f_s(t) - k[x_1(t) - x_2(t)] - f_{res1}(t) = m_1\ddot{x}_1(t) \tag{3.4}$$

then, $$f_s(t) = m_1\ddot{x}_1(t) + f_{res1}(t) + k[x_1(t) - x_2(t)] \tag{3.5}$$

Consider magnitudes for all instantaneous time; this continuous output signal can be transformed into discrete-time values measured at every sampling time *T*, and the individual discrete sample number is represented by *n* as follows:

$$f_s(n) = m_1\ddot{x}_1(n) + f_{res1}(n) + k[x_1(n) - x_2(n)] \tag{3.6}$$

By assuming that: $$\dot{x}_1(n) = \left[\frac{x_1(n)-x_1(n-1)}{T}\right] \tag{3.7}$$

and that: $$\ddot{x}_1(n) = \left[\frac{\dot{x}_1(n)-\dot{x}_1(n-1)}{T}\right], \tag{3.8}$$

then substituting Equations 3.7 and 3.8 into the Equation 3.6 gives:

$$f_s(n) = f_{res1} + k(n)x(n) + \left[\frac{m_1(n)}{T^2}\right]x_1(n) - \left[\frac{2m_1(n)}{T^2}\right]x_1(n-1) + \left[\frac{m_1(n)}{T^2}\right]x_1(n-2) \tag{3.9}$$

The continuous-time differential equation of the *receiver*, based on the free body diagram illustrated in Figure 3.3(b), is given as:

$$f_r(t) - f_{res2}(t) - k[x_1(t) - x_2(t)] = m_2\ddot{x}_2(t) \tag{3.10}$$

then, $$f_r(t) = m_2\ddot{x}_2(t) + k[x_1(t) - x_2(t)] + f_{res2}(t) \tag{3.11}$$

Reforming the continuous signal into discrete-time values gives:

$$f_r(n) = m_2\ddot{x}_2(n) + k[x_1(n) - x_2(n)] + f_{res2}(n) \tag{3.12}$$

By assuming that: $$\dot{x}_2(n) = \left[\frac{x_2(n)-x_2(n-1)}{T}\right] \tag{3.13}$$

and that: $$\ddot{x}_2(n) = \left[\frac{\dot{x}_2(n)-\dot{x}_2(n-1)}{T}\right], \tag{3.14}$$

then substituting Equations 3.13 and 3.14 into Equation 3.12 gives:

$$f_r(n) = f_{res2} + k(n)x(n) + \left[\frac{m_2(n)}{T^2}\right]x_2(n) - \left[\frac{2m_2(n)}{T^2}\right]x_2(n-1) + \left[\frac{m_2(n)}{T^2}\right]x_2(n-2) \tag{3.15}$$

Having determined the relationship between the human *handler* and *receiver*, the human behavioural characteristics while performing a task of a horizontal transfer object need to be investigated. Rahman et al. [2002] analysed and developed an appropriate human characteristics model of two humans carrying out a HHI task. Two human subjects were asked to jointly move a rigid object to a target, in which the force exerted by the participants and the object position were measured. In addition, the researchers proposed a model of human arm characteristics, which is mechanically similar to a mass-spring-dashpot system as presented in Figure 3.4.

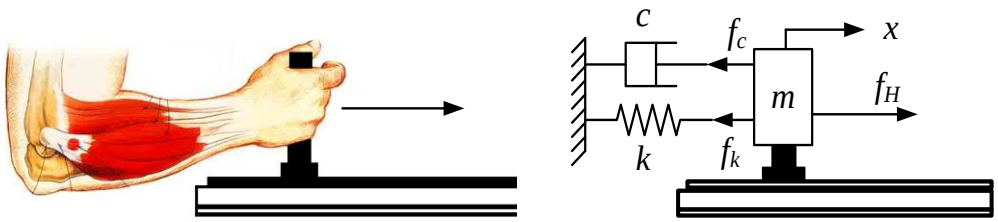

Figure 3.4 Impedance model of human arm in a spring-damper system based on Rahman et al. [2002]

From the dynamic model of the human arm based on Rahman et al. [2002], a diagram of mechanical models when a pair of participants working together with the one DOF HHI test apparatus is shown in Figure 3.5. In this study, the mechanical model is specifically considered for one-directional movement, so that gravitational effects can be ignored.

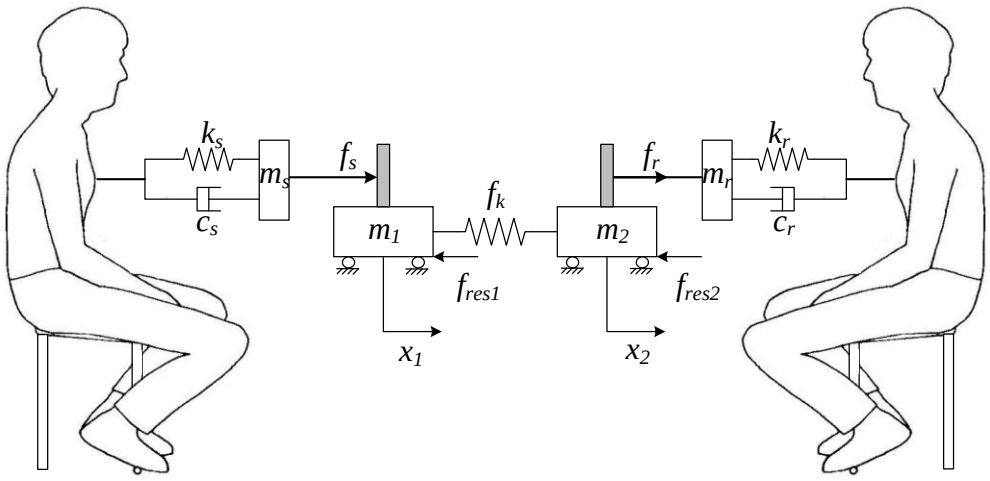

Figure 3.5 Schematic of the haptic human-human interactive mechanical model

A model of *handler*/*receiver* human arm dynamics can be derived as the following equations:

$$f_s(t) = m_s(t)\ddot{x}_1(t) + c_s(t)\dot{x}_1(t) + k_s(t)x_1(t) \tag{3.16}$$

Equation 3.16 can be transformed into discrete-time values measured at every sampling time *T* with the individual discrete number samples represented by *n* as given by:

$$f_s(n) = m_s(n)\ddot{x}_1(n) + c_s(n)\dot{x}_1(n) + k_s(n)x_1(n) \tag{3.17}$$

By assuming that: $$\dot{x}_1(n) = \left[\frac{x_1(n)-x_1(n-1)}{T}\right] \tag{3.18}$$

and that: $$\ddot{x}_1(n) = \left[\frac{\dot{x}_1(n)-\dot{x}_1(n-1)}{T}\right], \tag{3.19}$$

then substituting $\dot{x}_1(n)$ and $\ddot{x}_1(n)$ in Equation 3.17 gives

$$f_s(n) = m_s(t)\left\{\left[\frac{x_1(n)-x_1(n-1)}{T^2}\right] - \left[\frac{x_1(n-1)-1}{T^2}\right]\right\} + c_s(t)\left[\frac{x_1(t)-x_1(n-1)}{T}\right] + k_s(n)x_1(n) \tag{3.20}$$

The dynamic model equation of the *handler* is simplified in the following equations.

$$f_s(n) = \left[\frac{m_s(n)+c_s(n)+k_s(n)T^2}{T^2}\right]x_1(n) - \left[\frac{2m_s(n)+c_s(n)}{T^2}\right]x_1(n-1) + \left[\frac{m_s(n)}{T^2}\right]x_1(n-2) \tag{3.21}$$

or, $$f_s(nt) = a_1x_1(n) + a_2x_1(n-1) + a_3x_1(n-2) \tag{3.22}$$

where, $a_1 = \left[\frac{m_s(n)+c_s(n)+k_s(n)T^2}{T^2}\right]$,

$a_2 = \left[\frac{-2m_s(n)-c_s(n)}{T^2}\right]$, and

$a_3 = \left[\frac{m_s(n)}{T^2}\right]$.

In the same way, a model equation for the *receiver*'s arm dynamics is given by:

$$f_r(t) = \left[\frac{m_r(n)+c_r(n)+k_r(n)T^2}{T^2}\right]x_2(t) - \left[\frac{2m_r(n)+c_r(n)}{T^2}\right]x_2(n-1) + \left[\frac{m_r(n)}{T^2}\right]x_2(n-2) \tag{3.23}$$

or, $$f_r(n) = a_1x_2(n) + a_2x_2(n-1) + a_3x_2(n-2) \tag{3.24}$$

where, $a_1 = \left[\frac{m_r(t)+c_r(t)+k_r(t)T^2}{T^2}\right]$, $a_2 = \left[\frac{-2m_r(t)-c_r(t)}{T^2}\right]$, and

$a_3 = \left[\frac{m_r(t)}{T^2}\right]$.

The human arm impedance parameters, consisting of masses m_s and m_r, stiffness k_s and k_r and damping factors c_s and c_r, can be estimated using the differential variance of the recursive least-square technique, via the System Identification Toolbox in Matlab. To investigate the proposed impedance variables, the physical data captured from the preliminary HHI test have to be used, which are the forces f_s and f_r measured from both partners, object displacements x_s and x_r, velocities $\dot{x}_s$ and $\dot{x}_r$, accelerations $\ddot{x}_s$ and $\ddot{x}_r$, and sampling time T. Moreover, according to the studies of Rahman et al. [2002] and Feth et al. [2009], it has been concluded that this technique is also a promising approach for a robot in a human-robot haptic collaboration task.

Achieving an effective model of the one DOF haptic HHI task is one of the important challenges involved in designing a human-robot interactive strategy, which will allow the robot manipulator arm to interact safely with a human and to facilitate the dextrous transfer of objects in a timely manner. There is extensive research relating to the system model identification of the complex human operator. McRuer has proposed a human operator "crossover model" which could be used to predict operator behaviour whilst performing various human-machine interactive tasks. This model was first introduced for piloting simulated aircraft and is divided into a combination of sensing, computation and actuating components [McRuer et al. 1967; 1995].

3.2 Dynamic Model of the Human Operator in Human-Machine Interaction

Much of the relevant human operator modelling research has been concerned the manual control of vehicles. For example, Zhihao et al. [2007] and Trujillo et al. [2011] have considered the human abilities, which contribute to successful flying skills in studies aimed at developing pilot tests to enhance training effectiveness. The description of human-machine interaction based on the ability of an individual human operator is complicated. Arata (2009) analyzed human-machine interaction and proposed a human control model, as shown in Figure 3.6, which is useful for design, simulation and evaluation. The transfer function of the human operator, *H(S)*, is modelled as a combination of feed-forward and feedback signals. The important consideration in this test is to ensure an effective human behavioural model.

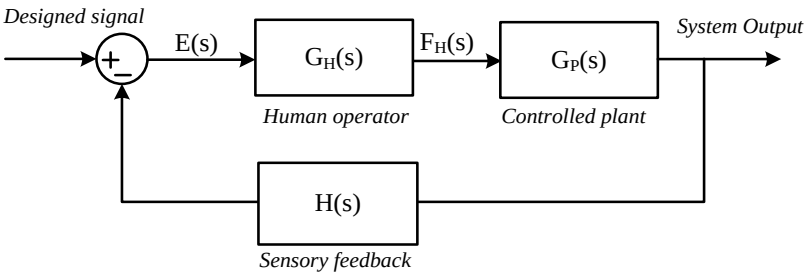

Figure 3.6 Simplified diagram of a human-machine interactive system [Arata, 2009]

3.2.1 McRuer Crossover Model

In the 1960s, a human characteristic model based on dynamic responses in human-machine interaction was designed and evaluated by McRuer et al. [1967; 1995]. The research was carried out using the McRuer crossover model, which assumes that the manual control of a vehicle is based on a combination of sensing, computation and actuating systems. In this research, the operator model was derived based on a human linear differential equation. However, the functional model also contains a noise added term, termed the remnant, which takes into account variations in individual human's performance. According to a general architecture of major human pathways, the human perceptual control can be divided into precognitive, pursuit and compensatory modes [McRuer, 1980]. Figure 3.7 shows the McRuer crossover model, in which the operator can be illustrated as a linear descriptive function. This model relates to visual, cognitive and neuromuscular systems along with a remnant representing time variation, noise and the non-linear behaviour of the human. Therefore the model can be considered to be a quasi-linear equation.

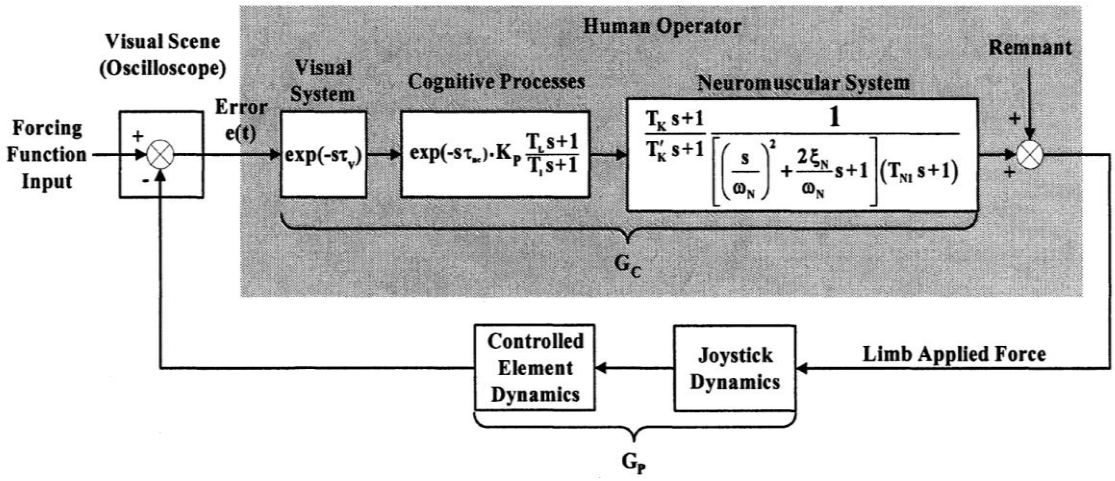

Figure 3.7 General architecture of the human operator model [McRuer et al.1980]

In the crossover model proposed by McRuer [1980] it is assumed that a human operator can adapt his/her behaviour to the overall human-machine plant characteristics and behave as a 'good servo' or, in other words, demonstrate good stability and response characteristics. The McRuer crossover region transfer function of the system (G_0) can be expressed as:

$$G_0(S) = G_h(s)G_p(s) = \frac{(\omega_C)e^{-\tau_d S}}{S} \tag{3.25}$$

where, G_h is a human transfer function as a linear feedback controller,
G_p is a machine or plant transfer function,
τ_d is reaction time delay of the human, and
ω_C is crossover frequency.

The extended crossover model in Equation 3.26 has been proposed to accommodate a residual phase lag which was not included in the original crossover model [McRuer, 1980]. Here, T_z and T_p are the lead and lag coefficients respectively, which can be adjusted by the human operator whilst performing different tasks:

$$G_H(s) = \frac{F(S)}{E(S)} = \frac{(\mathrm{K_H})(T_z S+1)(e^{-\tau_d S})}{(T_p S+1)} \tag{3.26}$$

Due to the complexity of the proposed human control system, a simplified model of a human-machine control system, based on experimental results and frequency response tests has been applied, as shown in Figure 3.8 [Rouse et al. 1980]. The term N(s) represents the system remnant, which could possibly be introduced by human non-linear behaviour, muscle tremors and variations in phase lag. There are four parameters in the human-machine control model, which are gain, time delay, smoothing and anticipation features. These components are able to be adjusted according to operator behaviour whilst performing different tasks. The quasi-linear equation is given as follows:

$$F^*(S) = G_H(s)E(S) + N(S) \tag{3.27}$$

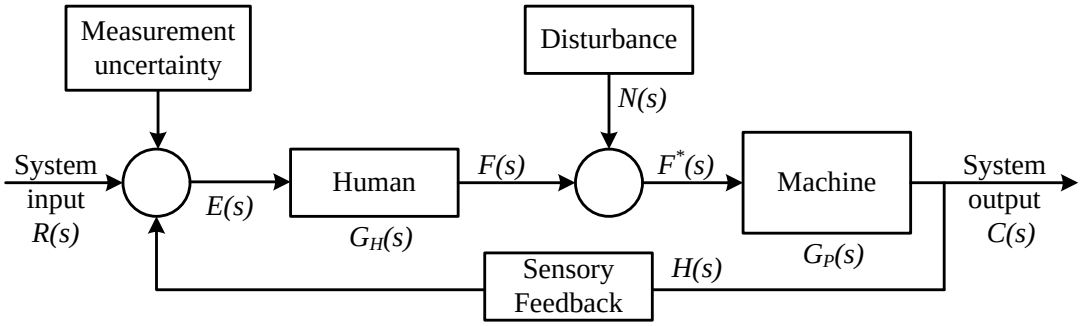

Figure 3.8 Simple model of a human-machine control system [Rouse, 1980]

3.2.2 Dynamic Model of Human Operator in a One DOF HHI System

The block diagram of HHI in the compliant object transfer task is shown in Figure 3.9. The models of the dynamic responses of the *handler* and *receiver* are represented by G_{h_s} and G_{h_r} respectively. In this study, the human operator transfer functions have been estimated based on the McRuer extended crossover model. The two human behavioural models are drawn as a system of parallel transfer functions. The block diagram of one DOF human-human interaction while performing the one-directional object transfer task can be depicted as follows, where x_{ref} is a reference target, and the force output F_H which is applied to the plant G_P can be computed as the summation of individual outputs G_{H_s} and G_{H_r}.

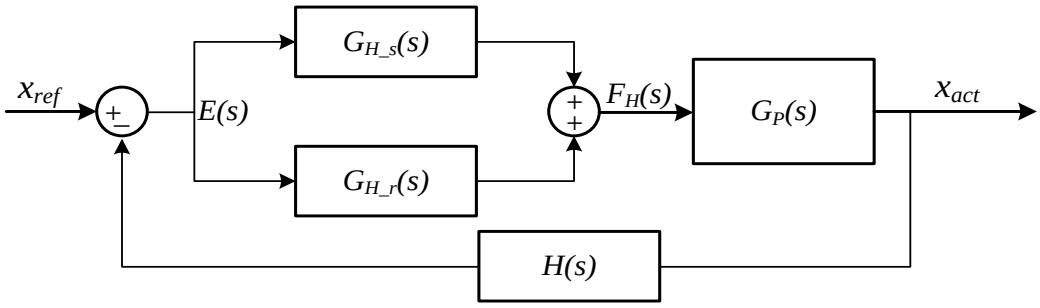

Figure 3.9 Control model of two humans working with a machine

The representation of the control system using a block diagram approach is a convenient method to illustrate how human dynamic characteristics based on the McRuer model can be applied to the human-human physical interaction test. The one DOF human-human interactive model can be principally used to estimate the system response behaviour. The machine mathematical model was derived based upon the schematic of the simple one DOF human-human interactive machine as schematically depicted in Figure 3.10. A human behaves so as to respond to the changes in a set of different transfer targets with continuous closed-loop control. The human operator model begins with a proposed transfer point, which enables a human visual scene, and then the human's cognitive processes lead to a decision to act based on the actual scene. Afterwards, the human's neuromuscular system is commanded to perform behaviour, and the human operator continues to respond to the HHI task until test completion is achieved.

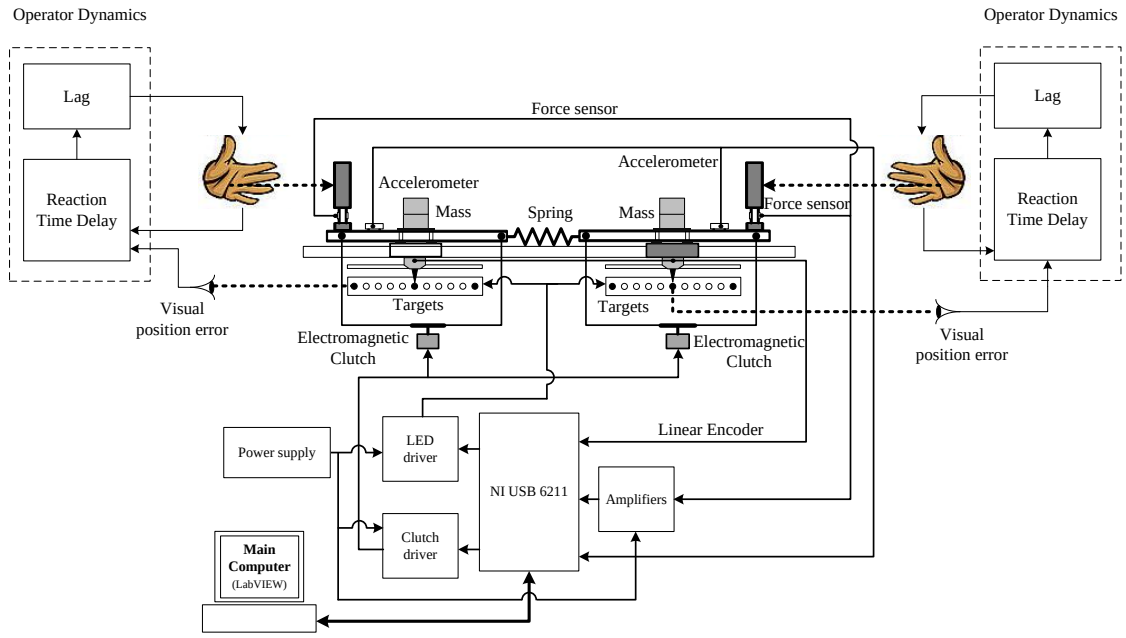

Figure 3.10 Schematic of the one DOF human-human interactive system

The dynamic equations of the *handler* and *receiver* derived earlier in Equations 3.6 and 3.10 can be simplified in terms of $\ddot{x}_1(n)$ and $\ddot{x}_2(n)$ as follows:

$$\ddot{x}_1(n) = \frac{f_s(n)}{m_1} - \frac{k}{m_1}x_1(n) + \frac{k}{m_1}x_2(n) - \frac{f_{res1}(n)}{m_1} \tag{3.28}$$

$$\ddot{x}_2(n) = \frac{f_r(n)}{m_2} + \frac{k}{m_2}x_1(n) - \frac{k}{m_2}x_2(n) - \frac{f_{res2}(n)}{m_2} \tag{3.29}$$

Figure 3.11 shows the equivalent of the one DOF human-machine interactive dynamics system, in which the human reaction forces f_s and f_r can be estimated using the McRuer crossover model. The displacement tracking errors Δx_1 and Δx_2 can be defined as the differences between the desired and measured object positions.

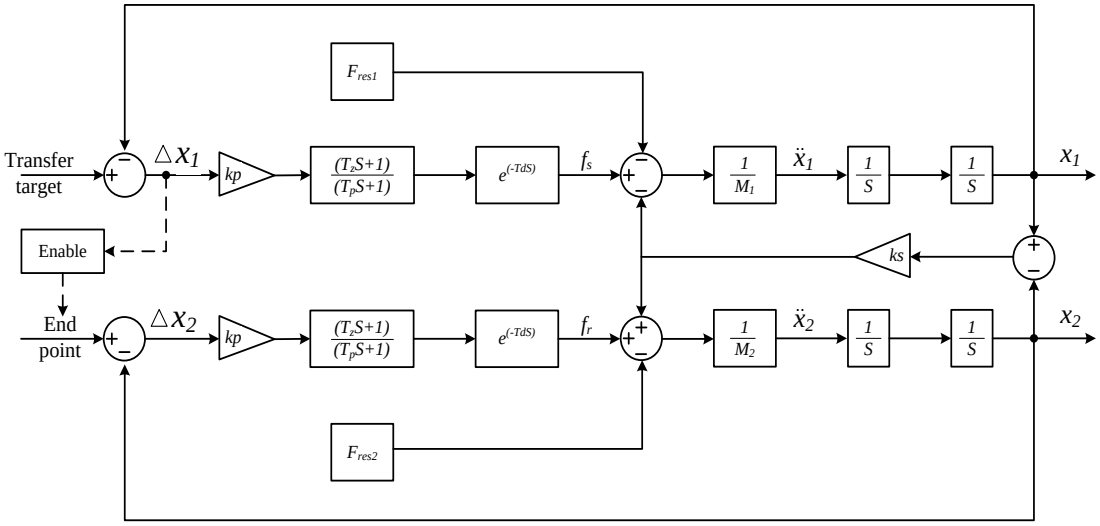

Figure 3.11 Block diagram of the human-machine interactive dynamics system

3.3 A One DOF Human-Human Interactive Rectilinear Task

A set of preliminary experiments involving a single DOF HHI rectilinear (sliding) task has been developed and carried out. The two key objectives of the study are as follows:

i. To evaluate the human dynamic response based on McRuer crossover model while undertaking a one DOF HHI task, and
ii. To undertake an appropriate set of trials, based on a number of participants, and sequence of the physical task, to satisfy:
    a. Box-Behnken design so as to provide statistically sufficient data, and the relationship between human applied force to the one DOF human-human interactive variables (mass, spring stiffness, frictional force and transfer target), and
    b. Substantive human-human and human-robot object handover tests which are detailed in Section 3.7 and Chapter 5, respectively.

The preliminary design requirements were set as follows:

- The design should facilitate the accomplishment of physical human-human interaction during the horizontal transfer of a compliant object.
- The compliant object is defined as a combination of two spring-coupled masses with opposite friction acting against their motion.
- Two electromagnetic clutches are employed to provide the generation of frictional force in the system.
- An array of light emitting diodes (LEDs) displays a random transfer target.
- The required system variables, namely mass, spring stiffness, frictional force and transfer target, should be easily adjustable.
- The physical parameters automatically measured in real-time are object position, acceleration and human force components.
- The experimental device should be able to provide a data collection and monitoring system in real-time.

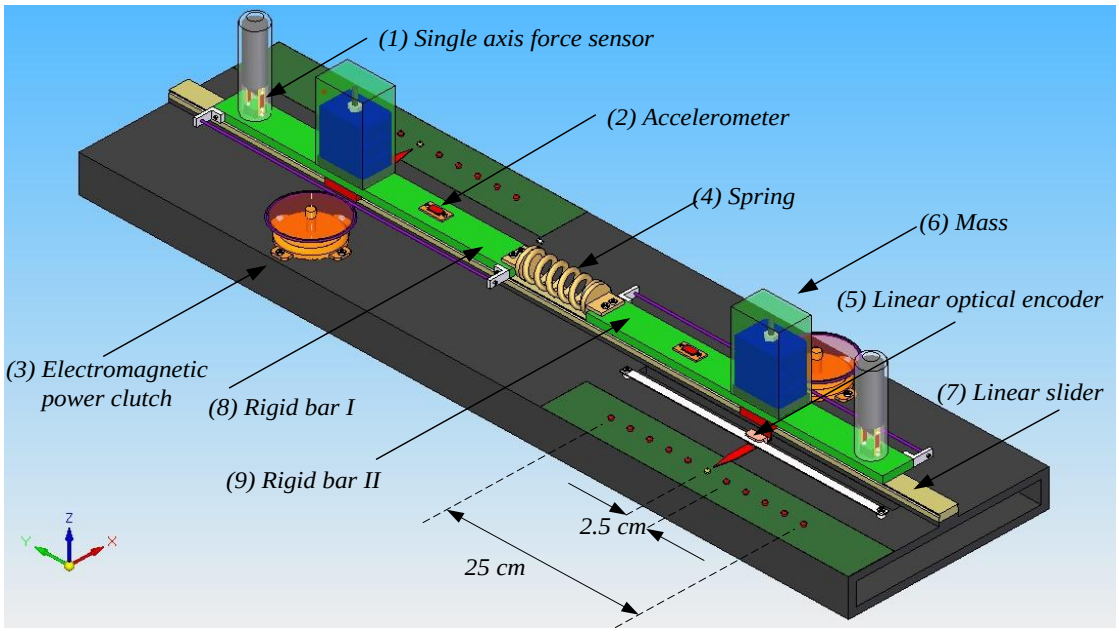

Figure 3.12 Design of a one degree of freedom human-human interactive slider task

A schematic of the HHI test apparatus designed for the preliminary study is illustrated in Figure 3.12, which is considered dynamically similar to a system of two spring-coupled masses, as illustrated in Figure 3.2.

An effective data acquisition system with an appropriate sampling rate was adopted. In sensor selections, the external forces applied by the human subjects (f_s and f_r) were detected by two sets of parallel strain gauges, packed into each handle. Two optical linear encoders were used to measure the object positions x_1 and x_2, whereas the object velocities $\dot{x}_1$ and $\dot{x}_2$ were able to be approximated by differentiating the displacement signals from the optical encoders. Accelerometers were suitably mounted on m_1 and m_2 in order to detect the object accelerations $\ddot{x}_1$and $\ddot{x}_2$. Furthermore, the system's frictional forces against the movement of the compliant object were electrically controlled and generated by two electromagnetic clutches.

The conceptual design and description of the one DOF HHI rectilinear test apparatus used to analyse the influential factors affecting the human forces applied to the system have been placed in Appendix A, including (1) mechanical design, (2) electronic design, and (3) data acquisition system and software design. The Mechanical design describes the specification for the linear test platform, sets of springs and masses. The Electronic design describes how the parameters of forces, object displacement and acceleration can be measured in real-time. Frictional forces acting against the motion of the masses was applied using electromagnetic clutches. The Laboratory Virtual Instrument Engineering Workbench (NI-LabVIEW), was based on a dataflow diagram and allows effective multiple operations to run in parallel for data collection and embedded graphical data monitoring. A full program and flow diagram developed for the one DOF HHI process are schematically shown in Appendix A (data acquisition system and software design), including two NI DAQ cards (USB 6211 and USB 6008) to meet specification data acquisition.

Conceptual software design for the LabVIEW virtual interface begins with hardware interface initialization. After this, the parameters required, which are a set of random targets, frictional forces and a number of tests are required for initial parameter setting. Before activation of the system timer, the user (*handler*) is required to move the object towards the starting point without any physical measurement being taken. This step is checked by an independent observer to ensure that the object had been precisely located, before the timer is manually activated. As soon as the first random target is enabled, the *handler* moves the object into the transfer position. When the object approaches its target, it is handed over to the *receiver*, and manipulated into its final position. This represents the completion of the task and the timer is deactivated. During the task execution, the physical responses, such as forces applied by each participant, completion times, object displacements and accelerations, are monitored, and collected in real time.

Figure 3.13 shows the layout of workspace of the preliminary one DOF HHI experiments, including sending, transfer and receiving features. There are a set of start, transfer and end positions, in which the transfer targets displayed by LEDs are digitally controlled by a LabVIEW virtual interface via the NI USB6008 card.

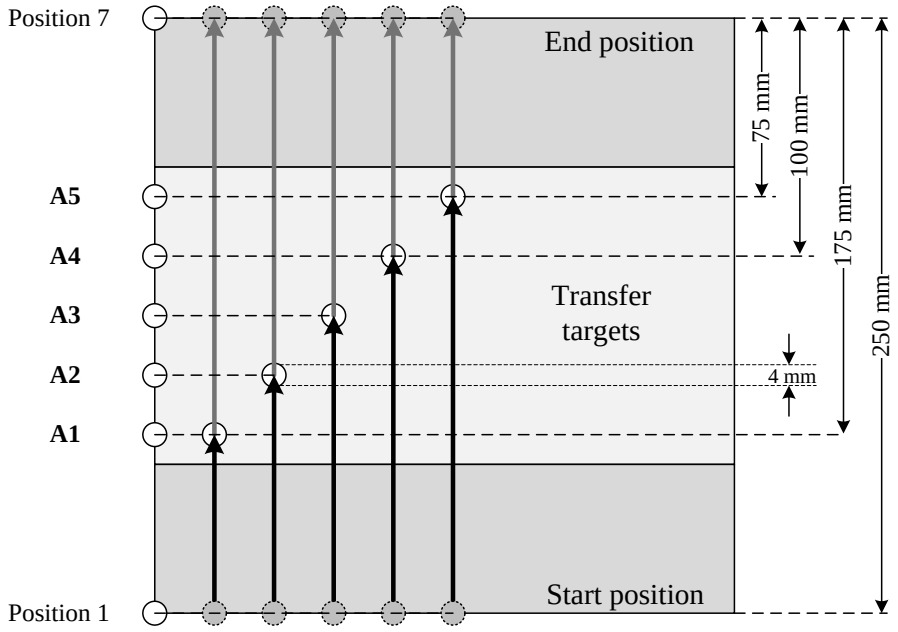

Figure 3.13 Layout of workspace of the one DOF HHI experiments

3.3.1 Force Sensor Calibration

Sensor calibration was carried out prior to conducting any tests. Two singe-axis parallel load cells were attached to each grip, as shown in Figure 3.14 to measure applied force, and calibrated using a standard spring balance, with the force applied horizontally at the centre of the grip. Both grips were calibrated, by applying a range of force of ±20N with 2N resolution.

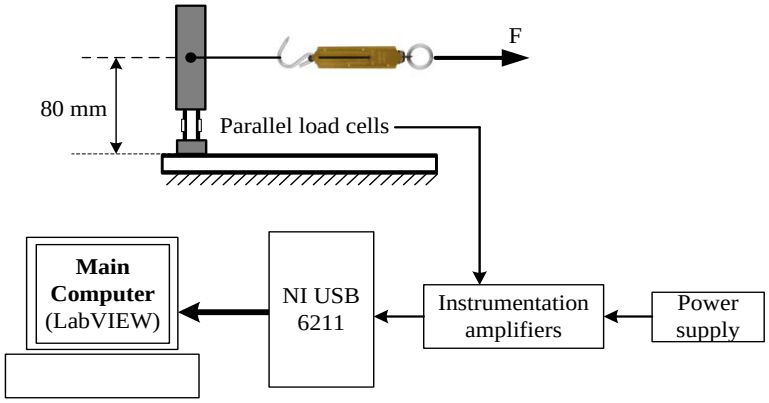

Figure 3.14 Schematic of force sensor calibration experiments

By determining the relationship between applied force and output voltage as shown in Figures 3.15(a) and (b), the calibration equations for the two handles were obtained as follows:

$$V_{left\ handle} = 0.66F_{left\ handle} - 0.003 \tag{3.30}$$

$$V_{right\ handle} = 0.70F_{right\ handle} - 0.06 \tag{3.31}$$

where, $V_{left\ handle}$ and $V_{right\ handle}$ are the output voltages of the left and right handles, and

$F_{left\ handle}$ and $F_{right\ handle}$ are the forces applied to the left and right handles respectively.

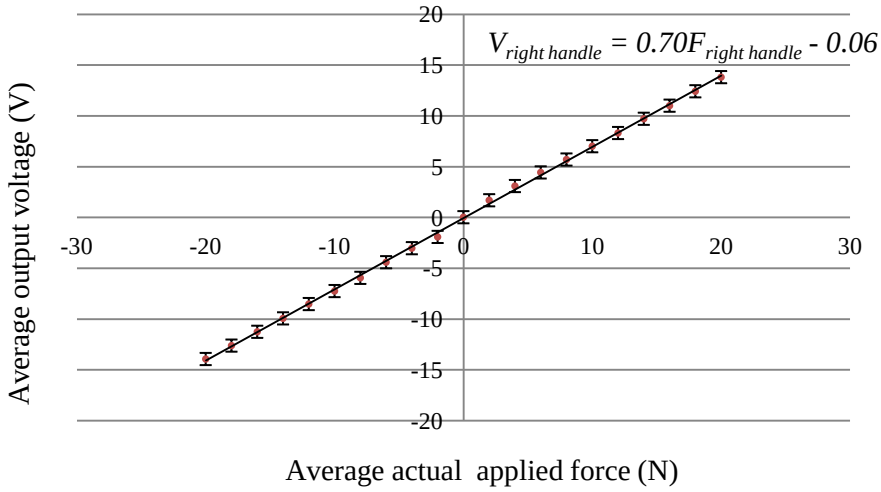

(a) Left handle

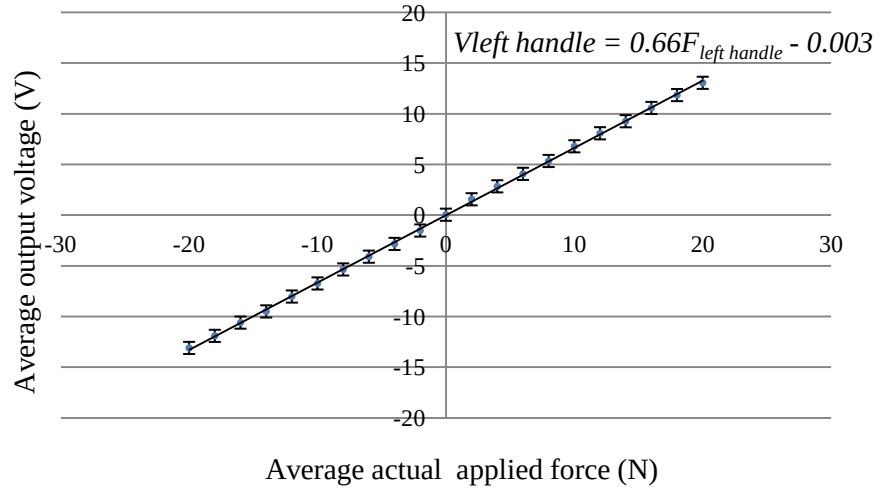

(B) Left handle

Figure 3.15 Relationship between voltage outputs and applied force

3.3.2 Frictional Force Evaluation

When an object is moving on a surface its motion is opposed by friction, with the force of resistance opposite to direction of the object's movement. Static frictional force occurs from the time when external force is applied to an object until the time when movement begins. Bashir [2005] presented an adopted friction model as illustrated in Figure 3.16. Since the electrical generation of frictional forces in real-time is a complicated process if smooth and accurate force profiles are to be obtained; therefore, in order to facilitate simple frictional force generation, the conditional assumption is made that the maximum static and kinetic frictions are equal.

Electromagnetic clutches (M.0113.2411), as described in Appendix A were used to generate variable friction capacities. Figure 3.17 depicts a simplified frictional force profile applied throughout the HHI experiments.

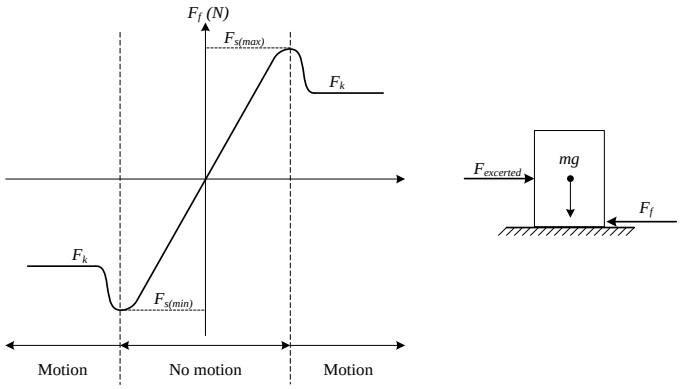

Figure 3.16 Friction occurring, when external force is applied to an object

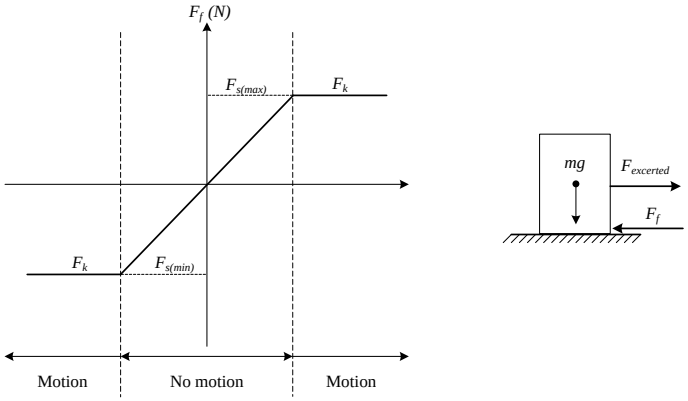

Figure 3.17 Modified frictional force profiles employed in the tests

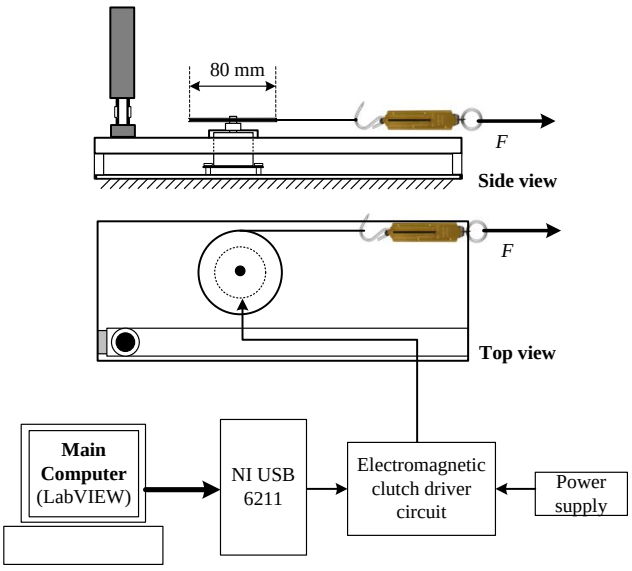

Figure 3.18 Schematic of frictional force calibration experiments

The relationship between the frictional forces generated and current supplied to the electromagnetic clutch was studied using the set-up shown in Figure 3.18, using a 80mm diameter pulley system and tensioned cable, which was attached to a spring balance to provide the tension force.

The relationship between the current generated from the electromagnetic clutch's current control circuits to provide variable torque, and the measured frictional forces from both electromagnetic clutches can be expressed as follows:

$$F_1 = 12.73I_1 - 4.88 \tag{3.32}$$

$$F_2 = 7.52I_2 - 1.92 \tag{3.33}$$

where, F_1 and F_2 are frictional forces produced by the right- and left- hand electromagnetic clutches respectively. I_1 and I_2 are current applied to the right- and left-hand clutches respectively. These equations can be specifically used in a range of 0.4-0.8A at $24V_{dc}$ (0-2N frictional forces).

3.3.3 System Block Diagram of One DOF Human-Human Interaction (HHI)

The study of the single degree of freedom HHI experiment was undertaken to establish an appropriate set of behaviour strategies for the design of the human-robot interactive architecture. Figure 3.19 schematically illustrates the conceptual design developed for the HHI test. The system involves a set of physical sensors including force sensors, optical linear encoders and accelerometers, and a signal conditioning system of buffers and line driver circuits, instrumentation amplifiers, current control circuits, and NI-DAQ cards, as well as actuators (i.e. electromagnetic clutches and LEDs). The forces applied by paired- participants whilst undertaking a one DOF HHI task were captured by the parallel load cells. The optical linear decoders and accelerometers were used to detect the displacement and acceleration of the object. LEDs were used to indicate the start, random transfer, and final positions. Frictional forces introduced by the electromagnetic clutches were individually and digitally regulated by the current control circuits. Furthermore, a LabVIEW virtual interface was developed to monitor and capture the physical signals, as mentioned, and control the actuators.

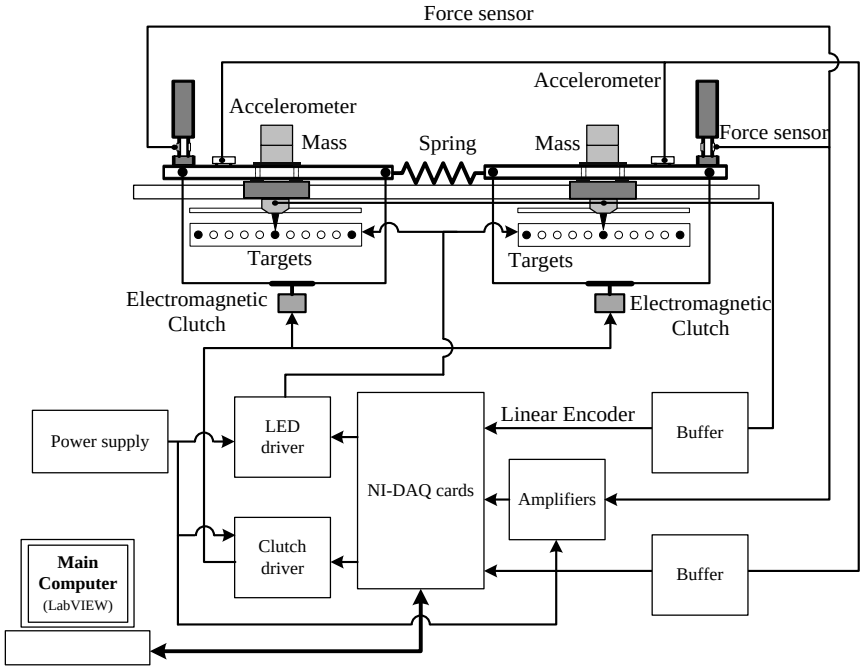

Figure 3.19 Schematic of the one DOF HHI task

3.3.4 Test Procedure for One DOF HHI

The preliminary HHI experimental apparatus is shown in Figure 3.20, and involves two human participants (randomly selected) to perform the object transfer tasks. Before the tests were executed, one participant was invited to be a *handler* and the other a *receiver*. . Both participants are requested to sit down in comfortable positions on opposite sides of the test rig. A random transfer target position was selected by the test administrator and the *handler* was instructed to move the compliant object horizontally to the *receiver* at a random desired target without any form of communication using only one hand. Whilst undertaking the HHI task, three key parameters are measured and collected in real-time for further investigation of the human characteristics, namely object position, acceleration and the external force exerted by the two participants. When the object reached the target position, it was passed to the *receiver* and moved towards the final position by the *receiver*. In the full-scale experiments, the participants were required to initially perform a preliminary set of trials in order to minimize the influence of human learning.

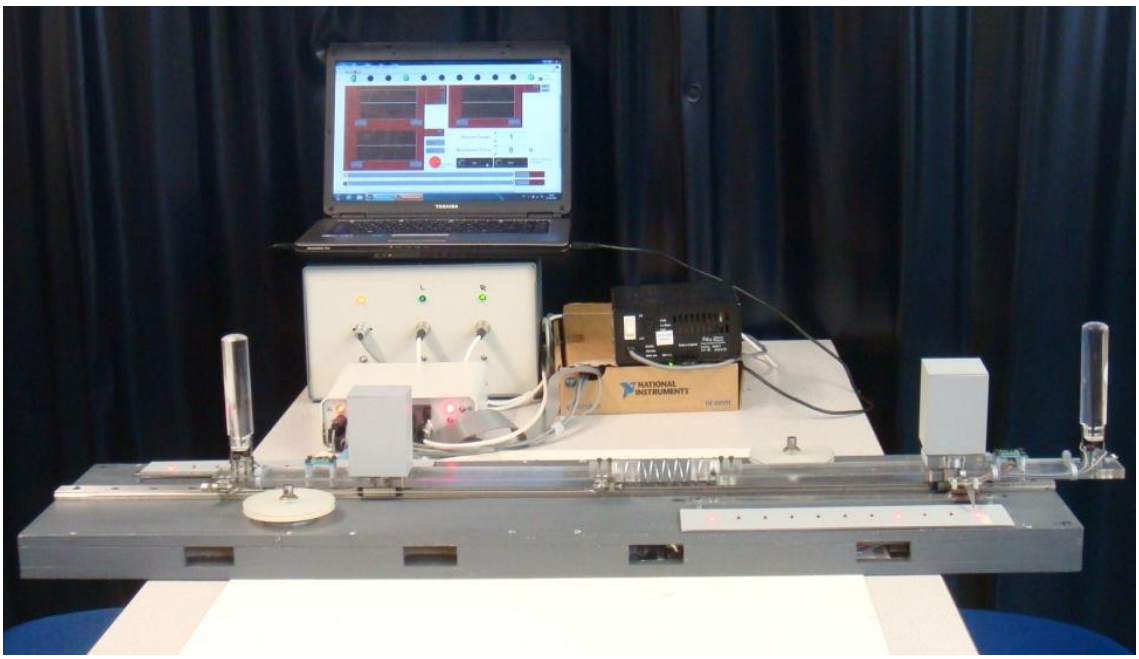

Figure 3.20 Preliminary experimental set-up

Prior to starting the pilot tests each participant was asked to agree to the following rules:

i. Each participant has to perform all assigned tasks to the best of their capacity.
ii. Only one hand is allowed to grasp the handle and twisting or bending the handle is not allowed.
iii. Two healthy participants, a *handler* and a *receiver*, are randomly selected to undertake the tests.
iv. The *handler* has to naturally release his/her grasp after completing an object transfer task in order to allow the *receiver* to move the object to the final point.

The pilot test sequence is summarised in the Flow diagram depicted in Figure 3.21.

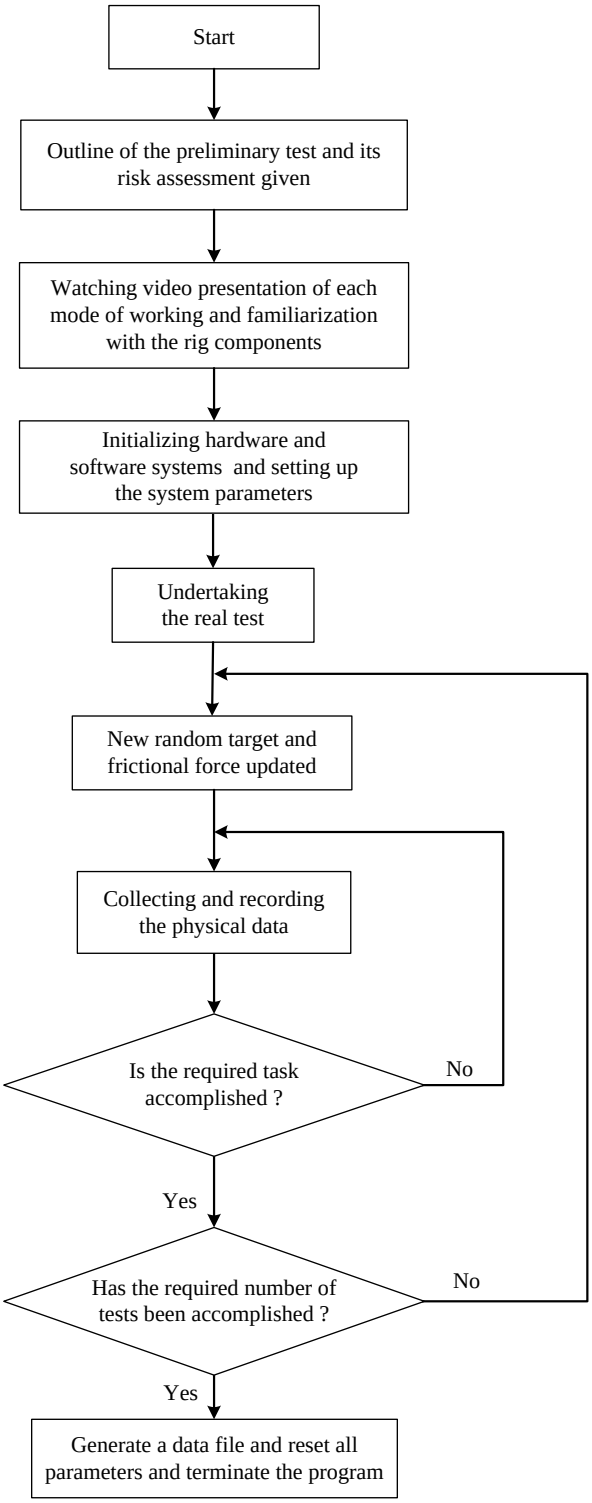

Figure 3.21 Flowchart illustrating the pilot test sequence

The sequence can be divided into three distinct phases, i.e. sending, transfer and receiving, which can be described as follows:

I. Sending Phase: Initially, the preliminary experimental apparatus is set-up, as depicted in Figure 3.22(a). When a random transfer target (*T*) LED appears, the timer trigger is activated. The *handler* is asked to move the compliant object horizontally from the start point *'S'* until it reaches the random transfer target position, as shown in Figure 3.22(b).

Key to Figures below
S – Start position
T – Transfer position
E – End position

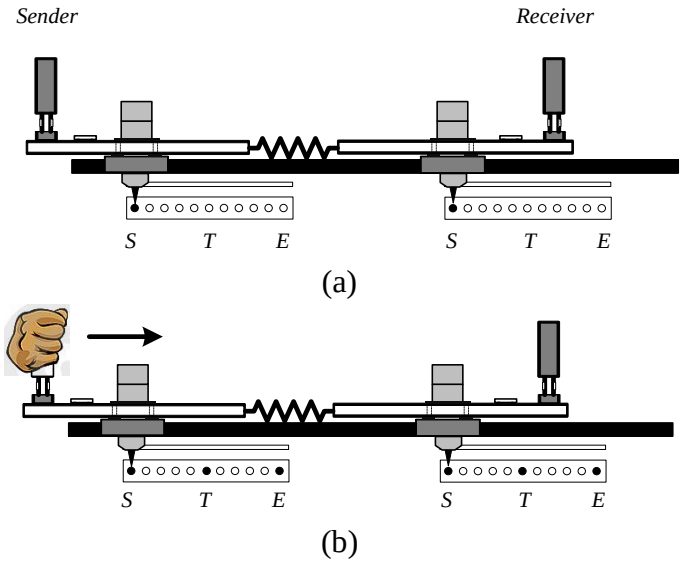

Figure 3.22 Sending phase in the real human-human interactive slider task

II. Transfer Phase: When the object arrives at the transfer position *'T'*, the *receiver* is permitted to grasp the object and move it towards the end point *'E'*. In this step, to carry out effective haptic collaboration, the *handler* has to naturally relax the grasping force, while the *receiver* firmly grasps the handle. Figures 3.23(a) - (c) depict the transfer procedure in a manner.

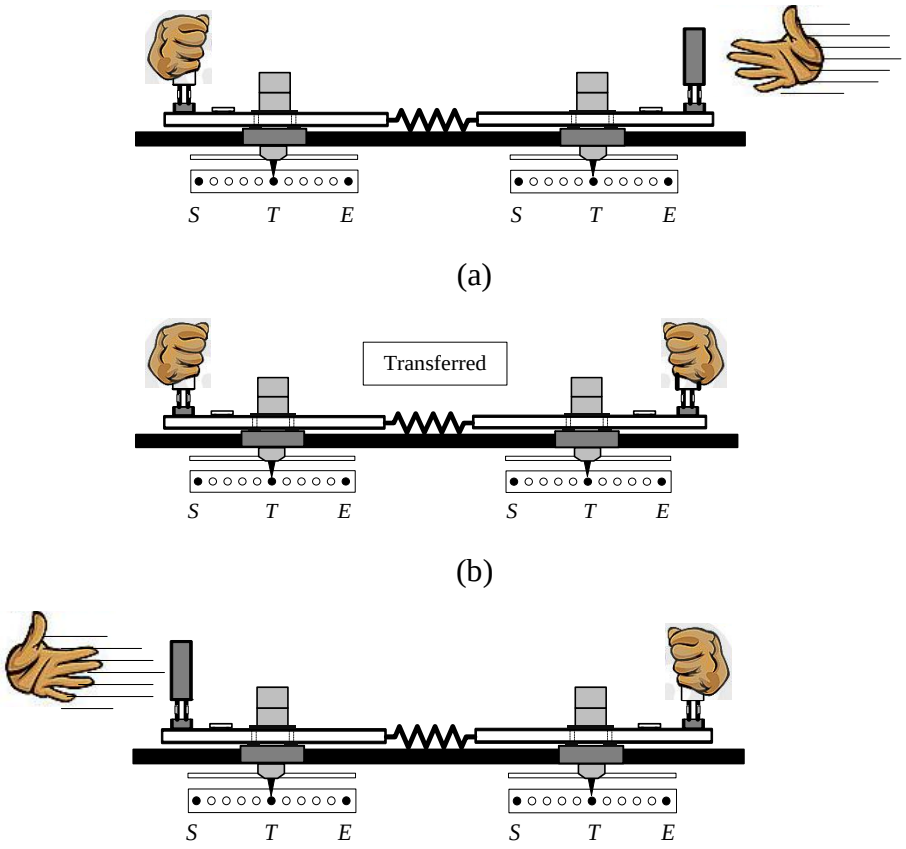

Figure 3.23 Transfer phase in the real human-human interactive slider task

III. Receiving Phase: Once the compliant object has been transferred, the *receiver* individually manipulates the object towards the end position *'E'*, as shown in Figures 3.24(a) and (b), (which stops the timer).

Once the first transfer test has been accomplished, a new random target is randomly initiated with a different time delay in order to determine the effect of the human familiarisation or expectation processes. Throughout the test runs, the completion times, physical displacements and accelerations of the object as well as forces exerted by both humans are captured and monitored in real-time.

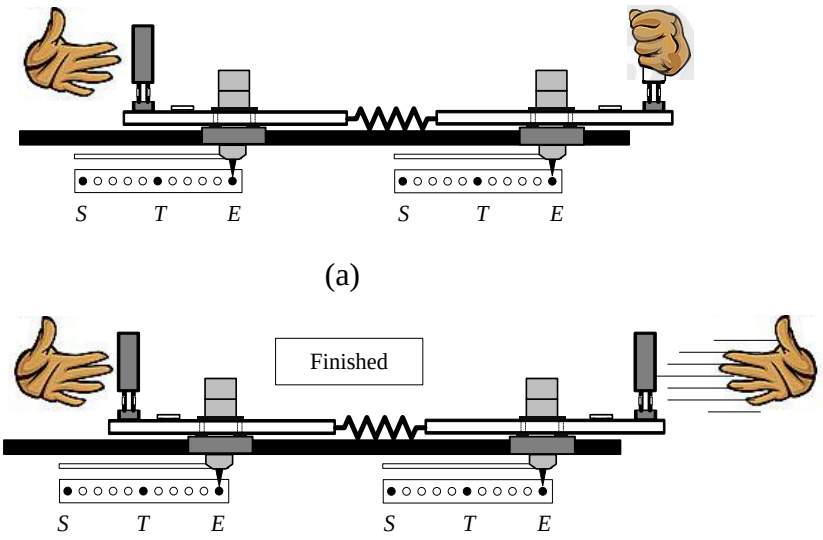

Figure 3.24 Receiving phase in the real human-human interactive slider task

3.4 Pilot Study Design for One DOF HHI

A pilot study is a small experiment in which test results are collected and statistically analysed prior to carrying out an appropriate set of large-scale experiments. This technique is often used in engineering experiments to optimize and conduct proper full-scale experiments along with attempting to reduce costs and avoid wasting time. The pilot study here was based on discussions with statisticians from the Industrial Statistical Research Unit (ISRU) at Newcastle University and the information gained from standard other sources such as *Essential Mathematics and Statistics for Science* [Currell, 2005] as well as *Design and analysis a researcher's handbooks* [Keppel, 1991]. The purpose was to determine a suitable number of participants and trials and appropriate sequence of transfer tasks in a main study. As suggested by Keppel [1991], an acceptable significance level (α) for a scientific experiment is generally recommended at 0.05, or the 95% confidence interval; therefore, this recommendation was applied throughout the pilot study.

3.4.1 Pilot study objectives

The pilot study objectives can be defined as:

- To determine the number of participants required in the full-scale study.
- To choose the number of trials to be used in the main study.
- To investigate the order or sequence of tasks.

3.4.2 Pilot study test design and results

Relevant studies have been previously carried out concerning the number of participants and the number of the test respectabilities applied to participants to familiarise them with tests before conducting the real trials [Keppel, 1991]. Experimental Design Generator and Randomiser (EDGAR) technique was used to generate a random order of experimental tests under the following conditions:

- The pilot study requires four pairs of human participants to complete the object transfer tasks.
- The selected participants are assigned to undertake five tests each with different sequences of transfer points.
- Each test involves five modes (or sets of data).

Table 3.1 Pilot study design of task sequence

	Paired Participants 1					Paired Participants 2					Paired Participants 3					Paired Participants 4				
	Trials / Order					Trials / Order					Trials / Order					Trials / Order				
	1	*2*	*3*	*4*	*5*	*1*	*2*	*3*	*4*	*5*	*1*	*2*	*3*	*4*	*5*	*1*	*2*	*3*	*4*	*5*
Time (s)	A3	A4	A5	A1	A2	A2	A4	A1	A3	A5	A1	A3	A2	A5	A4	A4	A5	A1	A2	A3
Time (s)	A2	A5	A1	A3	A4	A3	A5	A2	A4	A1	A3	A5	A4	A2	A1	A2	A1	A3	A5	A4
Time (s)	A4	A1	A3	A2	A5	A1	A3	A5	A2	A4	A2	A4	A3	A1	A5	A1	A4	A2	A3	A5
Time (s)	A5	A3	A2	A4	A1	A5	A2	A4	A1	A3	A5	A2	A1	A4	A3	A3	A2	A5	A4	A1
Time (s)	A1	A2	A4	A5	A3	A4	A1	A3	A5	A2	A4	A1	A5	A3	A2	A5	A3	A4	A1	A2

The HHI pilot study tests were carried out by the selected subject groups. The results including completion times and corresponding standard deviations, are summarized in Tables 3.2 and 3.3, respectively.

Table 3.2 Task completion times for each of pair of participants in the pilot test

(a) Paired participants 1

	Paired Participants1				
	Trial 1 (O1)	**Trial 2 (O2)**	**Trial 3 (O3)**	**Trial 4 (O4)**	**Trial 5 (O5)**
Time (s)	3.42	2.31	2.74	2.60	2.75
	3.34	2.80	2.70	2.63	2.60
	2.69	2.40	2.69	3.79	2.68
	3.56	2.40	2.50	2.40	2.93
	3.06	2.33	2.99	2.88	2.82
Mean	3.21	2.45	2.72	2.86	2.75
StDev	0.34	0.20	0.18	0.55	0.13

(b) Paired participants 2

	Paired Participants1				
	Trial 1 (O1)	**Trial 2 (O2)**	**Trial 3 (O3)**	**Trial 4 (O4)**	**Trial 5 (O5)**
Time (s)	4.33	2.80	2.94	3.23	2.50
	4.58	3.39	3.06	3.57	2.66
	4.01	3.20	3.43	2.61	3.29
	3.48	2.39	3.03	3.93	2.71
	3.28	2.77	2.81	3.03	2.98
Mean	3.94	2.91	3.05	3.27	2.83
StDev	0.55	0.39	0.23	0.51	0.31

(c) Paired participants 3

	Paired Participants1				
	Trial 1 (O1)	**Trial 2 (O2)**	**Trial 3 (O3)**	**Trial 4 (O4)**	**Trial 5 (O5)**
Time (s)	8.63	4.97	4.63	4.02	4.14
	4.49	4.36	5.01	4.75	4.59
	8.08	5.20	4.30	4.61	5.63
	5.16	3.93	5.01	3.87	4.56
	4.91	3.65	5.24	4.80	4.70
Mean	6.26	4.42	4.84	4.41	4.72
StDev	1.94	0.66	0.37	0.43	0.55

(d) Paired participants 4

	Paired Participants1				
	Trial 1 (O1)	**Trial 2 (O2)**	**Trial 3 (O3)**	**Trial 4 (O4)**	**Trial 5 (O5)**
Time (s)	3.31	3.71	2.91	3.22	2.93
	3.37	3.72	2.78	3.08	3.08
	4.00	4.51	3.39	2.83	3.65
	4.76	2.91	3.09	3.86	2.91
	3.99	4.41	3.03	3.17	2.63
Mean	3.89	3.85	3.04	3.23	3.04
StDev	0.59	0.65	0.23	0.38	0.38

Table 3. 3 Average completion times of each pair of participants

	Paired Participant			
	P1	**P2**	**P3**	**P4**
Trial 1	3.21	3.94	6.26	3.89
Trial 2	2.45	2.91	4.42	3.85
Trial 3	2.72	3.05	4.84	3.04
Trial 4	2.86	3.27	4.41	3.23
Trial 5	2.75	2.83	4.72	3.04
Mean	2.80	3.20	4.93	3.41
STD	0.28	0.45	0.77	0.43

The random tasks in the HHI pilot study were created using a balanced Latin Square design, which is the typical factorial design used to provide a task sequence [Brown, 2004]. All four pairs of participants were required to undertake five trials for each of five sets of data, as shown in Table 3.3. Here the transfer points A1, A2, A3, A4 and A5 represent the positions at which the compliant object has to be transferred from a *handler* to a *receiver*, as illustrated in Figure 3.13.

3.4.2.1 Determining the number of participants required

In any full-scale experimental design, the number of requisite participants should be sufficient to give statistically significant results. Theoretically, this should be as many participants as possible, since a higher number of human subjects utilized in a test are likely to give more effective and sensitive experimental results. In practice, to specify an appropriate number of human subjects in a full-scale test, a power analysis method can be used [Keppel, 1991].

Four sample pairs were assigned in the pilot study to undertake five test trials, in which each trial consists of five treatment conditional modes. The population treatment represented as the averages of the task completion time of five modes per human subject (μ_1, μ_2, μ_3 *and* μ_4), and all deviations from μ are illustrated in Table 3.4 and Table 3.5 respectively.

Table 3.4 Mean and standard deviation of completion times taken of all participants in the pilot study

	Accomplished time (s)			
	Paired participants (1)	**Paired participants (2)**	**Paired participants (3)**	**Paired participants (4)**
Mean	2.80	3.20	4.93	3.41
STD	0.28	0.45	0.77	0.43

Table 3.5 Means of modes and deviations of μ_i - μ_{mean} of all participants in the pilot study

Mean of modes (s)	**Deviation of μ_i - μ_{mean}**
$\mu 1$ = 2.80	-0.79
$\mu 2$ = 3.20	-0.39
$\mu 3$ = 4.93	1.35
$\mu 4$ = 3.41	-0.18
μ_{mean} = 3.59	

It can be assumed that an accurate estimation of the population variance ($\sigma^2_{S/A}$) is available and equal to μ_{mean} [Keppel, 1991]. Therefore the data in the above table can be used in the equations below, in which the following notation is used:

$\sigma^2_{S/A}$ is population variance.

$\emptyset_A$ is a value used in determining power quantity.

S' is the number of samples.

df_{demon} is demonstrator degrees of freedom.

df is sample degrees of freedom.

a is the number of treatment conditions.

α is the significance level of the test.

The unknown variables (df_{denom} and df) can be computed as:

$$df_{denom} = a\times(S'-1) = 5\times (18-1) = 85 \tag{3.34}$$

$$df = (a-1) = 5-1= 4 \tag{3.35}$$

The formula used to estimate a value in determining power quantity ($\emptyset_A$) is given by:

$$\emptyset_A^2 = \frac{S'\frac{\left[\sum(\mu_i-\mu)^2\right]}{a}}{\sigma^2_{S/A}} \tag{3.36}$$

Substituting the relevant parameters into Equation (3.36) gives:

$$\emptyset_A = 0.38\sqrt{S'} \tag{3.37}$$

If a power function value is equal to or greater than 0.8, then it can be concluded that a number of samples proposed is acceptable. By using the trial and error method, the sample size (S') of 18 participants was therefore chosen to obtain an appropriate value of power quantity ($\emptyset_A$), and subsequently the solution for $\emptyset_A$ gives:

$$\emptyset_A = 0.38\sqrt{18} = 1.62 \tag{3.38}$$

To determine the power function value, three parameters, which consist of df, $\emptyset_A$ and df_{demon}, are required. According the above calculation, the power value of the test can be estimated under the conditions as follows: $\emptyset_A$ is 1.62, S' is 18, df_{demon} is 125, df is 4, a is 5, and α is 0.05. Figure 3.25 shows that the power function value is approximately 0.82. If the result is equal to or greater than 0.80, it can be concluded that the number of samples proposed is acceptable; however, if the power value is less than 0.80, the selected sample size is rejected.

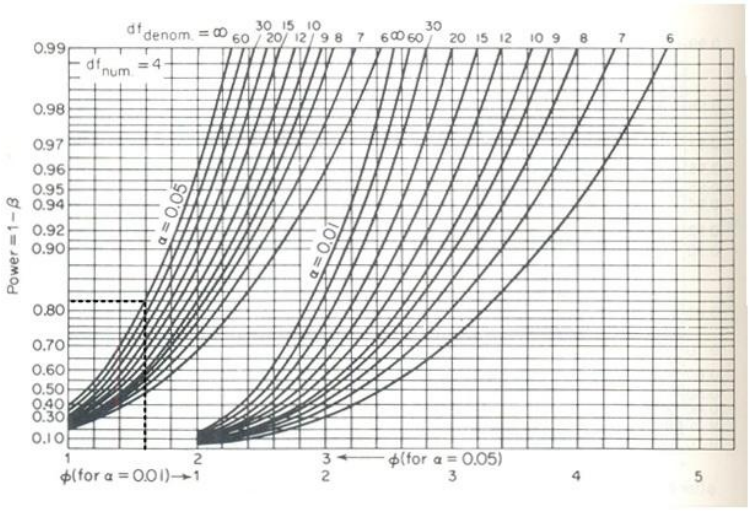

Figure 3.25 Chart of power function for analysis of variance tests [Keppel, 1991]

Figure 3.26 depicts the relationship between the power value and the number of participants required in the main experiments, in which if the number of participants is equal to or greater than 18, it is acceptable (the power function ≥ 0.80).

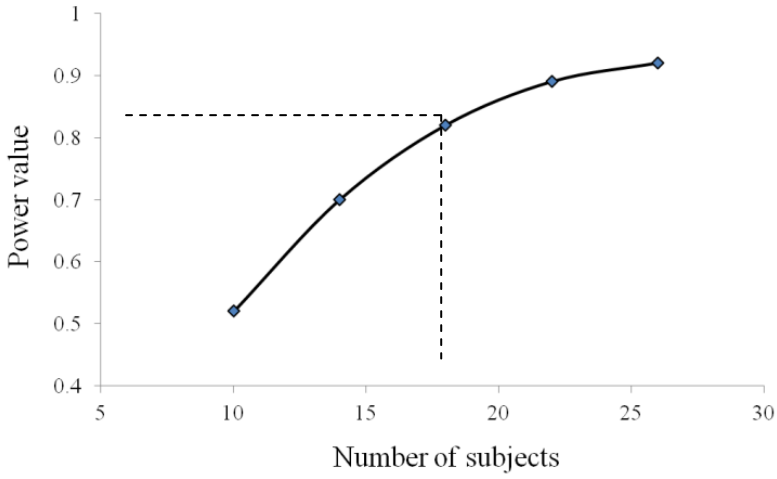

Figure 3.26 Number of participants required for the preliminary study

3.4.2.2 Determining the number of trials used

To counter any effects of human learning experience, all participants were required to complete a familiarisation process. The number of trials required in the full-scale experiment has to be statistically determined using a paired-test comparison technique. This method is normally used when sample groups to be compared are measured on different occasions, such as in student pre-test and post-test scores. Figure 3.27 illustrates the paired T-test comparison applied to the 4 selected participant pairs to determine the number of trials for an individual participant.

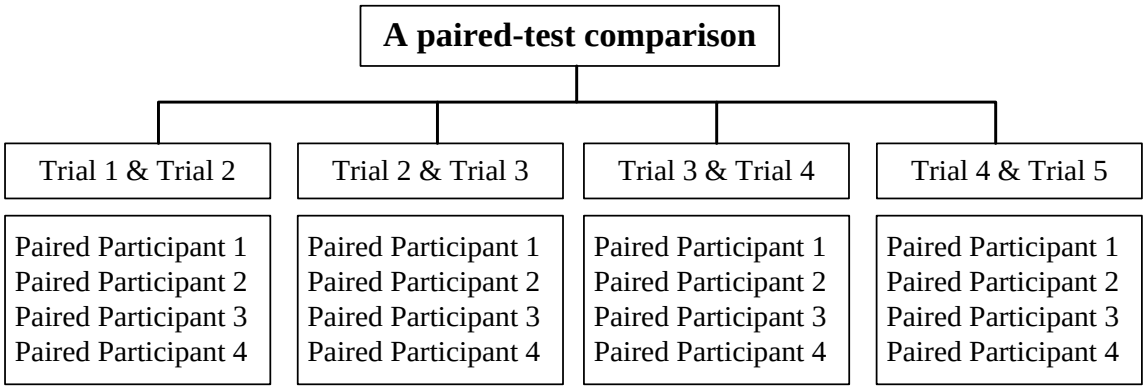

Figure 3.27 Paired T-test comparison chart

The two statistical hypotheses used in a paired-test comparison are a null hypothesis (H_0) and an alternative hypothesis (H_1). In this test, H_0 assumes that averages of the treatment population are equal, while in H_1 the averages of the treatment populations are not equal. The paired T-test analysis is used to prove whether H_0 should be rejected and then H_1 accepted or if H_0 should be accepted and H_1 rejected. The paired T-test formula is expressed in Equation 3.39:

$$t = \frac{\bar{x}_1 - \bar{x}_2}{\sqrt{\frac{{s_1}^2}{n_1} + \frac{{s_2}^2}{n_2}}} \tag{3.39}$$

where $\overline{x}_1, \overline{x}_2$ are the means of the first and second groups respectively, and

s_1, s_2, n_1, n_2 are the standard deviations and total numbers of samples (respectively) of the first and second sample groups.

As an example, consider the results of the paired participants 1, whilst performing trial 1 and 2. The hypothesis (H_0) and alternative hypothesis (H_1) for the dependent T-test for paired samples are given below:

H_0: $\mu_1 = \mu_2$ (the means of the two trials are equal)

H_1: $\mu_1 \neq \mu_2$ (the means of the two trials are not equal)

The Statistical Package for the Social Sciences (SPSS) is one of the most useful programs [Bergmann et al. 2000; Landau and Everitt 2004; Seeger et al. 2007] used to analyze a wide variety of statistical problems, and was employed to compute the T-test results, as shown in Table 3.6. These outcomes were calculated based on 95% confident interval or 0.05 of significant level.

Table 3.6 Dependent T-test results of the comparison between Trial 1 (T1) and Trial 2 (T2) carried out by paired participants 1

	Mean (s)	**N**	**Std. Deviation**	**Std. Error Mean**
Pair1_T1	3.21	5	0.35	0.15
Pair1_T2	2.45	5	0.20	0.09

Paired Samples Test	**Paired Differences**					**t**	**df**	**Sig. (2-tailed)**
	Mean (s)	**Std. Deviation**	**Std. Error Mean**	**95% Confidence Interval of the Difference**				
				Lower	**Upper**			
Pair1_T1 - Pair1_T2	0.77	0.37	0.17	0.30	1.23	4.61	4	**0.01**

According to the SPSS results, the calculated significance level was 0.01, which is less than 0.05. It can be conclude that the statistical probability of observing such a value by chance was less than 0.05. Therefore, the results were significant at the 95 % confidence level, i.e. there was a significant difference between the mean completion times of the first and second trial results of paired participants 1. The T-test results for all human participants performing the trials in each condition are summarized in Table 3.7 and Table 3.8.

Table 3.7 The summary of the dependent T-test results for paired participants 1 and 2

Paired samples		**Trial sample statistics**							**According to the calculated Sig. value, it can be statistically interpreted that:**
		N	***Mean*$_1$**	***Std Deviation*$_1$**	***Mean*$_2$**	***Std Deviation*$_2$**	***t value***	***Sig.***	
Paired Participants 1	Trial 1 and Trial 2	5	3.21	0.35	2.45	0.20	4.62	**0.01**	There is a significant difference between the mean completion times. *[Rejected H_0: $\mu 1 = \mu 2$]*
	Trial 2 and Trial 3	5	2.59	0.21	2.89	0.19	-2.10	**0.10**	There is no significant difference between the mean completion times. *[Accepted H_0: $\mu 2 = \mu 3$]*
	Trial 3 and Trial 4	5	2.72	0.18	2.86	0.55	-0.57	**0.60**	There is no significant difference between the mean completion times. *[Accepted H_0: $\mu 3 = \mu 4$]*
	Trial 4 and Trial 5	5	2.86	0.55	2.76	0.13	0.40	**0.72**	There is no significant difference between the mean completion times. *[Accepted H_0: $\mu 4 = \mu 5$]*
Paired Participants 2	Trial 1 and Trial 2	5	3.94	0.55	2.91	0.39	5.92	**0.00**	There is a significant difference between the mean completion times. *[Rejected H_0: $\mu 1 = \mu 2$]*
	Trial 2 and Trial 3	5	2.91	0.39	3.05	0.23	-0.91	**0.41**	There is no significant difference between the mean completion times. *[Accepted H_0: $\mu 2 = \mu 3$]*
	Trial 3 and Trial 4	5	3.05	0.23	3.27	0.51	-0.77	**0.48**	There is no significant difference between the mean completion times. *[Accepted H_0: $\mu 3 = \mu 4$]*
	Trial 4 and Trial 5	5	3.27	0.51	2.83	0.31	1.31	**0.26**	There is no significant difference between the mean completion times. *[Accepted H_0: $\mu 4 = \mu 5$]*

Table 3.8 The summary of the dependent T-test results for paired participants 3 and 4

Paired samples		**Trial sample statistics**							**According to the calculated Sig. value, it can be statistically interpreted that:**
		N	***Mean*$_1$**	***Std Deviation*$_1$**	***Mean*$_2$**	***Std Deviation*$_2$**	***t value***	***Sig.***	
Paired participants 3	Trial 1 and Trial 2	5	6.25	1.94	4.42	0.66	2.90	**0.04**	There is a significant difference between the mean completion times. *[Rejected H_0: μ1 = μ2]*
	Trial 2 and Trial 3	5	4.42	0.66	4.84	0.37	-0.91	**0.41**	There is no significant difference between the mean completion times. *[Accepted H_0: μ2 = μ3]*
	Trial 3 and Trial 4	5	4.84	0.37	4.41	0.43	1.80	**0.14**	There is no significant difference between the mean completion times. *[Accepted H_0: μ3 = μ4]*
	Trial 4 and Trial 5	5	4.41	0.43	4.72	0.55	-1.35	**0.25**	There is no significant difference between the mean completion times. *[Accepted H_0: μ4 = μ5]*
Paired participants 4	Trial 1 and Trial 2	5	3.89	0.59	3.85	0.65	0.08	**0.94**	There is no significant difference between the mean completion times. *[Accepted H_0: μ1 = μ2]*
	Trial 2 and Trial 3	5	3.85	0.65	3.04	0.23	3.02	**0.04**	There is a significant difference between the mean completion times. *[Rejected H_0: μ2 = μ3]*
	Trial 3 and Trial 4	5	3.04	0.23	3.23	0.38	-0.88	**0.42**	There is no significant difference between the mean completion times. *[Accepted H_0: μ3 = μ4]*
	Trial 4 and Trial 5	5	3.23	0.38	3.04	0.38	0.63	**0.55**	There is no significant difference between the mean completion times. *[Accepted H_0: μ4 = μ5]*

Note: In the above table, if the calculated *Sig*. value is ≥ 0.05 there is no statistically significant difference between the mean completion times of the trial results by these paired participants; however, if Sig. value is < 0.05 there is a significant difference between the mean completion times of the trial results by the paired participants.

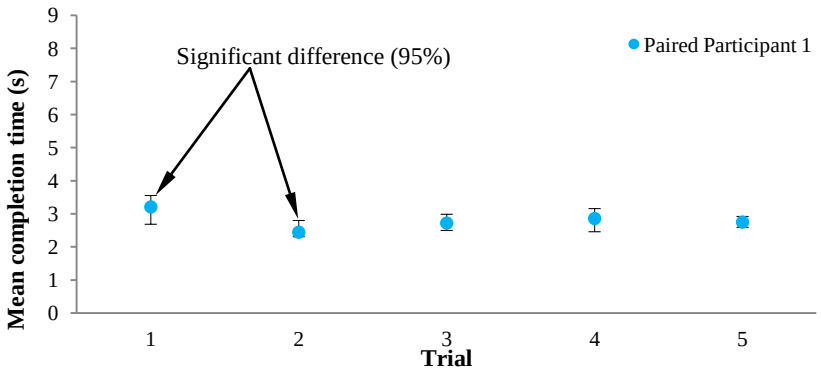

(a) Trial performed by paired participants (1)

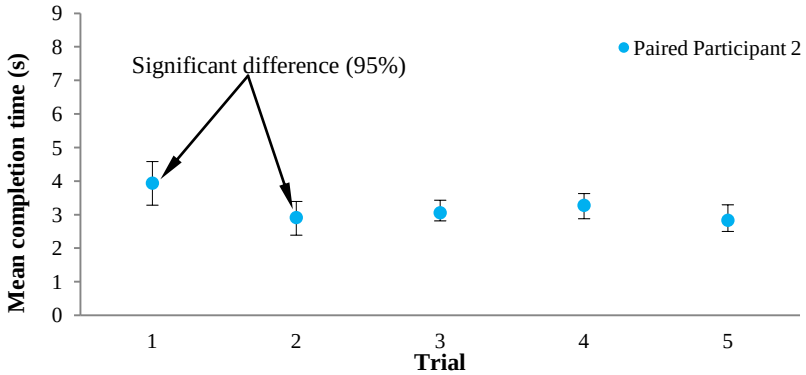

(b) Trial performed by paired participants (2)

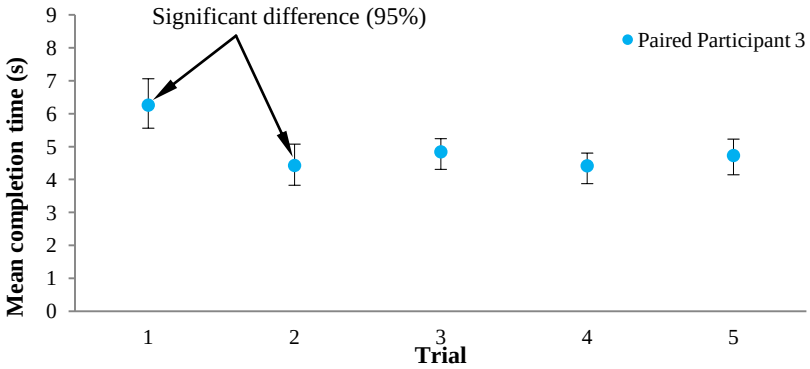

(c) Trial performed by paired participants (3)

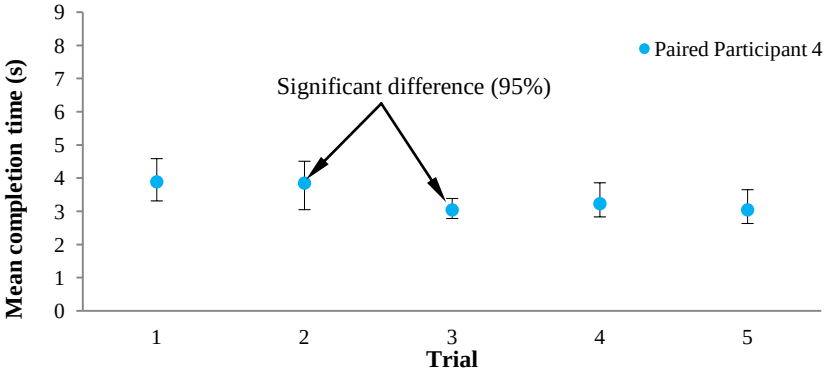

(d) Trial performed by paired participants (4)

Figure 3.28(a) – (d) Average completion times for all paired participants

Figures 3.28(a) – (d) highlight the results of the T-tests to indicate the difference at 95% confidence interval between means of task completion times for each coupled tests. It can be observed that there were statistically significant differences between the first and second trials for paired participants 1, 2 and 3. However, there was no statistically significant differences at 0.05 significance level between trial 2 versus trial 3, trial 3 versus trial 4 or trial 4 versus 5. Only for paired participants 4 indicated that it was significant difference between trial 2 and trial 3. In addition, there were no statistically significant differences at 95% confidence interval between trial 1 versus 2, trial 3 versus trial 4 and trial 4 versus trial 5.

3.4.2.3 Determining the order or sequence of tasks

For the comparison of the means of two sample groups, the T-test method is often used; however, this technique may be unreliable when comparing three or more sample groups [Keppel, 1991]. An appropriate method used to investigate the averages of more than two samples is analysis of variance, which is popularly called ANOVA. Here a one-way ANOVA technique was used to investigate the sequence of the HHI tasks, to find if the order of testing significantly affected on the task completion time. Figure 3.29 illustrates the one-way ANOVA comparisons applied to the 4 selected participant pairs to investigate the order or sequence of tasks.

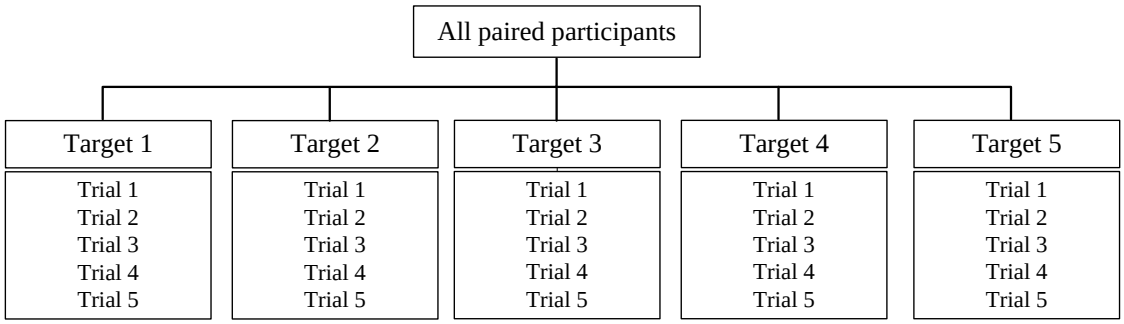

Figure 3.29 One-way ANOVA comparison chart

Consider the results of the paired participants 1, whilst performing trials 1 to 5 of the transfer target 1. The hypothesis (H_0) and alternative hypothesis (H_1) for the one-way ANOVA test for a sample group are given below:

H_0: $\mu_1 = \mu_2 = \mu_3 = \mu_4 = \mu_5$ the means of all trial groups are equal.

H_1: $\mu_1 \neq \mu_2 \neq \mu_3 \neq \mu_4 \neq \mu_5$ the means of all trial groups are not equal.

A significance level of $\alpha = 0.05$ was adopted. SPSS was again employed and the one-way ANOVA test results are shown in Table 3.9.

Table 3.9 One-way ANOVA test results of paired participant 1

Descriptive Statistics	**N**	**Minimum**	**Maximum**	**Mean**	**Std. Deviation**
Completion Time	25	2.31	3.79	2.80	0.38

Completion Time	**Sum of Squares**	**df**	**Mean Square**	**F**	**Sig.**
Between Groups	0.08	4	0.02	0.12	0.97
Within Groups	3.47	20	0.19		
Total	3.56	24			

Since the calculated significance value of 0.97 is greater than 0.05, there was no statistically significant difference between the mean completion times at the 95% confidence interval. The ANOVA results for all participants investigated for each condition are presented in Table 3.10.

Table 3.10 Summary of one-way ANOVA results conducted for all human participants

Paired participants		**Trial sample statistics**						**According to the calculated Sig. value, it can be statistically interpreted that:**
	N	***Minimum***	***Maximum***	***Mean***	***Std. Deviation***	***F-value***	***Sig.***	
Paired participant 1	25	2.31	3.79	2.80	0.38	0.12	**0.97**	There is no significant difference between the mean completion times. *[Accepted H_0: $\mu_1 = \mu_2 = \mu_3 = \mu_4 = \mu_5$]*
Paired participant 2	25	2.39	4.58	3.20	0.56	0.39	**0.81**	There is no significant difference between the mean completion times. *[Accepted H_0: $\mu_1 = \mu_2 = \mu_3 = \mu_4 = \mu_5$]*
Paired participant 3	25	3.65	8.63	4.93	1.14	0.35	**0.84**	There is no significant difference between the mean completion times. *[Accepted H_0: $\mu_1 = \mu_2 = \mu_3 = \mu_4 = \mu_5$]*
Paired participant 4	25	2.63	4.76	3.41	0.58	0.86	**0.50**	There is no significant difference between the mean completion times. *[Accepted H_0: $\mu_1 = \mu_2 = \mu_3 = \mu_4 = \mu_5$]*

Note: In the above table, if the calculated *Sig*. value is ≥ 0.05 there is no statistically significant difference between the mean completion times of the trial results by these paired participants; however, if Sig. value is < 0.05 there is a significant difference between the mean completion times of the trial results by the paired participants.

A one way Analysis of Variance (ANOVA) method was used to determine if there were any significant differences for the test orders. According to the test results shown in Figure 3.30, there are no statistically significant differences at 0.05 significance level between the first, second, third, fourth and fifth test orders among all participants.

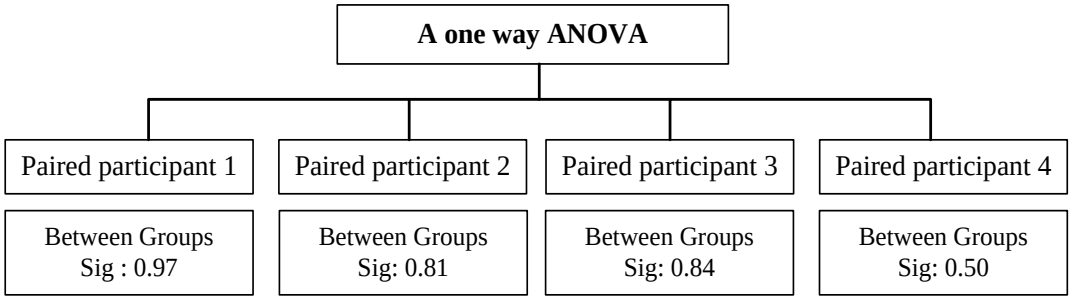

Figure 3.30 One-way ANOVA results comparison chart

3.4.3 Pilot Study Recommendations

A one DOF HHI pilot study was conducted in which the test results were statistically analysed at 95% confidence interval to establish the effective test sample size, number of trials and testing sequence for the large-scale one DOF HHI experiments designed using a Box-Behnken and the substantive main human-human/human-robot object handover tasks (as detailed in Section 3.7 and Chapter 5 respectively). In summary, these experiments are expected to be as follows:

- Based on the power analysis method, at least 18 paired participants should be adopted in the main study to ensure the test results are statistically significant.
- The participants will be required to become familiar with the test rig with no less than 2 repetition sets of five different transfer points. In the real full-scale experiment, 3 trial tests are used.
- In the pilot study, the sequence of tasks, which each participant pair executed, was randomly ordered. It was deemed that the test sequence had no statistically significant effects. However, in the main experiments, the EDGER calculator is used to generate a random Latin Square design in order to avoid the effects of human learning.

3.5 Response Surface Methodology (RSM)

This section investigates the relationship between the influential factors (mass, spring stiffness, frictional force and transfer target) affecting the human forces applied to the system. It is important to design an appropriate experiment, which will provide a statistically sufficient amount of complex data while also reducing costs in a timely manner. The Box-Behnken design [Box and Hunter, 1957], which is a type of a Response Surface Methodology (RSM) was adopted. RSM is a mathematical and statistical technique used to model and evaluate problematic issues in which the real physical relationships are not precisely known. A second order response surface is very useful, and is widely used in RSM because it is flexible in terms of functional forms. Additionally, all unknown coefficient parameters (β_i) can be solved using the least square method. The second order model comprises of the first order model, all quadratic terms ($\beta_{ii}x_i^2$) and all cross terms ($\beta_{ij}x_i x_j$). The functional equation can be expressed as in Equation 3.40, in which the first order equation of the relationship between an output *y* and a group of input variables $x_1, x_2, \ldots, x_k$ is also represented in Equation 3.41:

$$y = \beta_0 + \sum_{i=1}^{k} \beta_i x_i + \sum_{i=1}^{k} \beta_{ii} {x_i}^2 + \sum_{i<j} \sum \beta_{ij} x_i x_j + \varepsilon \qquad (3.40)$$

$$y = \beta_0 + \beta_1 x_1 + \beta_2 x_2 + \ldots + \beta_k x_k + \varepsilon \qquad (3.41)$$

where
- i, j are the process orders varying from 1 to the number of variables,
- β_0 is the mean of overall experimental responses,
- β_i is the coefficient effecting to the variable x_i, and
- ε is the error observed in response *y*.

An analysis of variance (ANOVA) is used to evaluate the depth of removal as a function of four parameters. According to the one DOF HHI preliminary test, Equation 3.42 can be defined based on the dependent variables x_1, x_2, x_3 and x_4, representing spring stiffness, mass, frictional force and transfer target components respectively, in terms of their relationship to the output *y* (human force). It is given by:

$$y = \beta_0 + \beta_1 x_1 + \beta_2 x_2 + \beta_3 x_3 + \beta_4 x_4 + \beta_{11} {x_1}^2 + \beta_{22} {x_2}^2 + \beta_{33} {x_3}^2 + \beta_{44} {x_4}^2 + \beta_{12} x_1 x_2 + \beta_{13} x_1 x_3 + \beta_{14} x_1 x_4 + \beta_{23} x_2 x_3 + \beta_{24} x_2 x_4 + \beta_{34} x_3 x_4 \qquad (3.42)$$

It should be noted that the RSM technique is not used to estimate the output across the whole range of all significant parameters; however, the method normally works well especially over a small area (Montgomery, 2001).

A crucial property of the RSM technique is to provide a good approach to prediction across the whole region of interest. Box and Hunter [1957] suggested the term *rotatable* which means that the predicted variance is the same for every point based on its distance from the centre point created. An example of this is where the variance of predicted response is the same for all points located on spheres. The Box-Behnken, which is efficiently utilized for 3-4 variable factors, is therefore used in the design of the experimental tests. The Box-Behnken cube design for three factors is demonstrated in Figure 3.31. The treatment combinations are positioned at the centre and the middle of edges of the cube, in which capabilities have been limited at +1 and –1, for upper and lower limits. In other words, it can be called a *rotatable* design, in which a centre point is rounded by the other points of $\sqrt{2}$ radius (Prakash, et al. 2010).

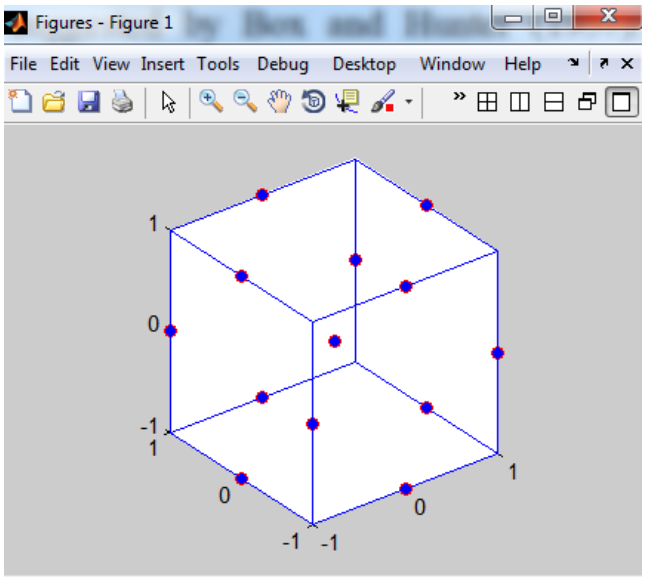

Figure 3.31 A Box-Behnken design for three factors generated by Matlab

Table 3.11 presents the Box-Behnken design with values of the four variables in a one DOF human-human interactive task (including frictional force, spring stiffness, target and mass), in which low, middle and high levels are defined as -1, 0 and 1 respectively. There are 33 different tasks of the Box-Behnken design generated by Matlab software [Aslan and Cebeci, 2007], which are listed in Appendix C.

Key to table 3.11 F_c: Frictional force T: Target
K: Spring stiffness M: Mass

Table 3.11 The Box-Behnken design with levels of variables

Factor level	**Value**	$\boldsymbol{K}$ (kN/m) $\boldsymbol{x_1}$	$\boldsymbol{M}$ (kg) $\boldsymbol{x_2}$	$\boldsymbol{F_c}$ (N) $\boldsymbol{x_3}$	$\boldsymbol{T}$ (m) $\boldsymbol{x_4}$
Lower level	-1	1	0	0	0.075
Middle level	0	1.5	1	2	0.125
Upper level	1	2	2	4	0.175

3.6 Evaluation of One DOF HHI Study

This section presents the investigation of the relationship of the four influential variables including mass, compliance, frictional force and transfer target affecting the human forces applied to the one DOF HHI system and the estimation of the human dynamic response based on McRuer crossover model.

3.6.1 Evaluation of the Developed Model Based on Box-Behnken Design

The human force profiles generated here are related to how fast the object is moved, i.e. the faster the object is moved, the narrower the force profile, and thus to effectively study the effects of the relevant parameters on surface roughness, the human force measured during performing the HHI task was required to be normalized. The lateral force shapes were first normalized based on the average completion time of each task before further analysis. Normalized object displacement, velocity and acceleration profiles were produced using the same technique.

Reed and Peshkin [2008] studied a haptic crank turning task and force profiles were normalized before further analysis. A study of human physical behaviour in tasks such as reaching, grasping or manipulating objects was presented by Ellen et al. [1985]. The characteristics of human arm movements were repeatedly measured and all physical trajectories were normalized for time and distance. Additionally, a comparison of actual and ideal force shapes of slow and fast human hand movements has been carried out based on the consideration of a normalized completion time [Wilsaan et al. 2010].

Having recommended graph normalization, this process was based on average completion time and achieved using Matlab. The function `xlsread(filename)` was used to transform the physical force information suitable for Matlab, and the program returns numerical data in time and force arrays. To average the force profiles for each Box-Behnken task, the instruction `polyfit(x,y,n)` was utilized to estimate polynomial equations before subtracting a fixed time interval in order to compute a mean trajectory. The physical profiles of the 33 Box-Behnken tasks undertaken by the 18 paired participants were then evaluated based on time normalization. Consider Task 1, where the variables were set as: K = 1.0kN/m, M = 0.0kg, F_c = 0.0 N and T = 0.125m. Figures 3.32 - 3.34 present the normalized and average force profiles, and Figures 3.35 - 3.37 illustrate the normalized and average velocity profiles from the 18 *handlers* and *receivers*.

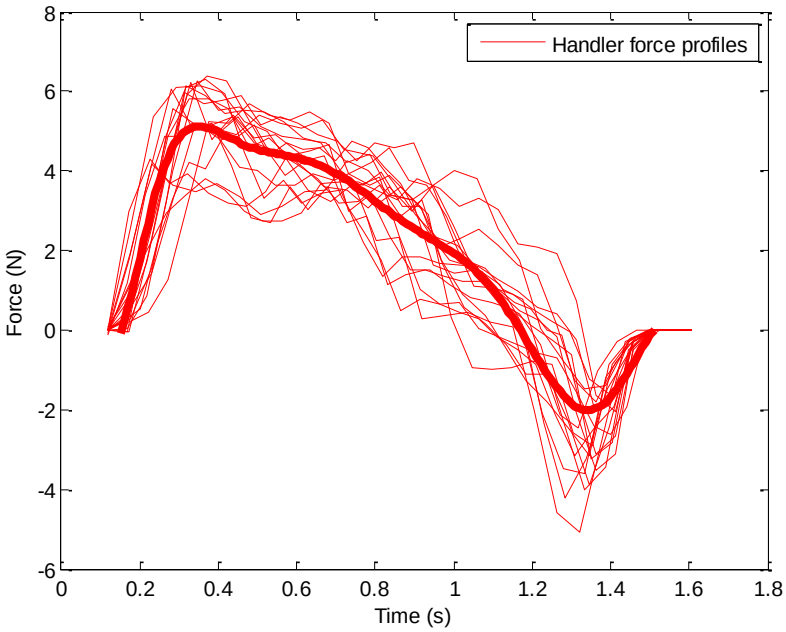

Figure 3.32 Normalized force profiles from all 18 *handlers* in Box-Behnken Task 1

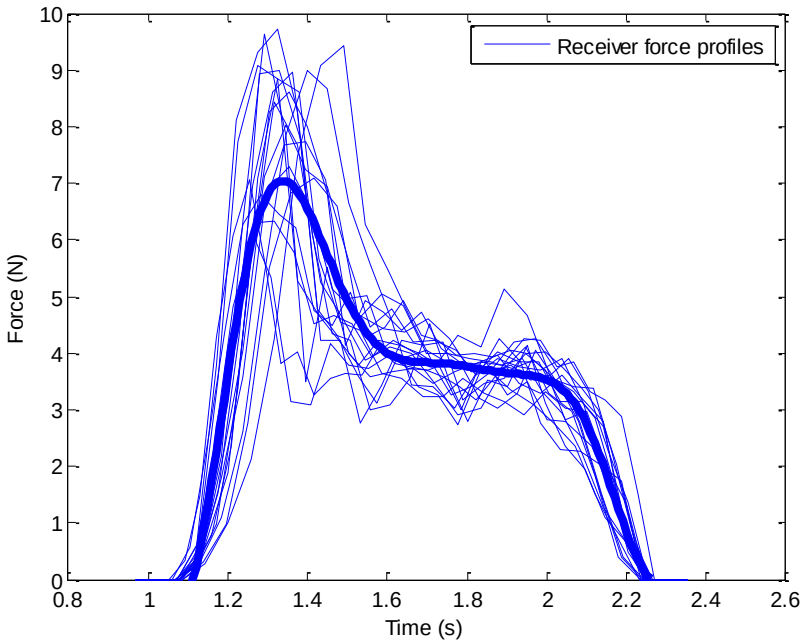

Figure 3.33 Normalized force profiles from all 18 *receivers* in Box-Behnken Task 1

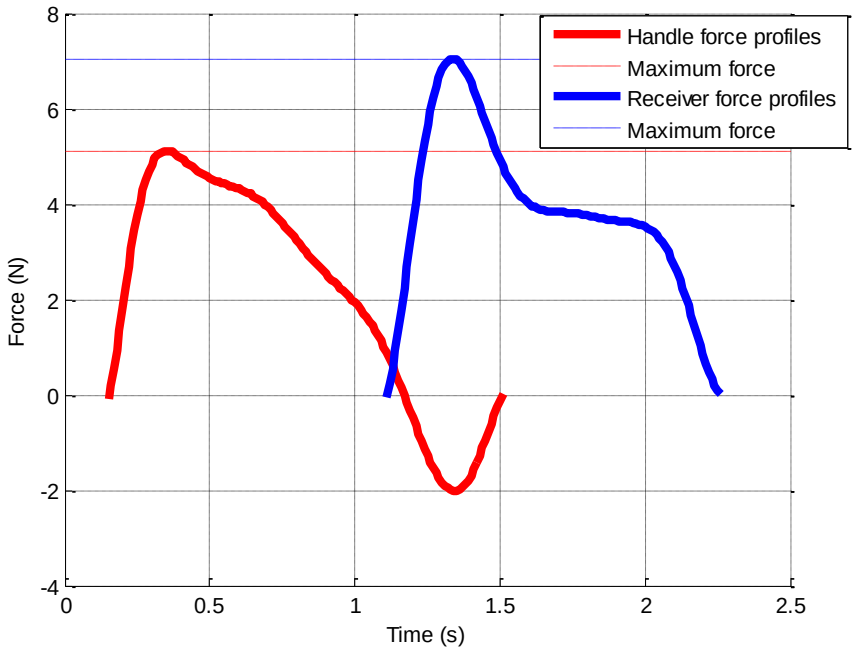

Figure 3.34 Average force profiles from all *handlers* and *receivers* in Box-Behnken Task 1

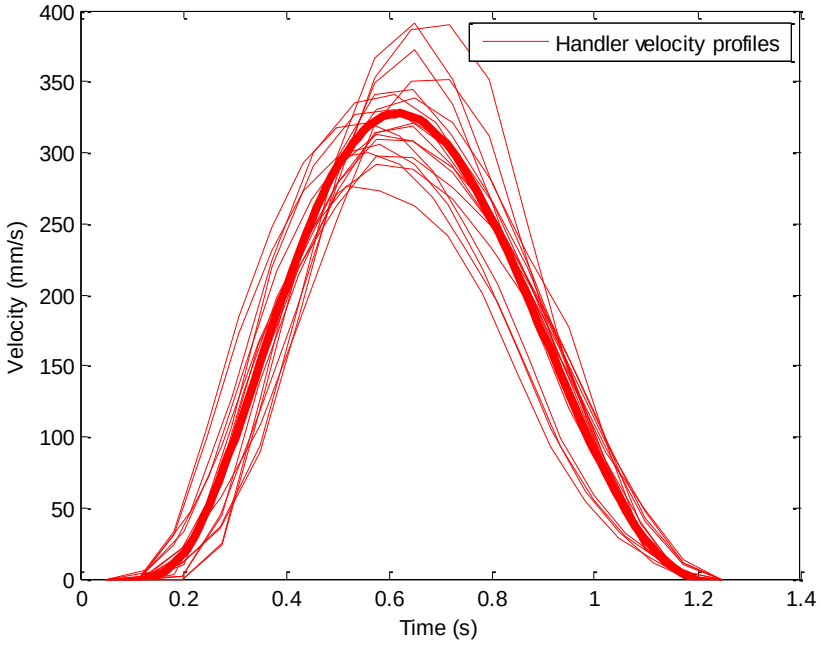

Figure 3.35 Normalized velocity profiles from all 18 *handlers* in Box-Behnken Task 1

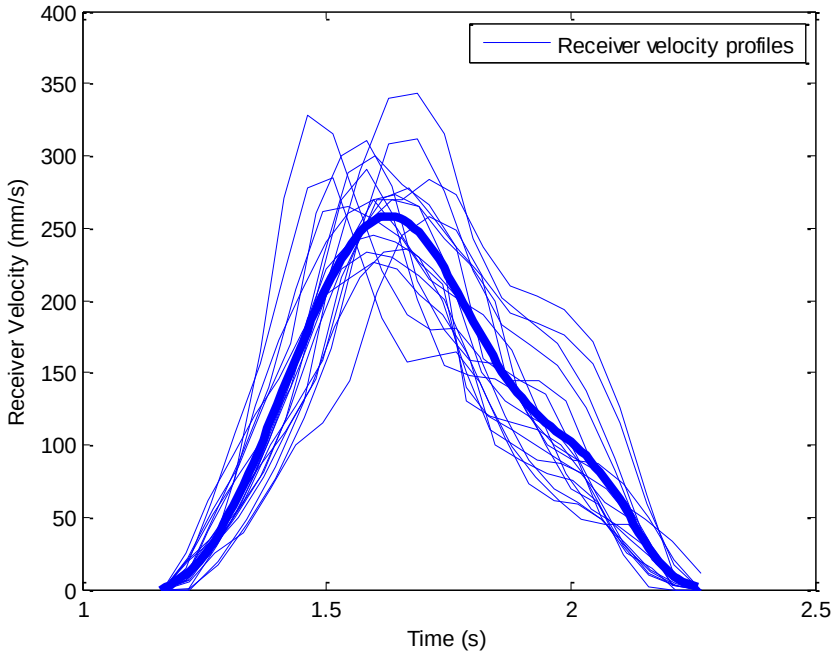

Figure 3.36 Normalized velocity profiles from all 18 *receivers* in Box-Behnken Task 1

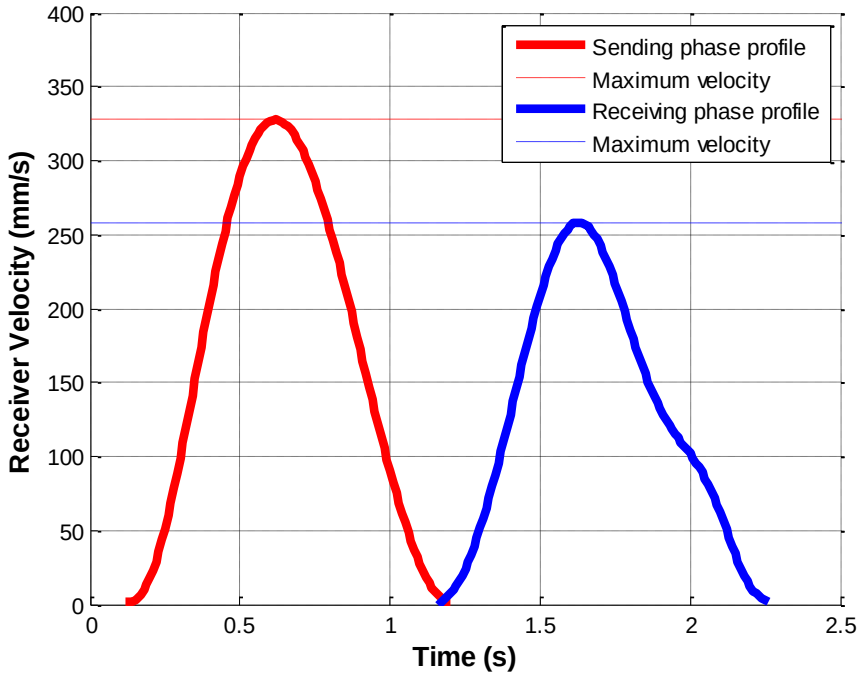

Figure 3.37 Average velocity profiles from all *handlers* and *receivers* in Box-Behnken Task 1

The human force profiles of the *handlers* and *receivers* were normalized based on an average transfer completion time. Figures 3.32 and 3.33 show the interactive force profiles of the *handler* and *receiver* from the time-domain during sending, transfer and receiving phases in one of the single DOF human-human interactive tests, and average force profiles from both operators are presented in Figure 3.34. Additionally, the normalized velocity profiles of the object are plotted in Figures3.35 and 3.36, and their average profiles in the time-domain are shown in Figure 3.37 respectively. In the sending phase the *handler* moved the object horizontally from the start point until it reached the transfer target, so that only the *handler* force profile was detected, where the maximum force was 5.11N. The velocity profile accelerated at the beginning of the movement and when the object's position approached close to the target demanded, the object then decelerated at the end of the trajectory, with the maximum velocity of 327.5mm/s, and the velocity profile provides an agreement with Flash and Hogan [1985].

In transfer phase, the *receiver* was permitted to grasp the object, so that the interactive force between the *handler* and *receiver* was conducted, where the maximum forces from the *handler* and *receiver* were -2.02N and 7.04N respectively. Once the *handler* relaxed the grasping, the object was individually manipulated towards the end position. The velocity profile of the receiving phase was deemed to be affected by the interactive force, and the maximum velocity was 258.5mm/s.

However, careful observation of the *receiver* force profiles revealed that they significantly relied on the interactive force between a *handler* and a *receiver*, rather than the system variables, as expected. In other words, the interactive forces in the HHI test depended more on how firmly a *handler* grasped the compliant object than on the effects of friction, transfer target, spring stiffness or mass components. The stronger the grasp, the greater force the *receiver* had to apply in order to complete the test and vice versa. Due to this observation, only the *handler*'s forces were therefore analysed to establish the relationship between the maximum amplitudes of the human forces and the system parameters proposed.

The estimation of the second-order polynomial model of the response surface can be developed using SPSS [Bergmann et al. 2000; Landau and Everitt 2004; Seeger et al. 2007]. The response surface is characterized using ANOVA for curve fitting and contour plots. In this HHI test, the maximum *handler* forces in each of the Box-Behnken tasks have been used to evaluate the effects of the four proposed influential variables. The analysis of variance of the response variables and regression coefficients using SPSS were carried out.

The 95% confidence interval (α = 0.05) was adopted, and the null hypothesis (H_0) and alternative hypothesis (H_1) are as follows:

- H_0: There is no statistically significant relationship between the input variables and the dependent output variable
- H_1: At least one of the input variables significantly affects the dependent output variable.

The coefficients of the second-order-polynomial equation can be estimated along with the proposed initial conditions as follows. It is assumed that the variance of the individual distribution has to be constant for all values of the independent variable, and that the relationship between the dependent variable and each independent variable has to be linear. Table 3.12 presents the output from SPSS, and includes the coefficients applied in the second-order-polynomial equation and significance values. The second-order polynomial equation shown below expresses the relationship between the surface roughness parameter *y* (human force) and the four variable parameters x_1, x_2, x_3 and x_4 representing respectively spring stiffness, mass, frictional force and transfer target, respectively.

$$y = 3.059x_1 + 0.120x_2 - 0.220x_3 + 0.017x_4 - 1.123x_1^2 - 0.001x_2^2 + 0.152x_3^2 - 0.008x_1x_2 + 0.082x_1x_3 - 0.002x_1x_4 - 0.002x_2x_3 + 0.001x_3x_4 - 0.740 \quad (4.43)$$

Once, the parameter coefficients in the second-order equation had been computed, the ANOVA method was subsequently used to assess the system response surfaces.

Table 3.12 Estimated regression coefficients

Model		Coefficients		Standardized Coefficients	*T*	*Sig.*
		β	Std. Error	Beta		
1	(Constant)	-0.740	0.809	-	-0.915	0.372
	K	3.509	0.768	0.958	4.568	0.000
	M	0.120	0.019	0.657	6.463	0.000
	F_c	-0.220	0.093	-0.240	-2.363	0.030
	T	0.017	0.007	0.453	2.518	0.022
	K×*K*	-1.123	0.247	-0.924	-4.548	0.000
	M×*M*	-0.001	0.001	-0.124	-1.774	0.093
	F_c×F_c	0.152	0.015	0.685	9.824	0.000
	T×*T*	0.000	0.000	-0.273	-1.613	0.124
	K×*M*	-0.008	0.007	-0.075	-1.238	0.232
	K×F_c	0.082	0.034	0.147	2.439	0.025
	K×*T*	-0.002	0.001	-0.132	-1.792	0.090
	M×F_c	-0.002	0.002	-0.031	-1.016	0.323
	M×*T*	0.000	0.000	0.194	3.733	0.002
	F_c×*T*	0.001	0.000	0.193	3.714	0.002

Table 3.13 One-way ANOVA results for the second-order polynomial equation

Model	R	R^2	Adjusted R^2	Std. Error of the Estimate
1	.998[a]	.996	.993	.13530

Model		Sum of Squares	df	Mean Square	F	Sig.
1	Regression	80.109	14	5.722	312.586	.000[a]
	Residual	.329	18	.018		
	Total	80.438	32			

a. Predictors: (Constant), $F_c \times T$, $K \times M$, $K \times K$, $T \times T$, $M \times F_c$, $F_c \times F_c$, $M \times T$, $M \times M$, $K \times F_c$, $K \times T$, F_c, M, T, K

b. Dependent Variable: Actual force (y)

By applying the ANOVA technique to statistically evaluate the relationship between the system variables and surface roughness, the test results presented in Table 3.13 have a significance value of 0, which clearly indicates that the hypothesis H_0 has to be rejected and H_1 accepted, i.e. at least one of the input variables significantly affected the dependent output at the 95% confidence interval.

To decide whether an estimated regression model is acceptable or not, the R^2 value is determined which theoretically can have a range from 0 to 1. A suitable correlation between predicted and actual force values will then confirm the appropriateness of the equation. In this case, the computed the number of R^2 is 0.996, which means that 99.6% of the surface roughness parameter (y) estimation is meaningfully related to the input variable parameters, and the adjusted R^2 value (0.993) indicates the second-order polynomial model is highly reliable. Table 3.14 shows a comparison of the predicted dependent variable y, to the actual values, and it can be noted that the maximum, minimum and average absolute errors are 16.0%, 0.2% and 3.5% respectively.

Table 3.14 Comparison of the predicted and actual force values [Neranon and Bicker, 2014]

Test	Spring stiffness (N/mm)	Mass (N)	Resistance Force (N)	Target (mm)	Measured Force (N)	Predicted Force (N)	Error (N)	Error (%)
1	1.0	0	4	125	5.12	5.28	-0.16	-3.0
2	1.0	0	0	125	2.86	2.90	-0.04	-1.3
3	1.0	0	2	75	3.16	3.03	0.13	4.2
4	1.0	0	2	175	3.59	3.73	-0.14	-3.8
5	1.0	10	4	75	5.89	5.67	0.22	3.8
6	1.0	10	4	175	7.09	6.57	0.52	7.4
7	1.0	10	0	75	3.56	3.57	-0.01	-0.2
8	1.0	10	0	175	4.26	4.07	0.19	4.6
9	1.0	20	4	125	7.56	6.96	0.60	8.0
10	1.0	20	0	125	5.12	4.74	0.38	7.5
11	1.0	20	2	75	5.21	4.79	0.42	8.1
12	1.0	20	2	175	6.53	5.49	1.04	16.0
13	1.5	0	4	75	5.15	5.17	-0.02	-0.3
14	1.5	0	4	175	6.12	5.97	0.15	2.5
15	1.5	0	0	75	2.78	2.82	-0.04	-1.5
16	1.5	0	0	175	3.11	3.22	-0.11	-3.6
17	1.5	10	2	125	4.97	4.73	0.24	4.9
18	1.5	20	4	75	7.06	6.77	0.29	4.2
19	1.5	20	4	175	8.23	7.57	0.66	8.1
20	1.5	20	0	75	4.82	4.58	0.24	4.9
21	1.5	20	0	175	5.67	4.98	0.69	12.1
22	2.0	0	4	125	5.48	5.49	-0.01	-0.3
23	2.0	0	0	125	2.63	2.79	-0.16	-5.9
24	2.0	0	2	75	3.02	3.18	-0.16	-5.4
25	2.0	0	2	175	3.45	3.68	-0.23	-6.7
26	2.0	10	4	75	6.11	5.90	0.21	3.4
27	2.0	10	4	175	7.09	6.60	0.49	6.9
28	2.0	10	0	75	3.57	3.48	0.09	2.6
29	2.0	10	0	175	4	3.78	0.22	5.6
30	2.0	20	4	125	7.71	7.01	0.70	9.0
31	2.0	20	0	125	5.01	4.47	0.54	10.9
32	2.0	20	2	75	5.02	4.78	0.24	4.7
33	2.0	20	2	175	5.86	5.28	0.58	9.9

3.6.2 Estimation of Human Behaviour based on the Extended Crossover Model

The main difficulty in modelling the human dynamics is to determine the unknown parameters which are influenced by the actual system's inputs and outputs. A preliminary test was carried out to measure operator reaction time (τ_d) using a visual indicator to stimulate the response. The schematic diagram of the preliminary experimental set-up is shown in Figure 3.38. Here an LED indicator was used to enable the participants to push the button as soon as possible; in the meantime LabVIEW Timer0 was started. Once the human pressed the stop button, the LED and Timer0 were simultaneously deactivated, and then the information was captured in real-time using a LabVIEW virtual interface

Table 3.15 presents the results of the evaluation of the human reaction time (τ_d). The mean human reaction time was 0.16s with a corresponding standard deviation of 0.01s. The test results were in agreement with those of McRuer [1980], in which the values of the human perceptual reaction time were in the range of 0.13 to 0.20s. This reaction time delay of 0.16s was applied in the remaining McRuer crossover parameters, i.e. gain K_H, and coefficients of lead T_z and lag T_p, which were identified using the prediction error method (PEM) in the Matlab Identification Toolbox™. The PEM technique is suitable for use in system process behaviour based upon the basic type of model.

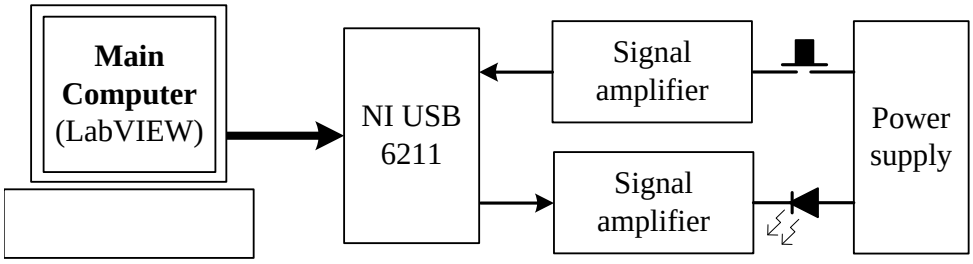

Figure 3.38 The experimental setup of human reaction time estimation test

Table 3.15 Human reaction time results and average time taken

Participant No.	Average taken time (s)
1	0.16
2	0.16
3	0.15
4	0.17
5	0.15
6	0.16
7	0.17
8	0.17
9	0.17
10	0.16
11	0.15
12	0.17
13	0.16
14	0.16
15	0.15
16	0.16
17	0.18
18	0.15
Std	**0.01**
Mean	**0.16**

In this study, the PEM input and output were defined as the human force exerted on the object and the displacement tracking error respectively. First, the PEM input and output data have to be transformed into an `iddata` object, which is the basic object for dealing with signals in the Matlab toolbox, using the command:

```
data = iddata(y,u,Ts)
```

where, y and u represent the time-domain input and output of PEM respectively; additionally, T_s is the time interval in seconds between successive data samples. Once the `iddata` object has been created, using the output structure of the PEM model specified by `P1Z1D1`, which represents pole, one zero and one delay element together, as in the McRuer crossover model. This can be expressed as:

```
PEM model = pem(data,'P1Z1D1')
```

Figure 3.39 illustrates the example of actual human force and displacement profile from one of the one DOF HHI tests. The PEM output for the functional McRuer model of human behavioural control, as shown in Figure 3.40, generated by Matlab is as follows:

```
Process model with transfer function
                1+Tz*s
G(s) = Kp * ---------- * exp(-Td*s)
                1+Tp1*s
with  Kp = 40.241+-5.9241e-006,        Tp1 = 0.02+-3.2212e-009,
      Td = 0.16+-2.5876e-008 and       Tz = 0.01+-1.9709e-009
```

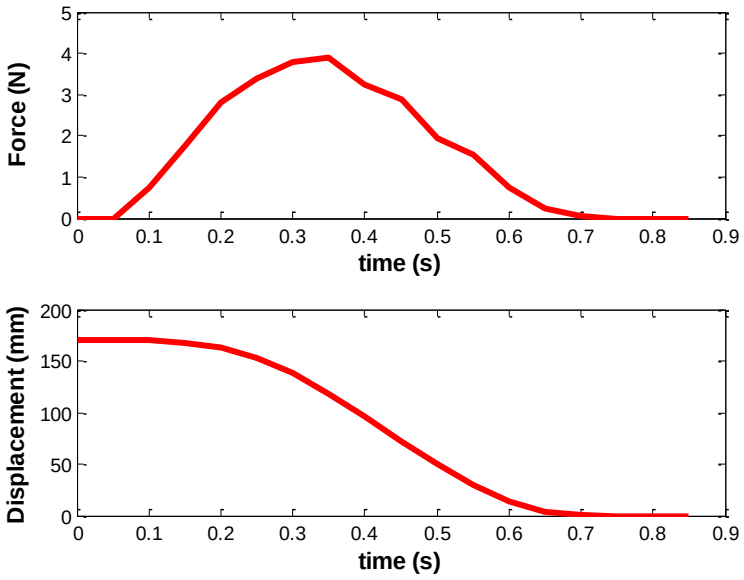

Figure 3.39 System input and output profiles required in Matlab PEM

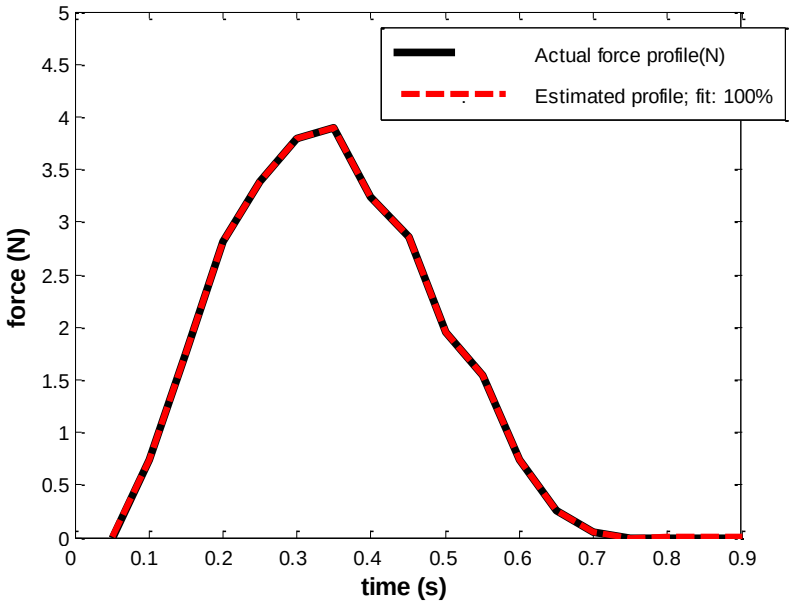

Figure 3.40 Comparison of actual and estimated human force profiles

Model validation was automatically utilized in the final step of system identification in order to provide a validation of the quality of the model in the simulation. The validation shows, whether or not a calculated model is a reasonable representation of an actual system, which is percentage best fit (100%). From the simulation results, the McRuer crossover parameters have been determined as K_H = 40.24, T_z =0.01, T_p = 0.02 and τ_d = 0.16. It can therefore be concluded that the model has provided a good estimation and effective validation based on performance criteria [Jahaya et al. 2011], and the computed models are deemed to be acceptable.

Careful observation of the *receiver* force profiles in the HHI test revealed that the *receiver* force signal significantly relied primarily on the interactive force associated with a *handler*, rather than on the system variables, as expected. Following this observation, only the *handler*'s forces were specifically examined to establish the human behavioural model. Consequently, the averages of the corresponding human parameters from the 18 samples, undertaking the 33 HHI preliminary experiments, were estimated.

Table 3.16 Results of the crossover model estimations and model validation using PEM

Test	*Stiffness (kN/m)*	*Mass (N)*	*Frictional force (N)*	*Target (mm)*	**McRuer crossover model parameters**				**Fit (%)**
					K_H	$\tau_d\ (s)$	$T_p(s)$	$T_z(s)$	
1	1	0	4	125	63.31	0.16	0.02	0.01	100.0
2	1	0	0	125	28.25	0.16	0.01	0.01	100.0
3	1	0	2	75	72.83	0.16	0.02	0.01	100.0
4	1	0	2	175	40.24	0.16	0.02	0.01	100.0
5	1	0.5	4	75	100	0.16	0.02	0.01	100.0
6	1	0.5	4	175	62.10	0.16	0.02	0.01	100.0
7	1	0.5	0	75	57.28	0.16	0.01	0.00	100.0
8	1	0.5	0	175	32.16	0.16	0.01	0.00	100.0
9	1	1	4	125	81.53	0.16	0.01	0.01	100.0
10	1	1	0	125	44.61	0.16	0.01	0.00	100.0
11	1	1	2	75	67.66	0.16	0.02	0.00	100.0
12	1	1	2	175	45.11	0.16	0.01	0.00	100.0
13	1.5	0	4	75	100	0.16	0.02	0.01	100.0
14	1.5	0	4	175	54.51	0.16	0.02	0.01	100.0
15	1.5	0	0	75	54.47	0.16	0.02	0.01	100.0
16	1.5	0	0	175	23.09	0.16	0.02	0.01	100.0
17	1.5	0.5	2	125	70.01	0.16	0.02	0.01	100.0
18	1.5	1	4	75	100	0.16	0.02	0.01	100.0
19	1.5	1	4	175	60.44	0.16	0.02	0.00	100.0
20	1.5	1	0	75	100	0.16	0.02	0.01	100.0
21	2	1	0	175	39.43	0.16	0.01	0.01	100.0
22	2	0	4	125	67.01	0.16	0.02	0.01	100.0
23	2	0	0	125	30.74	0.16	0.01	0.01	100.0
24	2	0	2	75	77.17	0.16	0.02	0.01	100.0
25	2	0	2	175	26.13	0.16	0.02	0.00	100.0
26	2	0.5	4	75	100	0.16	0.02	0.01	100.0
27	2	0.5	4	175	59.39	0.16	0.01	0.00	100.0
28	2	0.5	0	75	55.72	0.16	0.02	0.01	100.0
29	2	0.5	0	175	23.23	0.16	0.02	0.01	100.0
30	2	1	4	125	100	0.16	0.02	0.01	100.0
31	2	1	0	125	48.03	0.16	0.01	0.01	100.0
32	2	1	2	75	85.46	0.16	0.02	0.01	100.0
33	2	1	2	175	40.86	0.16	0.01	0.00	100.0

The extended McRuer crossover algorithms were successfully estimated using the Matlab PEM technique. Furthermore, model validation was employed in the final step of system identification in order to provide a measurement of the quality of the model in the simulation. The overall results can be concluded that the average reaction time was 0.16s with a standard deviation of 0.01s, which agreed with McRuer [1980] that the human perceptual reaction time is in the range 0.1-0.2s. The coefficients of lead time (T_z) and lag time (T_p) are between 0.00- 0.02s and 0.00-0.01s respectively.

Loop gain (K_H) is inversely proportional to the object distance moved and is associated with a faster response. In other words, the human muscle gain increases, when the object is moved over a shorter distance or with a faster reaction. In addition, K_H is directly proportional to the masses added and friction of the system; however, it is not affected by the system compliance. The model validation shows that the percentage of best fit is almost 100%, which is much higher than the normally acceptable percentage of model fitting at 80% of best fit. Neranon and Bicker [2014] showed that the McRuer crossover model is an effective way of matching the human behavioural characteristics whilst performing the one DOF human-human interactive tests and yields slightly better performance than the Auto Regressive Moving Average with Exogenous Input (ARMAX) system identification as suggested by Neranon and Bicker [2013] with the best fit percentages being between 88.7% - 97.2%.

The evaluation of the developed McRuer crossover model, based on Box-Behnken design and the estimation of human behavioural response were carried out in Sections 3.6.1 and 3.6.2 respectively, and this study was taken into account in the one degree of freedom constrained horizontal movement path, where a rectilinear slider was used to support low-friction movement. However it is appreciated that this linear horizontal movement does not imitate a real-world 3D human-human object handover task. Furthermore, the human-human collaborative operation does not function effectively as compared to a continuous object handover process because the *receiver* has to wait until the object completely approaches a transfer target and then, the *receiver* is allowed to move to the end position. Consequently, time delay is inevitably introduced. Therefore, a new set of substantive main human-human object handover experiments have been carried out to overcome the problems and will be detailed in the following section.

3.7 A One DOF Human-Human Object Handover Task

It is crucial to understand the kinematics and dynamics of human-human handover behaviour in order to design and develop an appropriate set of force and velocity control strategies for robust, behaviour-based, human-robot interaction (HRI). Thus a set of human-human object handover tests has been undertaken to investigate how the *handler* and *receiver* behave whilst performing a single DOF human-human handover task, similar to passing the baton in a relay race. Before starting the tests, each participant was asked to perform the assigned tests to the best of their ability, without twisting or bending the object. After understanding the HHI dynamic responses and establishing a robotic control system which enables a robot manipulator arm to interact with a human to facilitate the dextrous transfer of objects in a safe and speedy manner, finally, the performance of the human-robot handover tasks will be compared with the human-human handover tests in order to evaluate the control strategies proposed for the interactive task. Figure 3.41 depicts the outline of the sequence of the experiments.

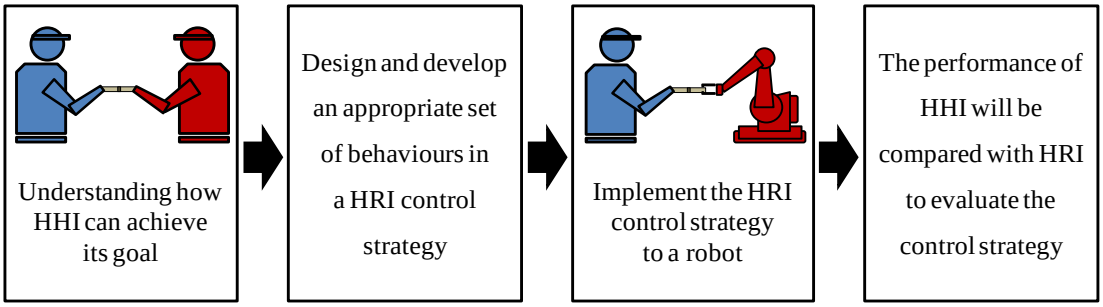

Figure 3.41 Outline of the sequence of principal experiments

The objectives of the one DOF human-human handover study are as follows:

- To evaluate human physical characteristics in a one DOF HHI handover task in order to design and develop an appropriate set of behaviours in a human-robot interactive control strategy in terms of:
    - How the *handler* and *receiver* regulate their interactive forces whilst executing the object handover tasks under different velocities and masses,
    - How the *handler* releases the object to be transferred in a natural and timely manner,
    - How long the object handover process takes (time (s) can be used),

    - How much work is done by the participant pair whilst performing the human-human handover interactive task, and
- To provide the information of the human-human handover characteristics and used to compare with the human-robot handover task in order to evaluate the performance of the robot control strategies designed.

The preliminary requirements were defined as follows:

- The equipment should facilitate the accomplishment of the characterization of the haptic human dynamic interaction.
- The object comprises an ATI mini40 F/T sensor (All detail of the sensor can be seen in Appendix D) coupled by cylindrical batons 40mm in diameter and 150mm in length, with a total mass 0.22kg.
- The equipment should facilitate the accomplishment of the characterization of the haptic human dynamic interaction.
- The object comprises an ATI mini40 F/T sensor (All detail of the sensor can be seen in Appendix D) coupled by cylindrical batons 40mm in diameter and 150mm in length, with a total mass 0.22kg.
- The handling interactive force applied by the subjects is measured by the ATI sensor and collected in real-time every 4ms (or 250Hz).
- Masses added can be to increase the load capacity of 0.2, 0.6 and 1.0kg in order to change the moment of inertia of the experimental device.

The preliminary human-human handover baton design is illustrated in Figure 3.42.

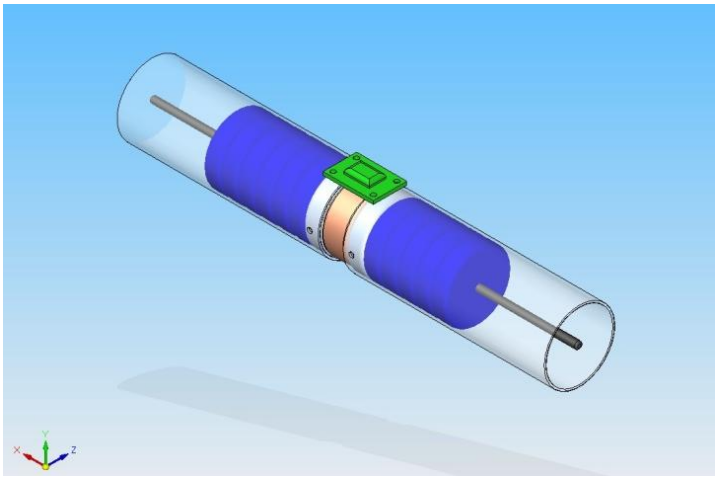

Figure 3.42 Design of a one DOF human-human handover baton

3.7.1 Design of One DOF Human-Human Handover Interaction

Two human participants were randomly selected to perform the one DOF human-human object handover task at three different conditions, i.e. 10, 50 and 100mm/s. In sending phase, the *handler* was first instructed to transfer the object to the *receiver* at a half of the fixed velocity (5, 25 and 50mm/s) without communication. When the object had arrived at the interactive zone, it was passed to the *receiver* similar to passing the baton in a relay race, and then manipulated towards the end point at the demanded conditional velocities. Whilst executing the interactive task, the interactive forces f_x, f_y and f_z were measured and collected in real-time using a ATI mini40 force/torque sensor. The ranges of the force and torque measurements of the ATI sensor are ±80N and ±2Nm with 0.02N and 0.00025Nm resolutions, respectively. In addition a DE-ACCM accelerometer was used to estimate the velocity of the object by integrating an output signal from the sensor.

The sensor system is made up of a DE-ACCM accelerometer, an ATI mini40 F/T sensor, electrically shielded and twisted transducer cables, a PCI based data acquisition board and an interface power supply (IFPS) box. The QNX Neutrino real-time operating system v6.4.0 supporting the implementation of the multi-tasking system was adopted to communicate with a power DAQ PCI board, PDL-ME-50 lab series. The PDL-ME DAQ card furnishes six channels of analog inputs (16-bit A/D converter, 50kS/s sampling rate) and offers the precise quantification of the strain gauge signals transmitted from the IFPS box and the acceleration data. Figure 3.43 shows the schematic of the systems of the ATI mini40 force/torque sensor and data acquisition.

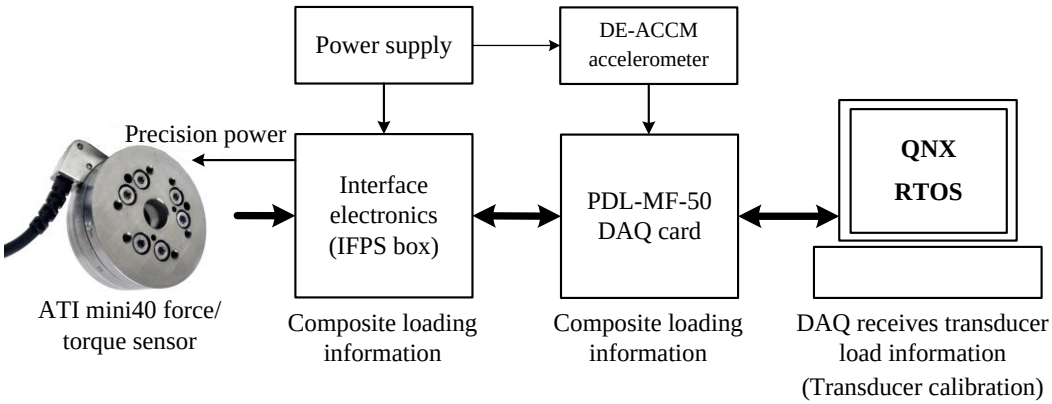

Figure 3.43 Schematic of force/torque sensor data acquisition

The corresponding flowchart is shown in Figure 3.44. The DAQ PCI board was first initialized to reset all configurations, and then the analog input was enabled for the data acquisition of the ATI force sensor in order to convert the raw data to its equivalent voltages. The data communication was based on a first-in-first-out (FIFO) method, i.e. the array of force signals was transmitted byte by byte until all had been sent according to an ordering process. The force/torque transducer was calibrated using a transducer stiffness matrix according to the default sensor reference frame. Before starting the test, the *handler* was instructed to hold the object horizontally and then the ATI mini40 transducer was initially set to restore all force bias readings to zero scale in order to eliminate the effects of other external forces.

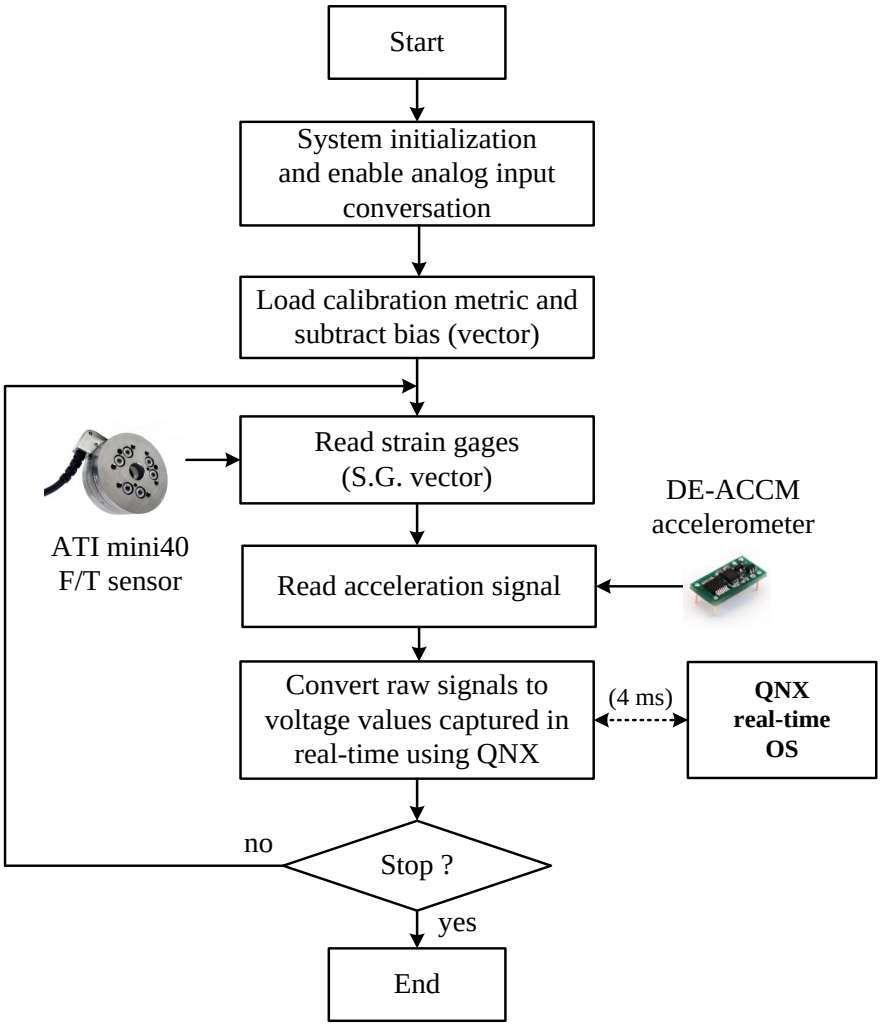

Figure 3.44 Flowchart of the human-human handover interaction

3.7.2 Test Procedure for One DOF Human-Human Handover Interaction

As recommended from the pilot study, 18 pairs of participants were required to perform three repetition sets of five object handover tasks. The *handler* was commanded to move the object horizontally using one hand from the start point to the transfer zone at the haft of demanded velocities of 5, 25 and 100mm/s. After passing the object to the *receiver*, it had to be manipulated to the end point by the *receiver* at the demanded velocities fixed at 10, 50 and 100mm/s. this process is similar to passing the baton in a relay race.

The workspace of the human-human handover task can be shown in Figure 3.45. The gripper of the Stäubli robot was moved along the x axis 700mm as a guide for the movement of the object for the *handler*. After each object handover test had been completed, a new test was enabled with a different time delay randomly set in the software. The physical interactive force signals along the x, y and z axes and the transfer times was detected and captured in real-time. Figure 3.46 shows the experimental apparatus, the execution of the human-human handover tests and a velocity guide used for the human movement while manipulating the object.

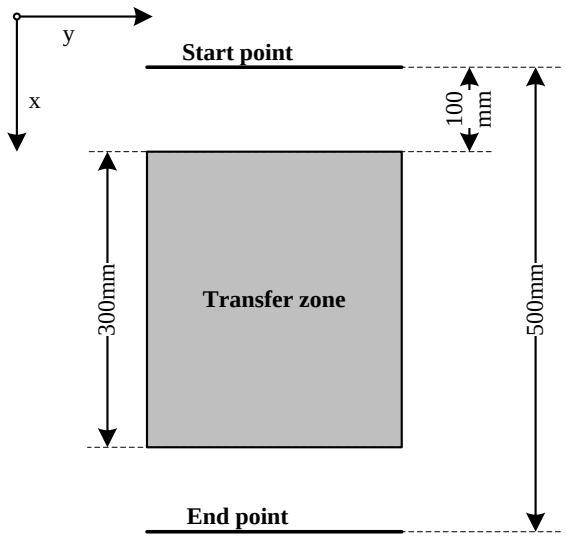

Figure 3.45 Flowchart of the human-human handover interaction

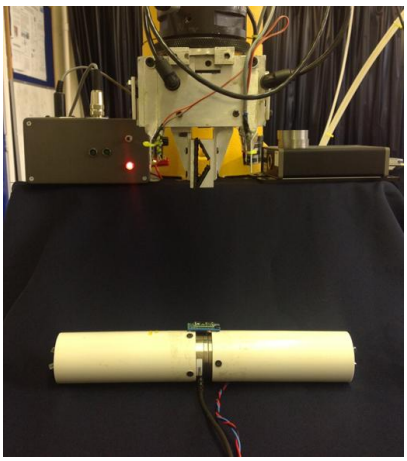

(a) Preliminary experimental set-up

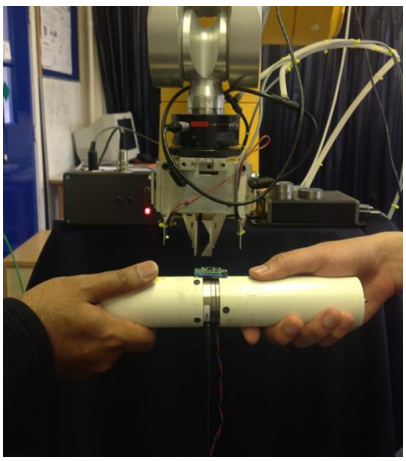

(b) Execution of the HHI

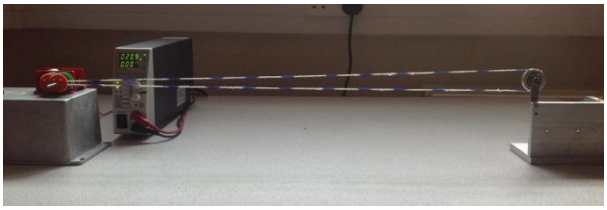

(c) A velocity guide of the movement of the object

Figure 3.46 Experimental set-up of a one DOF human-human handover task

3.7.3 Test Evaluation of One DOF Human-Human Handover Interaction

This study provides an understanding of the human dynamic responses in object handover tasks, where the one DOF human-human handover baton was designed to measure interactive force between the *handler* and *receiver* in real-time. Interactive force (f_{int}) profiles present the magnitude of the interactive forces between the (*handler* and *receiver)* participants against time (t) during the object transfer process, and how theyare regulated whilst performing the object handover tasks. The maximum interactive force (f_{max}) is used to indicate threshold force which represents how much the amount of magnitude of maximum force is taken into account when the *handler* decides to release the object to be transferred in a natural manner. The f_{max} can be calculated from the maximum magnitude of interactive forces. Transfer time (T_{trf}) which demonstrates how long the object handover process takes is computed by finding the difference between the times at which the *receiver* first grasps and starts pulling the handover baton and when the *handler* successfully releases the object. Furthermore, work done (W) by the participant pair in each collaborative task can be calculated by multiplying the area under the curve for interactive force (f_{int}) against time (t) by the instantaneous velocity (v) can be expressed as follows:

$$W = f_{int} \times s = (f_{int} \times t) \times v \tag{4.44}$$

or $$W = Area\ under\ force\ curve \times v \tag{4.45}$$

where, W is work done by F_{int},

f_{int} is interactive force,

s is object displacement,

t is time used, and

v is object velocity.

These features will be implemented in design and development of human-like robot control strategies able to effectively perform human-like functions in the human-robot handover tasks. Subsequently, the behavioural characteristics of the human-robot object handover tasks in terms of these parameters: maximum interactive force (f_{max}), transfer time (T_{trf}), and work done (W), will be evaluated and compared with the human-human handover task in order to determine the performance of the robot control strategies.

The tests were carried out to establish the relationship between f_{max}, T_{trf} and W, as a function of velocity and mass of the baton, and all results are summarised in Table 3.17. In this analysis, three standard deviations (3σ) defining 99% of the area under the curve of the force profile was appropriately used, and the interactive force profiles generated here are required to be subjected to the process of curve fitting due to the elimination of undesirable variations from the achieved interactive force data. Curve fitting was used to examine the relationships between the interactive force and time, and object velocity and time under different velocities and masses of the baton with the goal of defining best fit models. An analysis of the experimental HHI results revealed that the object velocity profiles were of a bell-shaped pattern, which provides an agreement with Shibata et al. [1997]; therefore a fourth-order polynomial was used to achieve an appropriate fit throughout the tests. Figure 3.47 shows the f_{max}, T_{trf} and W parameters computed from one of examples where the *handler* has to transfer the object of total mass 1.22kg at a demanded velocity of 100mm/s, in which the parameters were computed to be 3.96N, 0.31s and 49.2mJ respectively.

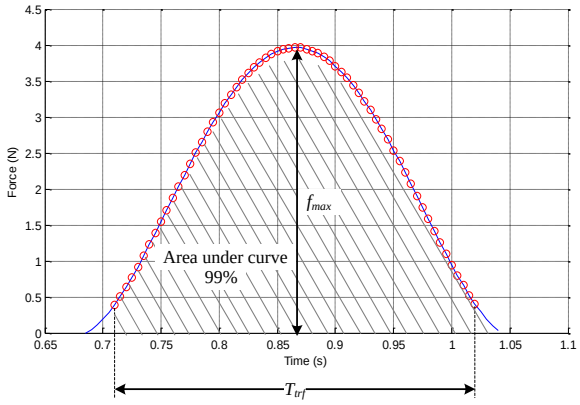

(a) Interactive force profile of a HHI test

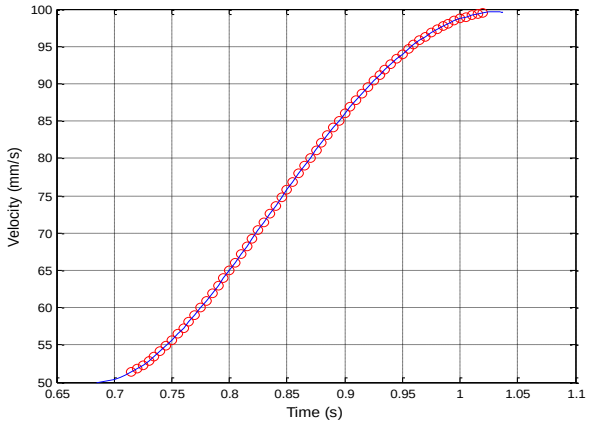

(b) Velocity profile of a HHI test

Figure 3.47 Human interactive force and velocity profiles

Table 3.17 Comparisons of the f_{max}, T_{trf} and W in HHI tasks under the conditions required

Transfer time (s)						
Velocity (mm/s)	Mass 0.42kg	SD (s)	Mass 0.82kg	SD (s)	Mass 1.22kg	SD (s)
10	0.54	0.05	0.52	0.08	0.48	0.08
50	0.44	0.04	0.43	0.04	0.38	0.04
100	0.37	0.03	0.35	0.04	0.30	0.03
Force max (N)						
Velocity (mm/s)	Mass 0.42kg	SD (N)	Mass 0.82kg	SD (N)	Mass 1.22kg	SD (N)
10	0.85	0.19	1.46	0.32	2.26	0.56
50	1.32	0.28	2.44	0.41	3.32	0.41
100	2.43	0.46	2.79	0.58	3.63	0.45
Work done (mJ or N.mm)						
Velocity (mm/s)	Mass 0.42kg	SD (mJ)	Mass 0.82kg	SD (mJ)	Mass 1.22kg	SD (mJ)
10	1.9	0.3	2.9	0.3	4.1	0.8
50	11.0	1.6	21.8	2.5	25.8	3.2
100	34.3	6.6	38.6	7.5	42.4	6.7

In summary, the findings in Figures 3.48(a) – (c) indicate the characteristics of the human *handler* and *receiver* whilst performing the human-human handover task of several demanded velocities of 10, 50 and 100mm/s and various object total masses of 0.42, 0.82 and 1.22kg. The results present how the *handler* and *receiver* regulate their interactive force (including maximum interactive force), how long the object handover process takes and finally how much work is done by the participant pair whilst performing the human-human handover interactive task.

The outcomes also identify how much work is done by the pair of the participants in the human-human handover interactive task. These features have then been used to design and develop an appropriate set of force and velocity control strategies for the Stäubli robot in the human-robot interaction (HRI) task. In the one DOF human-robot handover test, the object mass of 0.42kg was specifically considered for one-directional movement in the x-axis direction at the demanded velocities of 10, 50 and 100mm/s, so that a greater variety of object loads can be ignored. Finally, the data analysis of the human-human handover test identified as an ideal condition has been compared with the human-robot handover task to evaluate the force and velocity control strategies proposed for the interactive task.

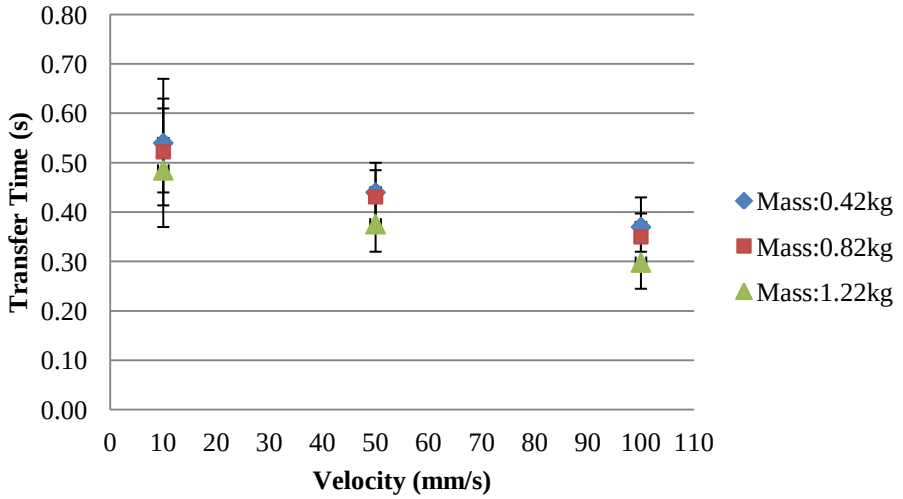

(a) Result of averages of transfer time

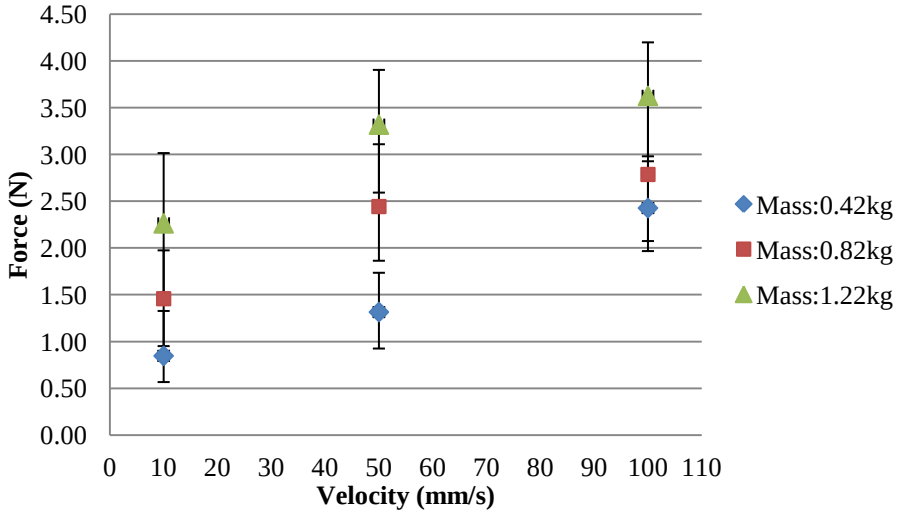

(b) Result of averages of interactive force

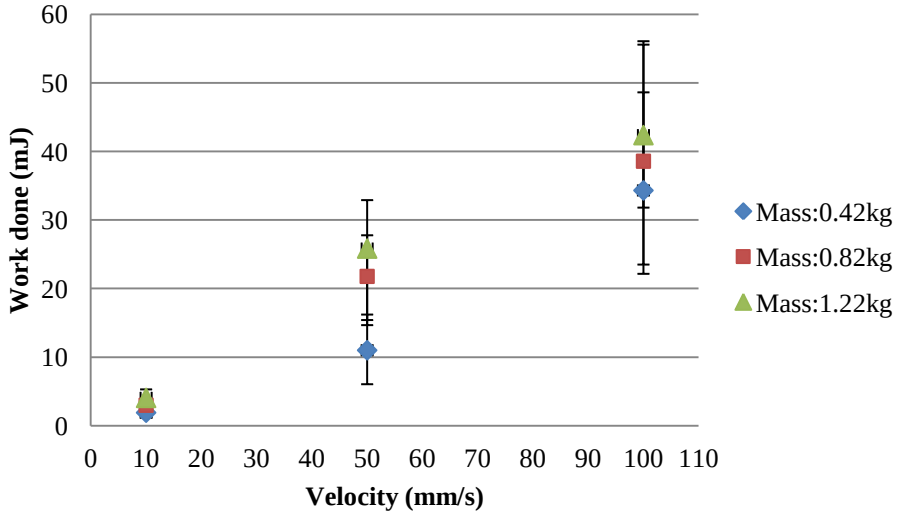

(c) Result of averages of work done

Figure 3.48 Average f_{max}, T_{trf} and W influenced by the weights added to the baton (0.2, 0.6 and 1kg) at various demanded velocities of 10, 50 and 100mm/s

3.8 Summary of a Human-Human Handover Task

The design and evaluation of single DOF HHI experiments used to analyse the physical HHI behavioural responses and force analysis for human-human interaction have been described in this chapter. A one DOF HHI pilot study was undertaken to statistically quantify the numbers of participants and trials, and appropriate sequence of transfer tasks. These recommendations have been applied to a full-scale one DOF HHI rectilinear tests designed using a Box-Behnken technique, a set of human-human object handover tests and the human-robot object handover tasks (as discussed in Chapter 5).

A Box-Behnken design was selected to generate a second order polynomial equation which expresses the relationship between the applied maximum force (y) and the four variables x_1, x_2, x_3 and x_4 representing respectively compliance, mass, friction and transfer target position. After applying an ANOVA technique to statistically evaluate the equation, it was concluded that at least one of the input variables significantly affected the dependent output at the 95% confidence interval. Additionally, the computed R^2 was 0.996, which shows that by employing the proposed second-order polynomial equation, 99.6% of the estimation of the human maximum force (y) is meaningfully related to the input variables.

Due to the complexity of the human control system, the McRuer crossover model was employed to simplify challenge of a human operator in human-machine interaction. By implementing the Matlab Prediction Error Method (PEM), the estimation of the McRuer crossover parameters was made, and the parameter estimates were deemed to be in agreement with those of McRuer [1980]. The results show that the average reaction time for the completion of the tasks was around 0.16s, with a corresponding standard deviation of 0.01s. The coefficients of lead time (T_z) and lag time (T_p) were in the ranges of 0.00–0.02s and 0.00–0.01s respectively. The human muscle gain (K_H) was directly proportional to the mass of the object, frictional force added and a faster response was inversely proportional to the distance moved by the object; however, it was not affected by compliance.

The investigation of the developed model based on Box-Behnken and human behavioural response using McRuer crossover model was restricted to the one degree of freedom constrained horizontal movement path, and a new set of substantive human-human object handover experiments were carried out to evaluate human physical characteristics in HHI tasks in order to design and develop an appropriate set of behaviours in a human-robot interactive control strategy. The set of tests were designed to determine how the *handler* and *receiver* regulate their interactive forces whilst performing the object handover tasks, and the maximum force when the *handler* decides to release the object, how long the handover process takes and how much work is done by the pair of participants whilst performing the task. Finally, the test evaluation of the relationship of interactive force, transfer time and work done components and the several conditions of added object weights and transfer speeds has been addressed. The understanding of the physical HHI behavioural characteristics was then adopted to establish the behavioural control strategy for robot force and velocity control in human-to-robot and robot-to-human handover tasks, which will be discussed fully in the following chapter.

CHAPTER IV

EXTERNAL FORCE CONTROL SYSTEM FOR HUMAN-ROBOT INTERACTION

The control of physical human-robot interaction is a challenging area of research, and a number of research projects have proposed force-feedback control using external force control algorithms to alter the robot trajectory. These can be categorized based upon the relationship between the position and/or velocity of the robot end effector and the force applied [Zeng and Hemami, 1997], as a form of active compliance for particular applications [Mason, 1981]. Position-based force control involves the difference between desired and actual interactive force and an equivalent position in the force-controlled direction. The robot's behaviour under force control is influenced by the interactive force exerted on the system [De Schutter and Van Brussel, 1988], and its ability to simultaneously control the robot so as to respond to positional variations in the contact surface. However, the accuracy and reliability of robot force control is limited mainly by the resolution of the force sensor and the precision of robot positioning.

4.1 Fundamentals of Robot Force Control

The term 'compliant motion' has been defined as a manipulation task which specifies the contact force between a robot manipulator and its environment. The positions of the robot end effector are appropriately controlled by the interactive forces whilst executing a physical interaction task. Motion control can be classified into two key groups: passive compliance and active compliance. Passive compliant motion modifies the position of the robot end effector by interaction forces of the contact and makes use of the compliance inherent in the robot structure. Active compliant motion uses force feedback to provide appropriately precise programmable robot movements [Mason, 1981]. Active compliance is used to ensure effective control and overcome the disadvantages of passive compliance.

Active compliance allows the robot end effector to be strategically controlled based on external force signals to control the robot's response can be grouped into two main categories: force and impedance control. In force control, both interactive force and robot position are controlled together, where the trajectory of the robot can be commanded using force feedback control. This is called position/force control or admittance control. In impedance control, the mechanical impedance of a robot end effector can be adjusted using various relationships between the interactive force and robot position. This method is based upon control of the difference between the desired and actual position, and the force feedback is required to facilitate impedance behaviour.

This section explains how compliant force/position control can be implemented in human-robot interactive tasks. De Schutter and Van Brussel [1988] reported that a fundamental requirement for the success of human-robot cooperation is the capability of the robot to handle the physical contact between the robot and the human. To modify the robot's trajectory, this method was successfully implemented on a PUMA 560 robot under several environmental constraints [Degoulange et al. 1993]. According to the tests conducted, the efficiency of system behaviour was closely related to the appropriate achievement of the force control gains. The most crucial aspect in this control method applied to the HRI task is to achieve a suitable compromise between the system response and stability, where the response time was required to be as short as possible. It should be noted that the system oscillations will be introduced when the control gains are too high.

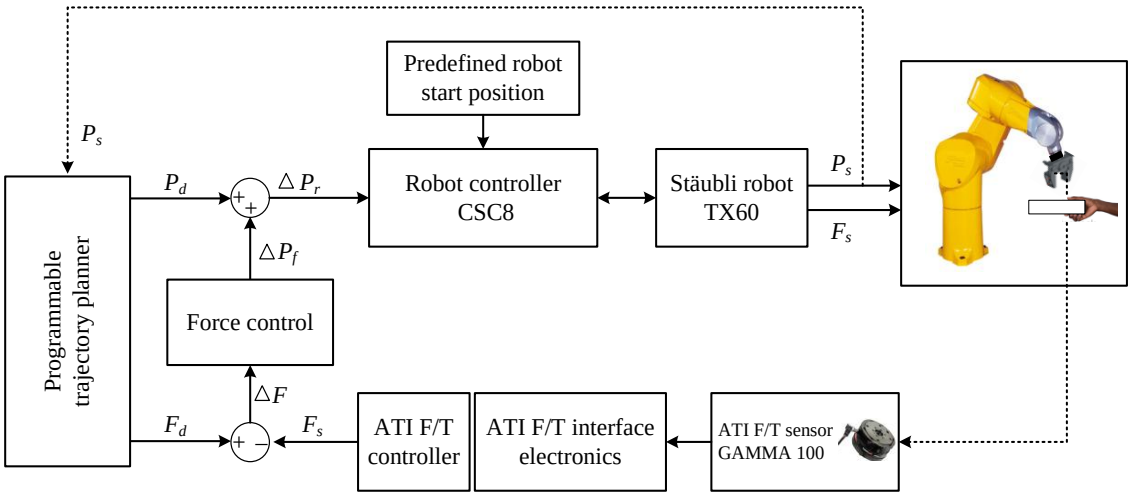

Figure 4.1 External force control for a human-robot interactive task based on De Schutter and Van Brussel [1988]

External force control provides effective stability when switching between position and force control, where the control outputs are defined in Cartesian coordinates, and can be directly transferred to the robot position control loop. In this study a 6-DOF Stäubli TX60 robot manipulator arm was used, as the ALTER real-time control (using the Cartesian space) provides the ability to modify the robot path externally, in real-time. The external force control developed for the human-robot interactive task is schematically illustrated in Figure 4.. Once the human operator physically grasps the object held by the robot manipulator, the interaction force (F_s) measured by an ATI F/T sensor is simultaneously compared with the desired force (F_d). A sequence of robot incremental positions (ΔP_r) are transmitted to the robot controller to modify the robot's instantaneous position (P_d) according to the force control outputs (ΔP_f) which are computed, based on an appropriate robot force control algorithm.

4.2 Implementation of Force and Velocity Robot Control for HRI

It is a crucial requirement for the success of effective human-robot interaction that the HRI control system operates in real-time. When an intelligent robot is required to work with a human in order to accomplish human-robot interactive (HRI) tasks, the robot should work collaboratively with the operator, where the physical communication between them, i.e. the interactive force and velocity of the object whilst performing the task, are seamless and transparent. This section describes the design and implementation of the force and velocity control of the robotic system in HRI object handover tasks.

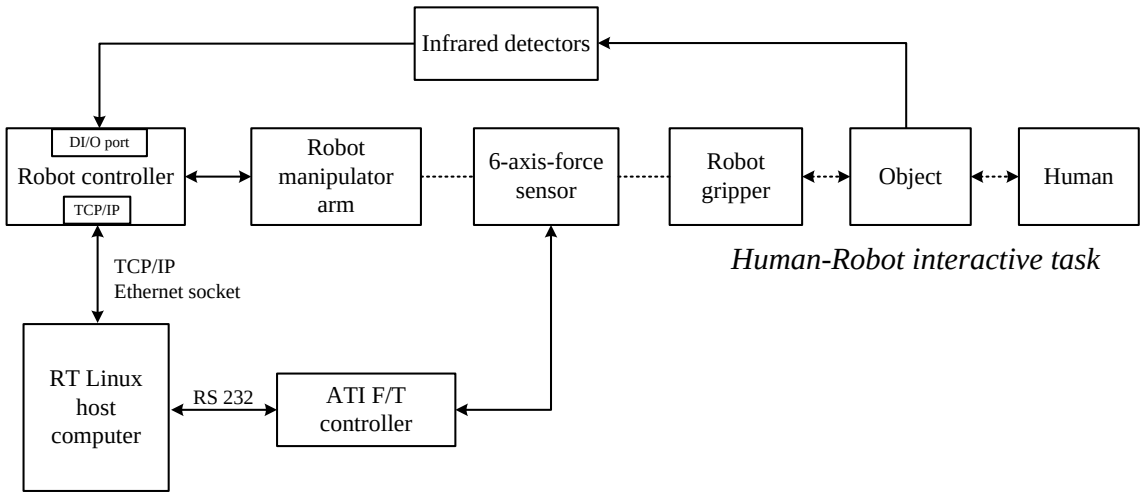

Figure 4.2 Overall schematic diagram of the proposed HRI system.

The design of the robotic control system should be capable of manipulating and transferring an object to a human in a timely and reliable manner. Figure 4.2 illustrates an overall schematic diagram of the human-robot interactive system, which has two key modes: object tracking and external force feedback control. The location and corresponding speed of the object are tracked by a set of infrared detectors, and the interactive force between the human and robot (via the robot end effector) is measured using a 6-axis force/torque sensor. The Stäubli robot controller communicates in real-time with an external PC via an Ethernet port using the TCP/IP protocol. The external PC (running under Linux) processes data transmitted by the sensors and generates changes in incremental position to modify the robot's path using an appropriate control algorithm. The conceptual design of the HRI control system was developed to meet the above requirements and is summarised below. A detailed description of both the hardware and software configuration and integration is given in Appendix D.

From a review of the commercial robot and manipulator systems which can satisfy the HRI requirements, a six-DOF Stäubli robot manipulator arm (TX60) with CS8C controller was chosen as it has the capability to perform real-time path control (which can be updated every 4ms) and also supports the transmission control protocol/ internet protocol (TCP/IP) interface. A pneumatic-two-finger gripper with three- point contact was designed, and is controlled electrically via a digital bidirectional input/output board of the Stäubli TX60 robot (CSC8) controller. A 6-axis ATI *Gamma* force/torque sensor with a stand-alone ATI controller was used to measure the interactive force between the human participant and robot manipulator arm during joint handling of an object, and was positioned between the robot end effector and the robot gripper.

For an appropriate object tracking system, infrared detectors were employed to estimate the velocity of the object in order to allow the robot to plan and execute a trajectory to the perceived transfer location. A real-time Linux PC with an Intel® Core TM 2 Duo CPU processor with a clock speed of 3GHz, which supports multi-task execution using the multi-tasking kernel to simultaneously run user programs, was used to process all sensor information, the robot force and velocity control, and the real-time updating of new targets for the modification of the robot's path. Transmit control protocol and internet protocol (TCP/IP) was established in the communication between the external real-time Linux PC and the CS8C controller using VAL3 ALTER communication.

Software development is one of the key requirements in the HRI system design. Two crucial software operating systems are used, consisting of the real-time Linux OS and Stäubli VAL3, in which the TCP/IP protocol was employed to provide communication between the Stäubli robot and the host PC running RT Linux. The CS8C Stäubli robot controller was selected to be the network server and the PC was adopted as the network client. The data transfer speed rate over TCP/IP was initially arranged at 100Mbit/s, and it can be guaranteed that all data transferred is accurately and reliably delivered due to the extensive error checking mechanisms provided.

Appendix D outlines the software flow diagrams, commands and functions for C programs in the RT Linux OS and VAL3 programs. There are four key programs running synchronously, which have to be strictly enforced with the synchronized communication rate at 4ms (250Hz), as follows:

1) Multi-axis force/torque sensor data acquisition: to receive the digitized force/ torque values transmitted from the ATI controller,
2) TCP/IP data acquisition: for communication between the RT Linux PC and the CS8C Stäubli robot controller using the TCP/IP protocol,
3) ALTER motion task: to control the real-time modification of the robot path using the ALTER motion command, and
4) Object velocity tracking task: involving the tracking of object velocity.

The system proposed has been designed and developed to meet the requirements specified for human-robot interaction tasks. An evaluation of the robot control system was performed to ensure its safe and timely operational characteristics specifically for the HRI application. The ATI *Gamma* multi-axis force/torque sensor and ALTER real-time control path systems were evaluated to quantify their effectiveness, and the results indicated satisfactorily stable performance of the external robot force control system, as detailed in Appendix D.

After an extensive review of relevant academic research, it was decided to initially apply simple proportional plus integral (PI) control. The PI robot force control algorithm is preferable to proportional-integral-derivative (PID) control since the derivative term is sensitive to noise and this could lead to a destabilizing effect on the HRI system. Although, the derivative gain (K_D) which gives a reduction in the system

overshoot and settling time has been removed, the overshoot response can be controlled using an appropriate proportional gain [Stankovic, 1988]. As suggested by De Schutter and Van Brussel [1988], Volpe and Khosla [1993] and Zeng and Hemami [1997], proportional integral (PI) control is appropriate for robot force/position control in order to provide the smallest possible force control error, and because this technique facilitates an increase in the accuracy and stability of the control system.

The two behavioural modules have different characteristic functions for PI closed-loop control. Increasing proportional gain, K_P, gives a decrease in the system rise time, and integral gain, K_I, is used to eliminate the system steady state error. However, optimized proportional integral control is normally employed to complete a specific task with satisfactory performance, and also has disadvantages in terms of high starting overshoot, sensitivity to controller gains and steady-state error [Khuntia et al. 2009]. To overcome these limitations, fuzzy logic control (FLC), which has higher capability dealing with non-linear dynamic nature of human behaviour and does not rely on complicated mathematical models, was adopted, as explained in the following sections.

4.3 Proportional Plus Integral (PI) Control

Proportional plus integral and derivative (PID) control and its combination such as P, PI and PD algorithms are most widely utilized in industrial process control applications because they are relatively easy to implement and no other types of control can match its simplicity and clear functionality [Vaishnav and Khan, 2007]. PID control is used for a wide range of applications, such as motor speed or position control, flight control, temperature control, and robot position control, whose relevant continuous equations are detailed in Appendix D. However, for the significant reasons mentioned above, proportional integral (PI) control was adopted in robot force and velocity control in the HRI study. In addition, this method is also often used in many practical applications with large disturbances and noise which are presented during operation of the processes because their stability is not containing the derivative term which is sensitive to noise [Zeng and Hemami, 1997].

4.3.1 Implementation of PI Force Control

An incremental discrete-time PI control algorithm with sampling time period τ and the discrete time interval k can be calculated by applying the equations 4.1 and 4.2. A detailed description of this algorithm is given in Appendix D for completeness.

$$u(k) = u(k-1) + k_P[e(k) - e(k-1)] + k_I e(k) \tag{4.1}$$

$$e(k) = f_d - f_s \tag{4.2}$$

where, $u(t)$ is the PI control output,

K_P is proportional gain,

K_I is integral gain,

f_d is the desired force, which was initially defined as 0, and

f_s is the actual force (measured by the ATI force sensor).

The PI force control implementation is chosen as shown in Figure 4.3, where e is the error defined as the difference in magnitude between the desired (f_d) and actual (f_s) forces, while de is the change in error (e). The PI control output was determined as the incremental displacement (ΔU_k) modified by the previous computed value of ΔU_{k-1}, which is scaled before being transferred to the Tx60 Stäubli robot's ALTER function to modify its trajectory.

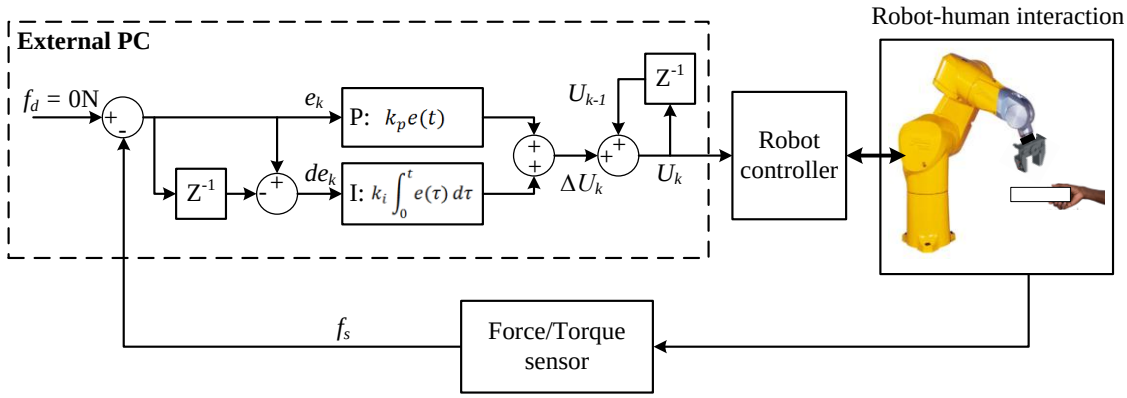

Figure 4.3 Schematic diagram of the force control strategy based on PI control

4.3.2 Implementation of PI Velocity Control

In the case of the human *handler* transferring the object to the robot, the robot has to first estimate the object's velocity and generate the perceived transfer position before grasping the object. A PI control algorithm, as shown in Figure 4.4, was used to control the robot's end effector velocity to facilitate the effective object handover task. The output of the velocity PI control was assumed to be the incremental position (ΔU_k) in three dimensions, where incremental PI velocity control can be calculated by applying Equation 4.1. The input *e* of PI control was generated as the difference in magnitude between the desired (v_d) and actual (v_s) velocities, as expressed in the following equation, and the input *de* is the change in error (*e*).

$$e(k) = v_d - v_s \tag{4.3}$$

where, v_d is the desired velocity, and

v_s is the actual velocity adopted by the robot controller.

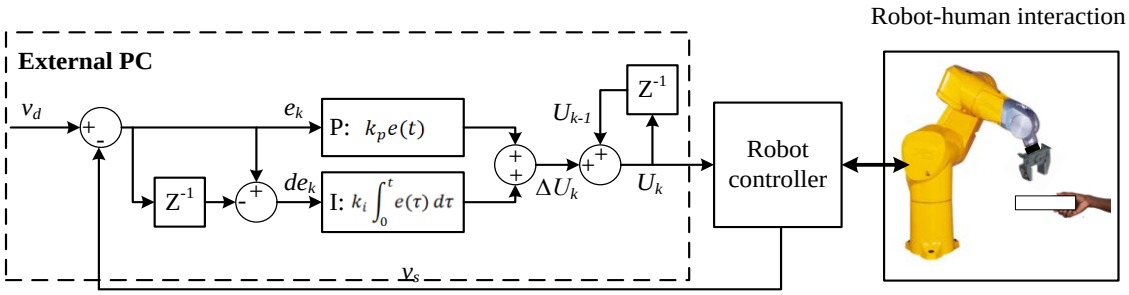

Figure 4.4 Schematic diagram of the velocity control strategy based on PI control

Proportional integral control gain tuning is the important stage to achieve an effective control response. Various techniques for PID gain tuning have been developed, such as the Ziegler-Nichols, Cohen-Coon, Chien-Hrones-Reswick or manual techniques. However, as complicated robot force control, once the proportional gain is set to an ultimate upper limit at which the system output starts to oscillating, this could cause the robot to venture into unstable regions and easily damage the robot manipulator, ATI *Gamma* force/torque sensor or the operator's hand. A trial and error tuning method, based on a virtual crank-turning preliminary experiment was adopted to establish appropriate PI gains for both the robot's force and velocity control.

The virtual crank-turning test is detailed in Appendix D. The ATI *Gamma* force/torque sensor was mounted between the robot end effector and gripper in order to measure the tangential (F_T) and radial (F_R) forces applied by a human participant. The RT Linux PC was also used to generate a set of incremental positions proportional to force applied and to update the robot trajectory every 4ms. The procedure of the virtual crank-turning task permitted the robot to move with a constrained trajectory around the virtual crank radius, at a diameter of 200mm, in a clockwise direction. The task was required to commence at the proposed home position, and the participant was required to manipulate the robot gripper around the circular path, whilst attempting to minimize the radial force (F_R). The performance of the system response can be evaluated in terms of the variation in the radial forces, in which a lower magnitude is considered to provide improved performance of the system.

In summary, the gain tuning for PI control applied to the robot's velocity and force control was implemented. Based on the results of the experiments, it can be concluded that the best performance as specified by the *E_RMS* of the radial force is observed with proportional and integral gains of K_P = 0.10 and K_I = 0.005, which values were subsequently implemented in the human-robot handover task.

4.4 Fuzzy Logic Control

Fuzzy logic control (FLC) introduced by Zadeh [1956] is normally used to control non-linear or complex systems based on 'IF-THEN' rules. It is a useful control method due to its ability to capture human qualitative control into control algorithms for the fuzzy rules. The design of FLC starts with the development of a fuzzy set, which is a set of elements having degrees of membership and clearly defined boundaries. The fuzzy set allows the gradual assessment of the membership of elements by representing the membership function in the interval [0, 1]. A membership function (μ) defines each degree of a membership value between 0 and 1, in which the fuzzy intersection (AND), union (OR) and complement (NOT) are fundamental logical operations of FLC. IF-THEN rules are designed based on knowledge of how good control of the system can be achieved, and are used to formulate the conditional statements comprising FLC. The fuzzy inference emulates decision-making by applying the rule base, and then the defuzzification process is applied to convert the results into a fuzzy output.

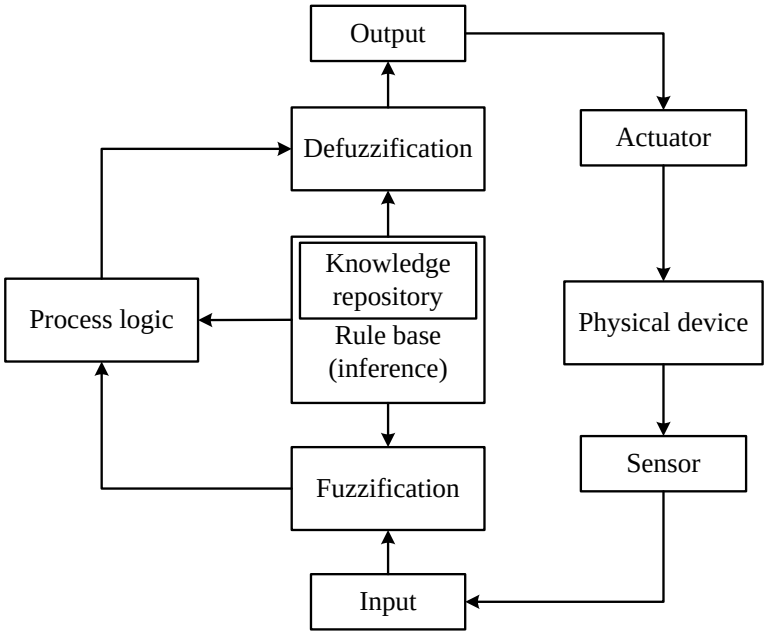

Figure 4.5 Building blocks of fuzzy logic control [Cox 1994]

Figure 4.5 demonstrates the process of a design of fuzzy logic control (FCL) system. The input signals are conveyed by a sensor which measures the physical environment. These are then converted and fuzzified into the fuzzy representation. A defuzzification technique is used to calculate output values for each set of input variables based on the rules proposed in the knowledge repository. The output signal is transferred to adjust the actuator in order to change the physical system. The basic structure of the FLC consists of the fuzzification, fuzzy rule-base, fuzzy inference and defuzzification.

Fuzzification of system input variables is the process of the scale transformation of the input data based on their membership functions, and is a process of changing the crisp values into grades of their membership functions in the interval between 0 and 1. Several shapes of the membership function are identified, such as triangular, trapezoidal, Gaussian or bell-shaped. Figure 4.6 illustrates the membership function (μ) on ZE (zero), NL (negative large) and PL (positive large) curves. If the crisp value (Error) of the fuzzy set is set as -0.2, and then the membership functions of negative large (NL) and zero (ZE) can be rated as 0.07 and 0.8 respectively, via a Gaussian-shaped evaluation.

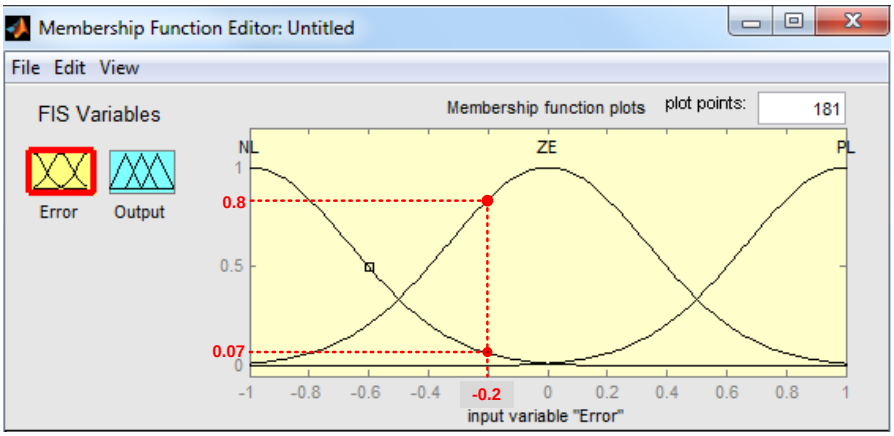

Figure 4.6 An example of a fuzzy set

Fuzzy rule-base is made up of two key parts, consisting of IF and THEN components. The capability of fuzzy logic control depends on the design of the fuzzy rules developed by human operators based on their experience. It can be defined as:

$$\text{If input}_1 \text{ is } A \text{ and } input_2 \text{ is } B \text{ then } output_1 \text{ is } C \tag{4.4}$$

where, A,B and C are linguistic values of the fuzzy sets $input_1$, $input_2$ and $output_1$ respectively.

For example, applying the IF-ELSE rule-base for a robot force control system which is composed of two inputs (force error and force error change) and an output (robot velocity), based on Mamdani [1947] may give the following rule:

rule: if force error (E) is positive big (PB) and force error change (ΔE) is positive big (PB), then robot velocity is positive big (PB) (4.5)

Whereas, based on the technique introduced by Sugeno [1988], the rule-base may be written as:

rule: if force error (E) is positive big (PB) and force error change (ΔE) is positive big (PB), then robot velocity = $a_1(error) + b_1\left(\frac{d(error)}{dt}\right) + c_1$ (4.6)

Fuzzy inference is the process of formulating inputs into an output based on the fuzzy membership functions and the decisions of the rule-base. It forms an intermediate stage between FLC fuzzification and defuzzification, and in this step the logic operations (AND, OR and NOT) are involved. Using the AND operation gives a minimum value and the OR operation provides a maximum value. Fuzzy inference can be implemented using two methods, consisting of max-min and max-product fuzzy inference, which can be expressed as in Equations 4.7 and 4.8 [Ross, 2004]:

$$\mu_{implied}{}^{k} = max^{k}\{\min[\mu_{antecedent}{}^{k}(i),\ \mu_{consequent}(j)]\} \tag{4.7}$$

$$\mu_{implied}{}^{k} = max^{k}\{\mu_{antecedent}{}^{k}(i).\ \mu_{consequent}(j)\} \tag{4.8}$$

where, $k = 1, 2, 3, \ldots r$ (number of fuzzy rules)

These two different techniques of fuzzy inference implementation are schematically explained in Figure 4.7.

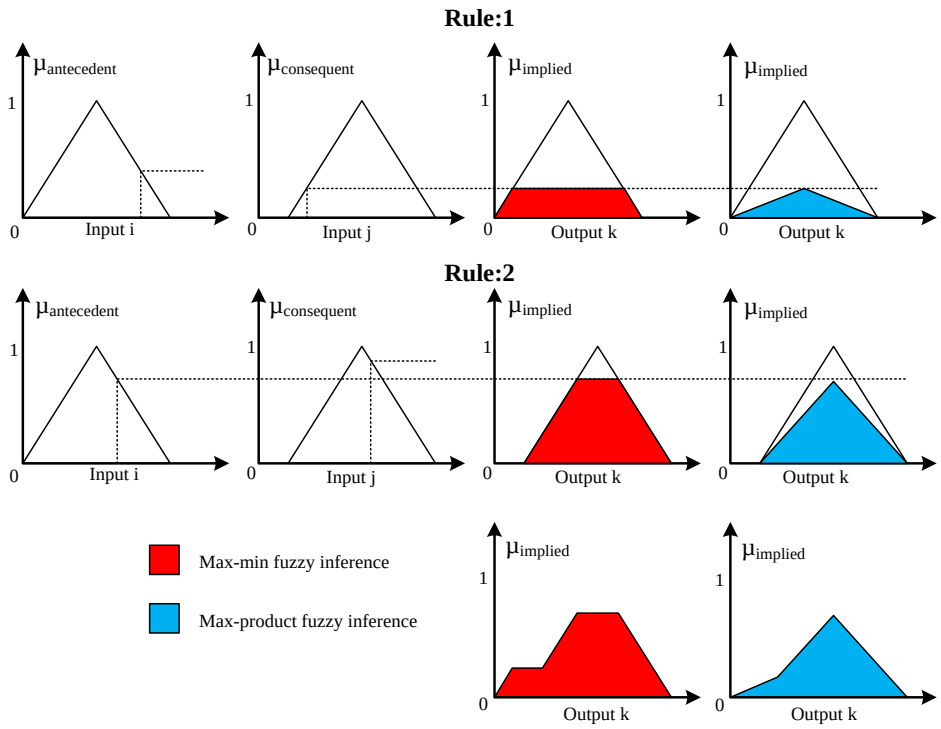

Figure 4.7 Fuzzy max-min and max-product inference methods

Defuzzification is the method of weighting and combining a number of calculated results derived by fuzzy inference and evaluating for each fuzzy output given as a single crisp value. In other words, the output of the fuzzy process can be computed by the fuzzy membership functions in order to convert fuzzy to precise quantities. Several techniques can be implemented, such as centroid, weight average, centre of sum, maximum membership and mean-max membership methods. However, the centroid method developed by Sugeno [1988] is a common, useful and most popular technique [Patyra and Mlynek, 1996], in which each effective output can be represented by the centre of the area under the curve and expressed as in Equation 4.9:

$$\mu^* = \frac{\int y.\mu(y)dy}{\int \mu(y)dy} \tag{4.9}$$

where, $\mu(y)$ is the membership function of *y*, and
$\int \mu(y)dy$ is the area of the fuzzy output.

Figure 4.8 illustrates the defuzzification process based on the centroid technique.

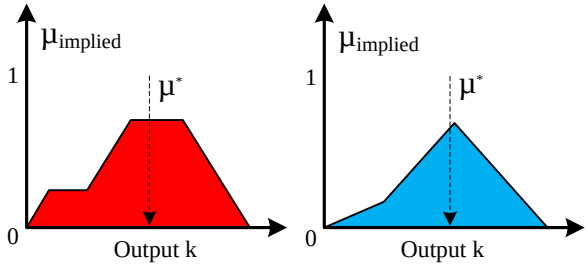

Figure 4.8 Defuzzification based on the centroid technique

4.4.1 Implementation of Fuzzy Logic Control for Robot Force Control

Figure 4.9 shows how FLC can be developed and implemented for robot force control based on the external force applied to the robot end effector, from which control outputs from the system were generated as a set of incremental displacements (ΔU) in three dimensions and sent to the robot's ALTER function. The fuzzy inputs were initially required to be identified in terms of the external force error (*e*) and change in the error (*de*), where f and f_d are the actual and desired forces respectively. Here f_d was defined as '0'.

$$e_k = f_d - f_s \tag{4.10}$$

$$de_k = e_k - e_{k-1} \tag{4.11}$$

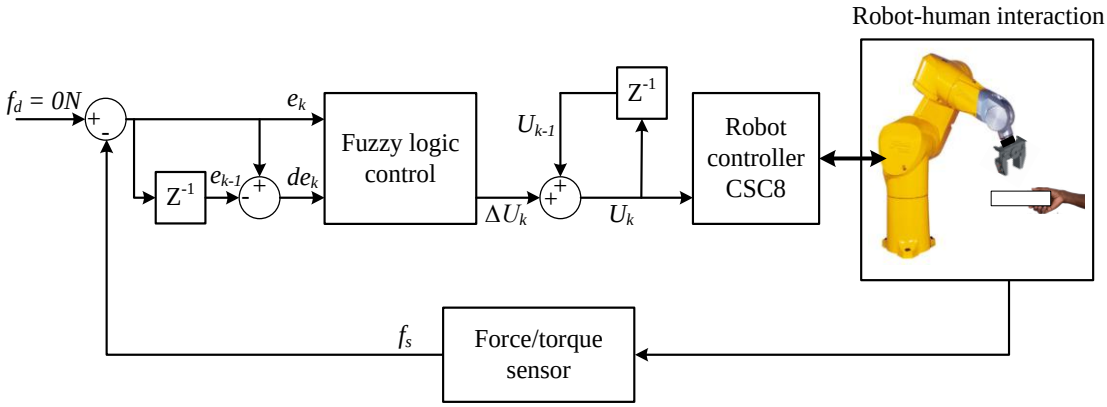

Figure 4.9 Schematic diagram of the force control strategy based on FLC

The output of the control system is the incremental displacement (ΔU). However, U is the displacement directly applied for the robot's ALTER real-time path control via TCP/IP communication.

$$U_k = U_{k-1} - \Delta U_k \tag{4.12}$$

The crisp sets of the fuzzy inputs and outputs have to be converted into linguistic forms using fuzzy membership functions. The input and output variables were normalized into five and seven linguistic levels respectively, in which the following notation is used:

NL is negative large,
NM is negative medium,
NS is negative small,
Ze is zero,
PS is positive small,
PM is positive medium, and
PL is positive large.

Figures 4.10(a) and (b) illustrate the membership functions for the inputs *e* and *de* respectively. Here the suitable membership functions of both inputs are established as (-5N, 5N) and (-0.5N, 0.5N) respectively and the degree of membership functions (μ) varies between 0 (non-member) and 1 (full member). There are five geometric membership functions of the input *e*, including NL (-5N,-2N), NS (-4N, 0N), ZE (-2N, 2N), PS (0N, 4N) and PL (2N, 5N) respectively. Additionally, five geometric membership functions adopted for the input *de* consist of NL (-0.5N,-0.2N), NS (-0.4N, 0N), ZE (-0.2N, 0.2N), PS (0N, 0.4N) and PL (0.2N, 0.5N).

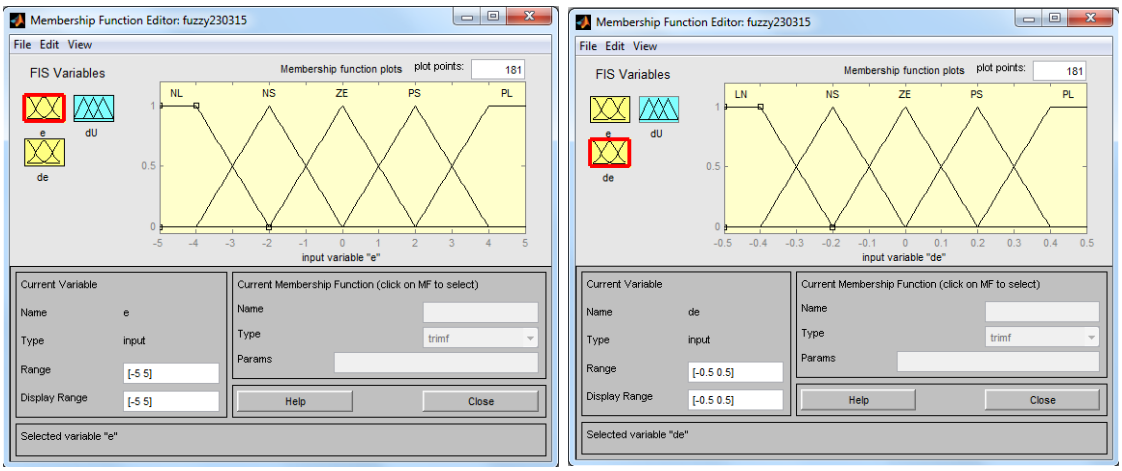

(a) (b)

Figure 4.10 Membership functions of (a) error *e* and (b) change of error *de* used for robot force control

Figure 4.11 demonstrates the membership functions for the output ΔU, where the universe of discourse of the output is defined as (-0.012mm, 0.012mm) and the degree of membership function (μ) varies between 0 and 1 representing non-member and full member respectively.

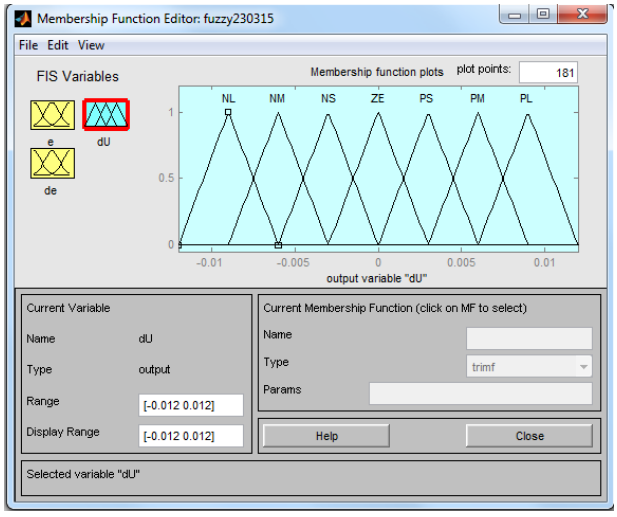

Figure 4.11 Membership function of the system output ΔU (incremental displacement) used for the robot force control

The rule base of the fuzzy logic control, as shown in Table 4.1, was developed based on the knowledge and experience of a system developer. In the case of negative large (NL) and positive large (PL) outputs, it can be seen that the large incremental displacements (ΔU_k) are required in the system. If positive and negative outputs ($+\Delta U_k$ and $-\Delta U_k$,) are introduced, this means that the displacements (U) directly applied for the robot's ALTER command are required to increase or decrease respectively to minimize the force error. On the other hand, in the case of negative small (NS) and positive small (PS) outputs, the small incremental displacements (ΔU_k) are required. Finally, if ΔU_k is conveyed as zero (ZE), the most recent displacement (U_{k-1}) is maintained.

Table 4.1 Fuzzy rule base used for robot force control

de \ *e*	NL	NS	ZE	PS	PL
NL	NL	NL	ZE	PS	PM
NS	NL	NL	ZE	PM	PL
ZE	NL	NL	ZE	PL	PL
PS	NL	NM	ZE	PL	PL
PL	NM	NS	ZE	PL	PL

The fuzzy logic toolbox in Matlab was used to develop the FLC robot force control. It also provides the rule base viewer, which can represent the entire output surface of the system as a three-dimensional curve. Figure 4.12(a) illustrates the surface viewer with two inputs *e* and *de* and one output ΔU. For the evaluation of the fuzzy outputs based on this rule base using Mamdani fuzzy inference systems, the centroid defuzzification method which calculates the centroid of the output area was utilized. Figure 4.12(b) displays the defuzzification outputs using the Matlab fuzzy logic toolbox. It can emulate the decision-making based on applying the rule base and convert the fuzzy outputs by entering specific input values or clicking to adjust each input. Subsequently, the aggregate outputs are carried out at the third column. For example, if the error (*e*) and change of error (*de*) are defined respectively as 1.5N and 0.15N, then the fuzzy output (ΔU) is delivered as 0.006mm.

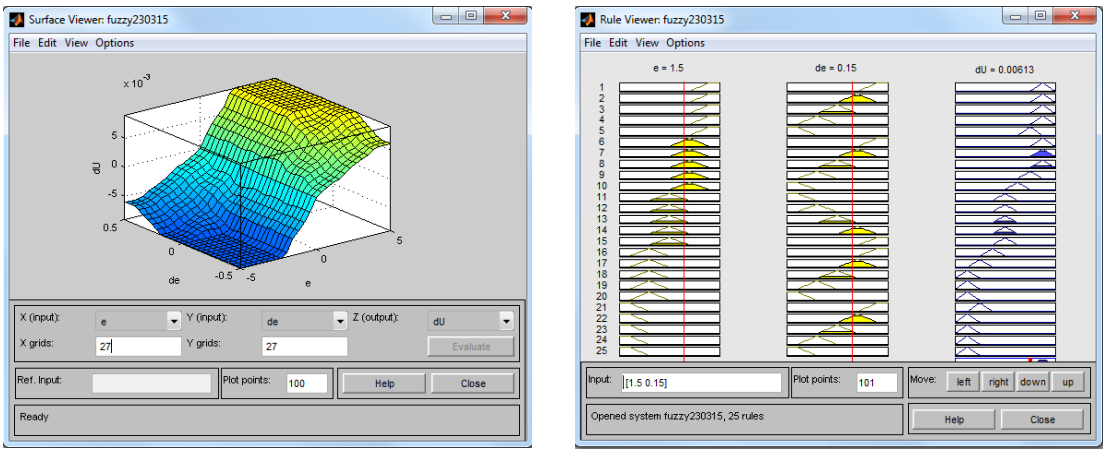

(a) (b)

Figure 4.12 (a) Surface viewer with two inputs *e* and *de* and one output Δ*U*; (b) defuzzification outputs computed by the Matlab fuzzy logic toolbox

4.4.2 Implementation of Fuzzy Logic Control for Robot Velocity Control

In the case of a human-to-robot handover task, it is necessary to control the velocity of the robot's end effector using the fuzzy logic control method in order to avoid jerky movements occurring whilst performing the task. Figure 4.13 shows how FLC can be applied to the system of robot velocity control in the human-to-robot handover task. The robot's velocity control was developed based on the velocity profile provided in the preliminary test of the human-human handover task. The CS8C robot controller was used to transfer the velocity data from the robot's end effector to the RT Linux PC, and the FLC outputs were generated as a set of incremental displacements (Δ*U*) in three dimensions and transmitted via the robot's ALTER function. Two fuzzy inputs were defined as the velocity error (e_v) and change in the error (de_v), where variables v_d and v_a are the desired and actual velocities respectively.

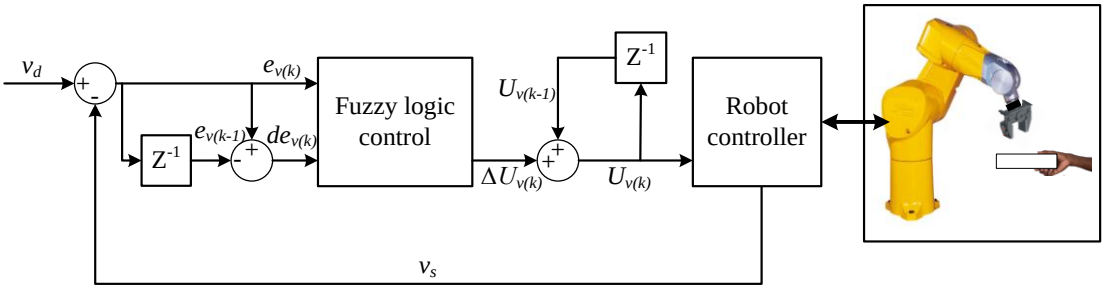

Figure 4.13 Schematic diagram of the velocity control strategy based on FLC

$$e_{v(k)} = v_d - v_s \tag{4.13}$$

$$de_{v(k)} = e_{v(k)} - e_{v(k-1)} \tag{4.14}$$

The fuzzy output is generated as an incremental displacement (ΔU_v). However, the parameter U is the displacement directly implemented for the robot's ALTER real-time path control via TCP/IP communication.

$$U_k = U_{k-1} - \Delta U_k \tag{4.15}$$

Figures 4.14(a) and (b) illustrate the crisp sets of the two fuzzy inputs e_v and de_v converted into linguistic form using fuzzy membership functions. The appropriate membership functions of the inputs are established as (-60mm/s, 60mm/s) and (-0.5mm/s, 0.5mm/s), while the degree of membership functions (μ) varies between 0 (non-member) and 1 (full member).

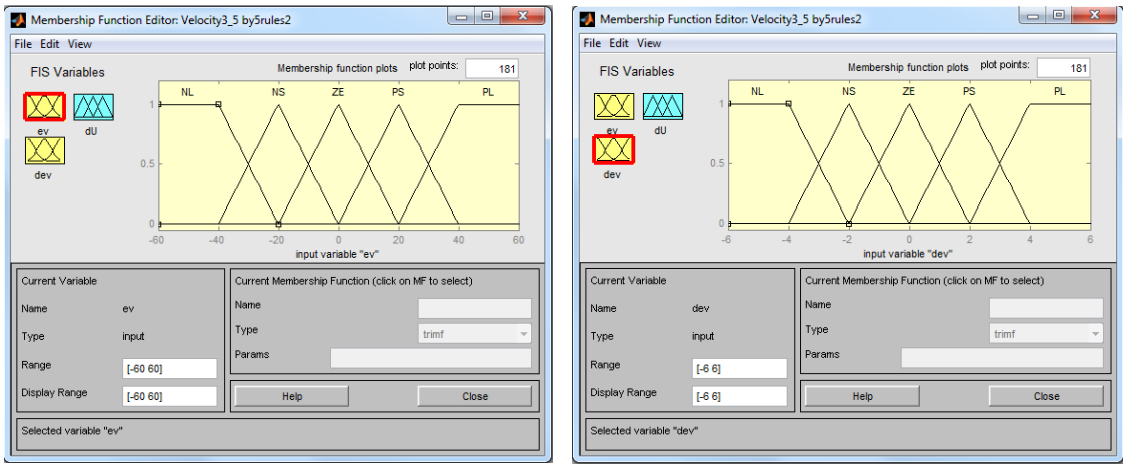

(a) (b)

Figure 4.14 Membership functions of (a) error *e* and (b) change of error *de* used for robot velocity control

Figure 4.15 demonstrates the membership functions for the output ΔU defined as the incremental displacement, in which the universe of discourse of the output is established as (-0.012mm, 0.012mm) and the degree of membership function (μ) varies between 0 and 1 representing non-member and full member respectively.

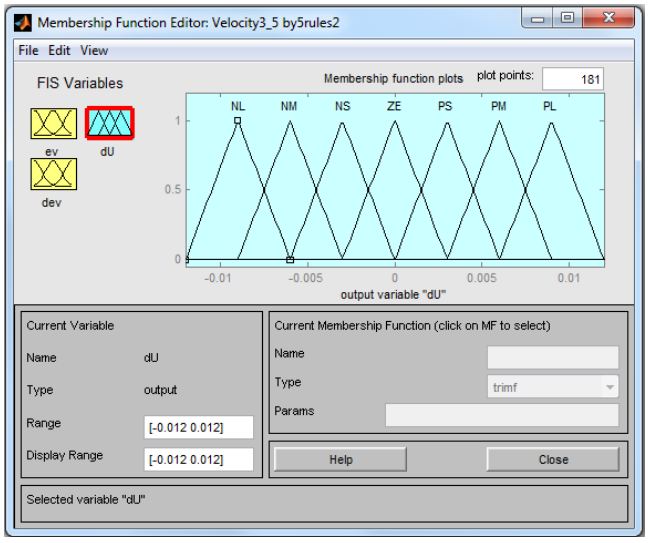

Figure 4.15 Membership function of the system output ΔU (incremental displacement) used for robot velocity control

The rule base of the FLC was developed as shown in Table 4.2. Negative large (NL) and positive large (PL) outputs represent large amount incremental displacements (ΔU_k) needed in the system, where the positive ΔUresults in the increment of the displacement (U) implemented for the robot's ALTER real-time path control, and vice versa. If ΔU_k is carried out as zero (ZE), the most recent displacement (U_{k-1}) dose not need to be changed.

Table 4.2 Fuzzy rule base used for robot velocity control

de \ *e*	NL	NS	ZE	PS	PL
NL	NL	NL	NS	NS	ZE
NS	NL	NM	ZE	ZE	PS
ZE	NM	NS	ZE	PS	PM
PS	NS	ZE	ZE	PM	PL
PL	ZE	PS	PS	PL	PL

Again, the fuzzy logic toolbox software in Matlab was used to achieve the FLC development for robot force control. Figure 4.16(a) shows the surface viewer with two inputs e_v and de_v and one output ΔU_v. The centroid defuzzification method was used to evaluate the fuzzy outputs based on this rule base using Mamdani fuzzy inference systems. Figure 4.16(b) presents the defuzzification outputs generated by the Matlab fuzzy logic toolbox. For example, if the error (e) and change of error (de) are assigned as 30 and 3mm/s respectively, then the aggregate outputs (ΔU_v) are 0.0075mm.

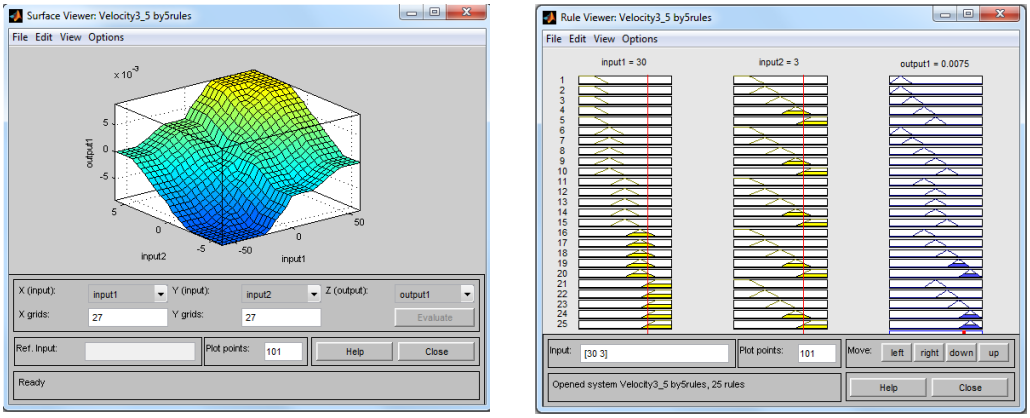

(a) (b)

Figure 4.16(a) Surface viewer with two inputs *e* and *de* and one output ΔU; (b) defuzzification outputs computed by the Matlab fuzzy logic toolbox

4.5 Safety Issues in Human-Robot Interaction

Safety is a key issue in human-robot interaction and one of the principal challenges in the development of the human-robot handover task because any failures which occur might become very critical. Several studies have investigated approaches related to safety and reliability issues in human-centred-robots, which include human factors, risk assessment, hazard analysis, and technologies for HRI safety. Accidents in HRI can be categorized in three groups: engineering error such as lost connections among parts or electronic faults, human operator mistakes such as accidents, fatigue or inobservance; and poor environmental conditions such as poor sensing in difficult weather or extreme temperatures [Vasic and Billard, 2013]. Duchemin et al. [2004] and Kulic and Croft [2005] have suggested conceptual designs to improve safety factors in a robot real-time controller applied for human-robot interaction. Two key features can be developed based on control software in order to facilitate an effective real-time control system. These consist of a validation phase and an appropriate emergency stop which can be activated as soon as any error occurs.

In this HRI task, the safety issues can be addressed in terms of hardware and software components as follows. Firstly, a safeguarded zone was introduced to conduct a safety strategy in the HRI test [Baerveldt, 1992]. If an unauthorised human enters the safeguarded zone, then the Stäubli robot will initiate an immediate emergency stop. The human-robot handover task was first established by setting up server-client communication via TCP/IP. The robot server has to create and bind a socket to a port, and then listen to the client acceptance acknowledgement of the connection from the RT-Linux PC. When bi-directional communication has been established, for safety reasons, the system requires an enter button to be pressed again before the HRI test is authorized. The speed of the Stäubli robot allowed in the human-robot handover test was limited to 150mm/s, and the robot working area was also optimized in order to minimize the risk of an injury occurring during HRI execution. If the robot was required to move more than the velocity or out of the range proposed, the ALTER command would be suddenly terminated and also the robot gripper would be immediately activated to open its fingers using a signal conditioning box, as shown in Figure 4.17. In addition, Figure 4.18 show stand-alone and manual control panel (MCP) emergency stop buttons, which can be manually activated by the human operator when accidents are detected.

Figure 4.17 A stand-alone signal conditioning box for the robot gripper located on the robot controller

Figure 4.18 Emergency stop buttons from MCP and external control box

Software safety has been considered to manage the risk to a human working together with the robot, as schematically shown in Figure 4.19. A timeout, which indicates the period of time allowed for a specified task to take place, was assigned for the serial and TCP/IP communication. The waits for data transfer; however, if the transmission has not been completed after the timeout has elapsed, then the communication will be terminated. Furthermore, if the process of information transmission along with the sampling rate of 4ms of the TCP/IP data communication or force sensor data acquisition fail; subsequently, the emergency indicator will be activated, while the TCP/IP communication and ALTER function will be immediately terminated.

As suggested by Traver et al. [2000], monitoring the interactive force feedback signal during the interaction provides valuable information about the safety of the interaction and this was also established. Three safety thresholds for all interactive force signals in three dimensions were defined. If force data (f_x, f_y and f_z) carried out from the ATI *Gamma* force sensor are greater than 30% of the threshold (f_{thr}), then the emergency light will be activated. However, if the measured forces are more than 50% of the limits, the emergency light will blink, and the robot gripper will be suddenly operated to release the object in order to ensure the safety of the human participant during the object handover process. In the meantime, the TCP/IP communication and ALTER function will be also terminated.

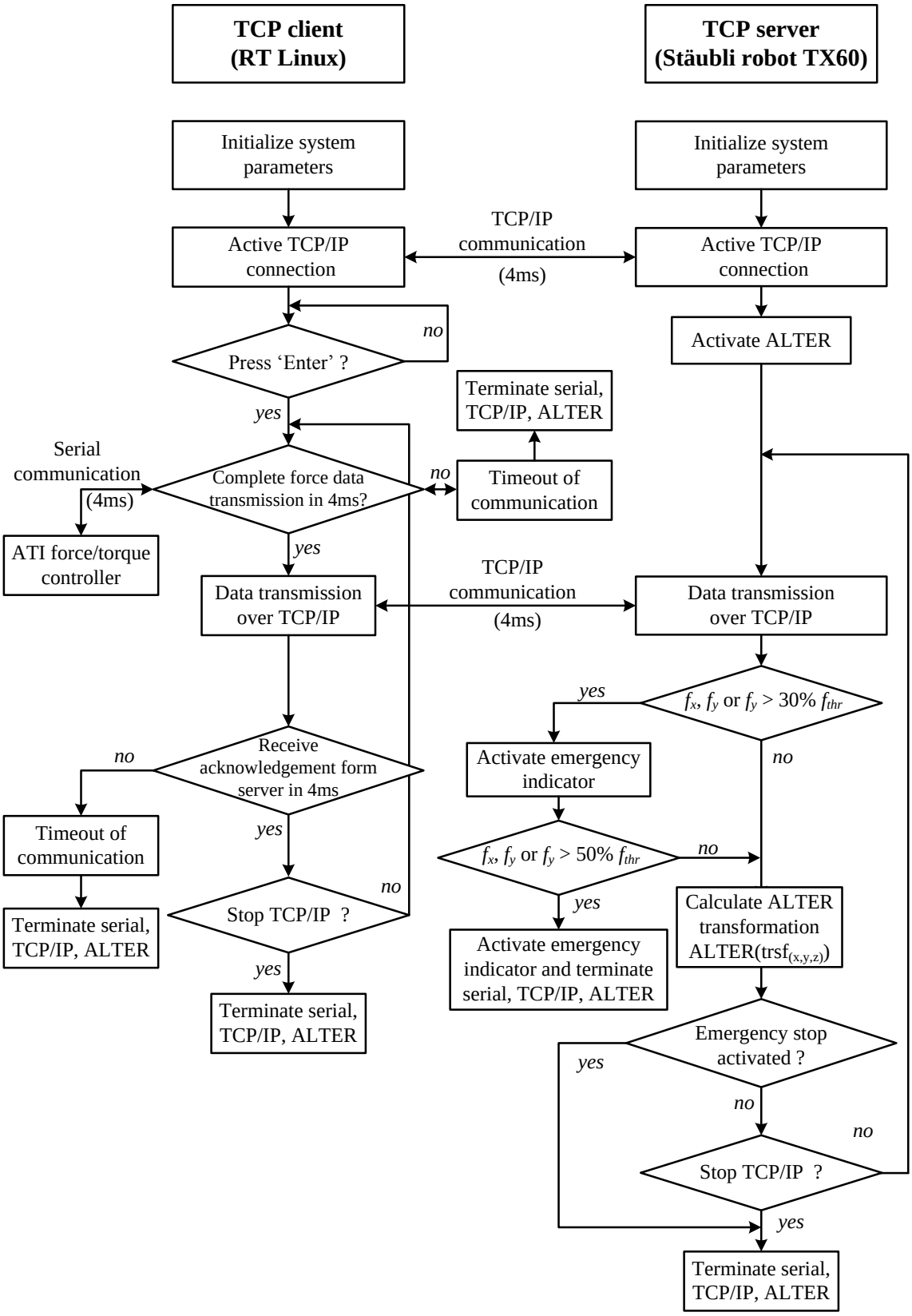

Figure 4.19 Flowchart of the safety software development in the human-human handover task

4.6 Summary

This chapter has focused on developing effective force and velocity control algorithms for the Stäubli robot manipulator, based on an understanding of the human physical characteristics in substantive human-human object handover experiments, as proposed in Chapter 3. The HRI hardware and software architectures have been discussed, including those for the Stäubli robot (TX60), gripper and ATI *Gamma* multi-axis force/torque sensor, and the real-time Linux operating system, transmit control protocol and internet protocol (TCP/IP) communication, and the multitasking software design were also outlined. Proportional plus integral (PI) control and fuzzy logic control (FLC) methods were adopted to achieve the robot position's control based on the velocity or force control systems. Additionally, the PI gains were experimentally tuned using the trial and error method based on the virtual crank-turning preliminary test, whereas the fuzzy inputs, outputs and rule base were developed based on the knowledge and experience of the developer. In addition, hardware and software safety issues in human-robot interaction, which is one of the principal challenges in this field, have been given due consideration.

CHAPTER V

EVALUATION OF CONTROL SYSTEM FOR HUMAN-ROBOT INTERACTION

The results concerning how human-human interactive cooperation can achieve its goal, as outlined in Chapter 3, have provided a better understanding of what is required in the design and development of an appropriate set of behaviours for a human-robot control strategy to facilitate the dextrous human-robot handover tasks in a safe and effective way. Control techniques, including proportional integral (PI) and fuzzy logic control (FLC), have been appropriately developed and implemented in order to improve the stability of the robot force and velocity control. In this chapter, the evaluation of the performance of the human-robot handover tasks is developed in order to conduct a quantitative assessment of the system's performance.

5.1 Experimental Design of Human-Robot Interaction

The dynamic characteristics of human behaviour whilst performing the human-human handover tasks at three different velocities of 10, 50 and 100mm/s were evaluated, as explained in Chapter 3. The HHI experimental results were used as a guideline to design and develop a robot control system for the effective human-robot object handover tasks. Three key parameters, i.e. maximum interactive force (f_{max}), transfer time (T_{trf}) and work done (W), were again employed to assess the robot's performance in the human-robot handover task and how close the performance of the HRI is to that of the HHI. Maximum interactive force (f_{max}) or threshold force represents how much maximum interactive force is applied when the *handler* decides to release the object. Transfer time (T_{trf}) which shows how long the object handover process takes. Furthermore, work done (W) by the robot and human can be calculated by multiplying the area under the curve for interactive force against time by the instantaneous velocity. The following sections explain the test procedures of the human-robot interactive tasks, which include two key experiments: human-to-robot and robot-to-human object handover tasks.

5.1.1 Test Procedure for Human-Robot Handover Task

In the case of the human passing the object to the robot, the *handler* was instructed to transfer the object naturally and smoothly to the robot (*receiver*) at different velocities. As in the HHI test, the baton is 40mm in diameter, 300mm in length and has a total mass of 0.42kg. The real-time speed monitoring along the trajectory of the object's movement was obtained by the robot controller using the specific command: `getSpeed(<tTool>)`, which returns the current Cartesian translation speed at the extremity of the specified tool `tTool`. An ATI mini40 force/torque sensor was used to measure the interactive force occurring between the human and robot, with a QNX Neutrino real-time PC to acquire the force information over RS-232, and collect the real-time trajectory of the object during transfer.

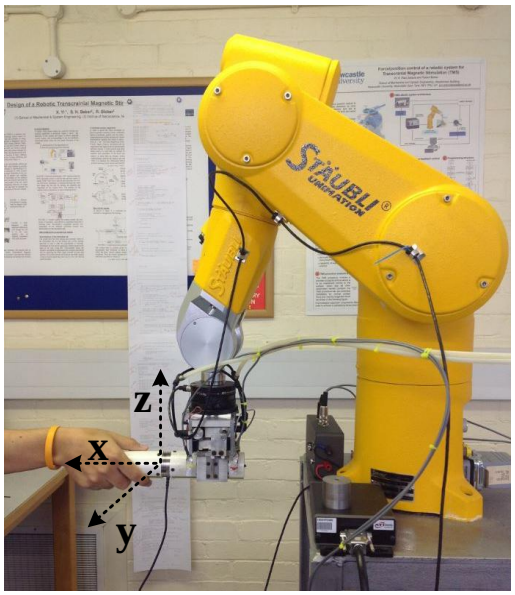

(a) Human-robot physical handover task

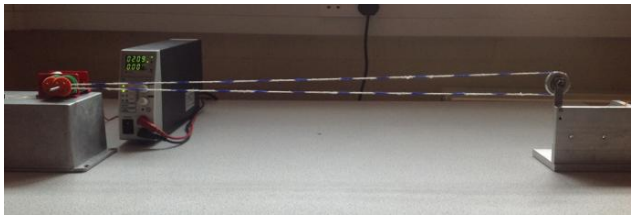

(b) Velocity guide

Figure 5.1 HRI experimental set-up

Figures 5.1(a) and (b) represent the HRI experimental set-up and a velocity guide used in the tests. A set of human-robot handover experiments was undertaken at a range of velocities (10, 50 and 100mm/s). Changing the transfer speed in the HRI task led to corresponding changes in the maximum interactive force (f_{max}), transfer time (T_{trf}), and work done (W). Eighteen participants, as recommended from the pilot study in Chapter 3, were employed in the human-robot handover tasks, in which the human passed the object to the robot and the robot passed the object to the human. Each of the tests was repeated 5 times to ensure that the results met the requirements of statistical significance. Additionally, three trial sets of five object handover tasks were allowed for the participants in order to minimize the effect of human learning. Both PI and fuzzy logic control algorithms were evaluated on the robot.

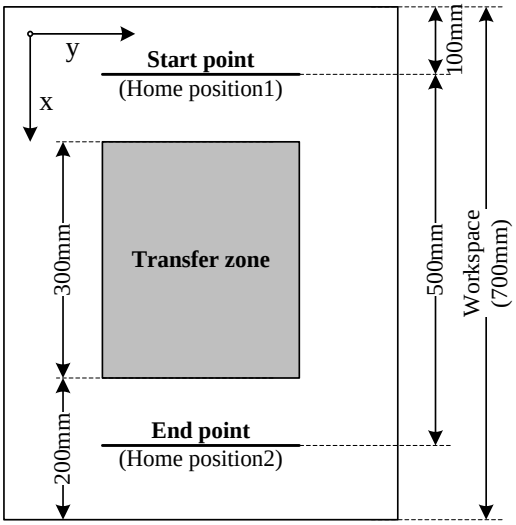

Figure 5.2 Layout of workspace of human-robot physical handover tasks

The test was specified as a one DOF HRI task, where the human and robot partners attempt to physically transfer the baton to each other along the x-axis. Figure 5.2 shows the workspace for the interaction test. The experimental test sequence can be summarized as follows. All participants were again asked to perform the assigned tests to the best of their capability. One hand was allowed to grasp the object, and twisting the baton was not allowed. Each human participant who worked as the *handler* had to release his/her grasp smoothly without dropping the baton. Subsequently, one of the two force control methods (PI and fuzzy logic control) was randomly selected to be implemented with the Stäubli robot for each collaborative task.

The *handler* has to horizontally manipulate the object from the start point to the transfer zone at the required velocity (5, 25 and 50mm/s) until the object reaches the transfer zone. Subsequently, the *receiver* is permitted to grasp the baton. A different time delay is introduced in order to minimize the effects of human anticipation processes.

5.1.2 Implementation of the Robot in the Robot-to-Human Handover Tasks

According to the requirements of the HRI tests, the Stäubli robot manipulator was required to effectively execute the human-to-robot and robot-to-human tasks. In the case of the robot transferring the object to the human, the robot working as the *handler* is responsible for safe and effective movement without dropping or damaging the object. The robot has to regulate the interactive force used and decide whether or not the object is safe to release. The PI and fuzzy logic control methods were developed for the robot's external force control in order for it to modify its behaviour based on force feedback.

The controlled trajectory of the robot needed in the robot-to-human handover task is illustrated in Figure 5.3. It can be divided into three key phases, consisting of: A, a sending phase; B, a transfer phase; and C, a receiving phase. Standard robot movement control is applied in phase A, after which movement control based on the PI or fuzzy logic force control algorithms in phases B and C. Typically, a point-to-point movement of the Stäubli robot was programmed using ALTER real-time path control, which can be defined with the ALTER geometrical transformation as `trsf_alter.x`, `trsf_alter.y` and `trsf_alter.z`. Prior to starting the handover tests, the robot was initialized by the program to grasp the baton and move to either home position1 in the case of robot-to-human handover task or a home position2 in the case of human-to-robot handover task, as illustrated in Figure 5.2.

According to the velocity trajectory of phase A, the robot is commanded to accelerate to its demanded velocity at the beginning of the movement. When the robot's speed approaches the required velocity target, its subsequently decelerates at the end of the trajectory in order to minimize any jerky movements of the robot end effector. Once the velocity of the robot reaches the velocities required in the sending phase, the robot has to maintain its velocity and move towards the interactive zone.

In phase B the human is required to interact with the object, and as soon as an external force is detected to the system, the robot's external force control based on PI or FLC was simultaneously activated. The *receiver* then accelerates the object until it reaches the demanded velocity. In the meantime, the velocity of the robot's end effector based on the force PI and fuzzy logic control schemes can be regulated. This is accomplished with a series of incremental displacements in the x, (y and z axes), which is directly proportional to the interactive force applied to the object. In this phase, the robot *handler* is also responsible for deciding when the object should be released. After the object transfer process has been completed successfully, it was observed that the robot's actual velocity was similar to that demanded, and the interactive force between the robot and the human was close to zero. At this point, the robot gripper is then opened and the object released, and the *receiver* then manipulates the object towards the end point, as shown in phase C.

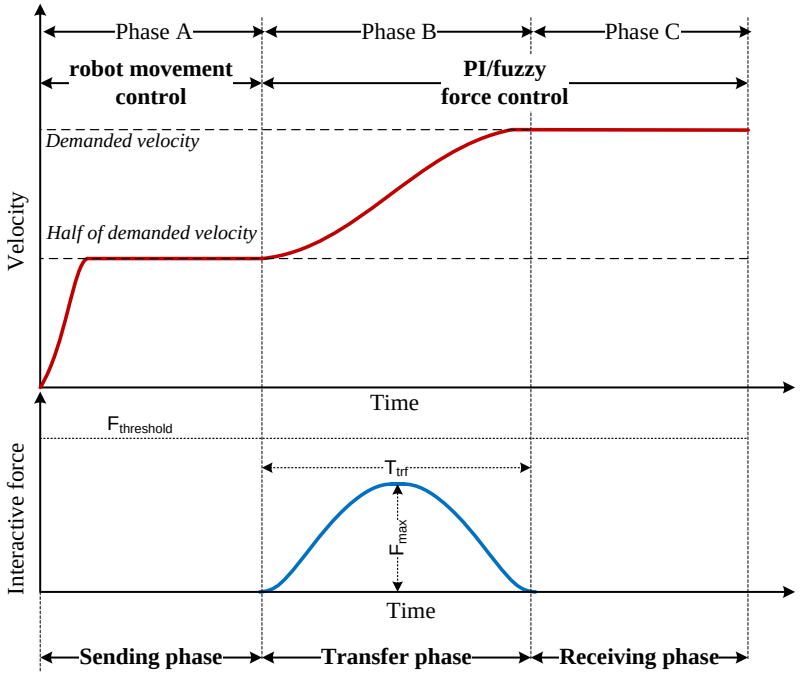

Figure 5.3 Velocity and interactive force profiles for robot-to-human handover tests

5.1.3 Implementation of Robot for the Human-to-Robot Handover Tasks

The robot-controlled trajectory in the human-to-robot handover task is shown in Figure 5.4, and can be categorized into four segments: A, the object's velocity tracking phase; B, the sending phase; C, the transfer phase; and D, the receiving phase. The robot is commanded using VAL3 programmed control in phase B and external control based on the PI and fuzzy logic velocity algorithms in phases C and D. At the beginning of the

task, the robot has to initially move to the home position$_2$ before the human *handler* is instructed to start passing the object to the robot. During this process, the robot needs to perceive and track the motion of the object. Thus the tracking of the object's velocity is modified, so that a first infrared sensor detects the object, and timer1 is then activated. Once the object is detected by the second infrared sensor, the timer is deactivated, and the velocity of the object is estimated.

Phase B allows the robot end effector to accelerate its motion to approach the calculated velocity of the object until reaching the interactive zone. In phase C, the robot gripper is activated to grasp the moving object after which PI and fuzzy logic velocity control is implemented to control the speed of the robot end effector in order to move the object at the demanded velocity. In the meantime, the human *receiver* regulates the interactive force and decides whether or not it is safe to release the object. However according to the safety strategy applied in cases of both robot-to-human and human-to-robot handover tasks, if the *receiver* exceeds the threshold force, then the gripper is opened and the emergency light is enabled to immediately release the object. In phase D, the object is manipulated by the *receiver* to the end position.

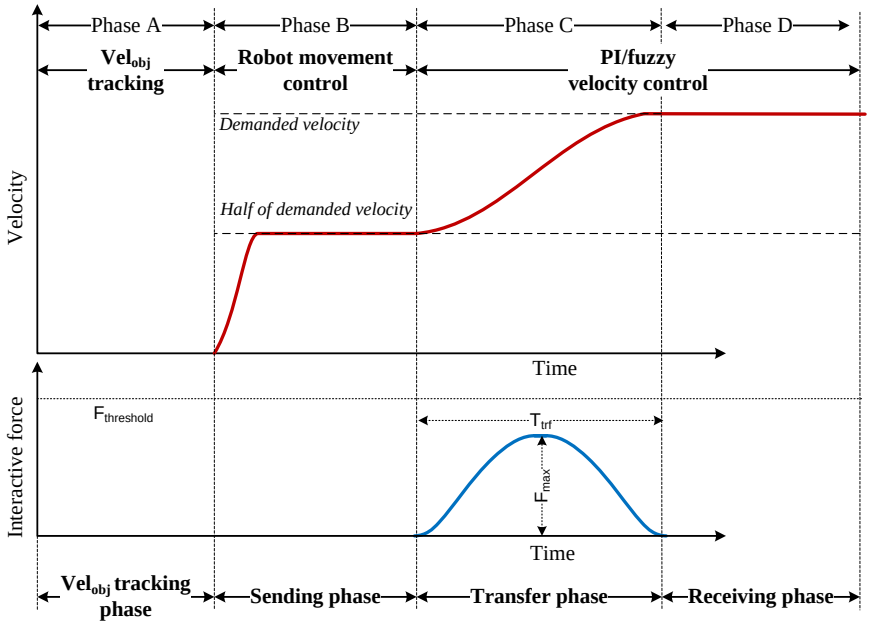

Figure 5.4 Velocity and interactive force profiles for human-to-robot handover tests

5.1.4 Questionnaire Design

A questionnaire was used in this study in order to gather information from the human participants concerning their evaluations of the robot control system in human-robot interaction. The questionnaire was designed based on the suggestions in a standard textbook of survey research [Marsden and Wright, 2010], and is made up of two types of items: rating scale questions and open questions. Questions in the first part are specified with a five points rating scale, which are: 1, poor (very dissatisfied); 2, fair (dissatisfied); 3, average (neither satisfied nor dissatisfied); 4, good (satisfied); and 5, very good (very satisfied). The rating scale technique was applied to convey how comfortable the participants were with the robot's performance in the human-robot handover task and how close the qualitative performance of the HRI is to that of the HHI. The second part of the questionnaire are open questions to provide an opportunity for the participants to express their opinions on their experience and to provide comments and suggestions concerning the strengths and weaknesses of the human-robot interactive system and whether or not it had been successfully developed.

5.2 Performance Evaluation of Human-Robot Interactive Task

In the following sections, the results of the performance evaluations of the human-to-robot and robot-to-human handover tasks are described. The appropriate robot control algorithms explained in Chapter 4 were implemented with the robot in order to execute the HRI handover tasks. Experiments were conducted to measure the stability of the robot's performance whilst performing the handover task with the human, and the results were then compared with the outcomes of the HHI tests. Furthermore, the questionnaire results were also used to reveal the opinion of the participants in seeking to support the test results.

5.2.1 Evaluation of Robot-to-Human Handover Task

The results for the robot-to-human handover tests are presented separately for each type of force control applied to the robot. These results are based on the extraction of time-domain features in quantitative form, such as the profiles of the velocity of the object and the physical interactive force between the human and robot, maximum interactive force (f_{max}), transfer time (T_{trf}), and work done (W). Similarly to the data for the human-human handover tests, three standard deviations (3σ) specifying approximately 99% of the area under the force curve were analysed.

5.2.1.1 Robot PI Force Control: Test Results and Discussion

A set of robot-to-human handover tests was undertaken to provide a comparison of the performance of the robot manipulator system based on PI and FLC to human behaviour. Figure 5.5 shows examples of the results of one of the robot-to-human handover tasks, where the robot was required to transfer the object to the human at the demanded velocity of 100mm/s using PI force control. The graph also shows the relationship between the velocity and interactive force profiles of the robot during the robot-to-human handover task using the proportional integral control method. These profiles are depicted in the time domain and are segmented into three main phases A, B and C representing sending, transfer and receiving phases. The robot *handler* moved the object horizontally from the start point to the interactive zone at a velocity of 50mm/s as shown in phase A. It can be observed that transfer phase B is also divided into two sub-phases B_1 and B_2 which indicate the actual interaction time between the robot and human and the time delay of the operational process of the robot gripper.

In phase B_1, the *receiver* was permitted to grasp the object and achieve the demanded velocity, during which the robot manipulator regulated the interactive force using the PI force control algorithm. This causes the acceleration of the velocity of the object at the beginning of the movement and when the object's speed approached the demanded velocity. The velocity profile provides an agreement with the paper by Flash and Hogan [1985]. In phase B_2, the control system activated the robot gripper to release its grasp after object transfer was successfully completed; however, a time delay of approximately 0.20s in the pneumatic gripper system is evident, and both partners were required to maintain their movements until the gripper had completely opened. It can be observed that the interactive force between them reduces to approximately zero, as the object reached the demanded velocity of 100mm/s. The velocity profile of the robot in phase C seemed to be significantly affected by the gripper, as its fingers were opening in order to release the object.

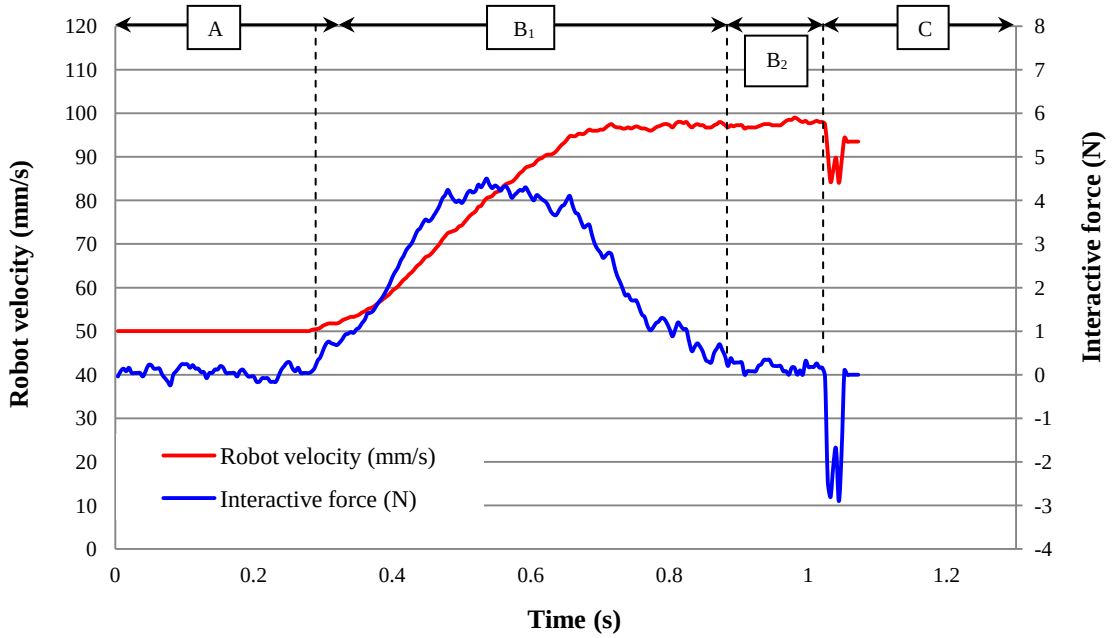

Figure 5.5 Actual velocity and interactive force profiles of a robot-to-human handover task based on PI control

A set of simple tests was undertaken to investigate the overall time delay of the robot gripper system. The force indicating the contact of the gripper fingers and the object was captured in real-time every 4ms by the robot mounted ATI *Gamma* multi-axis force/torque sensor and the PC running RT Linux. The time delay can be computed from the program's Timer1, which is activated once the gripper commands for opening or closing have been enabled from RT Linux, and deactivated when a maximum peak from the gripper operation occurs. The average time delays of the gripper opening and closing were 0.19s (with a standard deviation of 0.01s) and 0.22s (with a standard deviation of 0.01s).

In order to evaluate the results of the robot-to-human handover tasks based on PI robot control, curve fitting was implemented for the interactive force profiles. The following example reveals how the key parameters can be determined using Matlab. Figure 5.6 shows the actual interactive force, superimposed fitted curve and analysed force profile, and Figure 5.7 depicts the actual velocity, fitted curve and analysed velocity profile for the case where the *handler* has to pass the object to the *receiver* at a velocity of 100mm/s. The parameters (f_{max}, T_{trf} and W) were computed to be 4.29N, 0.55s and 114.3mJ respectively. Work done (W) was calculated by multiplying the area under the curve by the integrated velocity over time.

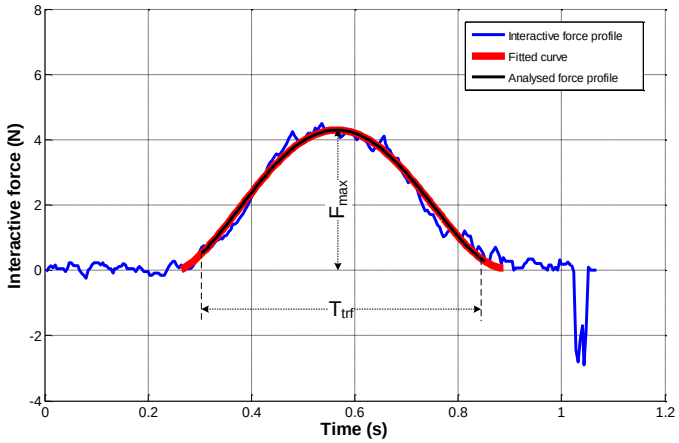

Figure 5.6 Interactive force profile of a robot-to-human handover test (PI) at 100mm/s

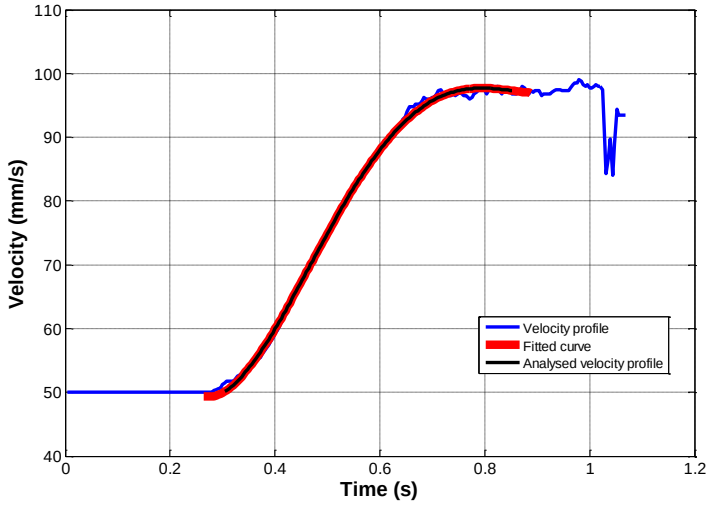

Figure 5.7 Velocity profile of a robot-to-human handover test (PI) at 100mm/s

5.2.1.2 Robot Fuzzy Logic Force Control: Test Results and Discussion

Figure 5.8 presents the time-domain profiles of the interactive force and velocity of the robot-to-human handover tasks based on fuzzy logic force control. The task is again categorized into three phases (A, B and C) and two sub-phases (B_1 and B_2). In the example shown, the robot manipulated the object at a constant velocity of 50mm/s and transferred it to the *receiver* at the demanded velocity of 100mm/s. In the transfer phase B, once the human grasped the object, the robot's fuzzy logic force control algorithm was activated. In the meantime, the human participant had to move the object with the required velocity. This movement trajectory is also in agreement with the bell-shaped velocity profile proposed by Flash and Hogan [1985]. It should be in noted in the chart that the velocity profile of the robot in phase C was affected by the operation of the gripper whilst releasing the object, but is smoother than when the PI control method was used illustrated in Figure 5.5.

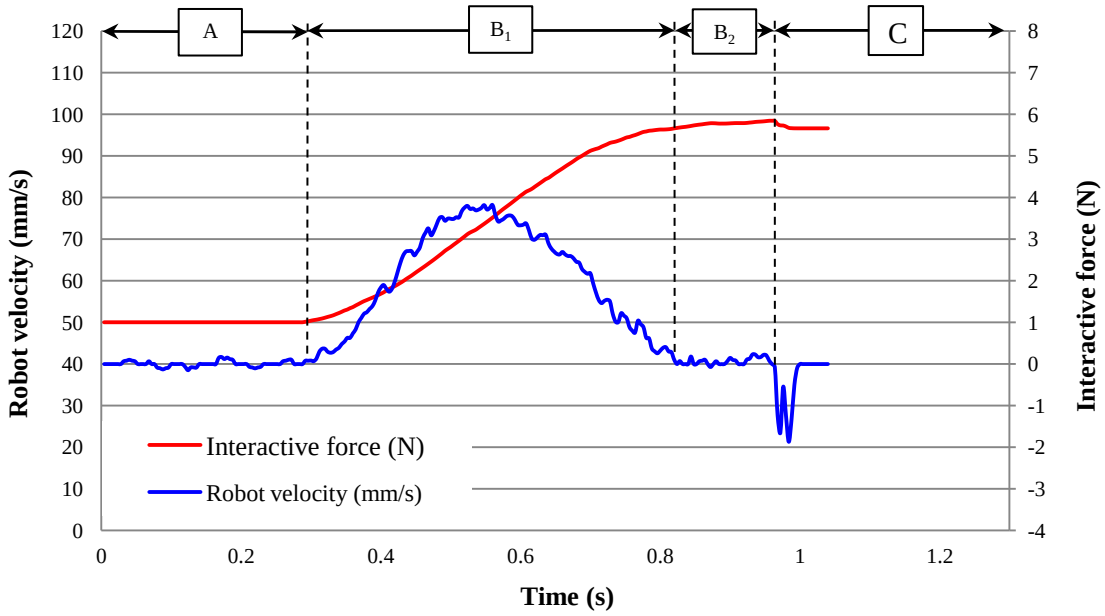

Figure 5.8 Velocity and interactive force profiles
of a robot-to-human handover task based on FLC

The curve fitting of the actual interactive force and velocity profiles based on the fuzzy logic force control algorithm for the case where the *handler* passed the object to the *receiver* at a velocity of 100mm/s, are shown in Figures 5.9 and 5.10 respectively, and used to evaluate the f_{max}, T_{trf} and W parameters. The results show that the maximum force applied was 3.54N, the transfer time was approximately 0.48s and finally the calculated work done was established as 86.7mJ.

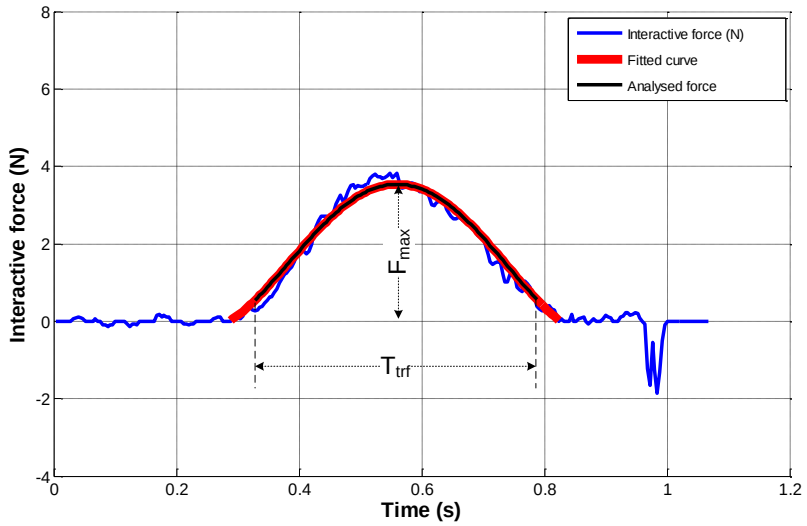

Figure 5.9 Interactive force profile of a robot-to-human handover test
based on FLC at 100mm/s

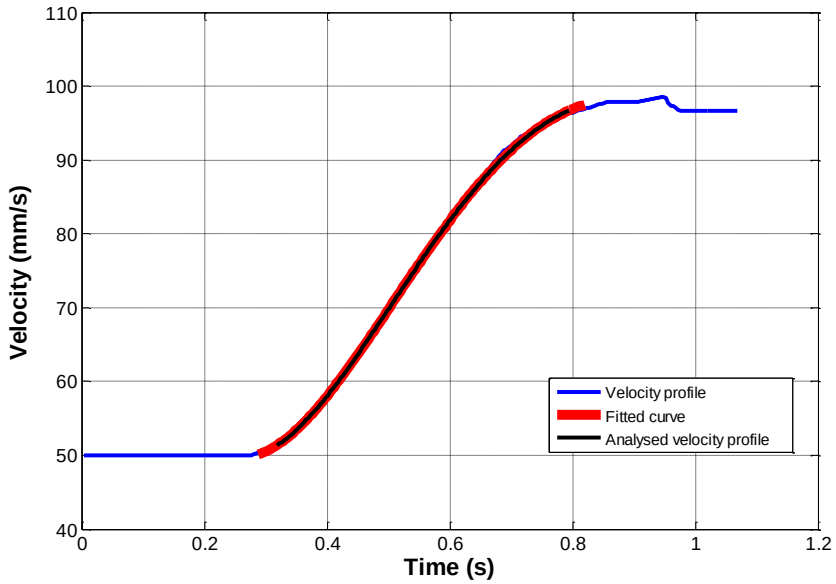

Figure 5.10 Velocity profile of a robot-to-human handover test based on FLC at 100mm/s

A comparison of the parameters for the two force control techniques is given in Table 5.1 and plotted in Figures 5.11-5.13. The following notation is used: RHI with PI and FLC represented the robot-to-human handover task based on the PI and FLC force control algorithms. Figures 5.11(a)-(c) compare the transfer time taken based on HRI with PI and FLC and HHI at the three demanded velocities. As expected it can be seen that the transfer times are reduced with an increase in velocity for all scenarios, with the transfer time in the human-human handover tasks the fastest. The transfer time of RHI with FLC is quicker than with PI; however, at a slow transfer speed of 10mm/s, the transfer times of RHI with the fuzzy logic control algorithm and HHI are similar around 0.54s, while the PI control scheme were slightly to show a difference with 0.63s.

Figures 5.12(a)-(c) indicate how the average maximum interactive force varies with transfer velocity. Generally, the interactive force increases with increasing demanded velocity, whereas the magnitudes of force in the HHI tests are the smallest. In addition, the maximum interactive forces of the robot-to-human tasks at all demanded velocities using FLC were seen to be lower than with the PI control method. The average magnitudes of interactive force in HHI and HRI with PI and FLC tasks at the demanded velocity of 10mm/s were closed to each other and varied between 0.85 and 1.05N. Conversely, at the higher transfer speed of 100m/s, the maximum interactive forces show most fluctuation, at 2.43, 3.65 and 4.54N respectively.

The work done as computed for the robot-to-human handover tasks at the different demanded velocities can be compared as depicted in Figures 5.13(a)-(c). It can be observed that the trends for work done and maximum force are quite similar, where the amount of work done between the human and robot for the handover tests increase significantly with higher demanded velocity. The test performance achieved in HHI tasks is again better than that of RHI with either PI or FLC, and furthermore the work done in RHI with PI control is also slightly greater than that of with FLC. However, at the demanded velocity of 10mm/s, it can be seen that the average work done in HHI and RHI tasks is similar, fluctuating between 1.29 and 2.4mJ,whereas the work done in the HHI and RHI with PI and FLC tasks at the demanded velocity of 100mm/s show significant differences, at 4.3, 82.5 and 116.0mJ respectively.

In these experiments, the quantitative performance of the robot external force control was investigated against a range of demanded transfer speeds. The test results based on both the proportional integral (PI) and fuzzy logic control (FLC) algorithms demonstrated dexterous human-human like object handovers, where the robot was able to successfully transfer the baton object to the human in smooth, safe and reliable manner. It can thus be concluded that both PI and FLC robot control strategies provide effective performance and reliability of the robot-to-human handover procedure. However, careful observation of the interactive force and velocity graphs for FLC revealed that these profiles are moderately smoother than the PI implementation (see Figures 5.5 and 5.8). Furthermore, FLC was shown to provide improved performance of the robot force control system over that of PI force control, in terms of reduced interactive force, shorter transfer time and lower work done. This also supports the conclusion that using FLC has a significant advantage when controlling non-linear systems, and is more insensitive than PI control to variations in small external force disturbances, which is an important requirement in robot force/position control schemes [Gaurav, 2012].

Table 5.1 Comparisons of the average values and corresponding standard deviations (std) of f_{max}, T_{trf} and W in robot-to-human handover tasks for PI and fuzzy logic control

Demanded velocity (mm/s)	**Human-human handover task**			**Robot-to-human handover task**					
				Robot PI force control			**Robot FLC force control**		
	Work done/std (mJ)	Time/std (s)	Force/std (N)	Work done/std (mJ)	Time/std (s)	Force/std (N)	Work done/std (mJ)	Time/std (s)	Force/std (N)
10	1.9/0.3	0.54/0.06	0.85/0.16	3.5/0.7	0.63/0.07	1.05/0.14	2.7/0.5	0.53/0.06	1.00/0.11
50	11.0/1.6	0.44/0.03	1.32/0.28	27.9/4.1	0.57/0.07	1.98/0.34	21.2/2.2	0.50/0.06	1.71/0.19
100	34.3/6.6	0.37/0.03	2.43/0.59	116.0/9.8	0.52/0.05	4.54/0.50	82.5/7.1	0.46/0.04	3.65/0.41

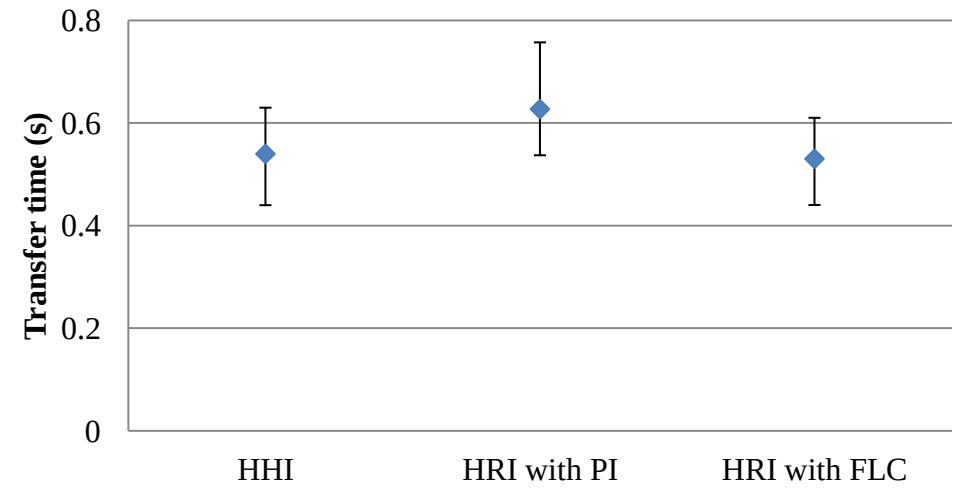

(a) Velocity = 10mm/s

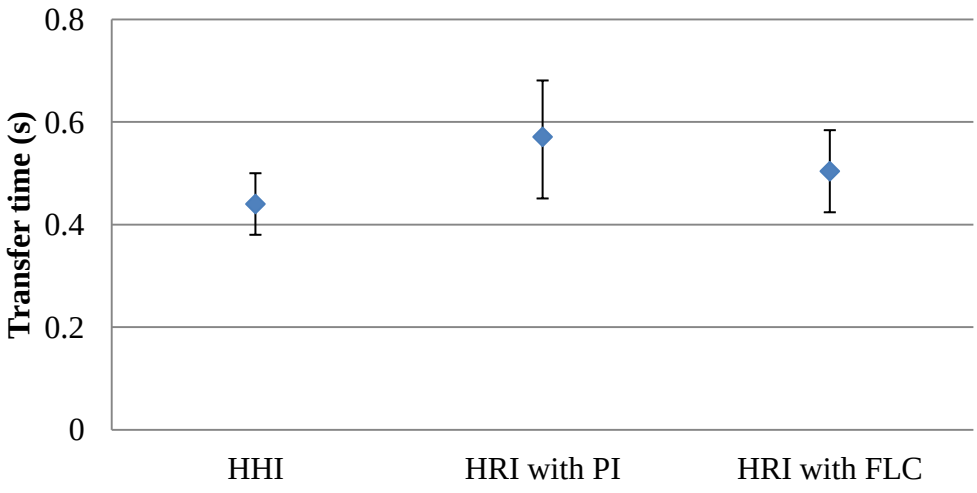

(b) Velocity = 50mm/s

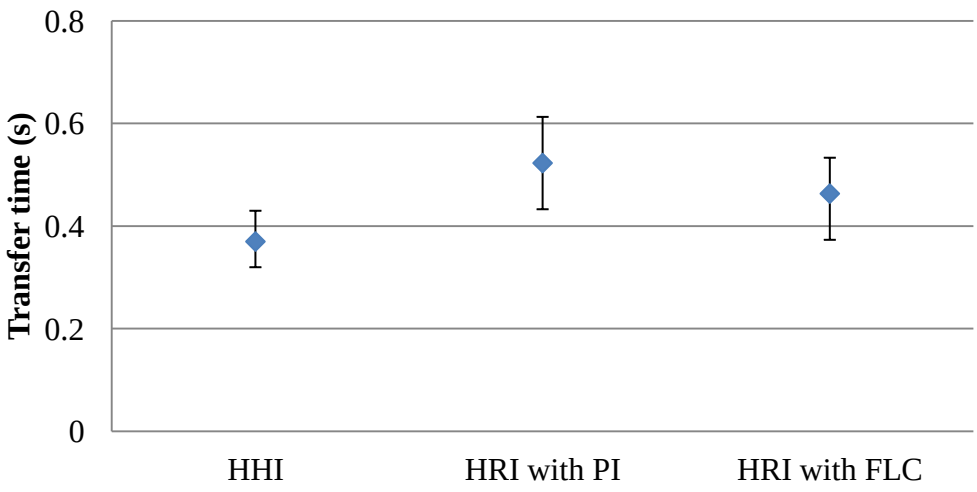

(c) Velocity = 100mm/s

Figure 5.11 Comparison of average transfer time based on HHI and HRI with PI and FLC against the demanded transfer speeds in robot-to-human handover tasks

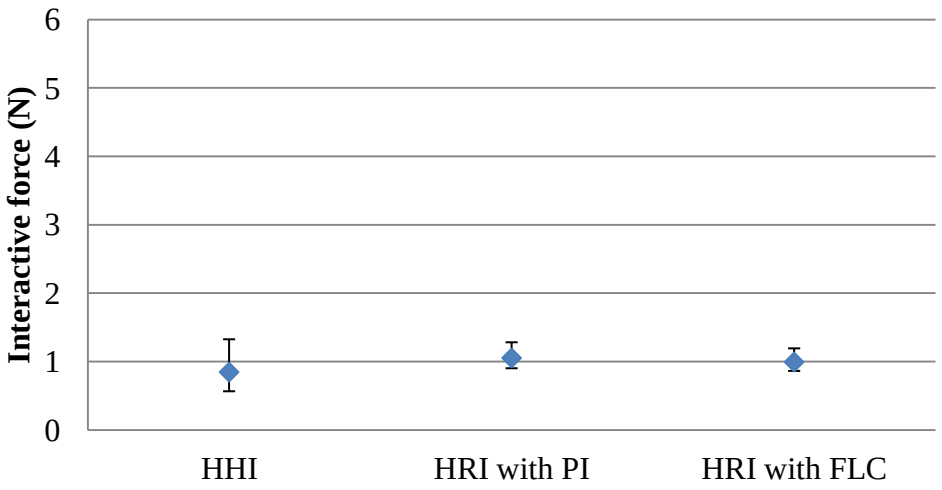

(a) Velocity = 10mm/s

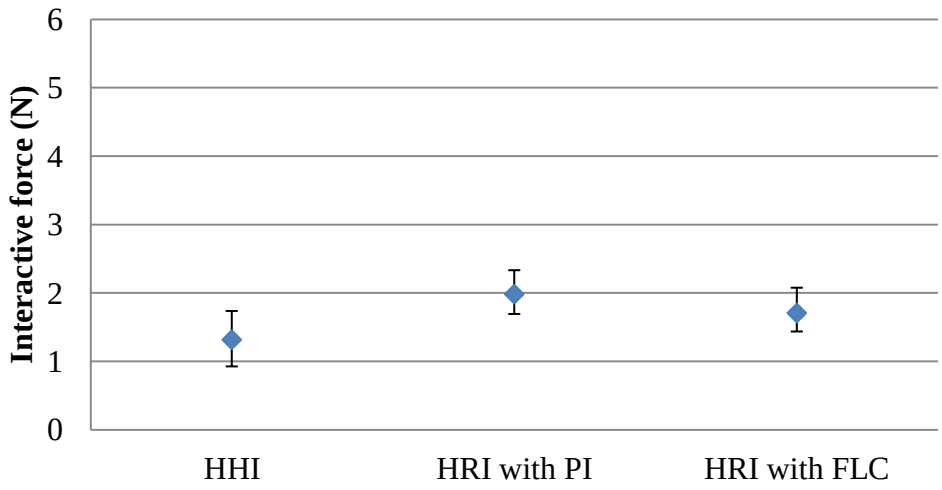

(b) Velocity = 50mm/s

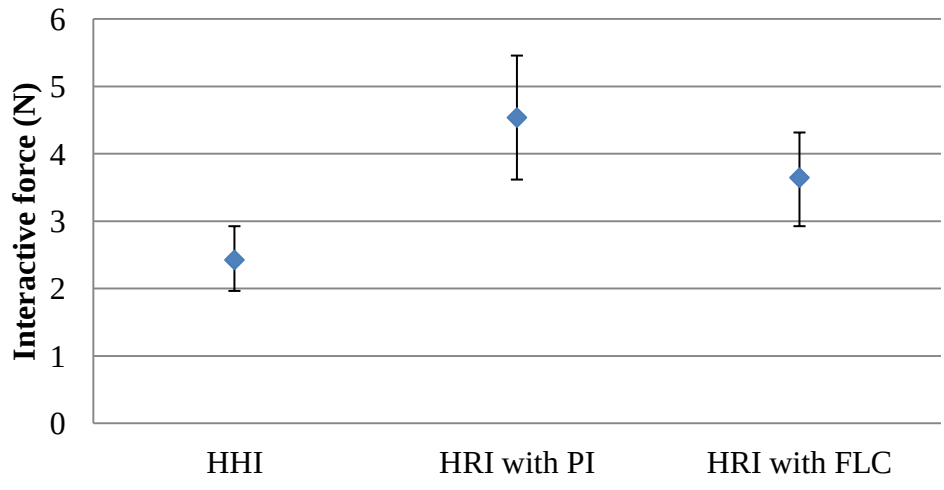

(c) Velocity = 100mm/s

Figure 5.12 Comparison of maximum interactive force based on HHI and HRI with PI and FLC against the demanded transfer speeds in robot-to-human handover tasks

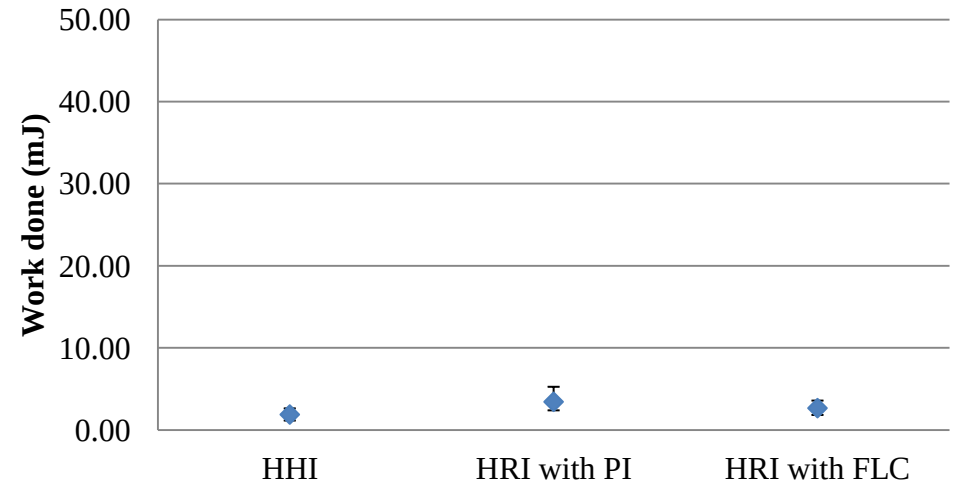

(a) Velocity = 10mm/s

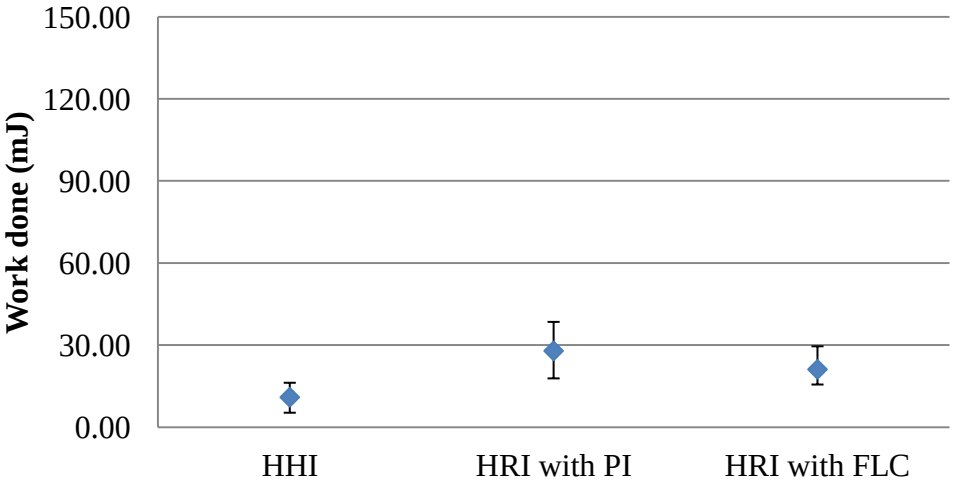

(b) Velocity = 50mm/s

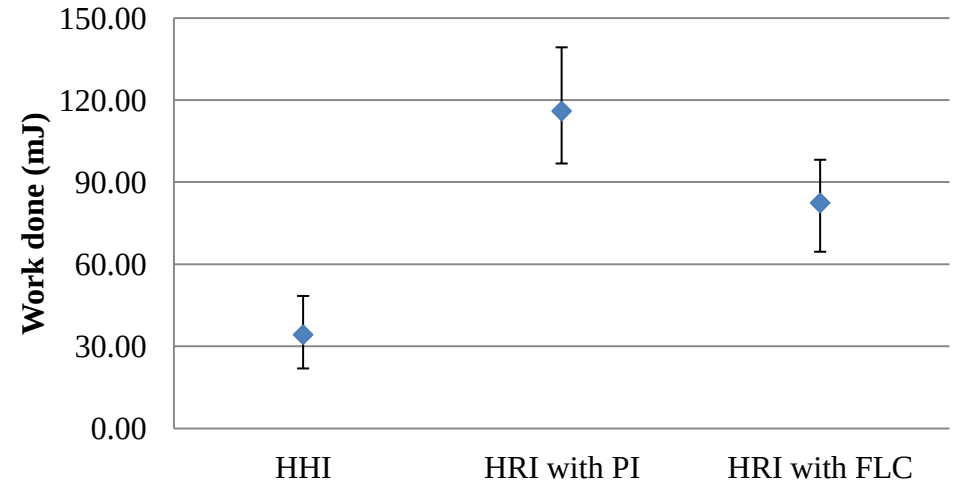

(c) Velocity = 100mm/s

Figure 5.13 Comparison of average work done based on HHI and HRI with PI and FLC against the demanded transfer speeds in robot-to-human handover tasks

5.2.2 Evaluation of the Human-to-Robot Handover Task

This section describes the evaluation of the system performance of the human-to-robot handover task using PI control and FLC at the three velocities of 10, 50 and 100mm/s. These experimental results are presented in the time-domain, which consist of both velocity and physical interactive force profiles, maximum interactive force (f_{max}), transfer time (T_{trf}), and work done (W).

5.2.2.1 PI Robot Velocity Control: Test Results and Discussion

The relationship between the actual velocity and interactive force profiles of the robot, using a PI velocity control algorithm whilst performing the human-to-robot handover tasks is illustrated in Figure 5.14. Phases A, B, C and D represent the object velocity tracking, sending, transfer and receiving postures. Once the velocity of the object in the handover process is estimated in phase A, then the robot is instructed to accelerate to the computed velocity in phase B_1. The movement of the robot end effector is maintained as shown in phase B_2.

The robot gripper is allowed to grasp the object in the interactive zone, as shown in phase B_3, where it can be noted that the interactive force profile was affected by the operation of the gripper whilst grasping the object. Subsequently, both robot and human partners have to maintain their simultaneous movement until phase C when the object is transferred. Therefore, the effect of irrelevant force exerted by the gripper during an operation can be avoided, thus ensuring reliability in performing effective and accurate HRI tasks. The human *handler* has to pass the object to the robot (*receiver*) at the transfer point in phase C, while the *handler* is responsible for regulating his/her force to decide whether or not the object is safe to release. Finally, phase D gives the velocity and interactive force curves when the robot individually holds and moves the object to the end point.

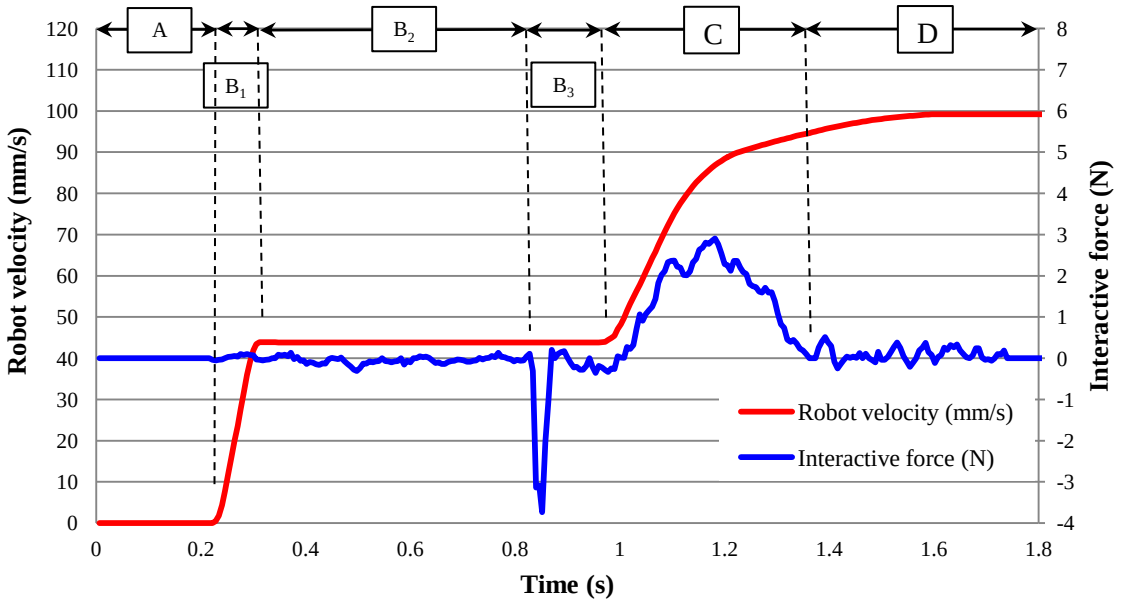

Figure 5.14 Actual velocity and interactive force profiles of a human-to-robot handover task based on PI control

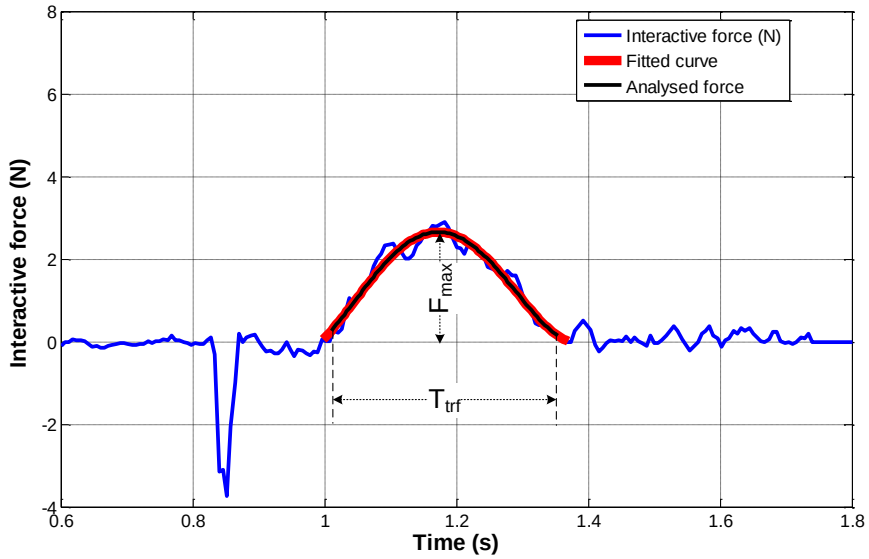

Figure 5.15 Interactive force profile of a human-to-robot handover test (PI)

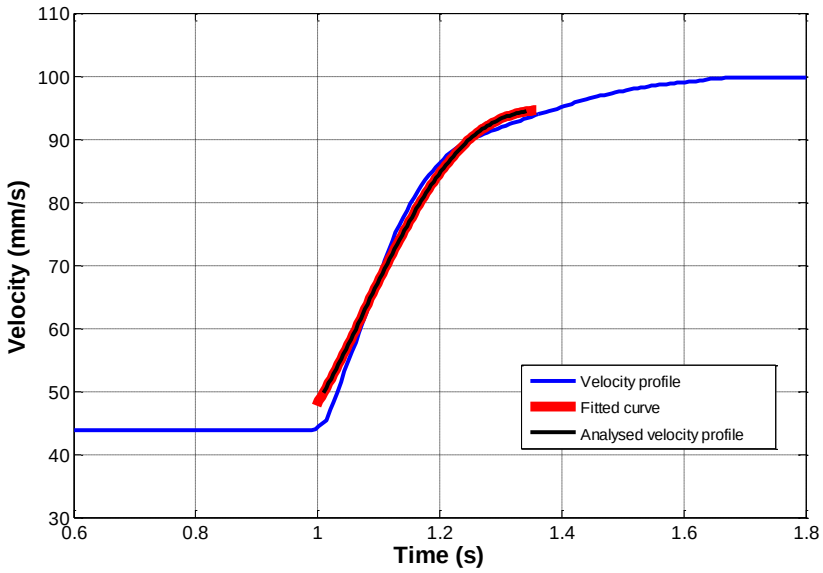

Figure 5.16 Velocity profile of a human-to-robot handover test (PI)

The following example presents how the relevant parameters can be calculated using Matlab software at a velocity of 100m/s. Figure 5.15 depicts the actual force profile, curve fitting and force profile analysed. Additionally, the actual velocity profile, fitted curve and analysed velocity profile are plotted in Figure 5.16, where the maximum force (f_{max}), transfer time (T_{trf}) and work done (W) were 2.66N, 0.36s and 49.6mJ respectively.

5.2.2.2 Fuzzy Logic Velocity Control: Test Results and Discussion

The relationship between the interactive force and velocity profiles in the time domain of the human-to-robot handover tasks while the robot was controlled by the fuzzy logic velocity control algorithm is shown in Figure 5.17, and once again it can be segmented into the four phases A-D as with the robot PI velocity control scheme, and can be observed that the performance show similar trends. However, as the fuzzy logic control is less sensitive to variations in external force disturbances, the velocity trajectory of the robot end effector is smoother than using PI control, as illustrated in phase C in Figure 5.14.

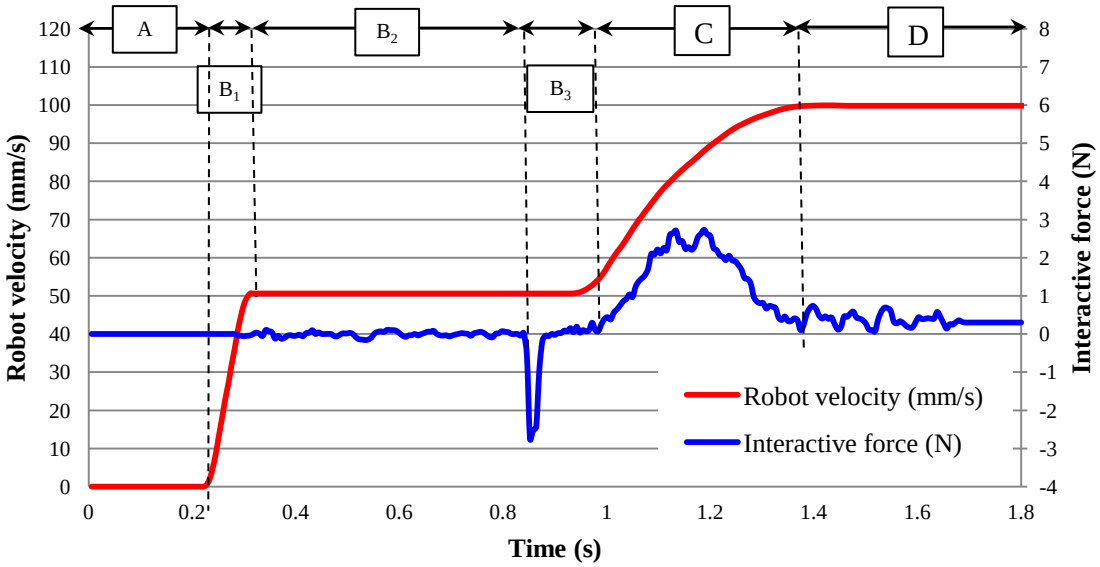

Figure 5.17 Actual velocity and interactive force profiles of a human-to-robot handover task based on FLC

Figure 5.18 presents the actual interactive force data, fitted curve and analysed force profile, whilst Figure 5.19 displays the actual velocity profile, fitted curve and analysed velocity profile used to estimate the parameters: f_{max}, T_{trf} and W. In the case of the human passing the object to the robot at a transfer speed of 100mm/s, the average maximum force was 2.51N, the transfer time 0.36s and the calculated work done 47.9mJ. Moreover, it can be observed that the fourth-order polynomial curve fitting for the velocity trajectory based on the robot fuzzy logic velocity control suggested an effective fit and provide better performance compared to PI control.

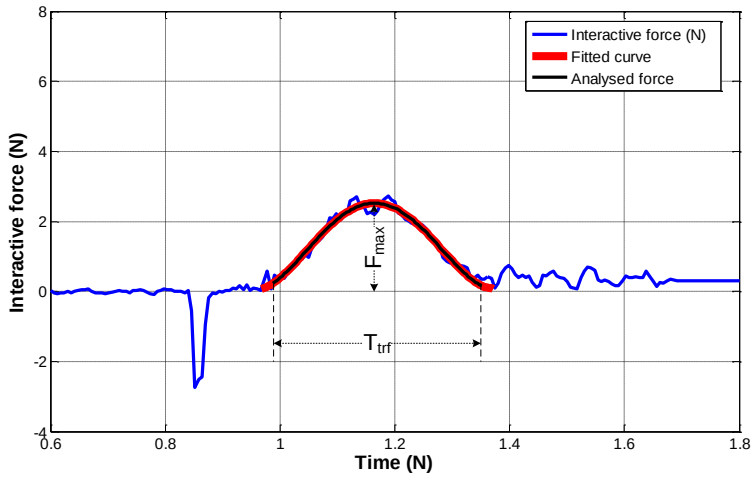

Figure 5.18 Interactive force profile of a human-to-robot handover test (FLC)

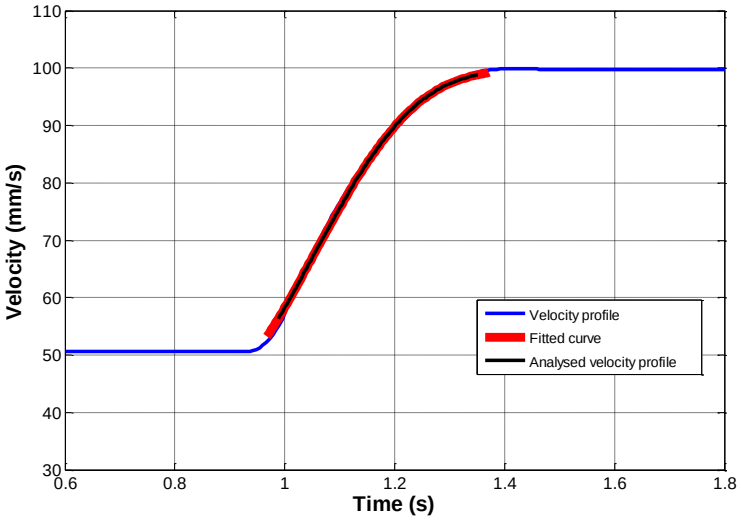

Figure 5.19 Velocity profile of a human-to-robot handover test (FLC)

Table 5.2 summarises a comparison of the interactive force, transfer time and work done between the human-to-robot and human-human handover tasks with the robot was controlled by the proportional integral and fuzzy logic velocity control schemes at the three different demanded velocities, as shown in Figures 5.20-5.22. Figures 5.20(a)-(c) depict the representative plots for the average transfer times. It can be observed that transfer time is reduced with increases in demanded velocity for all cases, including HRI based on robot PI velocity control (HRI with PI), HRI using fuzzy logic velocity control (HRI with FLC) and HHI. The outcomes from HHI are again generally the fastest, followed by HRI with FLC and then HRI with FLC. At the demanded velocity of 10mm/s, it can be concluded that the average transfer times taken in the human-to-robot and human-to-human handover tasks are similar, varying between 0.54-0.57s, whereas transfer times at the velocities of 50 and 100mm/s fluctuate between 0.44-0.54s and 0.37-0.44s respectively.

Figures 5.21(a)-(c) show a similar trend in the average maximum interactive force in all scenarios, with the magnitude of interactive force increasing as the transfer rates rise from 10 to 100mm/s. Notable differences in interactive force occurring in the human-to-human and human-to-robot handover tasks at the demanded velocities of 10, 50 and 100mm/s were found in the intervals of 0.85-1.33N, 1.32-1.63N and 2.43-2.78N respectively. The lowest magnitude of force was applied to the object in order to ensure effective object handover which was successful and safe in the case of HHI. In addition, the average force in the HRI tasks where the robot was controlled by the FLC algorithm is seen to be slightly less than that using the PI control method.

The average work done in all cases was calculated using the multiplication of the area under the interactive force curve by the average velocity and the results are shown in Figures 5.22(a)-(c). It can be seen that the work done increases significantly when the velocity demanded is higher. As with the trends of interactive force described above, the work done in HHI tasks is the lowest, followed by HRI tasks with FLC and then HRI with PI. Nevertheless, at the velocity of 10mm/s the mean work done in HHI, HRI with PI and HRI with FLC are similar in the range from 1.9 to 3.9mJ; whereas at the demanded transfer velocity of 100mm/s, significantly different results among all scenarios were obtained ranging between 34.3 and 60.6mJ.

The evaluation of the performance of the human-to-robot handover tasks against variations in the demanded transfer velocities have shown that the robot velocity control algorithms based on proportional integral and fuzzy logic control are both considered acceptable for HRI and can facilitate safe and timely natural collaboration between the human partner. At the demanded velocities of 10 and 50mm/s, the maximum interactive force, transfer time and work done between the human and robot, during HHI and HRI using FLC and PI are similar. Nonetheless, at the transfer speed of 100mm/s, the mean work done by the robot using FLC is slightly less than PI control where the work done in RHI with PI control is approximately 1.8 times higher than in HHI tasks, while the work done in RHI with FLC is only 1.4 times as much as the work done in the HHI experiments.

Table 5.2 Comparisons of the average values and corresponding standard deviations (std) of f_{max}, T_{trf} and W in human-to-robot handover tasks according to PI and fuzzy logic control

Demanded velocity (mm/s)	**Human-human handover task**			**Human-to-robot handover task**					
				Robot PI velocity control			**Robot FLC velocity control**		
	Work done/std (mJ)	Time/std (s)	Force/std (N)	Work done/std (mJ)	Time/std (s)	Force/std (N)	Work done/std (mJ)	Time/std (s)	Force/std (N)
10	1.9/0.3	0.54/0.06	0.85/0.16	3.99/0.7	0.57/0.05	1.33/0.24	3.8/0.6	0.57/0.06	1.26/0.22
50	11.0/1.6	0.44/0.03	1.32/0.28	24.4/3.7	0.54/0.06	1.63/0.18	21.9/3.1	0.54/0.07	1.59/0.18
100	34.3/6.6	0.37/0.03	2.43/0.59	60.5/5.5	0.44/0.05	2.78/0.27	49.9/5.2	0.40/0.04	2.51/0.25

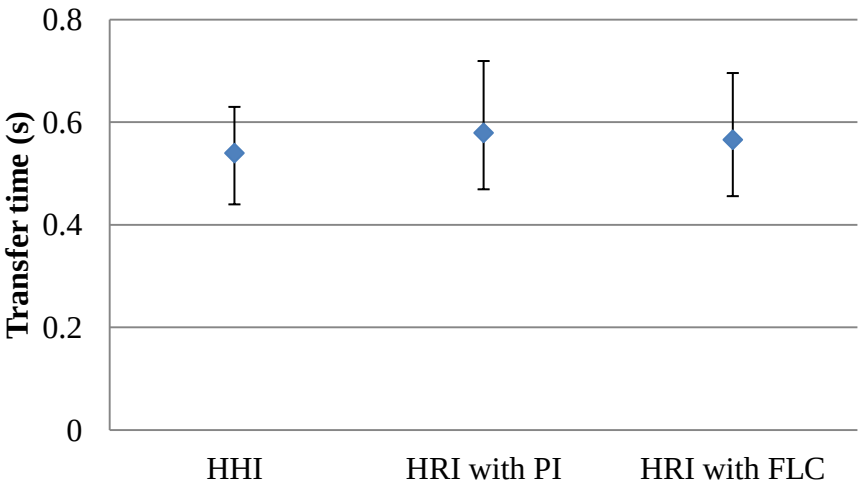

(a) Velocity = 10mm/s

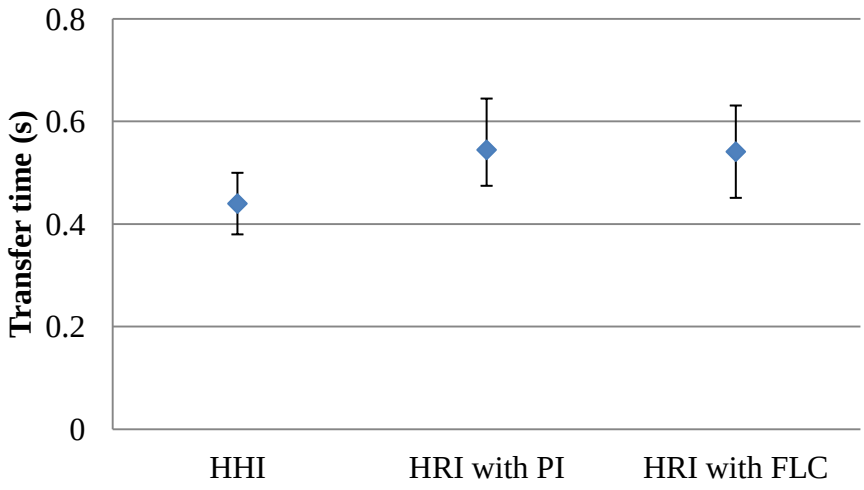

(b) Velocity = 50mm/s

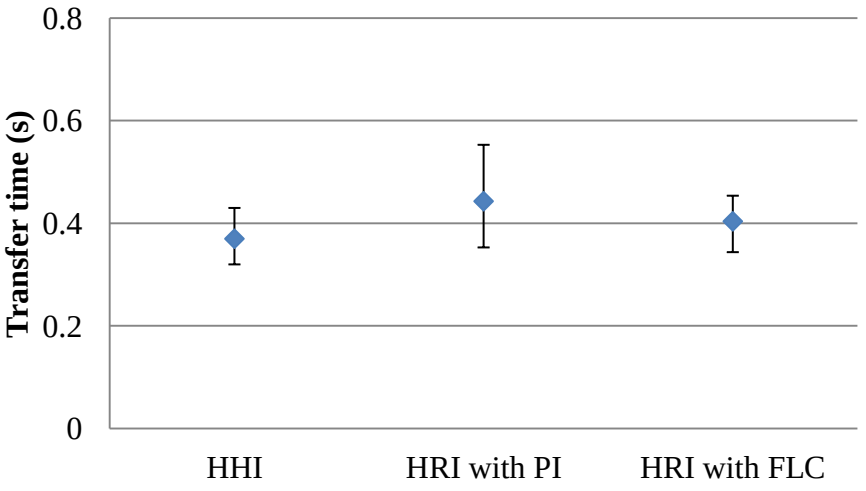

(c) Velocity = 100mm/s

Figure 5.20 Comparison of average transfer time based on HHI and HRI with PI and FLC against the demanded transfer speeds in human-to-robot handover tasks

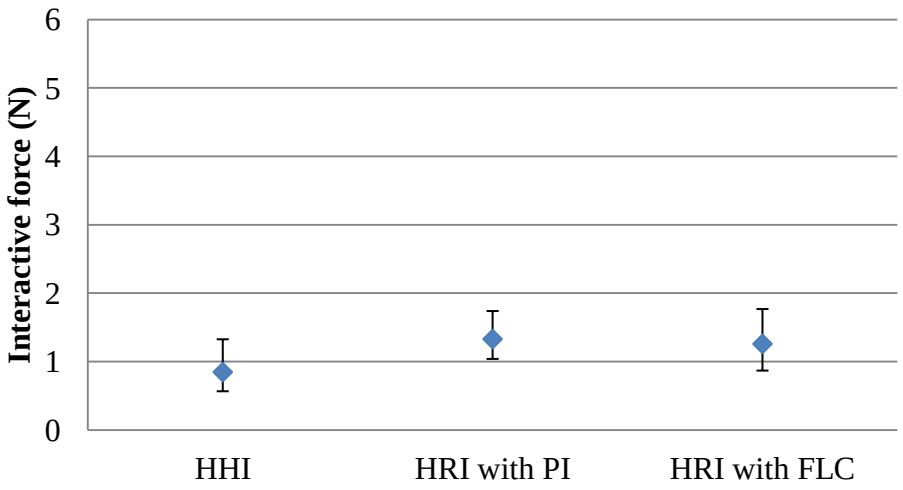

(a) Velocity = 10mm/s

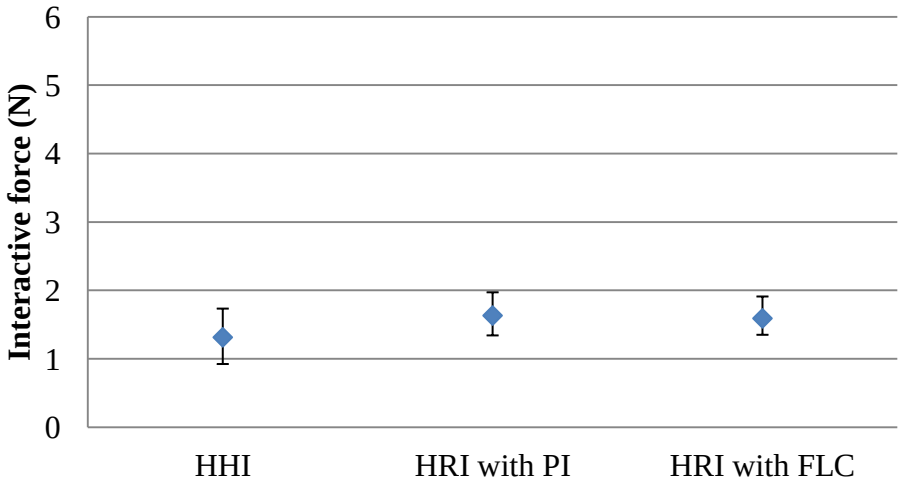

(b) Velocity = 50mm/s

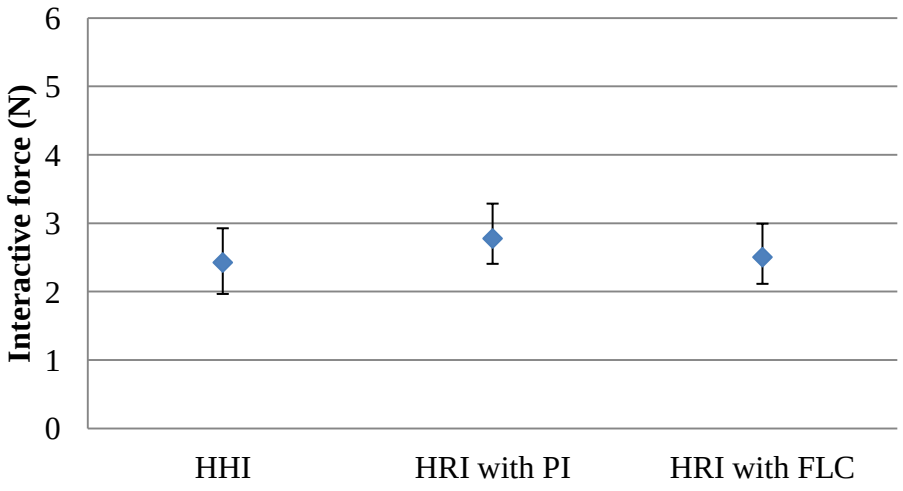

(c) Velocity = 100mm/s

Figure 5.21 Comparison of maximum interactive force based on HHI and HRI with PI and FLC against the demanded transfer speeds in human-to-robot handover tasks

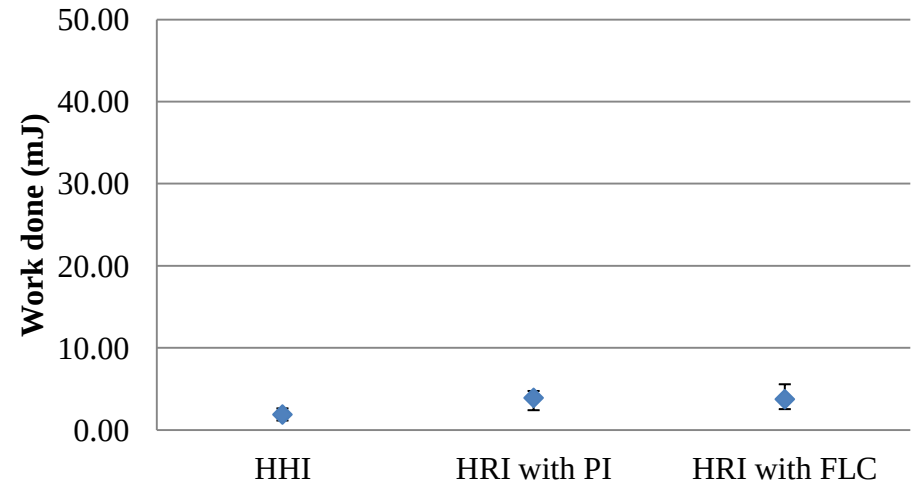

(a) Velocity = 10mm/s

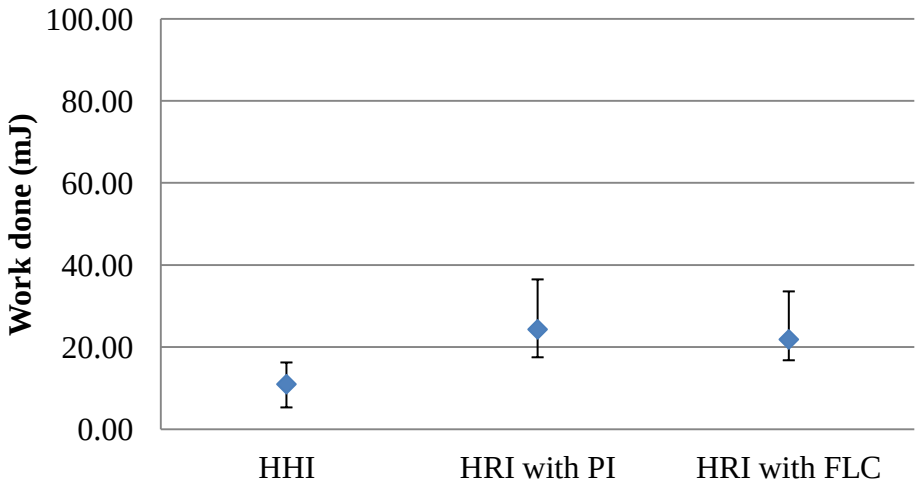

(b) Velocity = 50mm/s

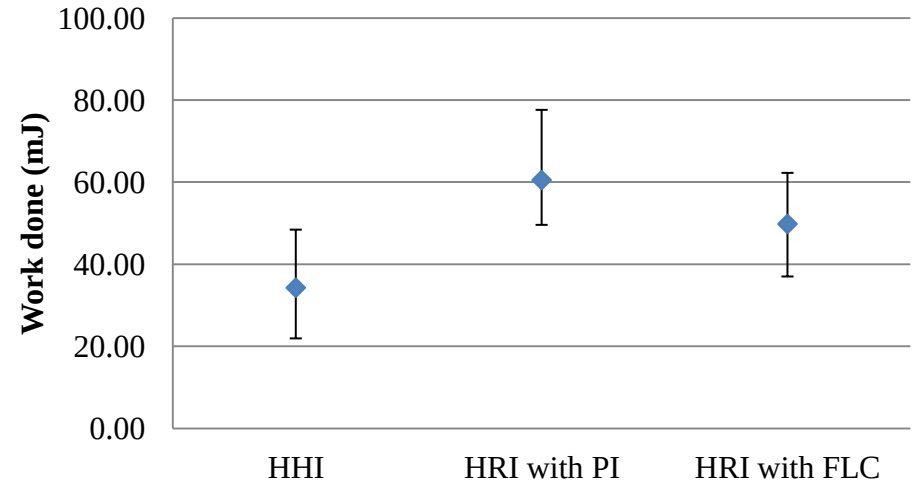

(c) Velocity = 100mm/s

Figure 5.22 Comparison of average work done based on HHI and HRI with PI and FLC against the demanded transfer speeds in robot-to-human handover tasks

5.2.3 Evaluation of Velocity Control Performance of HRI

The speeds required in the robot-to-human and human-to-robot handover tasks can be divided into the velocities in the sending and receiving phases. In the sending phase, the *handler* has to move the object to the interactive zone at velocities of 5, 25 and 50mm/s; afterwards, the object has to be transferred to the *receiver* and moved to the final position at velocities of 10, 50 and 100mm/s. Table 5.3 shows the performance of velocity control in the human-robot handover tasks where the robot was successfully controlled by two different methods: PI and FLC. Additionally, the percentages of the speed errors between the demanded and actual velocities of the object to be transferred were determined in order to compare the actual speed according to PI and fuzzy logic control applied to the robot to the results in the HHI tasks.

The test results illustrated in Table 5.3 provide information regarding the velocity of motion of the object. According to the results of the robot-to-human handover task as shown in Figure 5.23, the robot moved the object at speeds of 5, 25 and 50mm/s using the ALTER real-time path control command during the sending phase. The results suggest that the small error in speed between the demanded and actual velocities were very good across the speed range, with a 0.0mm/s standard deviation. In contrast to the human performance results in the receiving phase as illustrated in Figure 5.24, speed errors decrease when the demanded velocity increases. The percentage velocity errors during robot PI force control at the demanded velocities at 10, 50 and 100mm/s were 28.0%, 4.8% and 2.0%, with corresponding standard deviations of 1.6, 4.0 and 6.2 respectively. The percentage velocity errors under the same demanded speeds of 10, 50 and 100mm/s when using fuzzy logic force control were 31.0%, 9.4% and 5.1% with standard deviations of 2.0, 2.6 and 5.7 respectively. It can be observed that the errors from FLC are slightly greater than those of PI control, which could be due to the randomized experiments and the human learning.

In the human-to-robot handover process, the human (*handler*) transferred the object to the robot at speeds of 5, 25 and 50mm/s. The results for the *handler*, as plotted in Figure 5.25, show that there is a small increase in the percentage velocity error between the demanded and actual velocities when the velocity target is higher. Errors fluctuated between 5.06%-7.53% with standard deviation values in the range of 0.6-7.2 for both robot control algorithms. In the receiving phase, the robot was instructed to accelerate its speed towards the end position using PI and fuzzy velocity control techniques until approaching to the velocities demanded of 10, 50 and 100mm/s respectively.

It can be observed that the percentage velocity errors by the robot with PI velocity control at the demanded velocities (10, 50 and 100mm/s) were 1.00%, 0.40% and 0.30% with the corresponding standard deviations of 0.1, 0.0 and 0.0. However, with fuzzy logic velocity control the errors were respectively 0.00%, 0.20% and 0.20% with a standard deviation of 0.0. These results are graphically shown in Figure 5.26.

It can be concluded that the errors from fuzzy logic control are somewhat better than those of PI control, as a result of fuzzy logic velocity control having better overall stability, faster response, smaller overshoot and better control performance as compared to proportional integral control. Furthermore proportional integral control cannot provide effective control for non-linear systems, whereas the fuzzy logic control provides a better dynamic response [Fonseca et al. 1999; Garcia, and Domanguez, 2004; Isa et al. 2009; Gaurav and Amrit, 2012]

The results summarized in Table 5.3 indicate that fuzzy logic control yields slightly better performance than proportional integral control. When the human receives the object from the robot, the velocity error decreases with increasing demanded velocities, and the results show that the PI force control technique gives slightly smaller values of speed error than fuzzy logic control.

Table 5.3(a) Comparisons between the actual and demanded velocity in the robot-to-human handover tasks according to PI and fuzzy logic control

Robot-to-human handover task															
Robot PI force control								**Robot FLC force control**							
Velocity of sending phase (mm/s)				**Velocity of receiving phase**				**Velocity of sending phase**				**Velocity of receiving phase**			
Demanded	*Actual*		*Error (%)*	*Demanded*	*Actual*		*Error (%)*	*Demanded*	*Actual*		*Error (%)*	*Demanded*	*Actual*		Error (%)
	Average	SD			Average	SD			Average	SD			Average	SD	
5	5.0	0.0	0.00%	10	12.8	1.6	28.00%	5.0	5.0	0.0	0.00%	10.0	13.1	2.0	31.00%
25	25.0	0.0	0.00%	50	52.4	4.0	4.80%	25.0	25.0	0.0	0.00%	50.0	54.7	2.6	9.40%
50	50.0	0.0	0.00%	100	98.0	6.2	2.00%	50.0	50.0	0.0	0.00%	100.0	105.1	5.7	5.10%

Table 5.3(b) Comparisons between the actual and demanded velocity in the human-to-robot handover tasks according to PI and fuzzy logic control

Human-to-robot handover task															
Robot PI velocity control								**Robot FLC velocity control**							
Velocity of sending phase (mm/s)				**Velocity of receiving phase**				**Velocity of sending phase**				**Velocity of receiving phase**			
Demanded	Actual		Error (%)	Demanded	Actual		Error (%)	Demanded	Actual		Error (%)	Demanded	Actual		Error (%)
	Average	SD			Average	SD			Average	SD			Average	SD	
5.0	5.3	0.6	6.00%	10	9.9	0.1	1.00%	5.0	5.3	0.6	6.00%	10.0	10.0	0.0	0.00%
.25.0	23.6	1.9	5.60%	50	49.8	0.0	0.40%	25.0	23.3	2.1	6.80%	50.0	49.9	0.0	0.20%
50.0	46.3	7.2	7.40%	100	99.7	0.0	0.30%	50.0	46.4	6.5	7.20%	100.0	99.8	0.0	0.20%

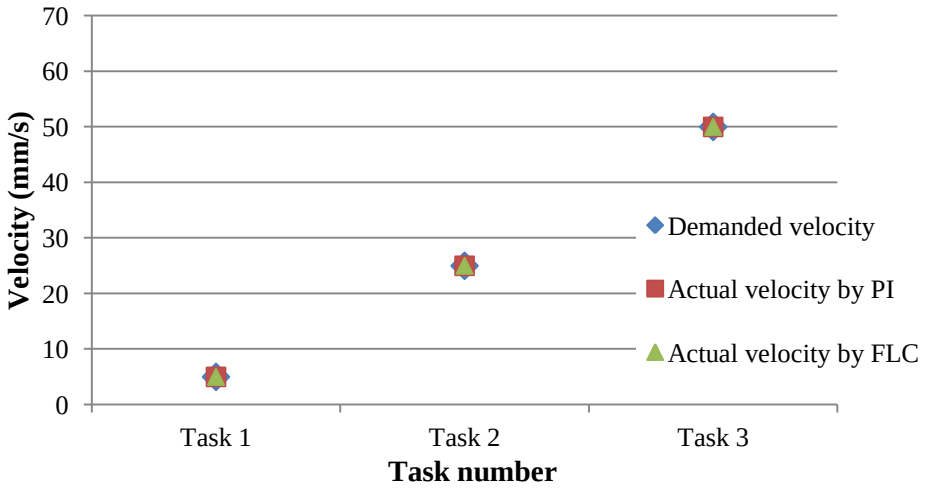

Figure 5.23 Actual and demanded velocity profiles based on PI and FLC in the object sending phase of robot-to-human handover tasks

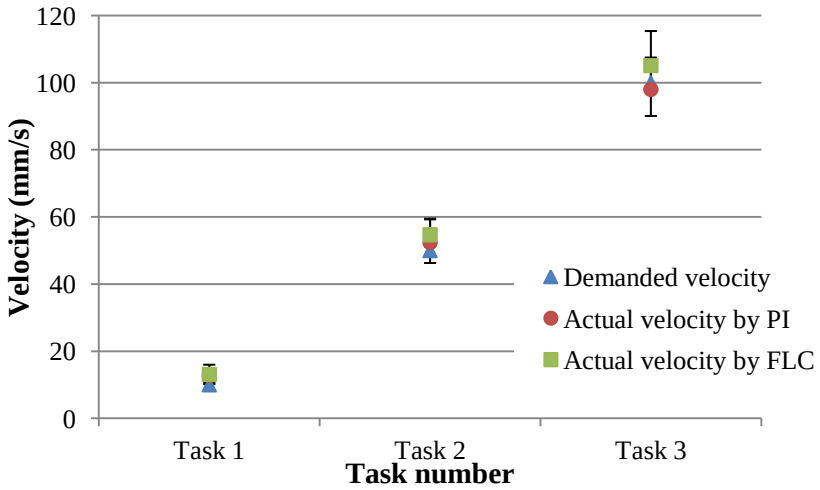

Figure 5.24 Actual and demanded velocity profiles based on PI and FLC in the object receiving phase of robot-to-human handover tasks

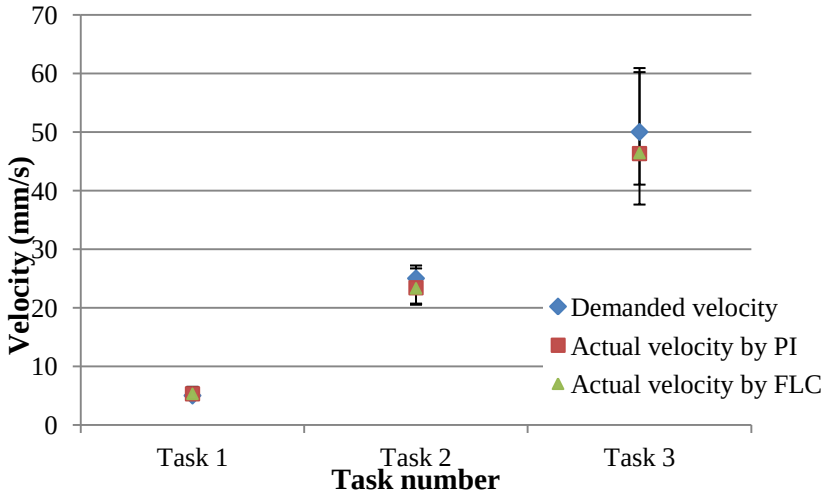

Figure 5.25 Actual and demanded velocity profiles based on PI and FLC in the object sending phase of human-to-robot handover tasks

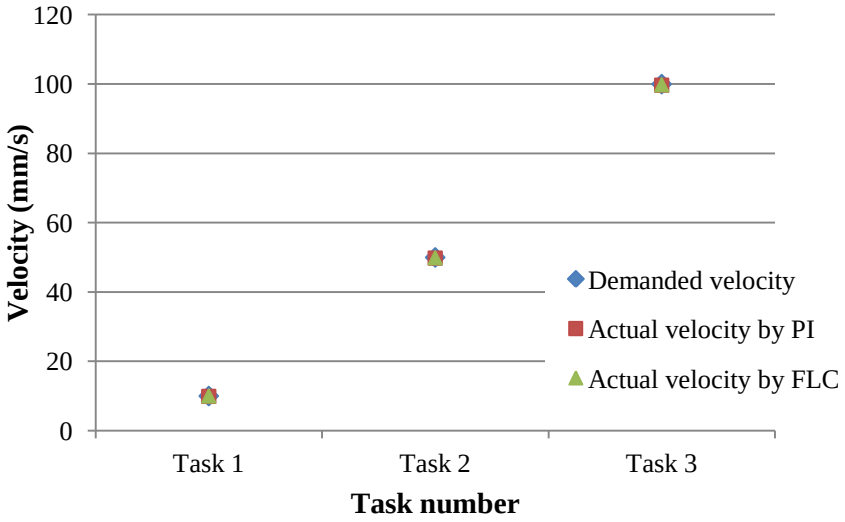

Figure 5.26 Actual and demanded velocity profiles based on PI and FLC in the object receiving phase of human-to-robot handover tasks

5.2.4 Frequency Domain Analysis of Human-Robot Handover Task

The previous two sections have presented the time domain evaluation of all force signals in HRI tests. In this section frequency domain analysis, by way of the fast Fourier transform (FFT), is used to determine the performance of the robot force and velocity control implemented for the robot-human interactive tasks. The FFT analysis technique, first used by Cooley and Tukey [1965], has been applied in many engineering applications. In this study, FFT was employed to identify changes in the power spectrum of the system at three demanded velocities (10, 50 and 100mm/s) for the object handover tasks, and when the Stäubli robot manipulator was controlled using PI and FLC force and velocity control schemes.

From the experimental results (Figures 5.5, 5.8, 5.14 and 5.17) showing the interactive force profiles of the HRI, it was observed that there was small oscillation moderating in the force signals. An FFT was applied to extract the noise frequencies, which were used to compare and evaluate the qualitative performance of the robot based on the proportional integral and fuzzy logic control schemes at various object transfer speeds. The following examples show how the performance in terms of the robot force and velocity control can be evaluated using FFT analysis where the robot was used to pass the object from/to the human at a velocity of 100mm/s.

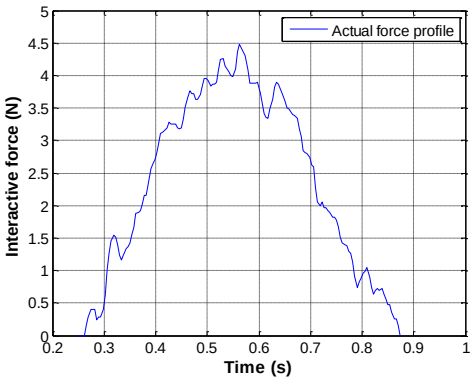

(a) Actual force profile

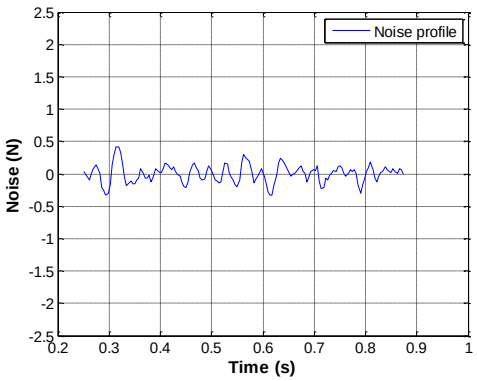

(b) High pass filtered data (noise signal)

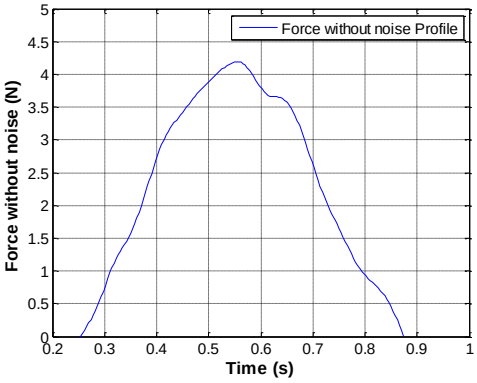

(c) Low pass filtered data

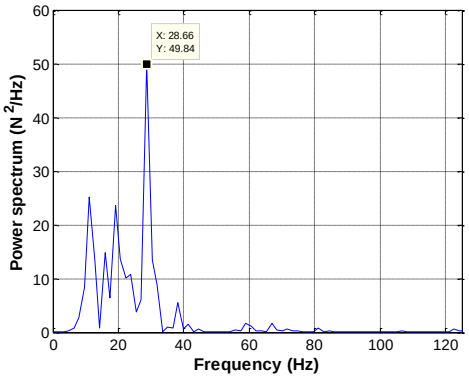

(d) Power spectrum

Figure 5.27 FFT analysis for robot-human interaction using PI control

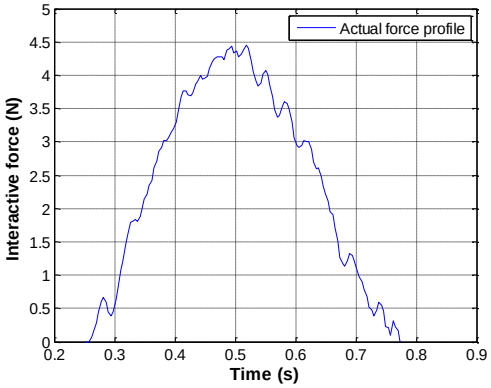

(a) Actual force profile

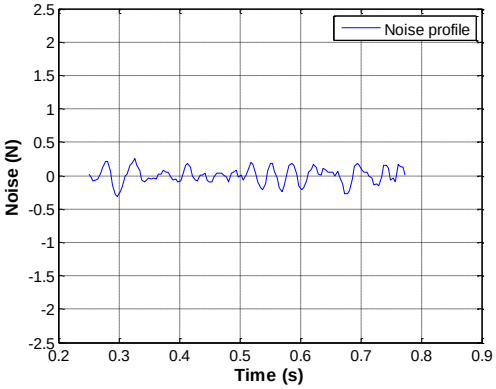

(b) High pass filtered data (noise signal)

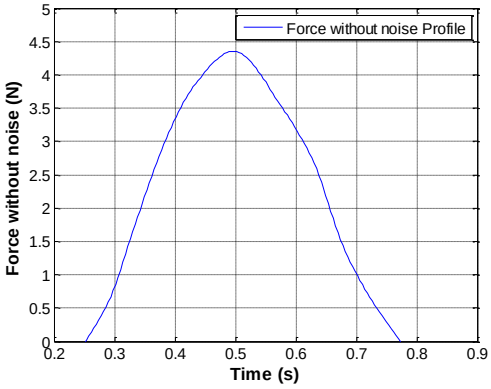

(c) Low pass filtered data

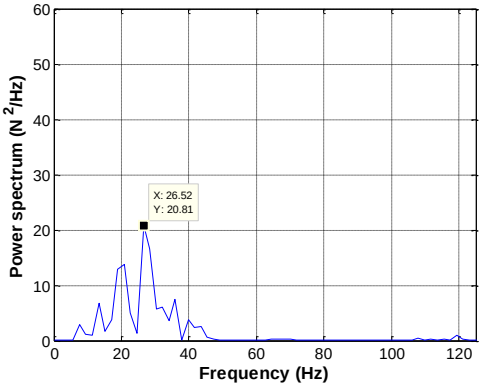

(d) Power spectrum

Figure 5.28 FFT analysis for robot-human interaction using FLC

Figure 5.27(a) illustrates the actual interactive force trajectory during the transfer phase using PI force control. To appropriately identify the noise signal, a high-pass filter (HPF) with a cut-off frequency at 10Hz was used to filter the data (see Figure 5.27(b)). The results of the FFT analysis are plotted in Figure 5.27(c), where the maximum power spectral density is approximately 49.8N^2 at a frequency of 28.66Hz. When the robot was controlled using FLC, a corresponding set of results shown in Figures 5.28(a)-(d) can be seen reduce the magnitudes of the filtered noise signal in the system, as depicted in Figure 5.28(b). Also, the maximum peak of the power spectrum is reduced to 20.81N^2 at the frequency of 26.52Hz.

Table 5.4 Qualitative performance measurement from FFT analysis in the robot-human handover tasks represented by the maximum power spectral values and their frequencies

Velocity (mm/s)	**Robot-to-human handover task**					
	PI			**FLC**		
	Mean (N^2)	**SD (N^2)**	**Frequency (Hz)**	**Mean (N^2)**	**SD (N^2)**	**Frequency (Hz)**
10	7.7	3.3	15.5 - 30.1	5.4	3.1	17.6 - 33.2
50	34.7	12.6	17.5 - 28.6	24.3	7.4	18.2 - 27.3
100	42.5	14.3	16.7 - 32.1	28.6	9.0	18.7 - 31.3
Velocity (mm/s)	**Human-to-robot handover task**					
	PI			**FLC**		
	Mean (N^2)	**SD (N^2)**	**Frequency (Hz)**	**Mean (N^2)**	**SD (N^2)**	**Frequency (Hz)**
10	9.4	6.3	20.5 - 25.7	8.3	3.4	24.5 - 26.3
50	14.7	6.7	14.7 - 35.7	11.5	4.1	15.2 - 34.1
100	27.0	9.2	13.8 - 28.4	18.5	4.0	14.1 - 28.2

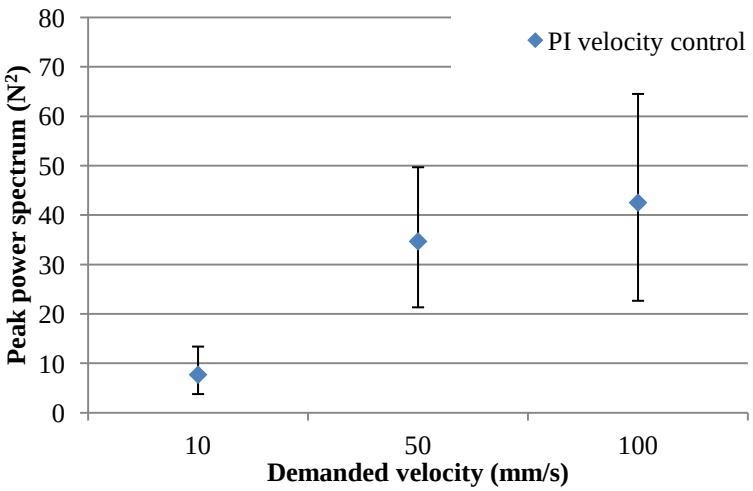

Figure 5.29 Comparison of the power spectral densities of robot using PI and fuzzy logic control at velocities of 10, 50 and 100mm/s in robot-to-human handover tasks

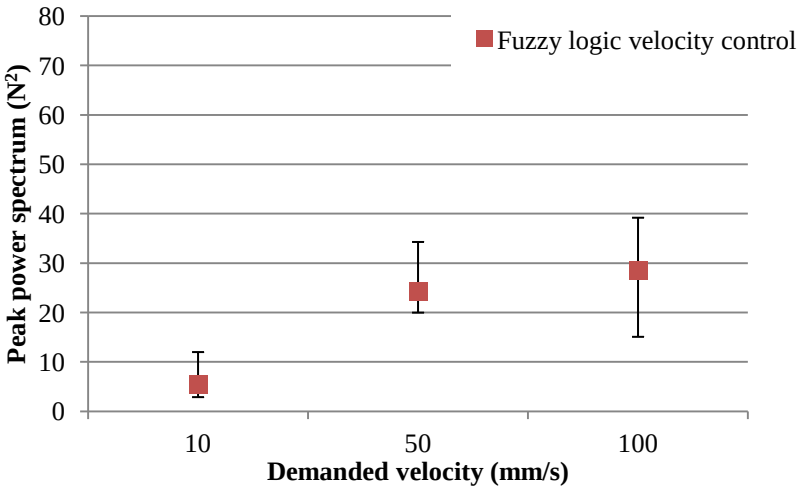

Figure 5.30 Comparison of the power spectral densities of robot using PI and fuzzy logic control at velocities of 10, 50 and 100mm/s in robot-to-human handover tasks

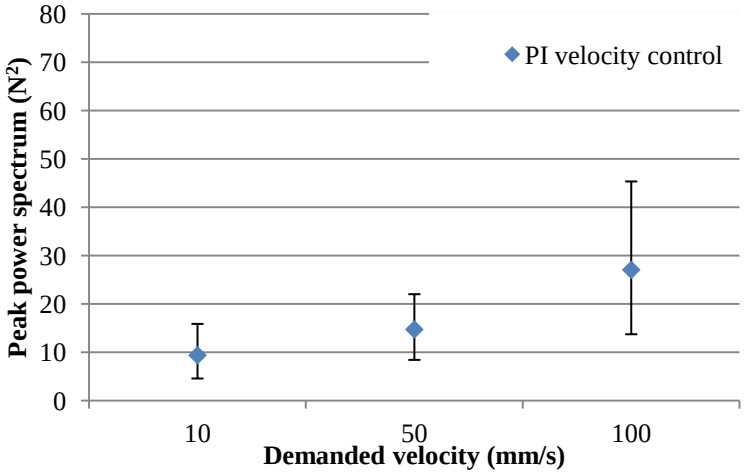

Figure 5.31 Comparison of the power spectral densities of robot using PI and fuzzy logic control at velocities of 10, 50 and 100mm/s in human-to-robot handover tasks

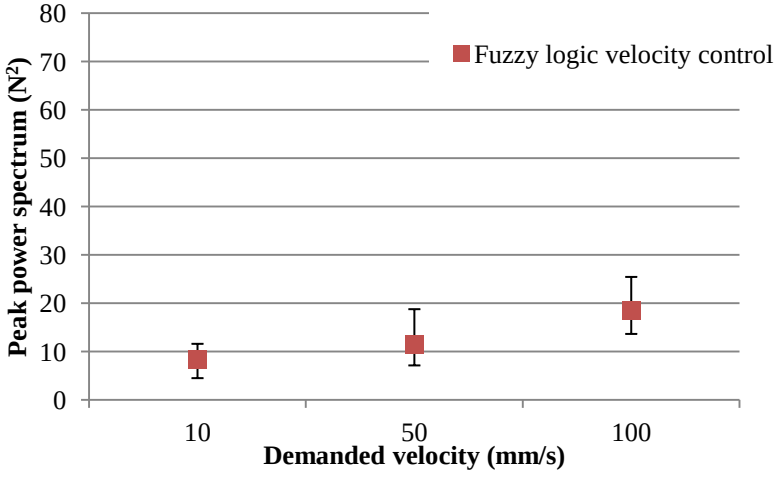

Figure 5.32 Comparison of the power spectral densities of robot using PI and fuzzy logic control at velocities of 10, 50 and 100mm/s in human-to-robot handover tasks

The evaluation of the robot performance for all demanded velocity conditions in the robot-to-human and human-to-robot handover tasks based on PI and fuzzy logic control algorithms is summarised in Table 5.4 and Figures 7.29-7.32. The results are expressed as the frequencies of the maximum power spectral densities delivered according to the proposed conditions, which varied slightly in the range of approximately 14-35Hz. These dominant frequencies were conducted from the dynamics of the robot force control system. Consider a simplest one DOF robot model developed, attempting to describe behaviour of the robot system [Eppinger, 1988] while executing HRI, as shown Figure 5.33 (with a single axis, link and joint), where an effective inertial (total moving mass) the axis is m_r associated with an effective viscous damping to ground is defined as b_r, and the force/torque sensor and human are modelled as a system of mass (m_h), compliance (k_s and k_h) and dashpot (b_s and b_h).

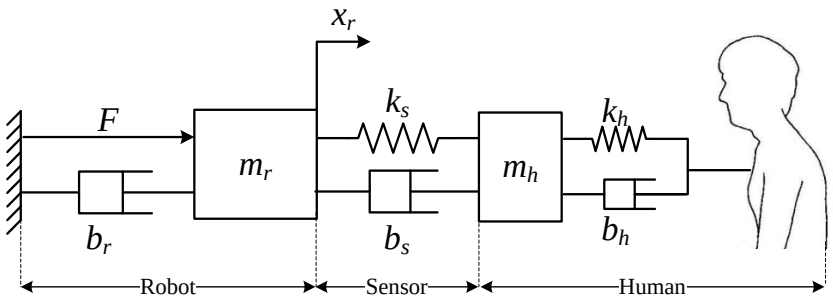

Figure 5.33 A simplest rigid-body model of the robot in HRI based on Eppinger [1988]

The magnitudes of the maximum power spectrum of the filtered data were examined to determine the oscillations of the noise signal for each scenario. Fuzzy logic force control provided better qualitative performance of the robot in all robot-to-human handover tasks, as shown in Figures 5.29-5.30. A comparison of the power spectral densities using FLC and PI control shows that the values of power spectrum were respectively 5.4, 24.3 and 28.6N^2 for FLC, and 7.7, 34.7 and 42.5N^2 for PI control. It can be concluded that the fuzzy logic force control method is more effective in giving enhanced stability and greater overall qualitative performance in the system.

Figures 5.31-5.32 present the power spectral results for the human-to-robot handover tasks based on the proportional integral and fuzzy logic velocity control schemes. The graph profile is similar to that in the robot-to-human handover tasks, insomuch that the noise signals from the PI control, was higher than with fuzzy logic control. The power spectrum values from PI and FLC at the three velocities (10, 50 and 100mm/s) were 9.4, 14.7 and 27.0N^2, and 8.3, 11.5 and 18.5 N^2 respectively. The conclusion of the qualitative performance in terms of stability of the robot velocity control using proportional integral and fuzzy logic control is similar to the results from the robot-to-human handover tests, where the effectiveness of FLC is seen to be better than the PI control, providing more effective dynamic performance and moderation in the force signals than proportional integral control over a wide operational range. Based on the results of the FFT analysis, fuzzy logic control was effectively implemented for force and velocity control in the robot in the human-robot handover tasks.

5.3 Analysis of Questionnaire Responses

The paired T-test comparison technique, as implemented in the preliminary pilot study test explained in Chapter 3, is typically used to compare the means of two different groups on different occasions with repeated measurements and the same samples. The initial assumption is that the data collected are normally distributed. However, the survey responses conveying participants' preferences concerning in the human-robot handover tasks are a statistically nonparametric type of data, which are not required to fit a normal distribution. The Wilcoxon [1945] signed-rank test was considered appropriate for use in determining if a significant overall difference exists in two independent sets of treatments, such as the PI and fuzzy logic control methods, as suggested by Bellera et al. [2010]. The survey responses based on the rating scale items and open questions giving the participants' opinions for the evaluation of the robot control system in human-robot interaction are showed in Table 5.5.

Table 5.5 Survey responses for the human-robot handover tasks

No	Question	Poor (1)	Fair (2)	Good (3)	Very Good (4)	Excellent (5)
1	How comfortable were you with the robot-to-human object handover task 1 (PI)		2	3	13	0
2	How comfortable were you with the robot to human object handover task 2 (FLC)		1	1	3	13
3	How comfortable were you with the human-to-robot object handover task 1 (PI)		1	5	10	2
4	How comfortable were you with the human-to-robot object handover task 2 (FCL)		1	2	13	2
5	Rate the reliability of the overall performance of HRI tests using PI		2	4	10	2
6	Rate the reliability of the overall performance of HRI tests using FLC		1	1	9	7
7	How do you compare the human-robot-object handover task to the human-human-object handover task?			2	13	3

5.3.1 Survey Responses of Robot-to-Human Handover Task

This section evaluates how comfortable the participants felt in participating in the robot-to-human handover tasks with the Stäubli robot manipulator based on the proportional integral and fuzzy logic force control schemes. The hypothesis H_0 and alternative hypothesis H_1 for the Wilcoxon signed-rank two-tailed test are given below:

H_0: The median difference between pairs of observations is zero, so that there is no significant difference in being comfortable with participation in the population distributions of the samples with the robot controlled by the PI and those with the fuzzy logic force control schemes.

H_1: The median difference between pairs of observations is not equal to zero, so that there is a significant difference in being comfortable with participation in the population distributions of the samples with the robot controlled by the PI and those with fuzzy logic force control schemes.

The statistical analysis by means of the Wilcoxon signed-rank test was conducted using the statistical package for the social sciences (SPSS), which is one of the most powerful programs used to analyze a wide variety of statistical problems and recommended by many researchers [Bergmann et al. 2000; Landau and Everitt 2004; Seeger et al. 2007]. A confidence interval of 95% or a significance level (α) of 0.05, which is typically accepted and recommended for scientific experiments [Keppel, 1991], was adopted in these statistical tests.

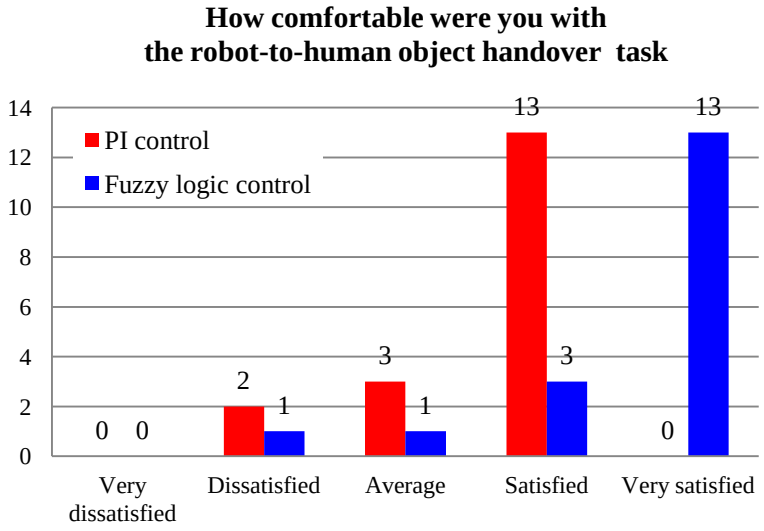

Figure 5.34 Responses of the human participants

Figure 5.34 shows a bar chart of the responses of the human participants comparing how comfortable the participants were whilst performing the physical robot-to-human handover tasks when the robot was implemented by the PI or fuzzy logic force control methods. The rating scale was specified as five points as follows: level 1 - poor or very dissatisfied; level 2 - fair or dissatisfied; level 3 - average or neither satisfied nor dissatisfied; level 4 - good or satisfied; and level 5 - very good or very satisfied. The results show that two largest groups of 13 participants each, or 72.2%, were either satisfied or very satisfied with the performance of the robot implemented by PI and fuzzy logic force control respectively. Additionally, 3 participants (16.6%) were merely satisfied with FCL, while no human subject was very satisfied with the PI control method. Approximately 27.8% and 11.2% respectively of the participants were dissatisfied or had neutral responses with the implementation of the PI and fuzzy logic force control schemes. However, there is no participant who claimed that any of the tests of haptic robot-to-human handover were very dissatisfactory.

To examine whether or not there is difference in the population distributions between paired observations for the PI and fuzzy logic force control techniques, the Wilcoxon test was produced the results shown in Table 5.6. The descriptive statistics include the sample size, mean and standard deviation of each treatment, and maximum and minimum values. The table shows the average satisfaction ratings based on PI and fuzzy force control are 3.61 and 4.56, with the corresponding standard deviations of 0.69 and 0.85 respectively.

Table 5.6 Statistical results

Descriptive Statistics

	N	Mean	Std. Deviation	Minimum	Maximum
PI and FLC	18	3.61	0.69	2	4
for RHI	18	4.56	0.85	2	5

Ranks

		N	Mean Rank	Sum of Ranks
FLC and PI for RHI	Negative Ranks	1[a]	7.50	7.50
	Positive Ranks	15[b]	8.57	128.50
	Ties	2[c]		
	Total	18		

a. FLC for RHI < PI for RHI, b. FLC for RHI > PI for RHI and c. FLC for RHI = PI for RHI

Test Statistics[a]

	FLC and PI for RHI
Z	-3.397[b]
Asymp. Sig. (2-tailed)	.001

a. Wilcoxon Signed-Ranks Test and b. Based on negative ranks.

The rank table provides information on the comparison of the control methods. The negative ranks present that only one participant preferred the PI force control scheme to fuzzy logic control. In contrast, the positive ranks indicate that 15 people thought that the qualitative performance of FLC was better than PI control. The number of ties demonstrates two participants who rated for both robot force control schemes equally. The negative mean rank value of 7.50 is less than the positive mean rank of 8.57, which suggests that the human participants were more comfortable while performing with the robot controlled by the fuzzy logic force control technique than with proportional integral control. The test statistics identify the overall significance of the difference between the two control methods. The significance value estimated was calculated as

0.001, which is less than 0.05, and therefore it can be concluded that the hypothesis H_0 has to be clearly rejected, and the alternative hypothesis H_1 has to be accepted. In other words, there is a significant difference in the population distributions from the samples derived, and the human participants were more comfortable in participating with the robot using the fuzzy logic force control rather than proportional integral control.

5.3.2 Survey Responses for the Human-to-Robot Handover Task

This bar chart in Figure 5.35 illustrates the human's opinions of how comfortable the participants were whilst executing the human-to-robot handover tasks, in which the robot motion was controlled based on the PI and fuzzy velocity control schemes. The rating scale technique was used with five rating levels. It can be observed from the results that the trends for both control schemes gave a similar pattern. The majority of the sample with 10 participants or 55.5% and 13 participants or 72.2% respectively were satisfied with the performance of the robot implemented by PI and fuzzy velocity control. For each control method, 11.1% of the human subjects were very satisfied with the effectiveness of the human-to-robot handover task, and only 1 participant (5.5%) was dissatisfied with the performance of the robot in the interactive task. Additionally, the performance of the robot based on the PI and fuzzy logic velocity control methods was rated as neither satisfactory nor dissatisfactory by 27.8% and 11.1% respectively of the participants.

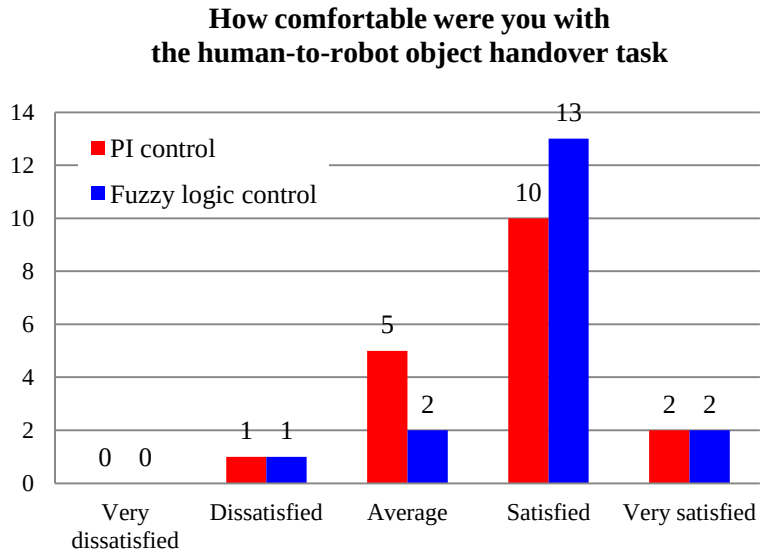

Figure 5.35 Responses of the human participants

With a confidence interval of 95% or at the significance level of 0.05, the hypotheses H_0 and H_1 tested using the Wilcoxon signed-rank two-tail test are given as follows:

H_0: The median difference between pairs of observations is zero, so that there is no significant difference in being comfortable with participation in the population distributions of the samples with the robot controlled by the PI and those with the fuzzy logic velocity control schemes.

H_1: The median difference between pairs of observations is not equal to zero, so that there is a significant difference in being comfortable with participation in the population distributions of the samples with the robot controlled by the PI and those with fuzzy logic velocity control schemes.

Table 5.7 Statistical results

Descriptive Statistics

	N	Mean	Std. Deviation	Minimum	Maximum
PI and FLC for HRI	18	3.72	0.75	2	5
	18	3.89	0.67	2	5

Ranks

		N	Mean Rank	Sum of Ranks
FLC and PI for HRI	Negative Ranks	0[a]	.00	.00
	Positive Ranks	3[b]	2.00	6.00
	Ties	15[c]		
	Total	18		

a. FLC for HRI < PI for HRI, b. FLC for HRI > PI for HRI and c. FLC for HRI = PI for HRI

Test Statistics[a]

	FLC for HRI – PI for HRI
Z	-1.732[b]
Asymp. Sig. (2-tailed)	.083

a. Wilcoxon Signed-Ranks Test and b. Based on negative ranks.

The SPSS statistical software was again used to analyse the results, as shown in Table 5.7. The mean of rating scale for the FLC velocity control, as shown in the descriptive statistics table, is 3.89 (with a standard deviation of 0.67), which is slightly higher than the mean value for the PI velocity control of 3.72 with the corresponding standard deviation of 0.75. In the ranks table, the 3 positive ranks indicate that three participants

were more comfortable with the FLC velocity control than the PI control method. In addition, the number of ties shows that fifteen participant ranked both control schemes similar. Furthermore, the test statistics demonstrate that the overall significance value calculated was 0.083, which is greater than 0.05, and it can be concluded that the hypothesis H_0 has to be accepted and the alternative hypothesis H_1 rejected. In other words, there is no significant difference in the population distributions of ratings concerning participation with the robot controlled by proportional integral and fuzzy logic force control whilst performing the human-to-robot handover task.

5.3.3 Stability of the Robot's Performance in the Human-Robot Interactive Task

Figure 5.36 shows the responses of the participants comparing the overall stability of the robot in human-robot interaction using the different control techniques of PI and FLC. It can be observed that 10 participants (55.5%) and 9 participants (50%) respectively were significantly satisfied with the overall stability of the HRI system using both PI and FLC techniques, with 2 (11.1%) and 7 (38.9%) very satisfied. Consequently, 6 participants (33.3%) were dissatisfied or had neutral responses with the robot performance based on PI control, compared to only 2 (11.1%) with FLC.

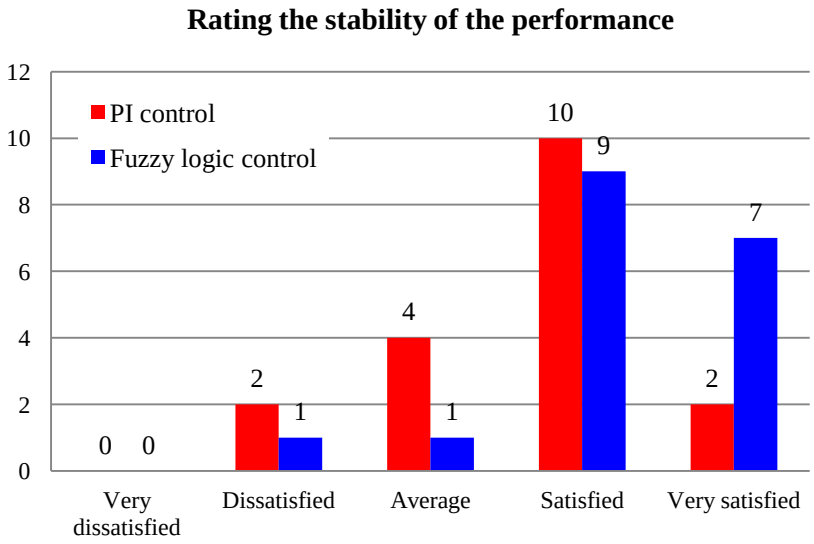

Figure 5.36 Responses of the human participants

The following hypotheses H_0 and H_1 were tested:

H_0: The median difference between pairs of observations is zero, so that there is no significant difference in the population distributions of the rating of the participants concerning the analysis of performance of the system stability for the PI and fuzzy logic control schemes.

H_1: The median difference between pairs of observations is not equal to zero, so that there is significant difference in the population distributions of the rating of the participants concerning the performance analysis of the system stability for both the PI and fuzzy logic control schemes.

Table 5.8 Statistical results

Descriptive Statistics

	N	Mean	Std. Deviation	Minimum	Maximum
Stability_of_PI	18	3.67	0.84	2	5
Stability _of_FLC	18	4.22	0.81	2	5

Ranks

		N	Mean Rank	Sum of Ranks
Stability of FLC and PI	Negative Ranks	1[a]	5.50	5.50
	Positive Ranks	10[b]	6.05	60.50
	Ties	7[c]		
	Total	18		

a. Stability of FLC < Stability of PI, b. Stability of FLC > Stability of PI and c. Stability of FLC = Stability of PI

Test Statistics[a]

	Stability _of_FLC and Stability _of_PI
Z	-2.673[b]
Asymp. Sig. (2-tailed)	.008

a. Wilcoxon Signed Ranks Test

b. Based on negative ranks.

The results of the statistical analysis show that ratings of the stability of the robot system in the HRI tests based on the PI and fuzzy logic control methods were 3.67 and 4.22 respectively, with corresponding standard deviations of 0.84 and 0.81. Only one of the samples (5.5%), as shown in the rank table preferred the stability of PI control to that of fuzzy logic control. Meanwhile ten participants (55.5%) were more appreciative of the performance in terms of stability of fuzzy logic control implemented for the HRI tests rather than the proportional integral velocity control scheme. The number of ties ranks identifies seven human subjects who perceived similar levels of stability for both robotic control techniques. The value of the positive mean rank was 6.05, which is higher than the negative mean rank value at 5.50, which suggests that the participants preferred the stability of the robot performance based on fuzzy logic control to that of proportional integral control. The overall significance value of the Wilcoxon signed-rank two-tailed test was 0.008, and it can be concluded that the hypothesis H_0 has to be rejected and the alternative hypothesis H_1 accepted. This means that there is a significant difference in the population distributions from the participants who were more comfortable with the robot's stability using fuzzy logic control rather than the proportional integral control scheme in the HRI tasks.

5.3.4 Comparison Human-Robot Handover Task to Human-Human Handover Task

The bar chart in Figure 5.37 shows the responses of the participants when comparing the overall performance of the human-robot handover task with that in the human-human handover task. In brief, the majority of the participants at 13 of the sample (72%) were satisfied with the robot's performance, while 2 people (11%) were neither satisfied nor dissatisfied. On the other hand, 3 participants (17%) were very satisfied with the effective implementation of the human-robot interaction during the object handover tests. Based on a five point rating, an average of 4.06 was obtained for satisfaction with the robot implementation of the HRI task as compared with the HHI task.

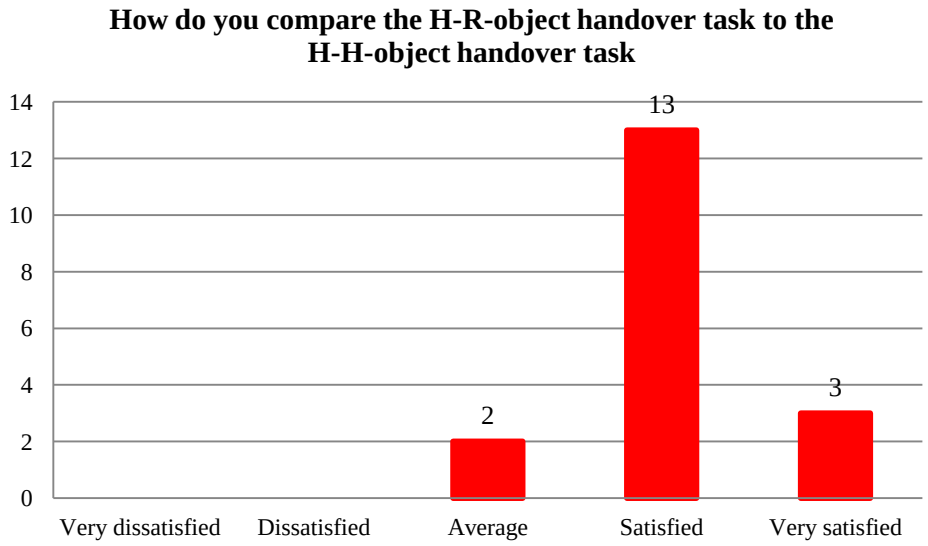

Figure 5.37 Responses of the human participants

In the second part of the questionnaire, from the evaluation of the survey responses the participants delivered their opinions in their own words, and expressed that there was greater satisfaction with the robot FLC force control rather than proportional control. Additionally, the overall stability of the robot was also deemed significantly higher with the FLC scheme than PI during human-robot interaction. This is largely due to the improved ability of the fuzzy logic control algorithm to compensate for the dynamic nature of the non-linear HRI system. However, the results in the survey responses for the human-to-robot handover section with regard to the participant's opinions suggested that the robot PI and fuzzy logic velocity control schemes afforded similar levels of performance, and these results did not agree with those of the parallel actual test results. This may be attributed to the smooth trajectory of the robot when using fuzzy logic control with the humans not sensitive enough to small variations in the robot's velocity. Finally, all participants indicated that the developed human-robot interactive system has been able to effectively perform human-like functions in the object handover tasks, and the overall mean rating of 4.06 (out of 5) indicates their satisfaction with the robot's performance.

5.4 Summary

This chapter has focused on the evaluation of robot force and velocity control based on two control schemes, i.e. proportional integral (PI) and fuzzy logic control (FLC) of the human-robot handover tasks. The experimental results have been presented in the time-domain in terms of the physical maximum interactive forces between the robot and human, transfer time and work done. After careful observation with regard to the human-robot handover test results, the motion of the robot end effector using FLC is significantly smoother than when using PI control, as it is less sensitive to small force disturbances. Fast Fourier transform (FFT) analysis was employed to identify the frequencies of noise signals moderated in interactive force between the robot and human. It has been found that when the robot was controlled by the FLC method, better performance of the controlled robot was achieved, where the power spectral densities of FLC illustrated lower amplitudes of the noise signals compared to PI control.

In addition, FLC which can compensate for the dynamic nature of the non-linear HRI system was deemed to provide an improvement in the robot force and velocity control in terms of reduced interactive force, shorter transfer time and lower work done. Moreover, the survey responded by the human participants in the tests agreed with the test outcomes, and the participants were satisfied with the overall performance of the robot system in the human-robot interactive tasks, where their average satisfaction rating was 4.06 based on a five-point rating scale.

An overall analysis of the results of the performance evaluations of the robot force and velocity control systems indicate that both the PI and FLC robot force control strategies demonstrate an acceptable HRI implementation, where the robot manipulator has been configured to provide the capability of natural and synchronized response with the human in ensuring effective human-robot object handovers.

CHAPTER VI

CONCLUSIONS AND RECOMMENDATIONS FOR FURTHER WORK

An appropriate set of behaviours in a human-robot control strategy has been developed based on understanding of how two humans pass an object to each other in a safe and reliable manner. This has enabled a Stäubli robot manipulator to naturally interact with a human participant in object handover tasks. A set of human-to-robot and robot-to-human handover tasks has been performed and studied. The results have been compared to a human-human interactive (HHI) task in order to evaluate the performance of the robot control force and velocity systems.

8.1 Conclusions

Understanding the human dynamic characteristics of physical HHI using a one degree of freedom (DOF) HHI rectilinear task, where the human *handler* passes the compliant object horizontally to the receiver by sliding it to different target positions, has been carried out. A human behavioural model based on dynamic responses in HHI was successfully evaluated using the extended crossover model proposed by McRuer et al. [1967; 1995]. The main challenge with the model identification is that these relevant model parameters vary considerably according to the characteristics of the system inputs which are influenced by changes in mass, compliance, friction and transfer distance; Matlab was used to determine the model parameters. The results show that the average reaction time for the completion of the tasks was approximately 0.16s, with a corresponding standard deviation of 0.01s, and the coefficients of lead time (T_z) and lag time (T_p) were in the ranges of 0.00–0.02s and 0.00–0.01s respectively, which agreed with the findings of McRuer [1980]. The human muscle gain (K_H) was found to be inversely proportional to the distance moved by the object, and proportional to its mass, friction and faster response; however, it was not affected by compliance.

Whilst the constrained movement of the one DOF rectilinear slider task does not reproduce real-world 3D human-human object handover, a new set of substitutive key HHI handover experiments was developed in order to establish appropriate guidelines for a behavioural control strategy in the robot force and velocity control schemes. Crucial aspects concerned in assessing and identifying the physical behavioural characteristics of the human participants were as follows:

- The interactive force profile (f_{int}) between the *handler* and *receiver* against time (t) describe how it is regulated whilst performing the physical collaborative tasks,
- The maximum interactive force (f_{max}) was used to specify the proportion of magnitude of maximum force that is taken into account when the *handler* decides to release the object to be transferred,
- Transfer time (T_{trf}) indicates how long the object handover process takes, and
- Work done (W) by the paired-participant in each object handover task.

The results for the above variables were used to design and develop an appropriate set of robot force and velocity control strategies in order to permit the robot manipulator arm to interact with a human so as to facilitate the dexterous transfer of objects in an effective manner. In the robot-to-human handover task, the external force control which allows the robot's trajectory to be moderated in real-time was based on applied force in world Cartesian coordinates. Robot velocity control was implemented in the human-to-robot handover tasks, where the trajectory of the robot can be modified according to the output from the velocity control scheme.

The development of the robot external force and velocity control schemes (Chapter 4), were implemented in the object handover tasks between the human and robot co-operators. The robot has to be capable of interacting with the human using velocity and force control to avoid dropping or damaging the object. The robot control was designed so that the location and velocity of the object are tracked using infrared sensors, and the interactive force applied by the human detected using an ATI *Gamma* six-axis force/torque sensor. RT Linux OS was used to communicate in real-time with the ATI controller over a serial port and with the CS8C robot controller via Ethernet using a TCP/IP protocol with data transfer rate of 4ms, or 250Hz. Controlled outputs based on the control schemes were computed and transmitted as incremental displacements.

As suggested by De Schutter and Van Brussel [1988], proportional integral control, which provides accuracy and stability in robot force control, was employed in the HRI tests. A set of preliminary tests of a virtual crank-turning task was conducted to identify the PI gains (K_P and K_I) which achieve the best performance of the robot force control system, based on minimising the variation in radial forces. This set of gains was used to complete tasks with a satisfactory stable performance in a specific environment. Nevertheless, because of the complicated dynamic nature of human behaviour in the human-robot handover tasks, the robot PI control was found to be limiting in terms of its performance and stability. To overcome these limitations an intelligent fuzzy logic control algorithm, which has the capability to accommodate the non-linear dynamic characteristics of the system, was successfully implemented to provide improved performance and stability.

In the robot-to-human and human-to-robot handover tests, the performance of the FLC robot force and velocity control systems has been evaluated and compared with that of proportional integral control. It was shown that the overall quantitative performance of robot control provided an efficient human-human like object handover, where the robot was able to successfully transfer the baton object to the human in a smooth, safe and timely natural manner. Thus it can be concluded that the external PI and FLC robot control strategy can provide the effective performance and reliability of the robot-to-human handover procedure and acceptable HRI implementation. Analysis of the test results revealed that the performance of FLC is superior to that of PI, where the levels work done, transfer time and interactive force in RHI with FLC are smaller than in RHI with PI in all scenarios, and are similar to the HHI tasks. A fast Fourier transform (FFT) analysis was employed to extract the features of the noise in the interactive force signals in the frequency-domain. The results show that the trajectory of the robot's real-time controlled path when the FLC scheme was implemented is significantly smoother than when using PI control.

The experimental results obtained have confirmed that using FLC is advantageous in dealing with non-linear systems and significantly improves the effective dynamic performance and robustness in the system, as shown in the successful HRI application. However, it is acknowledged that the performance of the fuzzy logic control method depends on the design and development of its control rule-base, and is sensitive to the membership function of the fuzzy logic's input and output variables.

A summary of the overall achievements of this research is as follows:

- Determination of an appropriate set of trials, based on a number of participants and a sequence of physical tasks, to satisfy preliminary one DOF HHI rectilinear and substantive one DOF human-human object handover tasks,
- Mathematical study of a dynamic model of human behaviour based on the McRuer crossover model whilst performing the horizontal transfer of the compliant object in the HHI rectilinear experiment, designed using a Box-Behnken statistical technique [Box and Hunter, 1957],
- Design and development of an appropriate set of dynamic behaviours (robot-to-human and human-to-robot handover) in a control strategy by understanding the physical characteristics of a key human-human object handover task. The behavioural control strategy has enabled the robot manipulator arm to effectively interact with the human to facilitate the dextrous transfer of objects in a safe and speedy manner,
- Design and development of robot force and velocity control systems based on PI and FLC algorithms in order to facilitate efficiency and robustness and real-time software modularity for RT Linux and the VAL3 Stäubli robotic language, and
- Performance validation of the capabilities and suitability of the robot's control scheme using the PI and FLC methods in human-to-robot and robot-to-human object handover tasks and which were compared to those of HHI tasks,

8.2 Recommendations and Future Work

From the investigation of HRI in the human-to-robot and robot-to-human handover tasks, it would be beneficial to further improve the system, and there are some opportunities for future work to be carried out in this research area. One such possibility suggested by Bailon et al. [1995] is that taking advantage of a higher sampling rate in the robot force control system will enhance the performance of the system. This can be achieved by changing the robot controller to overcome the limitation of the external ALTER command used on the Stäubli robot's real-time path control which can only be updated and synchronized with an external computer every 4ms.

The results in this study concerning HRI suggest that the qualitative measurement of the performance of robot velocity and force control using proportional integral and fuzzy logic control can lead to acceptable HRI implementation. The intelligent decision

making method of FLC, which can compensate for the dynamic nature of the non-linear HRI system was deemed to improve the performance of the robot control schemes compared to the use of PI force control in terms of reduced interactive force, shorter transfer time and less work done. Nonetheless, if the PI gains are appropriately optimized using such as the Ziegler-Nichols, Cohen-Coon and Chien-Hrones-Reswick techniques, then a formal comparison between the PI and FLC methods in the robot velocity and force control can be undertaken, and this is recommended for future investigation.

To enhance the stability of the controlled robot while it interacts in a complicated dynamic environment with the human operator, the possibility exists to enhance the system by implementing adaptive FLC, as suggested by Burn et al. [2003]. This technique has been developed and used successfully for robot and stable force control in unknown and varied environmental stiffness at the robot/task interface. Moreover, combined fuzzy logic control (FLC) and artificial neuron networks (ANNs), namely neuro-fuzzy control, can also be effectively used [Touati et al, 2002]. This type of control scheme integrates the advantages of both techniques, where the ANNs provides the appropriate tuning of the fuzzy sets, including shape and membership functions, and the rule-base in a controlled system. However, several considerations should be taken into account if such an option is used. For example, the design of neuro-fuzzy control requires large amounts of input and output information to be gathered for training using the learning algorithms of ANNs, and this could introduce longer processing times than when FLC is used on its own.

Finally, in order to improve the real-time object tracking and interaction, it would be beneficial to introduce 3D visual servoing; for example, using a Microsoft Kinect sensor through which the localization and speed of the object to be transferred can be extracted. A Kinect camera can provide the capability for advanced human skeleton tracking for the measurement of human handling gestures using a standard library (OpenNI), which can communicate with RT Linux OS. The performance of the sensor depends on the number of points observed and how many frames are captured per second (up to 30frames/s), so that it requires a very fast PC to process all of the necessary information. However, the higher the rate of detection, the longer time it will take to compute. Also the minimum operational distance between the object and camera is required to be approximately 0.5m.

LIST OF REFERENCES

Aaron, S., Terrence, F., David, K., Michael, L., Jean, S., Alan, S. and Michael, G. (2006) 'Common metrics for human-robot interaction', *Proceedings of the 1st ACM SIGCHI/SIGART conference on Human-robot interaction.* Salt Lake City, Utah, USA, ACM, pp.

Acosta-Calderon, C. A. and Hu, H. (2005) 'Robot imitation: Body schema and body percept', *Applied Bionics and Biomechanics,* 2, (3), pp. 131-148.

Aeolean Inc. (2002) 'Introduction to Linux for Real-Time Control', *National Institute of Standards and technology*. 2002

Aggarwal, P., Dutta, A. and Bhattacharya, B. (2007) 'Cooperation between a 4 DOF robotic hand and a human for carrying an object together', *SICE, 2007 Annual Conference.* 17-20 Sept. 2007. pp. 2354-2359.

Alami, R., Albu-Schaeffer, A., Bicchi, A., Bischoff, R., Chatila, R., De Luca, A., De Santis, A., Giralt, G., Guiochet, J., Hirzinger, G., Ingrand, F., Lippiello, V., Mattone, R., Powell, D., Sen, S., Siciliano, B., Tonietti, G. and Villani, L. (2006) 'Safe and Dependable Physical Human-Robot Interaction in Anthropic Domains: State of the Art and Challenges', *Intelligent Robots and Systems, 2006 IEEE/RSJ International Conference*. 9-15 Oct. 2006. pp. 1-16.

Almeida, F., Lopes, A. n. and Abreu, P. (1999) 'Force-impedance control: a new control strategy of robotic manipulators', *Recent advances in Mechatronics*, pp. 126-37.

Arai, H., Takubo, T., Hayashibara, Y. and Tanie, K. (2000) 'Human-robot cooperative manipulation using a virtual nonholonomic constraint', *IEEE,* pp. 4063-4069 vol. 4.

Arata, Y. E. (2009) 'Reaction Time Measurement Applied to Multimodel Human Control Modeling', *XIX IMEKO World Congress Fundamental and Applied Metrology,* ISBN 978-963-88410-0-1 pp. 2162-2167.

Aslan, N. and Cebeci, Y. (2007) 'Application of Box Behnken design and response surface methodology for modeling of some Turkish coals', *Fuel,* 86, pp. 90-97.

Azuma, R. T. (1997) 'A survey of augmented reality', *Presence-Teleoperators and Virtual Environments,* 6, (4), pp. 355-385.

Baerveldt, A. J. (1992) *Robot and Human Communication, 1992. Proceedings., IEEE International Workshop.* 1-3 Sep 1992.

Bailon, H., Vuskovic, M. I. and Ivankovic, B. (1995) *Systems, Man and Cybernetics, 1995. Intelligent Systems for the 21st Century., IEEE International Conference.* 22-25 Oct 1995.

Bakar, S. B., Yuichir, H., Ikeura, R. and Mizutani, K. (2006) 'Characteristic of 2 DOF cooperative task by two humans', *2006 SICE-ICASE International Joint Conference, Vols 1-13,* pp. 4034-4039.

Bakar, S. A., Ikeura, R., Salleh, A. F. and Yano, T. (2009) 'A study of human-human cooperative characteristic based on task direction', *Micro-NanoMechatronics and Human Science, 2009. MHS 2009. International Symposium.* 9-11 Nov. 2009. pp. 541-546.

Bakar, S. A. B. U., Ikeura, R., Handa, Y., Yano, T., Mizutani, K. and Sawai, H. (2010) 'Communication during the Cooperative Motion in the Task of Carrying an Object between Two Humans', *Journal of Biomechanical Science and Engineering,* 5, (2), pp. 104-118.

Barshir, A. M. (2005) *3D Kinaesthetic Virtual Reality System*, Thesis PhD dissertation. Newcastle University

Becker, M., Kefalea, E., Ma, E., Von Der Malsburg, C., Pagel, M., Triesch, J., VorbrÃ¼ggen, J. C., WÃ¼rtz, R. P. and Zadel, S. (1999) 'GripSee: A gesture-controlled robot for object perception and manipulation', *Autonomous Robots,* 6, (2), pp. 203-221.

Begum, M. and Karray, F. 'Visual Attention for Robotic Cognition: A Survey', *Autonomous Mental Development, IEEE Transactions on,* 3, (1), pp. 92-105.

Bellera, C. A., Julien, M. and Hanley, J. A. (2010) 'Normal approximations to the distributions of the Wilcoxon statistics: accurate to what n? Graphical insights', *Journal of Statistics Education,* 18, (2), pp. 1-17.

Bergmann, R., Ludbrook, J. and Spooren, W. P. J. M. (2000) 'Different outcomes of the Wilcoxon and Whitney test from different statistics packages', *The American Statistician,* 54, (1), pp. 72-77.

Bicchi, A. (2000) 'Hands for dexterous manipulation and robust grasping: a difficult road toward simplicity', *Robotics and Automation, IEEE Transactions on,* 16, (6), pp. 652-662.

Bicchi, A., Rizzini, S. L. and Tonietti, G. (2001) 'Compliant design for intrinsic safety: general issues and preliminary design', *Intelligent Robots and Systems, 2001.* pp. 1864-1869 vol.4.

Bicchi, A. and Tonietti, G. (2004) 'Fast and "soft-arm" tactics [robot arm design]', *Robotics & Automation Magazine, IEEE,* 11, (2), pp. 22-33.

Bicchi, A., Peshkin, M. A. and Colgate, J. E. (2008) 'Safety for physical human-robot interaction', *Springer handbook of robotics*, pp. 1335-1348.

Bicker, R. (1989) *Force feedback in remote tele-manipulation*, Thesis PhD dissertation. Newcastle University

Bien, Z. Z., Jung-Bae, K., Dae-Jin, K., Jeong-Su, H. and Jun-Hyeong, D. (2002) 'Soft Computing Based Emotion/Intention Reading for Service Robot', *Proceedings of the 2002 AFSS International Conference on Fuzzy Systems.*

Boud, A. C., Haniff, D. J., Baber, C. and Steiner, S. J. (1999) 'Virtual reality and augmented reality as a training tool for assembly tasks', *Information Visualization, 1999.* pp. 32-36.

Breazeal, C. and Scassellati, B. (2002) 'Robots that imitate humans', *Trends in Cognitive Sciences,* 6, (11), pp. 481-487.

Breazeal, C., Buchsbaum, D., Gray, J., Gatenby, D. and Blumberg, B. (2005) 'Learning from and about others: Towards using imitation to bootstrap the social understanding of others by robots', *Artificial Life,* 11, (1-2), pp. 31-62.

Brown, F. M., Agah, A., Gauch, J. M., Schreiber, T. and Speer, S. R. (1999) 'A cognitive robot with reconfigurable mind for studying theories of ambiguity resolution', *Systems, Man, and Cybernetics, 1999. IEEE SMC '99.* pp. 994-999 vol.6.

Bruckner, H. P., Spindeldreier, C., Blume, H., Schoonderwaldt, E. and Altenmuller, E. *Wearable and Implantable Body Sensor Networks (BSN), 2012 Ninth International Conference*. 9-12 May 2012.

Burdea, G. and Brooks, F. P. (1996) *Force and touch feedback for virtual reality.* Wiley New York.

Burghart, C., Holzapfel, H., Haeussling, R. and Breuer, S. (2007) 'Coding interaction patterns between human and receptionist robot', *Humanoid Robots, 2007 7th IEEE-RAS International Conference*. Nov. 29 2007-Dec. 1 2007. pp. 454-460.

Burn, K. (1993) *Control of a force reflecting telerobotics system.* Thesis PhD dissertation. Newcastle University.

Burn, K., Short, M. and Bicker, R. (2003) 'Adaptive and nonlinear fuzzy force control techniques applied to robots operating in uncertain environments', *Journal of robotic systems,* 20, (7), pp. 391-400.

Cakmak, M., Srinivasa, S. S., Min Kyung, L., Forlizzi, J. and Kiesler, S. 'Human preferences for robot-human hand-over configurations', *Intelligent Robots and Systems (IROS).* 2011. pp. 1986-1993.

Calderon, C. A. A. and Huosheng, H. (2004) *Intelligent Robots and Systems, 2004. (IROS 2004). Proceedings. 2004 IEEE/RSJ International Conference.* 28 Sept.-2 Oct. 2004.

Cannon, D. J. and Leifer, L. J. (1990) 'Speed and accuracy for a telerobotic human/machine system: experiments with a target-threshold control theory model for Fitts' law', *Systems, Man and Cybernetics, 1990. IEEE International Conference.* 4-7 Nov 1990. pp. 677-679.

Chang, L. Y., Zeglin, G. J. and Pollard, N. S. (2008) 'Preparatory object rotation as a human-inspired grasping strategy', *Humanoid Robots, 2008. Humanoids 2008. 8th IEEE-RAS International Conference.* 1-3 Dec. 2008. pp. 527-534.

Chang, L. Y. and Pollard, N. S. (2009) 'Video survey of pre-grasp interactions in natural hand activities', *Robotics: Science and Systems (RSS) 2009 Workshop on Understanding the Human Hand for Advancing Robotic Manipulation*.

Chanhun, P., Jin-Ho, K. and Dong-Il, P. 'Development of an industrial robot manipulator for the easy and safe human-robot cooperation', *Control Automation and Systems (ICCAS), 2010 International Conference.* 27-30 Oct. 2010. pp. 678-681.

Cooley, J. W. and Tukey, J. W. (1965) 'An algorithm for the machine calculation of complex Fourier series', *Mathematics of computation,* 19, (90), pp. 297-301.

Cox, E. (1994) 'The Fuzzy Systems Handbook: A Practitioner's Guide to Building, Using, and Maintaining Fuzzy Systems, AP Professional', *The Fuzzy Systems Handbook: A Practitioner's Guide to Building, Using, and Maintaining Fuzzy Systems, AP Professional*.

Currell, G., Dowman, A., Stewart Jr, C. N., Irving, P., Rampton, D., Shanahan, F., Cohen, Y., Cohen, J. Y. and Reece, R. J. (2005) 'Essential mathematics and statistics for science', *AMC*, 10, pp. 12.

Dautenhahn, K. and Nehaniv, C. L. (2002) 'The agent-based perspective on imitation', MIT Press, pp. 1-40.

Dautenhahn, K. (2004) 'Robots we like to live with - a developmental perspective on a personalized, life-long robot companion', *Robot and Human Interactive Communication, 2004. ROMAN 2004. 13th IEEE International Workshop*. 20-22 Sept. 2004. pp. 17-22.

Dave, K. (1997) *Accelerated MCSE Study Guide, TCP/IP*. McGraw-Hill, Inc.

De Schutter, J. and Van Brussel, H. (1988) 'Compliant robot motion II. A control approach based on external control loops', *Int. J. Rob. Res.*, 7, (4), pp. 18-33.

Degoulange, E., Dauchez, P. and Pierrot, F. (1993) *Robotics and Automation, 1993. Proceedings., 1993 IEEE International Conference.* 2-6 May 1993.

Dong Il, P., Chanhun, P. and Jin-Ho, K. (2009) 'Design and analysis of direct teaching robot for human-robot cooperation', *Assembly and Manufacturing, 2009. ISAM 2009. IEEE International Symposium.* 17-20 Nov. 2009. pp. 220-224.

Duchemin, G., Poignet, P., Dombre, E. and Peirrot, F. (2004) 'Medically safe and sound [human-friendly robot dependability]', *Robotics & Automation Magazine, IEEE,* 11, (2), pp. 46-55.

Earnshaw, R. A., Gigante, M. A. and Jones, H. (1993) *Virtual reality systems.* Academic press.

Eppinger, S. D. (1988) 'Modeling robot dynamic performance for endpoint force control', *MIT, Artificial Intelligence Laboratory, 1988 - 138 pages*.

Erkorkmaz, K. and Altintas, Y. (2001) 'High speed CNC system design. Part I: jerk limited trajectory generation and quintic spline interpolation', *International Journal of Machine Tools and Manufacture*, 41, (9), pp. 1323-1345.

Erlhagen, W., Mukovskiy, A., Bicho, E., Panin, G., Kiss, C., Knoll, A., Van Schie, H. and Bekkering, H. (2006) 'Goal-directed imitation for robots: A bio-inspired approach to action understanding and skill learning', *Robotics and Autonomous Systems*, 54, (5), pp. 353-360.

Espinosa-Perez, G. and Ortega, R. (1997) *Industrial Electronics, Control and Instrumentation, 1997. IECON 97. 23rd International Conference.* 9-14 Nov 1997.

Farid, F. and Redouane, T. (2009) 'Dynamic External Force Feedback Loop Control of a Robot Manipulator Using a Neural Compensator-Application to the Trajectory Following in an Unknown Environment', *Int. J. Appl. Math. Comput. Sci.*, 19, (1), pp. 113-126.

Feth, D., Groten, R., Peer, A. and Buss, M. (2009) *Robot and Human Interactive Communication, 2009. RO-MAN 2009. The 18th IEEE International Symposium.* Sept. 27 2009-Oct. 2 2009.

Fisher, W. D. and Mujtaba, M. S. (1991) 'A Kinematically Stable Hybrid Position/Force Control Scheme'.

Fitts, P. (1954) 'The information capacity of the human motor system in controlling the amplitude of movement', *Journal of Experimental Psychology*, 47, (6), pp. 381-391.

Flash, T. and Hogan, N. (1985) 'The coordination of arm movements: an experimentally confirmed mathematical model', *The journal of Neuroscience,* 5, (7), pp. 1688-1703.

Fong, T., Thorpe, C. and Baur, C. (2003) 'Collaboration, dialogue, human-robot interaction', *Robotics Research*, pp. 255-266.

Fonseca, J., Afonso, J. L., Martins, J. l. S. and Couto, C. (1999) 'Fuzzy logic speed control of an induction motor', *Microprocessors and Microsystems,* 22, (9), pp. 523-534.

Fritsch, J., Kleinehagenbrock, M., Haasch, A., Wrede, S. and Sagerer, G. (2005) *Robotics and Automation, 2005. ICRA 2005. Proceedings of the 2005 IEEE International Conference.* 18-22 April 2005.

Gambier, A. (2004) 'Real-time control systems: a tutorial', *Control Conference, 2004. 5th Asian.* 20-23 July 2004. pp. 1024-1031 Vol.2.

Garcia, J. M. and Domnguez, J. A. (2004) 'Comparison between Fuzzy logic and PI controls in a Speed scalar control of an induction machine', *CIRCE Departamento deIngeniera CPS, Universidad de Zaragoza, Conf. Paper.*

Garcia, L. M., Oliveira, A. A. F., Grupen, R. A., Wheeler, D. S. and Fagg, A. H. (2000) 'Tracing patterns and attention: humanoid robot cognition', *Intelligent Systems and their Applications, IEEE,* 15, (4), pp. 70-77.

Gaurav, A. K. 'Comparison between Conventional PID and Fuzzy Logic Controller for Liquid Flow Control: Performance Evaluation of Fuzzy Logic and PID Controller by Using MATLAB/Simulink', *International Journal of Innovative Technology and Exploring Engineering (IJITEE) ISSN,* pp. 2278-3075.

Gaurav and Amrit, K. (2012) 'Comparison between Conventional PID and Fuzzy Logic Controller for Liquid Flow Control: Performance Evaluation of Fuzzy Logic and PID Controller by Using MATLAB/Simulink', *International Journal of Innovative Technology and Exploring Engineering*.

Glasauer, S., Huber, M., Basili, P., Knoll, A. and Brandt, T. (2010) 'Interacting in time and space: Investigating human-human and human-robot joint action', *RO-MAN, 2010 IEEE.* 13-15 Sept. 2010. pp. 252-257.

Glattfelder, A. H. and Schaufelberger, W. (1986) 'Start-up performance of different proportional-integral-anti-wind-up regulators', *International Journal of Control,* 44, (2), pp. 493-505.

Geidenstam, S., Huebner, K., Banksell, D. and Kragic, D. (2009) 'Learning of 2D grasping strategies from box-based 3D object approximations', Citeseer 10-16.

Gini, M. (2002) *Intelligent autonomous systems 7.* IOS Press Inc.

Giuliani, M., Lenz, C., Müller, T., Rickert, M. and Knoll, A. 'Design principles for safety in human-robot interaction', *International Journal of Social Robotics,* 2, (3), pp. 253-274.

Goodrich, M. A. and Olsen, D. R., Jr. (2003) 'Seven principles of efficient human robot interaction', *Systems, Man and Cybernetics, 2003. IEEE International Conference.* 5-8 Oct. 2003. pp. 3942-3948 vol.4.

Gordon, A. M., Westling, G., Cole, K. J. and Johansson, R. S. (1993) 'Memory representations underlying motor commands used during manipulation of command and novel objects', *Journal of Neurophysiology,* 69, (6), pp. 1789-1796.

Groten, R., Feth, D., Goshy, H., Peer, A., Kenny, D. A. and Buss, M. (2009) 'Experimental analysis of dominance in haptic collaboration', *Robot and Human Interactive Communication, 2009. RO-MAN 2009. The 18th IEEE International Symposium.* Sept. 27 2009-Oct. 2 2009. pp. 723-729.

Haddadin, S., Suppa, M., Fuchs, S., Bodenmuller, T., Albu-Schaffer, A. and Hirzinger, G. 'Towards the Robotic Co-Worker', *At-Automatisierungstechnik,* 58, (12), pp. 695-708.

Haddadin, S., Albu, S., x, ffer, A., De Luca, A. and Hirzinger, G. (2008) 'Collision detection and reaction: A contribution to safe physical Human-Robot Interaction', *Intelligent Robots and Systems, 2008. IROS 2008. IEEE/RSJ International Conference.* 22-26 Sept. 2008. pp. 3356-3363.

Heinzmann, J. and Zelinsky, A. (1999) 'The safe control of human-friendly robots', *Intelligent Robots and Systems, 1999. IROS '99. Proceedings. 1999 IEEE/RSJ International Conference.* 1999. pp. 1020-1025 vol.2.

Heinzmann, J. and Zelinsky, A. (2003) 'Quantitative safety guarantees for physical human-robot interaction', *The International Journal of Robotics Research,* 22, (7-8), pp. 479-504.

Heyer, C. 'Human-Robot Interaction and Future Industrial Robotics Applications', *Ieee/Rsj 2010 International Conference on Intelligent Robots and Systems (Iros 2010)*, pp. 4749-4754.

Hogan, N. (1984) 'Impedance Control: An Approach to Manipulation', *American Control Conference, 1984.* 6-8 June 1984. pp. 304-313.

Huber, M., Rickert, M., Knoll, A., Brandt, T. and Glasauer, S. (2008) 'Human-robot interaction in handing-over tasks', *Robot and Human Interactive Communication, 2008. RO-MAN 2008. The 17th IEEE International Symposium.* 1-3 Aug. 2008. pp. 107-112.

Huebner, K. and Kragic, D. (2008a) 'Selection of robot pre-grasps using box-based shape approximation', *Intelligent Robots and Systems, 2008. IROS 2008. IEEE/RSJ International Conference.* 22-26 Sept. 2008. pp. 1765-1770.

Huebner, K., Ruthotto, S. and Kragic, D. (2008b) 'Minimum volume bounding box decomposition for shape approximation in robot grasping', *Robotics and Automation, 2008. ICRA 2008. IEEE International Conference.* 19-23 May 2008. pp. 1628-1633.

Ikeura, R. and Inooka, H. (1995) 'Variable impedance control of a robot for cooperation with a human', *Robotics and Automation, 1995. Proceedings., 1995 IEEE International Conference.* 21-27 May 1995. pp. 3097-3102 vol.3.

Ikeura, R., Morita, A. and Mizutani, K. (1997) 'Variable damping characteristics in carrying an object by two humans', *Robot and Human Communication, 1997. RO-MAN '97. Proceedings., 6th IEEE International Workshop.* 29 Sep-1 Oct 1997. pp. 130-134.

Ikeura, R., Moriguchi, T. and Mizutani, K. (2002) 'Optimal variable impedance control for a robot and its application to lifting an object with a human', *Robot and Human Interactive Communication, 2002. Proceedings. 11th IEEE International Workshop.* 2002. pp. 500-505.

Ikuta, K., Ishii, H. and Nokata, M. (2003) 'Safety evaluation method of design and control for human-care robots', *The International Journal of Robotics Research,* 22, (5), pp. 281.

Jahaya, J., Nawawi, S. W. and Ibrahim, Z. 'Multi input single output closed loop identification of two wheel inverted pendulum mobile robot', *Research and Development (SCOReD), 2011 IEEE Student Conference.* 19-20 Dec. 2011. pp. 138-143.

Jianming, Z., Ning, W. and Shuqing, W. (2004) 'A developed method of tuning PID controllers with fuzzy rules for integrating processes', *American Control Conference, 2004. Proceedings of the 2004.* June 30 2004-July 2 2004. pp. 1109-1114 vol.2.

Johansson, R. S. (1998) 'Sensory input and control of grip', *Sensory Guidance of Movement,* pp. 45-63.

Keppel, G. (1991) *Design and analysis: A researcher's handbook.* Prentice-Hall, Inc.

Khuntia, S. R., Mohanty, K. B., Panda, S. and Ardil, C. (2009) 'A comparative study of PI, IP, fuzzy and neuro-fuzzy controllers for speed control of DC motor drive', *International Journal of Electrical Systems Science and Engineering,* 1, (1).

Kilgus, C. C. and Gore, W. C. (1972) 'Root-Mean-Square Error in Encoded Digital Telemetry', *Communications, IEEE Transactions on,* 20, (3), pp. 315-320.

Kleinehagenbrock, M., Fritsch, J. and Sagerer, G. (2004) 'Supporting advanced interaction capabilities on a mobile robot with a flexible control system', *Intelligent Robots and Systems, 2004. (IROS 2004).* pp. 3649-3655 vol.4.

Komati, B., Pac, M. R., Ranatunga, I., Popa, D. O. and Lutz, P. 'Explicit force control vs impedance control for micromanipulation', *ASME 2013 International Design Engineering Technical Conferences and Computers and Information in Engineering Conference.* American Society of Mechanical Engineers, pp. V001T09A018-V001T09A018.

Kosuge, K. and Hirata, Y. (2004) *Robotics and Biomimetics, 2004. ROBIO 2004. IEEE International Conference.* 22-26 Aug. 2004. pp. 8-11.

Kulic, D. and Croft, E. A. (2005) 'Real-time safety for human - robot interaction', *Advanced Robotics, 2005. ICAR '05. Proceedings., 12th International Conference.* 18-20 July 2005. pp. 719-724.

Landau, S. and Everitt, B. (2004) *A handbook of statistical analyses using SPSS.* Chapman & Hall/CRC Boca Raton, FL.

Lawitzky, M., Mo, x, rtl, A. and Hirche, S. 'Load sharing in human-robot cooperative manipulation', *RO-MAN, 2010 IEEE.* 13-15 Sept. 2010. pp. 185-191.

Lederman, S. and Klatzky, R. 'Designing haptic and multimodal interfaces: a cognitive scientist™ perspective', *the Workshop on Advances in Interactive Multimodal Telepresence Systems.* pp. 71-80.

Lenz, C., Nair, S., Rickert, M., Knoll, A., Rosel, W., Gast, J., Bannat, A. and Wallhoff, F. (2008) 'Joint-action for humans and industrial robots for assembly tasks', *Robot and Human Interactive Communication, 2008. RO-MAN 2008.* pp. 130-135.

Lew, J. Y., Yung-Tsan, J. and Pasic, H. (2000) 'Interactive control of human/robot sharing same workspace', *Intelligent Robots and Systems, 2000. (IROS 2000).* pp. 535-540 vol.1.

Luh, J. Y. S. and Shuyi, H. (1998) 'Comparison of various models of robot and human in human-robot interaction', *Systems, Man, and Cybernetics, 1998.* pp. 1139-1144 vol.2.

Macfarlane, S. and Croft, E. A. (2003) 'Jerk-bounded manipulator trajectory planning: design for real-time applications', *Robotics and Automation, IEEE Transactions on,* 19, (1), pp. 42-52.

Mamdani, E. H. (1974) 'Application of fuzzy algorithms for control of simple dynamic plant', *Electrical Engineers, Proceedings of the Institution of,* 121, (12), pp. 1585-1588.

Marsden, P. V. and Wright, J. D. (2010) *Handbook of survey research.*Second Edition ed: Bingley, UK: Emerald Publishing Group Limited.

Mason, M. T. (1981) 'Compliance and Force Control for Computer Controlled Manipulators', *Systems, Man and Cybernetics, IEEE Transactions on,* 11, (6), pp. 418-432.

Mason, A. and MacKenzie, C. (2005) 'Grip forces when passing an object to a partner', *Experimental Brain Research,* 163, (2), pp. 173-187.

Mataric, M. J. (2007) 'The robotics primer'. MIT Press Cambridge, MA, USA ©1998.

McRuer, D. T. and Jex, H. R. (1967) 'A Review of Quasi-Linear Pilot Models', *Human Factors in Electronics, IEEE Transactions on,* HFE-8, (3), pp. 231-249.

McRuer, D. T., Systems Technology, i. and Hugh, L. D. F. R. C. (1995) *Pilot-induced oscillations and human dynamic behavior.* NASA.

Meltzoff, A. N. and Brooks, R. (2001) 'Like me as a building block for understanding other minds: Bodily acts, attention, and intention', *Intentions and intentionality: Foundations of social cognition*, pp. 171-191.

Miossec, S. and Kheddar, A. (2008) 'Human motion in cooperative tasks: Moving object case study', IEEE, pp. 1509-1514.

Mitka, E., Gasteratos, A., Kyriakoulis, N. and Mouroutsos, S. G. (2012) 'Safety certification requirements for domestic robots', *Safety Science,* 50, (9), pp. 1888-1897.

Monica, N. N. and Maja, J. M. (2002) 'A hierarchical architecture for behavior-based robots', *Proceedings of the first international joint conference on Autonomous agents and multiagent systems: part 1*. Bologna, Italy, ACM.

Morimoto, C. H. and Flickner, M. (2000) 'Real-time multiple face detection using active illumination', *Automatic Face and Gesture Recognition, 2000.* pp. 8-13.

Napier, J. R. (1956) 'The prehensile movements of the human hand', *Surger,* 38, (4), pp. 902-913.

Olsen, D. R. and Goodrich, M. A. (2003) 'Metrics for evaluating human-robot interactions', *PERMIS. 2003: Gaithersburg, Maryland, USA.* Citeseer.

Patrick, J. B. (1999) *Introduction to TCP/IP Internetworking.* South-Western Educational Publishing.

Patyra, M. J. and Mlynek, D. M. (1996) *Fuzzy logic: implementation and applications.* John Wiley & Sons, Inc.

Peng, P., Lynch, K. M., Peshkin, M. A. and Colgate, J. E. (2005) 'Human interaction with passive assistive robots', *Rehabilitation Robotics, 2005. ICORR 2005.* pp. 264-268.

Perdereau, V. r. and Drouin, M. (1993) 'A new scheme for hybrid force-position control', *Robotica,* 11, (05), pp. 453-464.

Pham, D. T. and Heginbotham, W. B. (1986) *Robot grippers.* Bedford : IFS, 1986.

Qining, W., Lianghuan, L., Guangming, X. and Long, W. (2006) 'Learning from Human Cognition: Collaborative Localization for Vision-based Autonomous Robots', *Intelligent Robots and Systems,* pp. 3301-3306.

Rahman, M. M., Ikeura, R. and Mizutani, K. (2000a) 'Control characteristics of two humans in cooperative task and its application to robot control', *Iecon 2000: 26th Annual Conference of the Ieee Industrial Electronics Society, Vols 1-4,* pp. 1773-1778.

Rahman, M. M., Ikeura, R. and Mizutani, K. (2000b) 'Control characteristics of two humans in cooperative task', *International Conference on Systems, Man & Cybernetics,* pp. 1301-1306

Rahman, M. M., Ikeura, R. and Mizutani, K. (2002) 'Investigation of the impedance characteristic of human arm for development of robots to cooperate with humans', *Jsme International Journal Series C-Mechanical Systems Machine Elements and Manufacturing,* 45, (2), pp. 510-518.

Raibert, M. H. and Craig, J. J. (1981) 'Hybrid Position/Force Control of Manipulators', *Journal of Dynamic Systems, Measurement, and Control,* 103, (2), pp. 126-133.

Rani, P., Sarkar, N., Smith, C. A. and Kirby, L. D. (2004) 'Anxiety detecting robotic system–towards implicit human-robot collaboration', *Robotica,* 22, (01), pp. 85-95.

Raphael, W. 'Grasp sensing for human-computer interaction', *Proceedings of the fifth international conference on Tangible, embedded, and embodied interaction.* Funchal, Portugal, ACM, pp. 221-228.

Reed, K. B., Patton, J. and Peshkin, M. (2007) 'Replicating human-human physical interaction', *Proceedings of the 2007 Ieee International Conference on Robotics and Automation, Vols 1-10,* pp. 3615-3620.

Reed, K. B. and Peshkin, M. A. (2008) 'Physical Collaboration of Human-Human and Human-Robot Teams', *Ieee Transactions on Haptics,* 1, (2), pp. 108-120.

Rezzoug, N. and Gorce, P. (2003) 'A biocybernetic method to learn hand grasping posture', *Kybernetes*, 32, (4), pp. 478-490.

Rivas, M. A. and Harbour, M. G. l. (2001) 'MaRTE OS: An Ada kernel for real-time embedded applications', in *Reliable SoftwareTechnologies-Europe 2001*. Springer, pp. 305-316.

Rofer, T. and Jungel, M. (2003) 'Vision-based fast and reactive Monte-Carlo localization', *Robotics and Automation, 2003. Proceedings. ICRA '03. IEEE International Conference.* pp. 856-861 vol.1.

Romero, L., Morales, E. and Sucar, E. (2001) 'An exploration and navigation approach for indoor mobile robots considering sensor's perceptual limitations', IEEE, pp. 3092-3097 vol. 3.

Ronald, C. A. (1998) *An Behavior-based Robotics.* MIT Press Cambridge, MA, USA ©1998.

Ross, T. J. (2004) *Fuzzy logic with engineering applications.* John Wiley & Sons.

Rotman, G., Brenner, E. and Smeets, J. B. J. (2004) 'Quickly tapping targets that are flashed during smooth pursuit reveals perceptual mislocalisations', *Experimental brain research*, 156, (4), pp. 409-414.

Rouse, W. B. (1980) 'Systems engineering models of human-machine interaction '. New York : North Holland, USA 1980.

Salisbury, J. K. (1980) 'Active stiffness control of a manipulator in cartesian coordinates', *Decision and Control including the Symposium on Adaptive Processes*, pp. 95-100.

Sangtungtong, W. and Dadthuyawat, W. *Electrical Engineering/Electronics, Computer, Telecommunications and Information Technology (ECTI-CON), 2013 10th International Conference.* 15-17 May 2013.

Saxena, A., Driemeyer, J. and Ng, A. Y. (2008) 'Robotic grasping of novel objects using vision', *The International Journal of Robotics Research*, 27, (2), pp. 157.

Scheidt, R. A., Dingwell, J. B. and Mussa-Ivaldi, F. A. (2001) 'Learning to move amid uncertainty', *Journal of Neurophysiology*, 86, (2), pp. 971-985.

Schmitt, T., Hanek, R., Beetz, M., Buck, S. and Radig, B. (2002) 'Cooperative probabilistic state estimation for vision-based autonomous mobile robots', *Robotics and Automation, IEEE Transactions on*, 18, (5), pp. 670-684.

Schutter, J. D. and Brussel, H. v. (1988) 'Compliant robot motion II. A control approach based on external control loops', *Int. J. Rob. Res.*, 7, (4), pp. 18-33.

Sebanz, N., Bekkering, H. and Knoblich, G. (2006) 'Joint action: bodies and minds moving together', *Trends in Cognitive Sciences*, 10, (2), pp. 70-76.

Seeger, F. H., Tonn, T., Krzossok, N., Zeiher, A. M. and Dimmeler, S. (2007) 'Cell isolation procedures matter: a comparison of different isolation protocols of bone marrow mononuclear cells used for cell therapy in patients with acute myocardial infarction', *European heart journal*, 28, (6), pp. 766-772.

Seow, S. C. (2005) 'Information Theoretic Models of HCI: A Comparison of the Hick-Hyman Law and Fitts' Law', *Human"Computer Interaction,* 20, (3), pp. 315-352.

Shannon, C. E. (2001) 'A mathematical theory of communication', *ACM SIGMOBILE Mobile Computing and Communications Review,* 5, (1), pp. 3-55.

Shibata, S., Sahbi, B. M., Tanaka, K. and Shimizu, A. (1997) 'An analysis of the process of handing over an object and its application to robot motions', *Systems, Man, and Cybernetics, 1997. Computational Cybernetics and Simulation., 1997 IEEE International Conference.* 12-15 Oct 1997. pp. 64-69 vol.1.

Shibata, S., Yamamoto, T., Jindai, M. and Shimizu, A. (2003) 'A fundamental approach of avoidance planning of robots considering human emotions', *Jsme International Journal Series C-Mechanical Systems Machine Elements and Manufacturing,* 46, (1), pp. 270-277.

Siciliano, B., Khatib, O., Villani, L. and De Schutter, J. (2008) 'Force Control', in *Springer Handbook of Robotics.* Springer Berlin Heidelberg, pp. 161-185.

Smeets, J. B. J. and Brenner, E. (1995) 'Perception and action are based on the same visual information: distinction between position and velocity', *Journal of Experimental Psychology: Human Perception and Performance,* 21, (1), pp. 19.

Soroka, S. (2002) *Modern Problems of Radio Engineering, Telecommunications and Computer Science, 2002. Proceedings of the International Conference.* 2002.

Soros, G., Resko, B., Solvang, B. and Baranyi, P. (2009) 'A cognitive robot supervision system', *Applied Machine Intelligence and Informatics, 2009. SAMI 2009.* pp. 51-55.

Stankovic, J. A. (1988) 'Misconceptions about real-time computing: a serious problem for next-generation systems', *Computer,* 21, (10), pp. 10-19.

Stevens, W. R. (1993) *TCP/IP illustrated (vol. 1): the protocols.* Addison-Wesley Longman Publishing Co., Inc.

Stiefelhagen, R., Yang, J. and Waibel, A. (2002) 'Tracking focus of attention for human-robot communication'.

Strabala, K. W., Lee, M. K., Dragan, A. D., Forlizzi, J. L., Srinivasa, S., Cakmak, M. and Micelli, V. 'Towards seamless human-robot handovers', *Journal of Human-Robot Interaction,* 2, (1), pp. 112-132.

Sugeno, M. and Kang, G. T. (1988) 'Structure identification of fuzzy model', *Fuzzy Sets and Systems,* 28, (1), pp. 15-33.

Sukhan, L., Hun-Sue, L., Seung-Min, B., Jongmoo, C., Dong-Wook, S., ByoungYoul, S. and Young-Jo, C. (2006a) 'Caller Identification Based on Cognitive Robotic Engine', *Robot and Human Interactive Communication, 2006.* pp. 417-423.

Sukhan, L., Hun-Sue, L. and Dong-Wook, S. (2006b) 'Cognitive Robotic Engine for HRI', *Intelligent Robots and Systems, 2006 IEEE/RSJ International Conference.* 9-15 Oct. 2006. pp. 2601-2607.

Sutcliffe, A. (1988) *Human-computer interface design.* Macmillan Education, London.

Tan, J. T. C. and Arai, T. (2010) 'Information support development with human-centered approach for human-robot collaboration in cellular manufacturing', *RO-MAN, IEEE*. pp. 767-772.

Takubo, T., Arai, H., Hayashibara, Y. and Tanie, K. (2002) 'Human-robot cooperative manipulation using a virtual nonholonomic constraint', *International Journal of Robotics Research*, 21, (5-6), pp. 541-553.

Touati, Y., Djouani, K. and Amirat, Y. (2002) 'Neuro-fuzzy based approach for hybrid force/position robot control', *Industrial Technology, 2002. IEEE ICIT '02. 2002 IEEE International Conference*. 2002. pp. 376-381 vol.1.

Tsumugiwa, T., Yokogawa, R. and Hara, K. (2002) 'Variable impedance control with virtual stiffness for human-robot cooperative task (human-robot cooperative peg-in-hole task)', *SICE 2002. Proceedings of the 41st SICE Annual Conference*. pp. 2329-2334 vol.4.

Traver, V. J., del Pobil, A. P. and Perez-Francisco, M. (2000) 'Making service robots human-safe', *Intelligent Robots and Systems, 2000. (IROS 2000). Proceedings. 2000 IEEE/RSJ International Conference*. 2000. pp. 696-701 vol.1.

Trujillo, A. C. and Gregory, I. 'Piloting changes to changing aircraft dynamics: What do pilots need to know?', *Digital Avionics Systems Conference (DASC), 2011 IEEE/AIAA 30th.* 16-20 Oct. 2011. pp. 6A5-1-6A5-12.

Vaishnav, S. R. and Khan, Z. J. (2007) *Design of PID & Fuzzy Logic controller for higher order system*. International MultiConference of Engineers & Computer Scientists.

Vasic, M. and Billard, A. 'Safety Issues in Human-Robot Interactions', *2013 IEEE International Conference on Robotics and Automation*.

Visioli, A. (2006) *Practical PID control.* Springer.

Volpe, R. and Khosla, P. (1993) 'A theoretical and experimental investigation of explicit force control strategies for manipulators', *Automatic Control, IEEE Transactions on*, 38, (11), pp. 1634-1650.

Vukobratovic, M., Surdilovic, D. and Ekalo, Y. (2008) *Dynamics and Robust Control of Robot-environment Interaction.* World Scientific Publishing Co., Inc.

Weiss, A., Bernhaupt, R., Lankes, M. and Tscheligi, M. (2009) 'The usus evaluation framework for human-robot interaction', Citeseer.

Wesley, P. C., Chris, A. C. P., Loos, H. F. M. V. d. and Elizabeth, A. C. (2012) 'Grip forces and load forces in handovers: implications for designing human-robot handover controllers', *Proceedings of the seventh annual ACM/IEEE international conference on Human-Robot Interaction*. Boston, Massachusetts, USA.

Wilcoxon, F. (1945) 'Individual Comparisons by Ranking Methods', *Biometrics Bulletin*, 1, (6), pp. 80-83.

Wolpert, D. M., Doya, K. and Kawato, M. (2003) 'A unifying computational framework for motor control and social interaction', *Philosophical Transactions of the Royal Society of London Series B-Biological Sciences*, 358, (1431), pp. 593-602.

Won-Kyung, S., Dae-Jin, K., Jong-Sung, K. and Zeungnam, B. (2001) 'Visual servoing for a user's mouth with effective intention reading in a wheelchair-based robotic arm', *Robotics and Automation, 2001. Proceedings 2001 ICRA. IEEE International Conference.* 2001. pp. 3662-3667 vol.4.

Xiangyang, Z. and Jun, W. (2003) 'Synthesis of force-closure grasps on 3-D objects based on the Q distance', *Robotics and Automation, IEEE Transactions on,* 19, (4), pp. 669-679.

Yamada, Y., Hirasawa, Y., Huang, S., Umetani, Y. and Suita, K. (1997) 'Human-robot contact in the safeguarding space', *Mechatronics, IEEE/ASME Transactions on,* 2, (4), pp. 230-236.

Yanco, H. A., Drury, J. L. and Scholtz, J. (2004a) 'Beyond usability evaluation: Analysis of human-robot interaction at a major robotics competition', *Human-Computer Interaction,* 19, (1), pp. 117-149.

Yanco, H. A. and Drury, J. (2004b) 'Classifying human-robot interaction: an updated taxonomy', *Systems, Man and Cybernetics*. pp. 2841-2846 vol.3.

Yoshikawa, T., Koeda, M. and Fujimoto, H. (2008) 'Shape recognition and grasping by robotic hands with soft fingers and omnidirectional camera', *Robotics and Automation, 2008.* pp. 299-304.

Yoshikawa, T., Koeda, M., Fujimoto, H., Khatib, O., Kumar, V. and Pappas, G. (2009) 'Shape Recognition and Optimal Grasping of Unknown Objects by Soft-Fingered Robotic Hands with Camera Experimental Robotics', in. Vol. 54 Springer Berlin / Heidelberg, pp. 537-546.

Zadeh, L. (1956) 'On the Identification Problem', *Circuit Theory, IRE Transactions on,* 3, pp. 277-281.

Zeng, G. and Hemami, A. (1997) 'An overview of robot force control', *Robotica,* 15, (05), pp. 473-482.

Zhihao, G., Haojun, X. and Lin, L. (2007) 'A Variable Strategy Pilot Modeling and Application', *Mechatronics and Automation, 2007. ICMA 2007.* pp. 210-214.

APPENDIX A

DESIGN OF A ONE DEGREE OF FREEDOM HUMAN-HUMAN INTERACTIVE RECTILINEAR TASK

LIST OF CONTENTS

A.1 Mechanical Design

The test platform was based on a hollow box with a wooden frame with dimensions of 900mm×200mm×10mm, which allowed cables to neatly pass through and provide a sufficiently rigid structure to stabilize the system. A linear slider was firmly packed to the workspace on the top of the wooden box in order to support a smooth and low-friction movement path. The linear slider used was the RSR 12w model made from high grade stainless steel, with a 900mm-linear guide rail as shown in cross-section in Figure A.1.

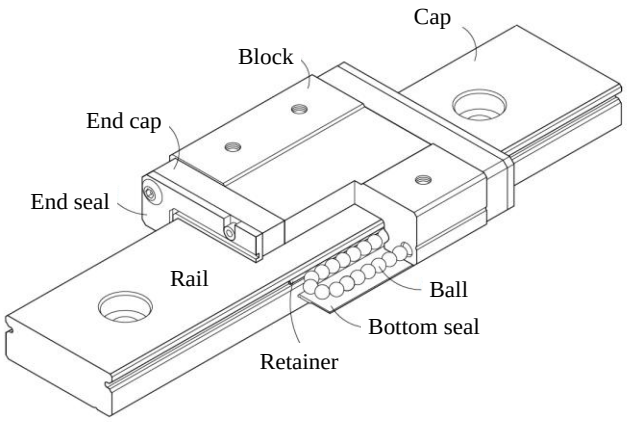

Figure A.1 The linear slider, RSR 12w model

For the system of spring-coupled-masses, two sets of masses m_1 and m_2 were placed individually on the top surfaces of the rigid rectangular bars, which were connected by a spring as demonstrated in Figure A.2. Plastic handles were shaped as cylinders 0.5inches in diameter and 6inches high. The spring stiffness capacities were required to be adjustable at 1.0, 1.5 and 2.0kN/m; therefore the spring's ends were properly designed so that comfortable replacement was possible in order to avoid wasting time in the test preparation.

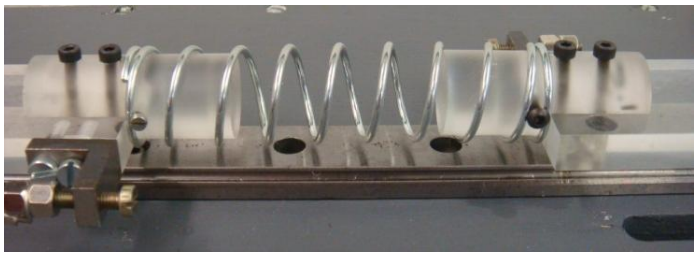

Figure A.2 Modified spring ends

The set of masses utilized to regulate the system moment of inertia were made from mild steel, which involved in load capacities of 0.5, 1.0 and 1.5kilograms. During the tests, it was covered by a gray box to prevent the visualization from the human subjects as illustrated in Figure A.3.

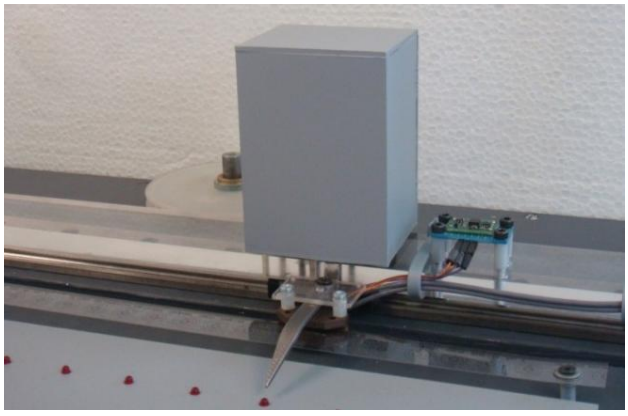

Figure A.3 The set of masses covered by an opaque gray box

A.2 Electronic Design

The aim of the one DOF HHI test was to investigate how the *handler* and *receiver* behave in an object handover task. The parameters of external human forces and object displacement and acceleration needed to be measured in real-time. The assumption that the human force would act in the horizontal direction was addressed first. Load cell sensors were adopted to establish the measurement of human forces f_s and f_r applied. An individual grab handle was notched and attached by two parallel LCL-005 load cells, which can detect force magnitude up to 4.54kg force capacity. Strategically, it was necessary to employ the coupling strain gauges, in order to reduce the more bending of the force sensors, whilst applying higher force. The LCL-005 load cell products were designed and developed by integrating four strain gauges arranged in a full Wheatstone bridge configuration, as shown in Figure A.4.

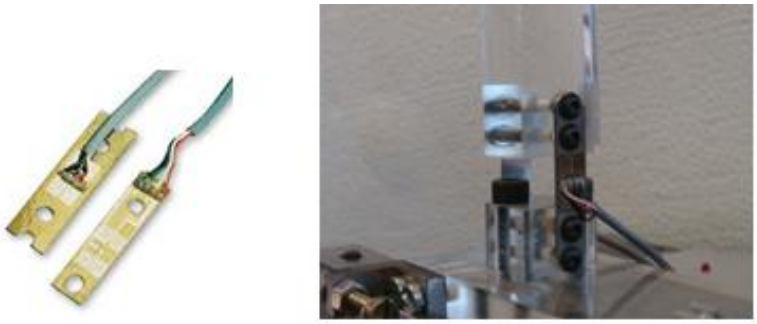

Figure A.4 Two parallel full-bridge-thin-beam load cells and their installation

The precision INA128 instrumentation amplifiers were used to deliver the enhance signals from the full-bridge-thin-beam load cells, in which the INA128 circuit diagram is schematically illustrated in Figure A.5. The INA 128 amplifiers were used due to their low power consumption as well as excellent stability and accuracy. Additionally, electrically twisted and shielded high-flex transducer cables were employed in order to avoid signal distortion. The INA 128 amplifiers can be implemented for a wide range of variable gains by varying an external resistor, R_G, in order to obtain a signal gain from 1 to 10,000. The formula below demonstrates the relation between R_G and output gain. To offer a gain of 500, which was appropriate for the load cell signals, an estimated resistor of 1-$k\Omega$ was considered suitable for use in the circuit.

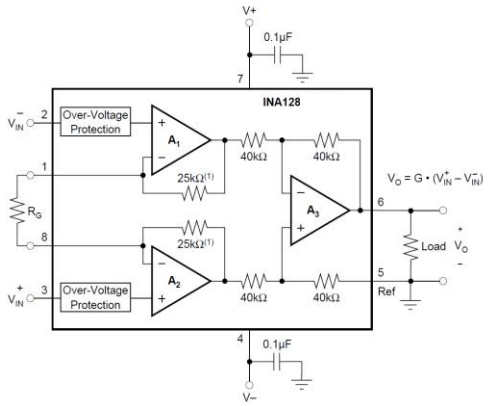

Figure A.5 Power instrumentation amplifier, INA 128

$$Gain = 1 + \frac{500\ k\Omega}{R_G} \tag{A.1}$$

The output gain of 500 can be found from:

$$R_G = \frac{500\ k\Omega}{500-1} \approx 1k\Omega \tag{A.2}$$

As the accurate detection of position is a prime consideration, two optical incremental linear encoders were employed to detect the object displacements x_1 and x_2. The encoder selected is composed of two main components: a transmissive linear strip, LIN-120-12-N model, 12inches in length; a transmissive optical encoder module, EM1-0-120, with a resolution of 120cycles per inch. The EM1 modules are able to generate digital quadratic signals with 5voltage excitation and the resolution values of these modules and linear strips have to strictly match. Figure A.6 illustrates the schematic of a transmissive optical encoder module and linear strip. Converting object displacement signal into three digital pulse trains of square waves is processed by an optical encoder. The output signals could be quantized using 32-bit counters, furnished in a National Instrument Data Acquisition (NI DAQ) Card, prior to being latched over LabVIEW.

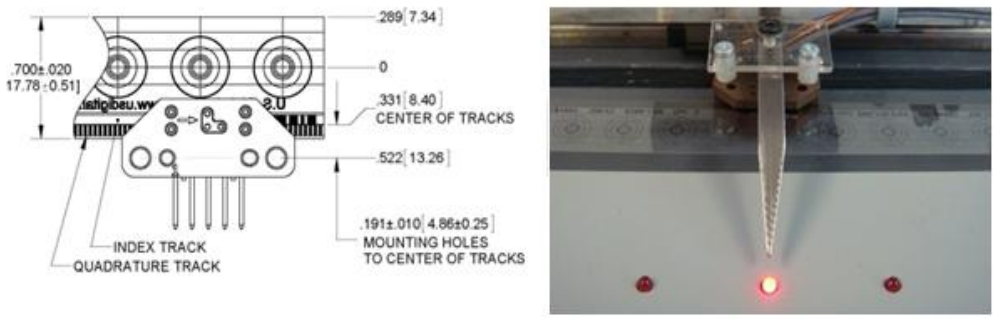

Figure A.6 Transmissive optical encoder module and linear strip

Although the object velocities $\dot{x}_1$ and $\dot{x}_2$ can be calculated from the high accuracy and resolution of optical linear encoders, the output signals could not effectively be conveyed as clean signals of accelerations $\ddot{x}_1$ and $\ddot{x}_2$ by double differentiating because the acceleration profiles achieved are normally moderated by noise. Nevertheless, the undesirable signals can be filtered out using digital or analog filters, and this process requires time delay to be applied in the real-time recording system. Therefore two accelerometers were employed to measure accelerations in the system.

Figure A.7 shows the schematic of a two-axis seismic accelerometer, DE-ACCM 6G model. The inertia of mass *m* is connected to a spring *k* and dashpot *c* through a moving object x^*. The mass displacement *x* can be electrically detected through a linear distance sensor, and to calculate its acceleration Newton's second law of motion is then applied. The accelerometers were strategically mounted onto the compliant object and the signal output is a variable (0-3.3) DC voltage corresponding to the magnitude of object acceleration and its direction. To minimize signal loss and achieve device interface protection, the sensor output was dispatched to a buffer and driver device, SN74LS241 model, before further transmission to a NI DAQ card.

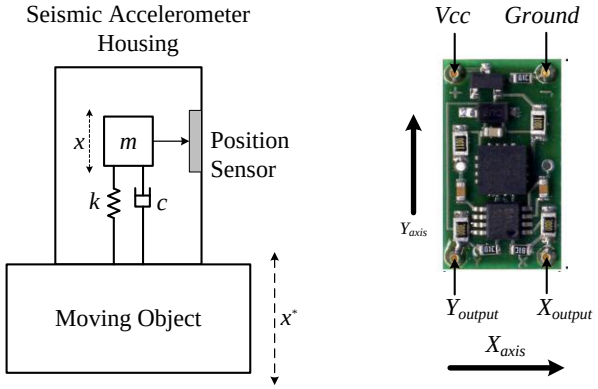

Figure A.7 Schematic of a DE-ACCM 6G seismic accelerometer

The frictional forces (f_{res1} and f_{res2}) acting against the movement of the object were required to be consistently, smoothly and quickly generated, and it was therefore necessary to be electrically operated. M.0113.2411 electromagnetic clutches, as shown in Figure A.8, were employed to efficiently introduce a set of system frictions. This electromagnetic clutch is able to produce up to 2.83-Nm torque.

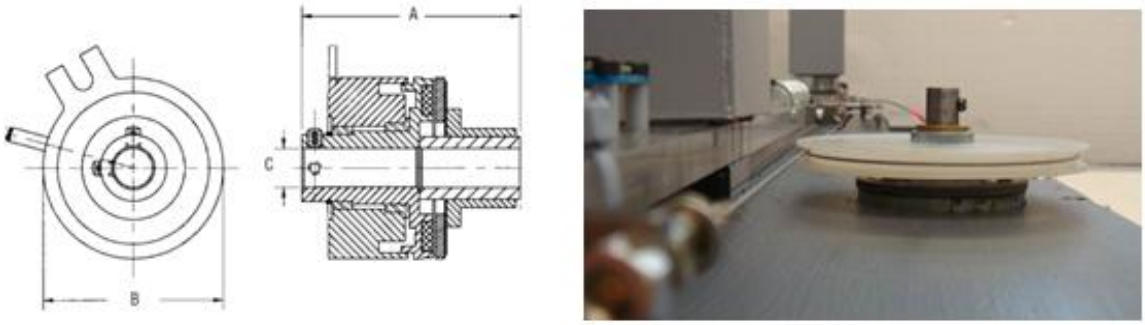

Figure A.8 Cross-section and the installation of the electromagnetic clutch

To activate the electromagnetic clutch engagement, current flows directly through the electromagnet to generate a magnetic field. Consequently, the rotor portion of the electromagnetic clutch becomes magnetized and produces a magnetized loop to attract the armature against the rotational movement of the clutch. Conversely, removing the current exiting from the electromagnetic clutch leads to its disengagement, which allows the armature to rotate freely without any attraction force. This implies that the frictional force is electrically controlled by changing the strength of the magnetic field. The primary advantage of using an electromagnetic clutch is that it results in a fast dynamic response in a system. Transfer efficiency is also high and, in addition, the torque induced is linear to the associated field current. Xiaogang and his colleagues proposed a simple relationship between the applied current and the transmission torque of an electromagnetic clutch as shown in Equation A.3 [Xiaogang et.al 2008], where the transmission is directly proportional to the current supplied to the clutch coil:

$$T_e = k_f \times I_h \tag{A.3}$$

where, T_e is transmission torque.

k_f is proportion factor.

I_h is current of clutch coil.

The M.0113.2411 electromagnetic clutches were firmly mounted to the wooded frame and their armature hubs were strategically fitted to the pulley systems in order to transmit frictional forces in the system. To regulate the various stabilized transmission torques, two digitized adjustable 0-30 DC voltage power supplies with current control circuits were individually used, as schematically illustrated in Figure A.9 Here the terminals P_3, P_4 and P_5 are connectors for a X9C103 digital potentiometer in order to facilitate the effective performance of digital torque control.

Figure A.10 displays a block diagram of the X9C103 digital potentiometer, which consists of a 99-resistor array, a set of wiper switches, a control selection and non-volatile memory, and recalling upon a power up operation. The connectors of the 3-wire serial-interface digital potentiometer are made up of CS U/D and INC pins, and these are utilized to control the position of the wiper element in order to obtain the variable digital voltage outputs.

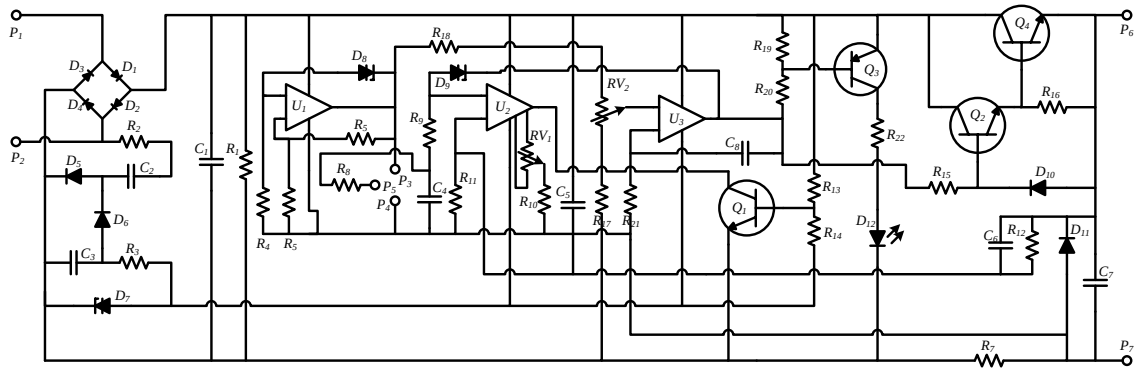

Figure A.9 The adjustable 0-30 DC voltage power supply with current control circuit

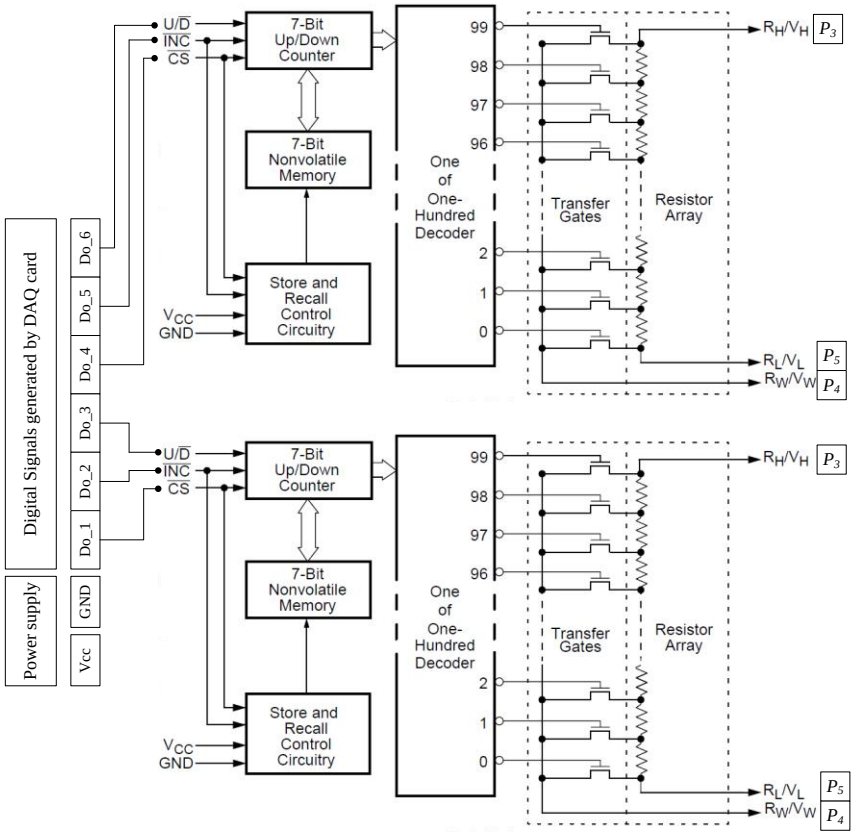

Figure A.10 Block diagram of the X9C103 digital potentiometer

A.3 Data Acquisition System and Software Design

The Laboratory Virtual Instrument Engineering Workbench (NI-LabVIEW) software was used for data collection and embedded graphical data monitoring. In this study, the need for a more cost-effective solution was highlighted. Two NI DAQ cards (USB 6211 and USB 6008) were chosen to meet requirements as follows. The object displacements (and directions) are detected by optical incremental linear encoders. The pulse trains from the encoders were directly ×4 decoded using a 32-bit counter in the USB 6211 card. Velocity is estimated by measuring the number of sequential quadratic pulses in a fixed time interval. Each analog signal from the force sensors and accelerometers was quantized using a 16-bit analog to digital converter for further processing. Additionally, the individual electromagnetic clutch was digitally controlled using the digital potentiometer, so that it required three channels of digital outputs.

A LabVIEW virtual interface served to provide automatic computer-based data collection and embedded graphical data monitoring in real time, and Figure A.11 shows the LabVIEW specification requirements as follows:

- 4×16-bit analog inputs for the 4 full-bridge-thin-beam load cells,
- 2×16-bit analog inputs supplied for the accelerometer outputs,
- 2×32-bit counter channels offered for the incremental encoders, and
- 2×3-bit digital channels prepared for the 2 digital potentiometers.

The USB-6211 furnishes sixteen analog inputs (16-bit A/D converter, 400kS/s sampling rate), two analog outputs (16-bit D/A converter, 250kS/s sampling rate), and 32 bi-directional digital input/output pins. Additionally, two 32-bit counters/timers support two generated quadratic pulse trains from the incremental linear encoders. The USB-6008 utilises eight analog inputs (12-bit A/D converter, 10kS/s sampling rate), two analog outputs (12-bit D/A converter, 150S/s sampling rate), and twelve bidirectional digital input/output channels. A 32-bit counter is also available on the card.

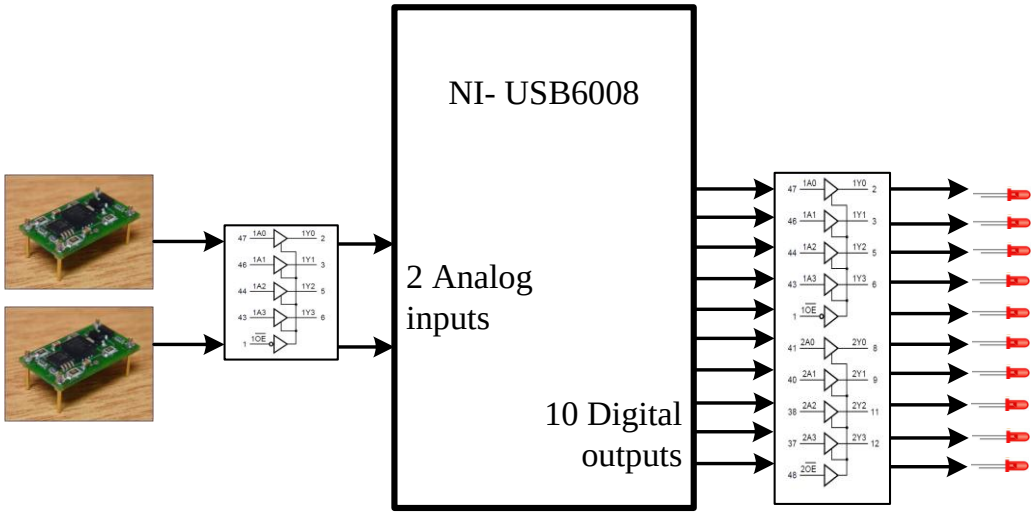

(a) Requirements for NI-USB6008

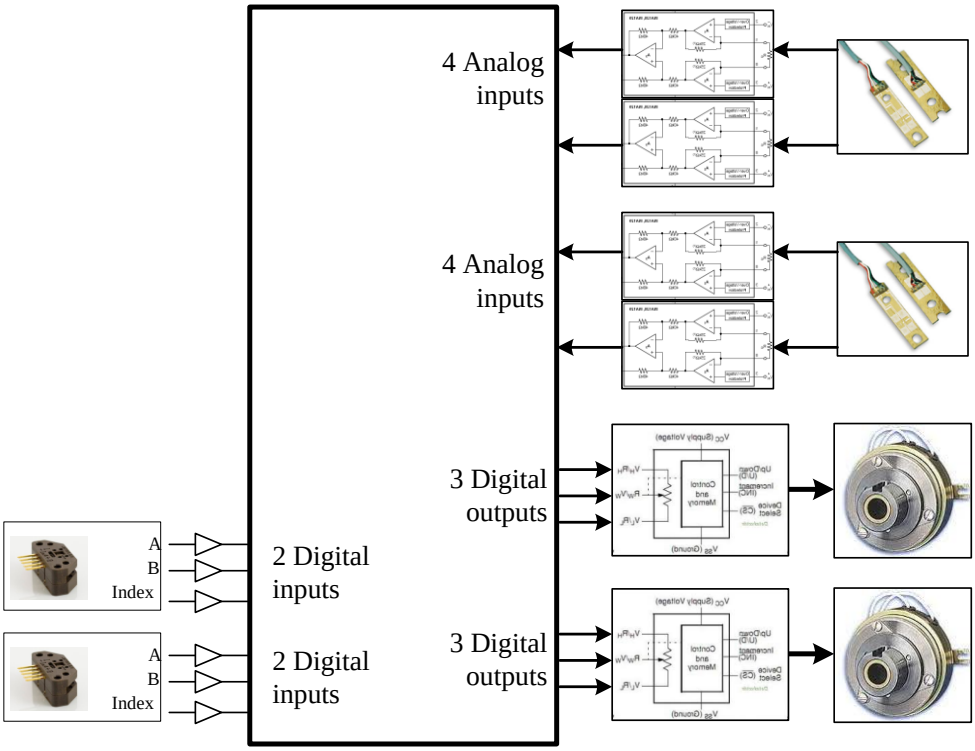

(b) Requirements for NI-USB6211

Figure A.11 Specification requirements for the LabVIEW data acquisition card

LabVIEW software used to support instrument access is based on a dataflow diagram. The data flow programming allows effective multiple operations to run in parallel. The program developed for the preliminary one-degree of freedom human-human interactive process is presented in Figures A.12(a) and (b), where the full program is attached in Appendix B.

(a) LabVIEW front panel

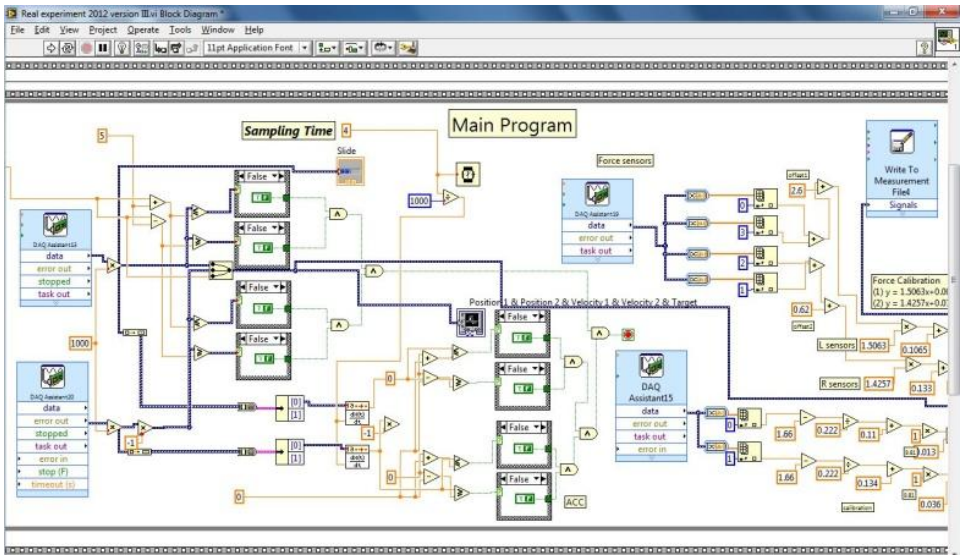

(b) LabVIEW block diagram

Figure A.12 Developed LabVIEW program

The Flow diagram for the LabVIEW virtual interface is schematically depicted in Figure A.13.

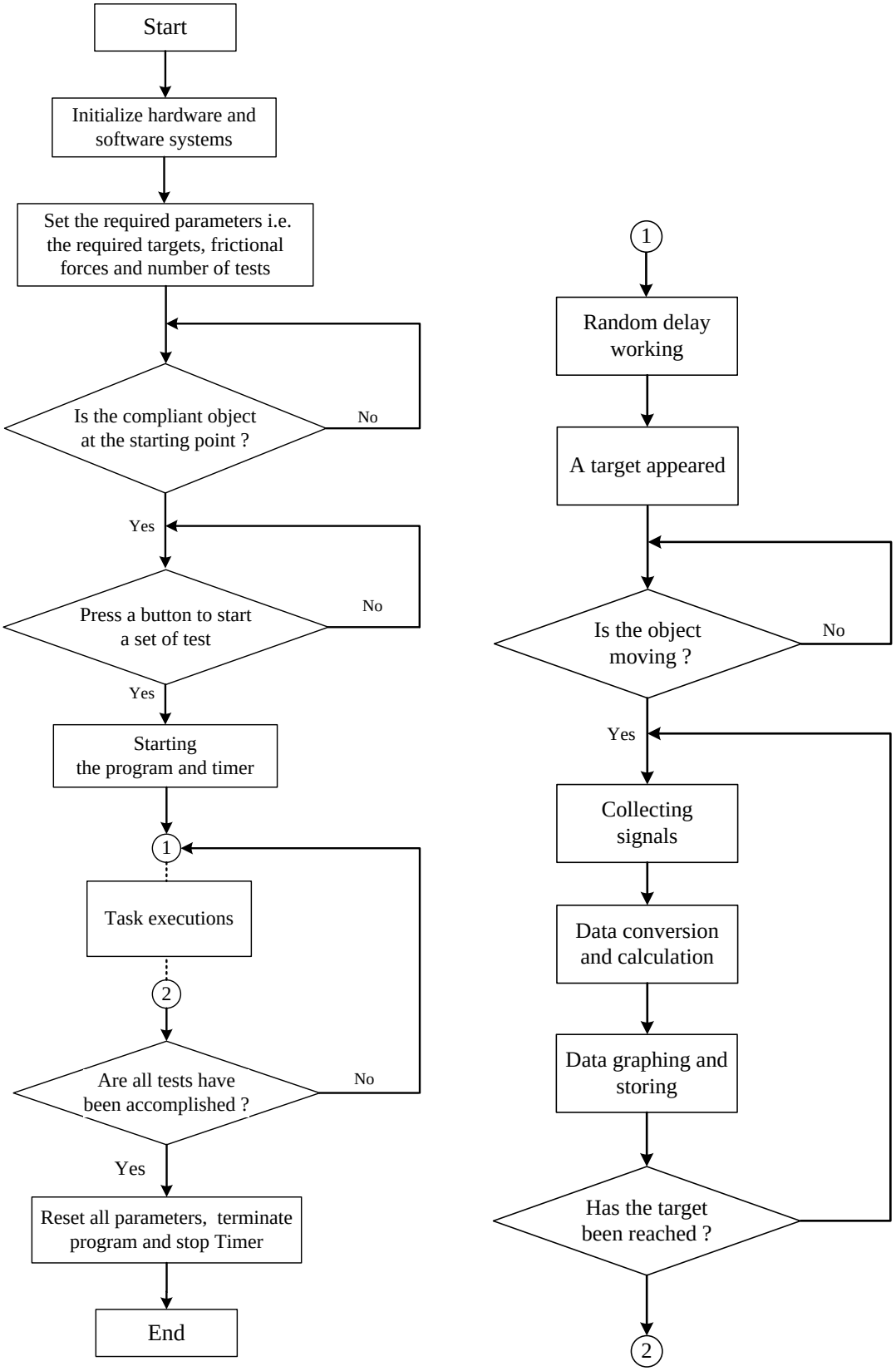

Figure A.13 Guidance flowchart for LabVIEW virtual interface

APPENDIX B

LABVIEW BLOCK DIAGRAM FOR A ONE DOF HHI TEST

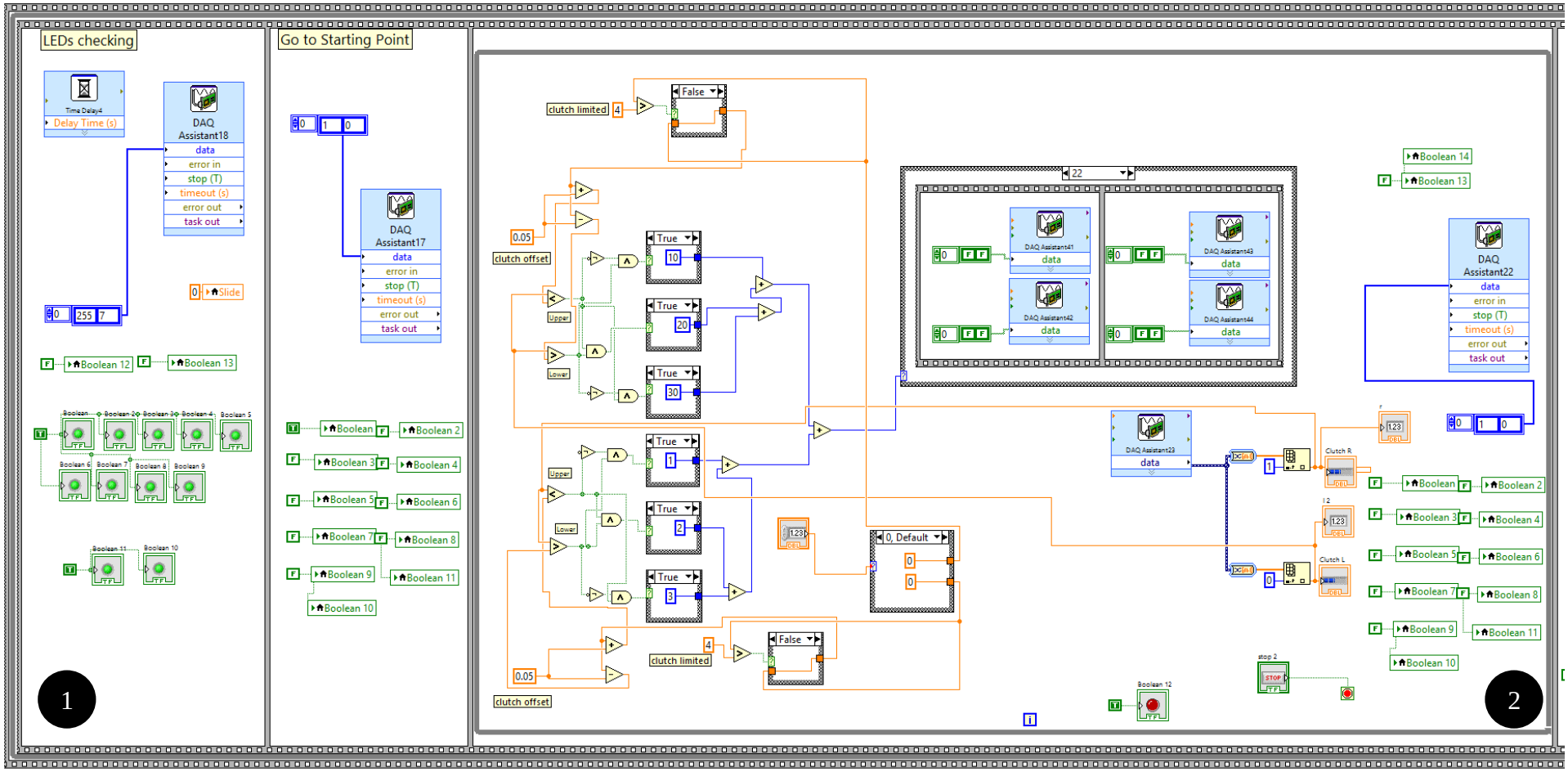

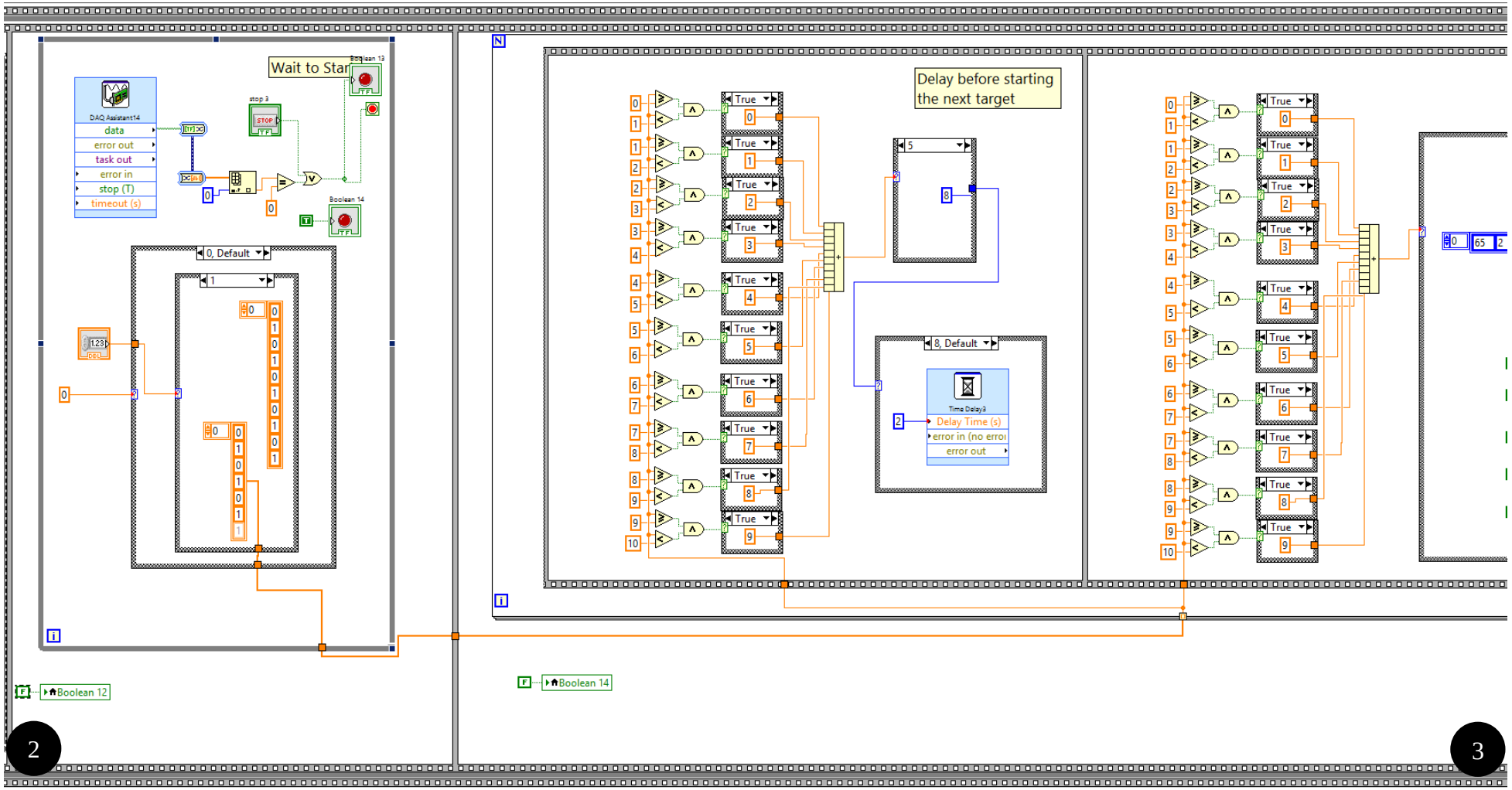
Wait to Star
DAQ Assistant14
data
error out
task out
error in
stop (T)
timeout (s)
Boolean 13
stop 3
Boolean 14
0, Default
1
Boolean 12
Delay before starting the next target
True
5
8
8, Default
Time Delay3
Delay Time (s)
error in (no error)
error out
Boolean 14
2
3

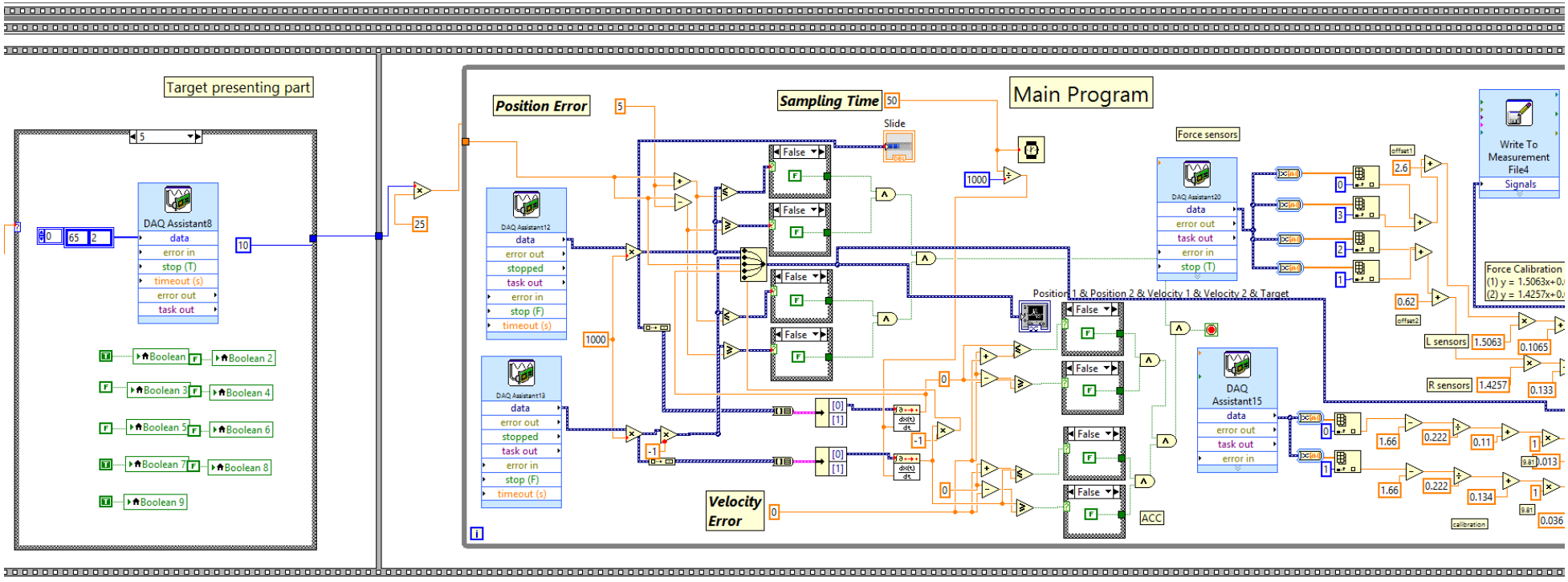
Target presenting part
DAQ Assistant8
data
error in
stop (T)
timeout (s)
error out
task out
Boolean
Boolean 2
Boolean 3
Boolean 4
Boolean 5
Boolean 6
Boolean 7
Boolean 8
Boolean 9
Main Program
Position Error
Sampling Time
Slide
Force sensors
DAQ Assistant12
DAQ Assistant13
DAQ Assistant20
DAQ Assistant15
Velocity Error
Position 1 & Position 2 & Velocity 1 & Velocity 2 & Target
ACC
Write To Measurement File4
Signals
Force Calibration
L sensors
R sensors
calibration

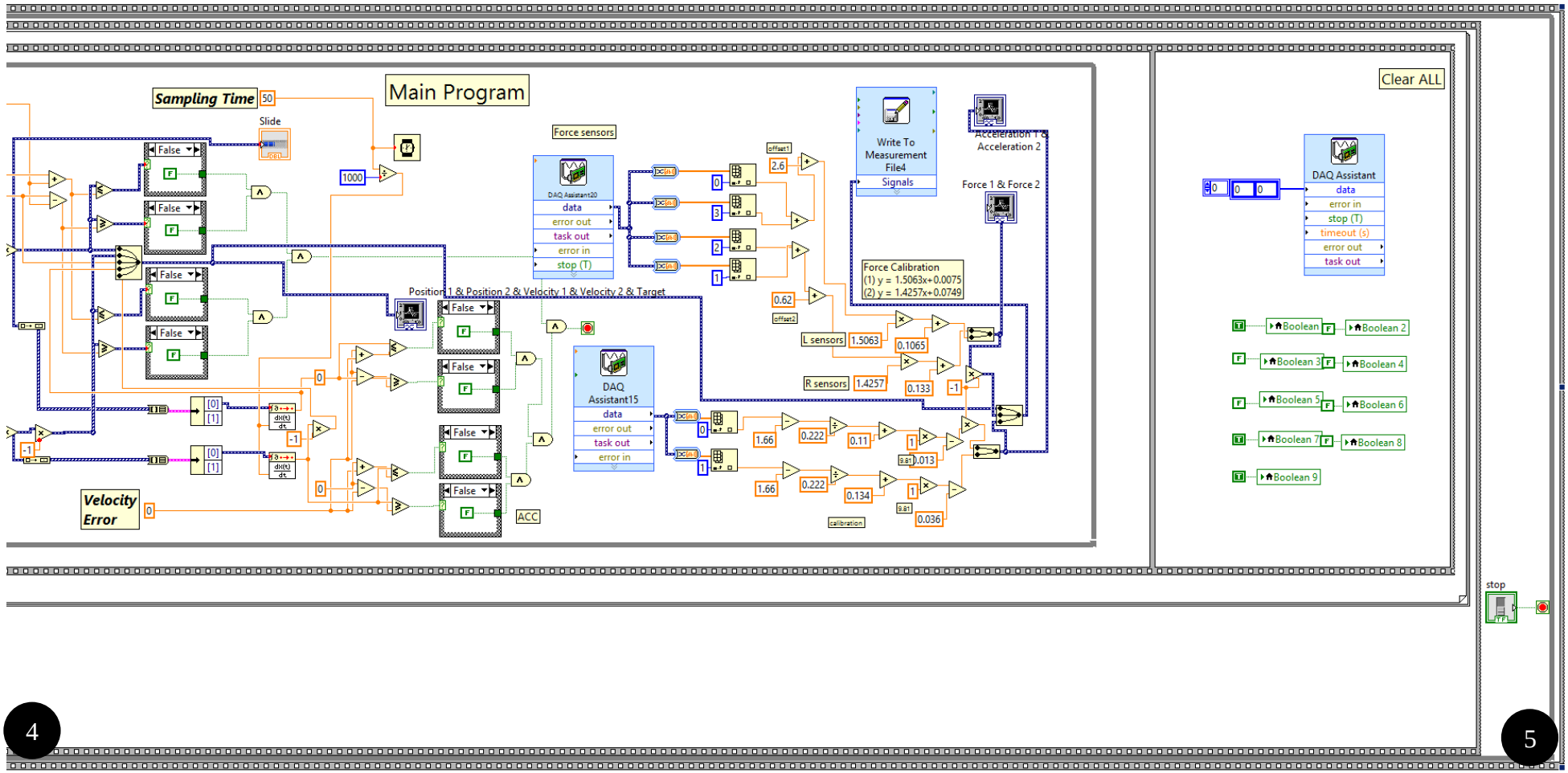
Main Program
Sampling Time
50
Slide
1000
Force sensors
DAQ Assistant20
data
error out
task out
error in
stop (T)
Write To Measurement File4
Signals
Acceleration 1 & Acceleration 2
Force 1 & Force 2
Force Calibration
(1) y = 1.5063x+0.0075
(2) y = 1.4257x+0.0749
Position 1 & Position 2 & Velocity 1 & Velocity 2 & Target
DAQ Assistant15
L sensors
1.5063
R sensors
1.4257
Velocity Error
ACC
Clear ALL
DAQ Assistant
timeout (s)
Boolean
Boolean 2
Boolean 3
Boolean 4
Boolean 5
Boolean 6
Boolean 7
Boolean 8
Boolean 9
stop
4
5

APPENDIX C

RESULTS OF BOX-BEHNKEN DESIGN

All 33 different tasks of the Box-Behnken design generated by Matlab software are illustrated in the following table.

Table C.1 The Box-Behnken design with four variables

Test	K (1 to 2kN/m)	M (1 to 2kg)	F_c (0 to 4N)	T (0.075 to 0.175m)
1.0	1.0	0.0	0	0.125
2.0	1.0	0.0	2	0.075
3.0	1.0	0.0	2	0.175
4.0	1.0	0.0	4	0.125
5.0	1.0	0.5	0	0.075
6.0	1.0	0.5	0	0.175
7.0	1.0	0.5	4	0.075
8.0	1.0	0.5	4	0.175
9.0	1.0	1.0	0	0.125
10.0	1.0	1.0	2	0.075
11.0	1.0	1.0	2	0.175
12.0	1.0	1.0	4	0.125
13.0	1.5	0.0	0	0.075
14.0	1.5	0.0	0	0.175
15.0	1.5	0.0	4	0.075
16.0	1.5	0.0	4	0.175
17.0	1.5	0.5	2	0.125
18.0	1.5	1.0	0	0.075
19.0	1.5	1.0	0	0.175
20.0	1.5	1.0	4	0.075
21.0	1.5	1.0	4	0.175
22.0	2.0	0.0	0	0.125
23.0	2.0	0.0	2	0.075
24.0	2.0	0.0	2	0.175
25.0	2.0	0.0	4	0.125
26.0	2.0	0.5	0	0.075
27.0	2.0	0.5	0	0.175
28.0	2.0	0.5	4	0.075
29.0	2.0	0.5	4	0.175
30.0	2.0	1.0	0	0.125
31.0	2.0	1.0	2	0.075
32.0	2.0	1.0	2	0.175
33.0	2.0	1.0	4	0.125

APPENDIX D

DESIGN OF FORCE AND VELOCITY ROBOT CONTROL SYSTEM

LIST OF CONTENTS

Appendix D describes how the real-time force and velocity robotic control was designed and implemented on the HRI system. Sections D.1-2 detail the hardware and software configuration and integration requirements, respectively, and D.3 focuses on implementation and evaluation of external force and velocity control, and the ATI force data acquisition and the ALTER real-time path control were also evaluated to quantify their performance. The proportional integral (PI) control implementation adopted in the controlled robotic system is presented in Sections D.4, using a trial and error tuning method based on a virtual crank-turning test to establish appropriate PI gains for both the robot's force and velocity control as described in D.5.

D.1 Hardware Configuration

D.1.1 Stäubli Robot Manipulator Arm (TX60)

The 6-DOF Stäubli TX60 robot manipulator arm, as illustrated in Figure D.1, is able to perform real-time path control, with appropriate speed, accuracy and reliability. The TX60 robot has a normal payload capacity of 3.5kg (maximum of 9kg) and repeatability of ±0.02mm. The real-time path control can be updated every 4ms, and the transmission control protocol/internet protocol (TCP/IP) interface is available with a net bit rate capacity of 100Mbit/s. The Stäubli robot system is made up of three key components consisting of a Stäubli manipulator, a robot controller and a robot manual control panel (MCP).

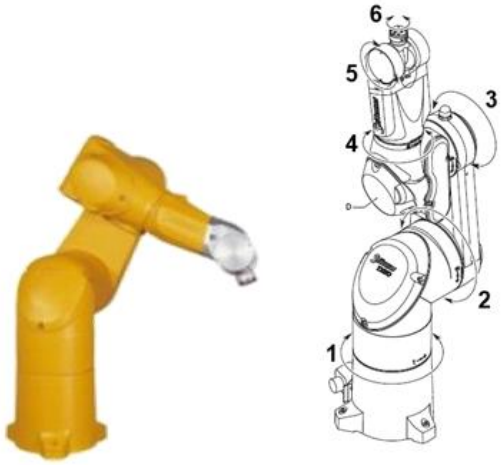

Figure D.1 Six-DOF Stäubli robot manipulator arm (TX60)

The CS8C Stäubli robot controller is a multi-processor system which is able to control the basic robot inputs/outputs, with a fieldbus interface board (supporting Modbus, Profibus, DeviceNet, CANOpen and TCP client), an Ethernet-Modbus-digital/analog-input-and-output port, two serial ports, and four USB devices. The CS8C controller controls the TX60 robot via the digital power amplifiers devoted to each robot arm axis. The VAL3 language is a high-level robot programming language developed by Stäubli, and incorporates external real-time force and velocity control via TCP/IP communication.

The MCP is available for a user to facilitate interaction with the robot in the design and development stages. The robot is positioned by defining the Cartesian coordinates in order to move the robot in the x, y and z directions, which is easier for the user's visualization of the robot movement. The VAL3 language was especially designed to control a Stäubli robot, not only using the basic features but also for developing a standard real-time path control function in which the robot has to be able to finish the execution of a motion task within the minimum period of 4 milliseconds.

The ALTER real-time control path is a key requirement in a robot architecture control designed for external path control. The principle of the control system for robot movement is that the robot normally fetches and then executes instructions without waiting for its current movement to be completed before processing the next command, i.e. the robot can execute and store several commands in advance. For example, the robot is programmed to move from position A to B and C by applying three joint movement instructions, consisting of *Movej (positionA, RTool, mNomSpeed), Movej (positionB, RTool, mNomSpeed)* and *Movej (positionC, RTool, mNomSpeed)* respectively.

Typically, the description of the *MOVEj (pPosition, RTool, mDesc)* instruction is a robot joint movement command to allow the robot to move towards to the "pPosition" using the "RTool" along with the movement speed of "mDesc". Initially, the robot fetches the first instruction, *Movej (positionA, RTool, mNomSpeed),* to be executed, and then the robot starts moving towards point A using *RTool* at the speed of mNomSpeed. Before the robot reaches to the point A, the second instruction may be immediately processed. Furthermore, the third command may probably be executed while the robot is still moving to positions A or B. Based on all the instructions

executed and stored in its available memory, the robot is required to move from positions A to B and then to C, whereas its trajectory cannot be interrupted until the robot reaches the final position C. The key challenge in real-time robot force control in human-robot interaction is that the incremental positions of the robot trajectory are calculated from human external forces in real-time. By the using ALTER command with the Stäubli TX60, the robot can modified its movement based on the external human force applied to the robot end effector via the object.

D.1.2 Robot Gripper Design

A robot gripper mounted at the robot end effector enables the robot to grasp, pick up, hold and release an object in the human-robot handover process. Several gripper types were tested in different schemes for each specialized application, and a three-point contact gripper was finally adopted. In the design of the gripper, several basic requirements were considered, including reliability, stability and the absence of slipping, twisting or rotational movement. A pneumatic-two-finger type with three-point contact was selected to handle this HRI application. Although various geometrical types of object could have been used in this test, a cylindrical plastic tube was selected to be used. This choice builds on the results of the study carried out by Pham and Heginbotham [1986], where a three-point contact gripper was found to be suitable for properly engaging a cylindrical component. The surfaces of the gripper fingers are covered by semi-soft synthetic rubber layers 3mm thick. When the plastic tube is in contact with the rubber surfaces, an appropriately high coefficient of friction is generated.

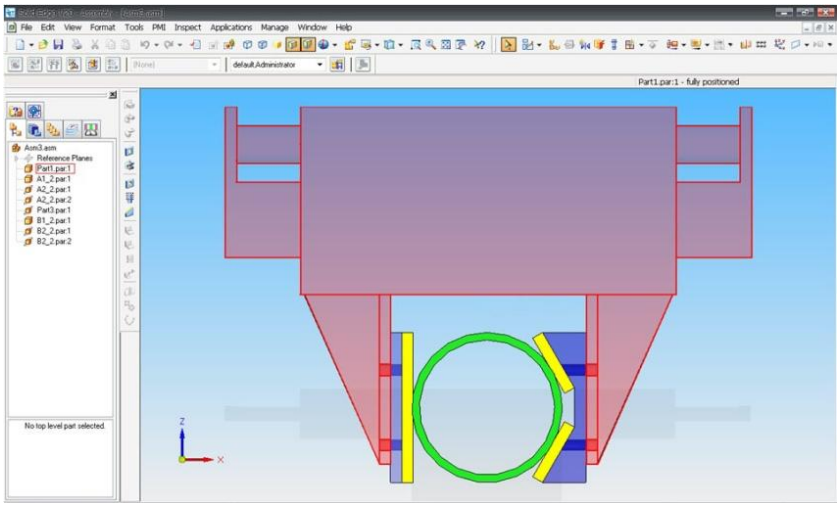

Figure D.2 Design of a simple three-point contact robot gripper

In the HRI process, the gripper can hold the object firmly in cases of heavy induced strain to present the object sliding, rotation or twisting can be avoided. The robot gripper design adopted for the HRI test is illustrated in Figure D.2. A four-way-two-state electrical solenoid valve, Univer E-0320 model, was employed to actuate the robot gripper. The system requires a DC power supply of 12 volts and 1.5 to 10 bar working pressure for suitable actuation in the haptic HRI task.

To control the electrical solenoid valve, a transistor-transistor logic (TTL) signal established in the digital output port of the CS8C robot controller was utilized. The digital bidirectional input/output board of the TX60 robot is fitted with 16 digital inputs (port: J602, pins: Di0-Di15) and 16 digital outputs (port: J602, pins: Do0-Do15). All input and output pins have individual displays indicating whether or not each is being activated. The capacity of the power supply used for the digital outputs is between 10-30 VDC, in which the maximum functional current is 700 mA per channel. Figure D.3 illustrates the schematic diagram of the digital output board and shows how the 12V electrical solenoid valve is connected to the board.

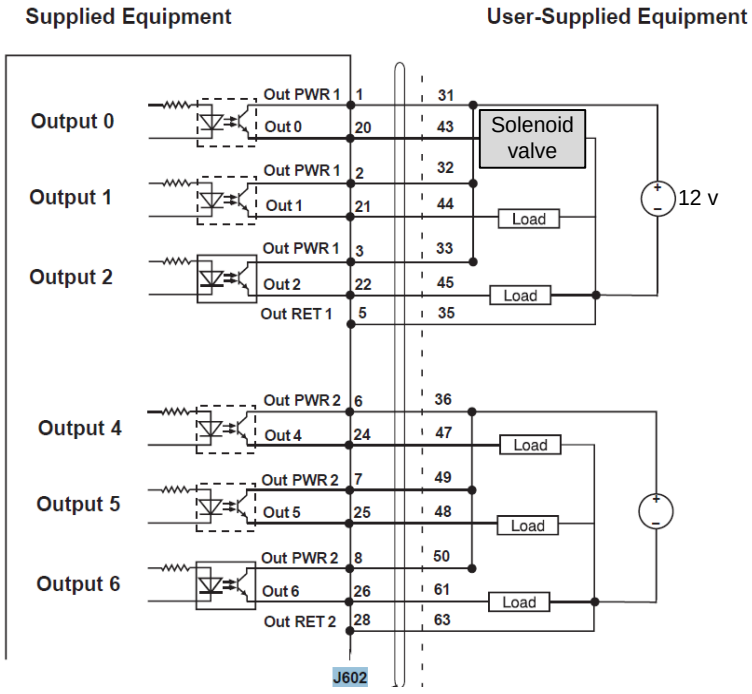

Figure D.3 Schematic diagram of the digital output board in the CS8C controller

D.1.3 Multi-Axis Force/Torque Sensor

A 6-axis force/torque sensor was used in the HRI application to detect the interaction force between the human participant and robot manipulator arm during joint handling of the object. The ATI *Gamma* Multi-Axis Force/Torque sensor, as shown in Figure D.4, was mounted between the robot end effector and gripper. The sensor system is made up of an ATI F/T *Gamma* sensor, an electrically shielded and twisted transducer cable and a stand-alone ATI controller in which optional analog, parallel and serial outputs have been already attached (see Figure D.5). The *Gamma* sensor has high stiffness, and can measure all six components of force, F_x, F_y and F_z, and torque, T_x, T_y and T_z, using a monolithic instrumented transducer. The ranges of force/torque measurements are up to ±130 N with 0.1N resolution and ±10Nm with 0.0025Nm resolution respectively.

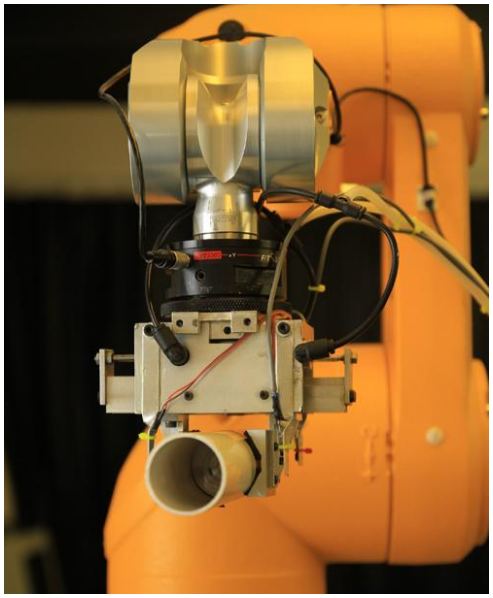

Figure D.4 Design of a simple three-point contact robot gripper

The ATI controller converts all strain gauge signals into the magnitudes of the Cartesian force/torque components using a calibration matrix computation. The ATI controller provides the sensor power and also can deliver the output communication either through an analog output port, discrete I/O connections, a serial port or a parallel port. The 12-bit analog to digital converter (ADC) channels are used to quantify the strain gauge signals before they are sent to the processor. The ATI CPU not only performs the executions of most commands and calculates the results but also is responsible for checking whether or not the captured forces/torques exceed the saturation limits.

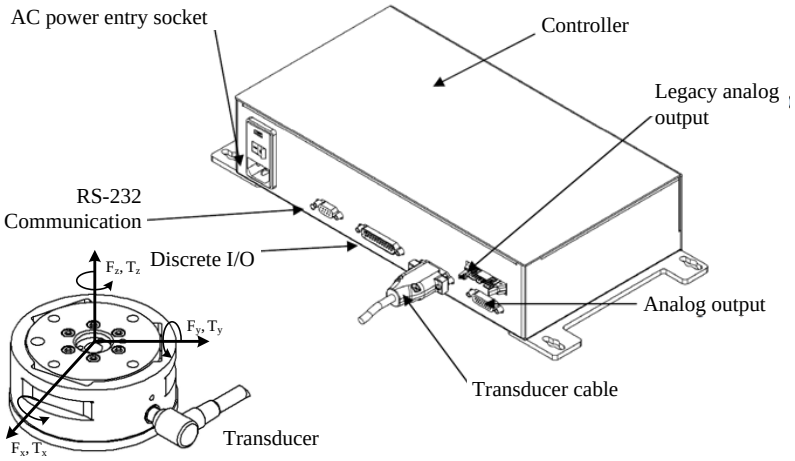

(a) ATI *Gamma* multi-axis force/torque sensor system

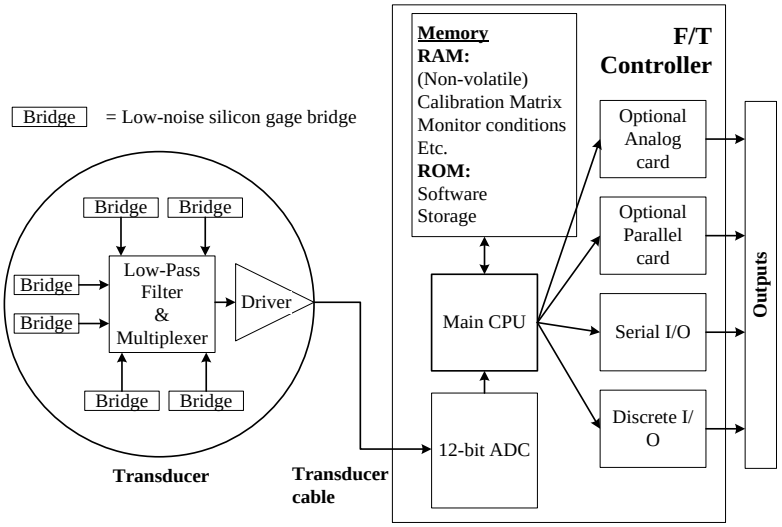

(b) Scheme of an ATI force/torque sensor system stand-alone controller

Figure D.5 ATI *Gamma* multi-axis force/torque sensor system and its scheme

D.1.4 Real-Time Linux Operating System

The human-robot interactive system is categorized as a hard real-time system, and a real-time Linux operating system (RT Linux OS) was employed to ensure robust control could be achieved. The updated Linux operating system Ubuntu with Linux 3.2.0-23-realtime version was adopted because it is effective stable, reliable, fast and powerful. Other outstanding features of Linux are that it allows program multitasking, multiplatform, multiprocessor and multithreading operation as well as also supporting a number of networking protocols (such as IPv4, IPv6, AX.25, X.25, IPX, DDP or TCP/IP networking, which includes FTP, telnet and NFS.

The Linux operating system, which is freely available to software developers, is a Unix-like operating system, and is made up of three key components: a base set of utilities, scripts, and the kernel, which is the key aspect of the OS and is responsible for the system hardware management. The base set of utilities and subscripts cooperate with the kernel to execute any task and also provide basic functionalities for a user. The Linux OS has a modular monolithic kernel, in which the memory task scheduler, device drivers and filesystem are in the kernel space. In addition, the RT Linux OS supports multi-task execution using the multi-tasking kernel to manage user programs so that they can run simultaneously. In this project, the Linux operating system was upgraded for real-time control applications by modifying the Linux kernel to guarantee that higher priority kernel processes can be appropriately executed before lower priority processes.

Figure D.6 illustrates the four stages of a standard real-time Linux modification, which achieves real-time capacity by adding a highly efficient second kernel called the micro-kernel implementation [Rivas and Harbour, 2001]. The micro kernel provides the interface between the standard kernel and the hardware, which controls and executes the real-time tasks and also runs the standard kernel as background tasks. Therefore, the latency of the real-time task process is able to be minimized into the micro-scale. The standard Linux task interrupt is approximately 20-4800 microseconds under varying load conditions. The improvement to real-time Linux can reduce the interrupt latency to around 2.4-4.4 microseconds under the same conditions [Aeolean, 2002].

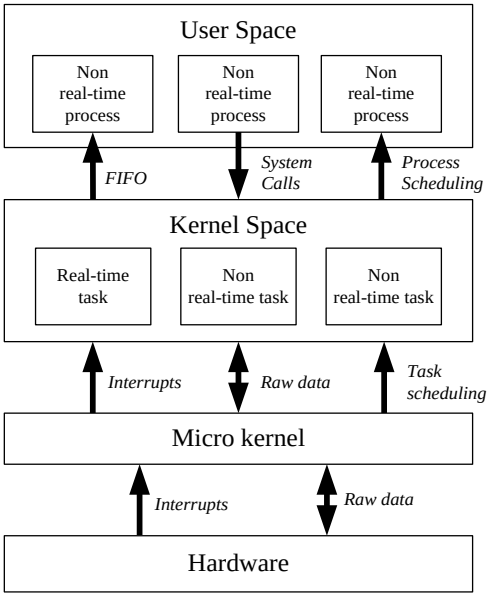

Figure D.6 Four stages of a standard real-time Linux modification [Aeolean, 2002]

D.1.5 Ethernet Communication

Recent, advances in networking allow computers to transfer information to each other over local area network (LAN) or wide area network (WAN) technologies. Transmit control protocol and internet protocol (TCP/IP) are the most reliable industry-standard methods used in the internet and networks worldwide, and were developed to facilitate the transfer of information between computers in shared networks, that can be easily explained as follows: In the process of general mailing, *handler* and *receiver* addresses are required to be printed into a letter and then a postman is able to deliver the letter to the correct *receiver*. This is similar to the basic functions of the TCP/IP network communication, in which every user has an individual network address. The data to be transmitted are packed into a single package of additional information including a *handler* address, a *receiver* address and a checksum used to verify the effective data transmission [Patrick, 1999].

As mentioned above, TCP/IP is typically named as one entity; however, there are two different protocols: the transport control protocol (TCP) and internet protocol (IP). The internet protocol is able to provide an individual network address to facilitate the data exchange between two specific network stations; however, the IP is normally unsecured. Consequently, for more reliable data transmission, it is always associated with the TCP in order to provide the effective security and handling of user data. The IP address is a set of unique identifier numbers, and there are two versions consisting of IP version 4 (IPv4) and IP version 6 (IPv6), which involve 32bits and 128bits respectively. In the present HRI application, IPv4 was employed and the set of 32-binary bits can be into sets of 4 numbers grouped by dots.

Internet Protocol datagrams are the messages which are transmitted over the internet. The IP datagram packet of IPv4 is shown as Figure D.7, which can be divided into: *header* and *data array*. The *IP header* contains many blocks, which can be defined as follows: the first 4bits are the current protocol version of the IP. *Service type* contains 8bits, including 4bits for the type of service precedence, 1 bit for delay, 1bit for maximize throughput, 1bit for maximum reliability and the last bit to minimize monetary costs. Total length is represented within 16bits, which varies from 46 to 65535bytes. The 16bits are later reserved for the unique IP datagram identification. There are 3bits of flags used to identify and control *fragments*. *Fragment offset* involves 13bits and can obtain a maximum offset of 65,528bytes [Dave, 1999].

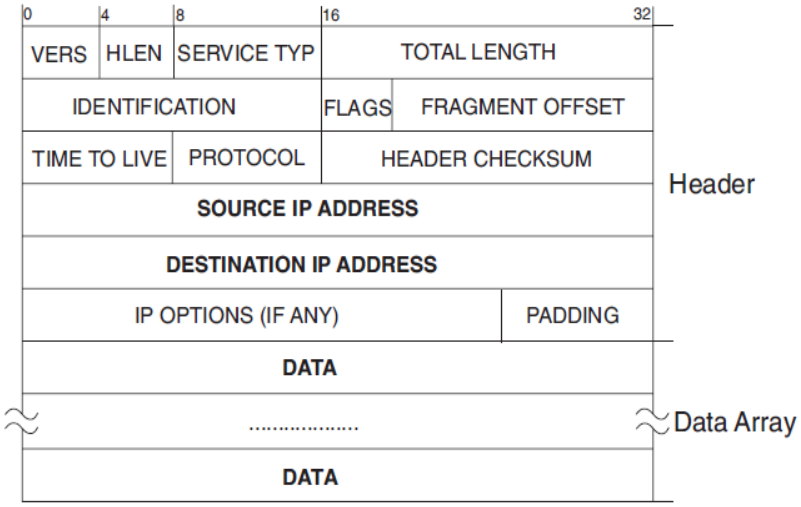

Figure D.7 IP datagram packet of IPv4 [Dave, 1999]

However, as mentioned, data transferred over the IP do not include a *checksum* to guarantee effective data transmission. Consequently, for more reliable data transmission, it is required to be associated with the TCP, which establishes the communication between two network stations which are a client and a server. During data transmission, all data are verified using a *checksum* and an individually sequential number is assigned to each packet to achieve more correct and reliable delivery. There is an 8-bit protocol in the IP data transmission, in which its header checksum is employed in a data error checking stage of the header which holds 16 bits.

Figure D.8 illustrates the TCP packets of IPv4. The first 32 bits are reserved for the *port numbers* of both a *handler* and a *receiver*. The subsequently 32 bits are employed for a sequence number to demonstrate the incremental number from the starting data byte of the TCP. The *acknowledgement-number* takes 32 bits to present the sequence number expected in the coming TCP packet. *Header length* contains 4 bits and the other 3 bits are reserved for use in the future but are always set to '0'. The 9-bit code is composed of 9 key control bits. *Window block*, which is used to specify the number of *window* size units, involves 16 bits. To give reliable data transmission, the 16-bit *checksum* is required for data and header error checking. An *urgent* pointer contains 16 bits to represent the last urgent data byte. *Options* contain 32 bits, which include padding. Finally, the last block is a set of data to be transmitted through the TCP layer [Dave, 1999].

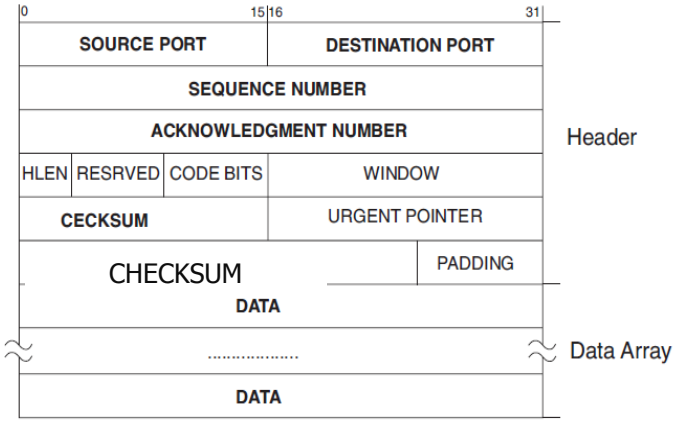

Figure D.8 TCP packets of IPv4 [Dave, 1999]

D.1.6 Object Tracking System

In the human-to-robot handover task, the robot is required to estimate the velocity of the object in order to plan and execute a trajectory to the perceived transfer location, i.e. the robot's motion was adapted based on the speed of the object manipulated by the human *handler*. As shown in Figure D.9, the velocity of the object held by the human is detected by the set of infrared sensors attached on the robot gripper, in which the first and second pairs of infrared emitters and *receivers* were used to activate and deactivate Timer1. Once the velocity of the object is estimated, the robot starts moving synchronously and accelerates to the estimated speed of the object's using the ALTER command. The robot gripper is then activated to grasp the object at the perceived transfer location and the PI velocity control applied to the robot has been enabled respectively to manipulate the object to the final position.

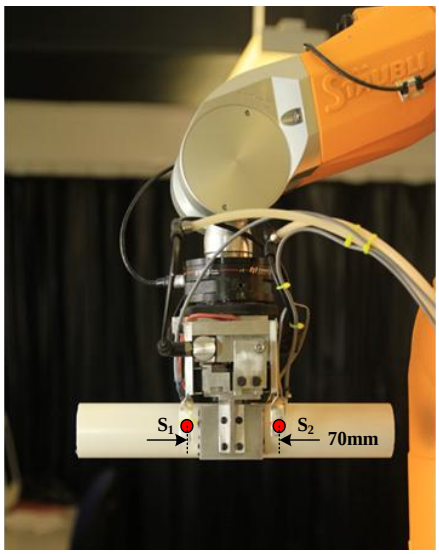

Figure D.9 Robot gripper with infrared sensors in an object tracking task

The two sets of infrared emitters and *receivers* (S_1 and S_2) were employed in the velocity tracking system of the object based on computing the average speed between two ports as shown in Figure D.9. A GaAs infrared emitter, LD242 model and sharp IS471F light detector were utilized to detect the object. This emitter has high reliability and wide beam along with wavelength at peak emission of 950nm. The Sharp IS471F IR detector has an integrated modulation system, and is modulated via a two-wire connection. High intensity stray light is eliminated by the comparator and is output as a TTL signal, which prevents inaccurate measurements. Figure D.10 illustrates the implementation of the circuit schematic of the infrared emitter and detector proposed, in which a silicon power transistor, TIP31C model, was intended for use in medium linear and switching the digital input of the Stäubli robot controller. In addition, a light-emitting diode (LED) was employed as an indicator lamp. When the object breaks the beam from the sensor S_1, the timer1 in the CS8C controller starts counting until the second beam of the sensor S_2 is activated.

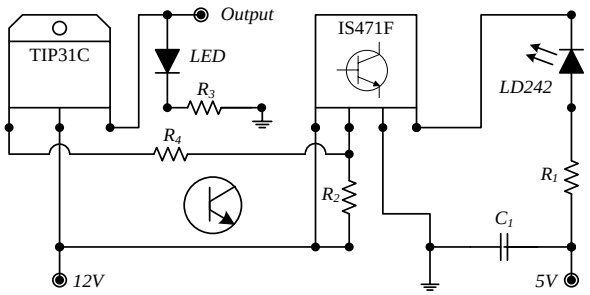

Figure D.10 Schematic diagram of an infrared sensor circuit

The system proposed was required to deliver an evaluation of the velocity tracking system of the object to ensure the effectiveness and accuracy of the speed measurement. Therefore, a set of preliminary tests has been carried out, where the robot gripper furnished by the two pairs of the emitters and *receivers* (S_1 and S_2) was needed to move along the x axis of 70mm in various different speed conditions from 5 to 100mm/s with 5mm/s resolution. RT Linux was used to capture the time taken in the fixed displacement mentioned. The mean velocity of the object can be estimated by dividing a distance fixed between the two sensor locations (70mm) with time taken. Figure D.11 shows the comparison of the actual and calculated velocities of the object in the calibration of the velocity tracking system for the Stäubli robot. The average errors fluctuated between ±0.50mm/s in the speed interval of 10 to 80mm/s, in which, from 80mm/s onwards, the average error increases to approximately ±2.00mm/s. This is probably due to reduced time taken to track the speed at higher velocities.

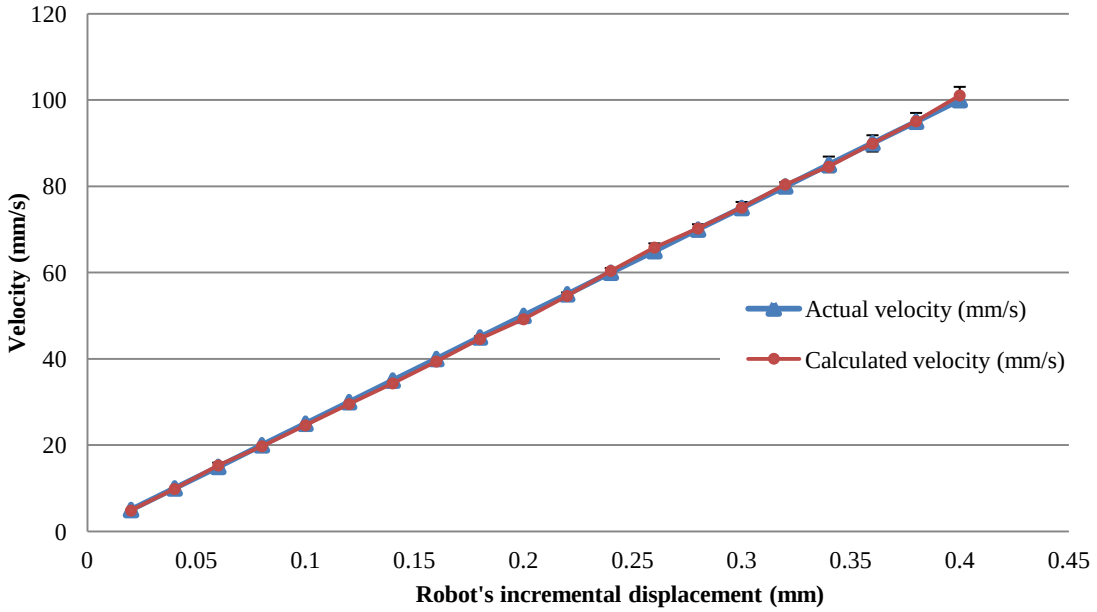

Figure D.11 Comparison of the actual and calculated velocities of the object

D.2 Software Configuration

This section describes the software development, which is one of the key requirements in the HRI system design. Two crucial software operating systems are used, consisting of the real-time Linux and Stäubli VAL3 OS. To create a program, the RT Linux OS requires three components, including a text editor, a compiler and a C standard library. The text editor is a program employed for writing and editing texts, and the GNU compiler collection (GCC), C compiler, is available in the RT Linux and associated with the standard C library. The library is a collection of sub-programs officially developed by programmers and can be used to reduce the amount of complex and repetitive source code. C code was developed to communicate with the ATI F/T *Gamma* sensor and the CS8C Stäubli robot controller over TCP/IP communication, and to facilitate the effective force feedback PI and fuzzy logic controls. The VAL3 language is a high-level programming language developed to control Stäubli robots. It combines the basic features of a standard real-time computer language with several specified functions, such as robot control, geometrical modelling and input/ output control tools. A VAL3 program was designed to handle the applications of the path modification of the robot moving in real-time, object velocity tracking, gripper operation control and multitasking systems.

D.2.1 Software Design for Multi-Axis Force/Torque Sensor Data Acquisition

The ATI F/T transducer was mounted between the robot end effector and gripper. The sensor is required to eliminate the effect of gravity and the other forces occurring during initialisation by biasing. To communicate with the ATI controller, RS-232 serial data communication was employed. The commands and data exchanges between the host PC and the ATI F/T controller were required to follow a standard serial data packet format. The packet is made up of a start bit, data bits, a parity bit and stop bits, at a speed of baud rate of 38,400 bits per second. In this application, the robot end effector is not required to be rotated, and to maximise data transfer rate, the sensor data transferred in binary form at using only 3-axis forces (*Fx*, *Fy* and *Fz*). The digitized force/torque values are received by the host PC memory based on a first-in-first-out (FIFO) method, which means that the array of F/T data are sent byte by byte until all have been transferred according to an ordering process or a queue. The software flow diagram for the F/T controller data acquisition is illustrated in Figure D.12.

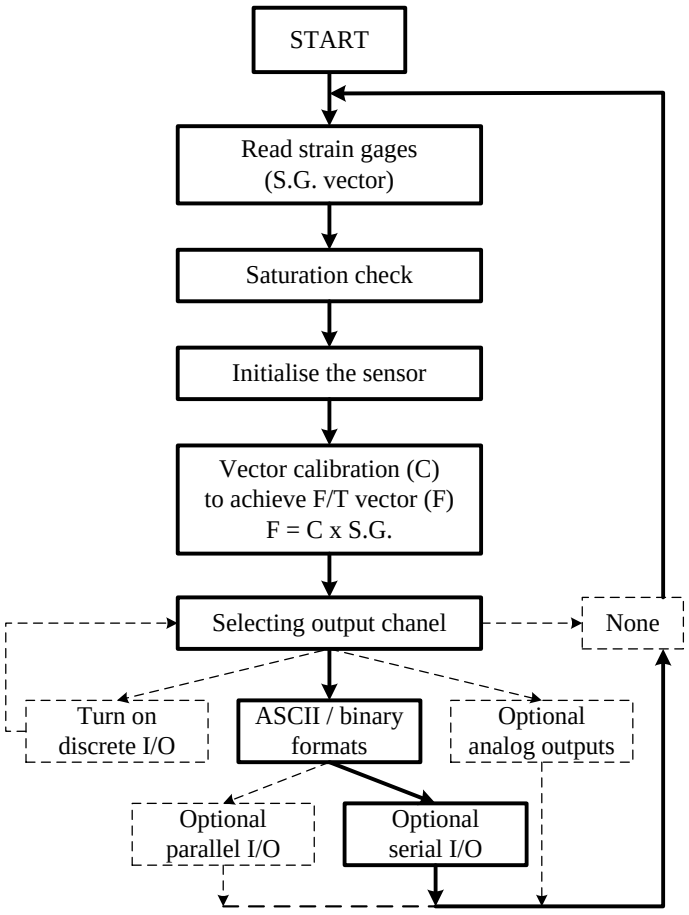

Figure D.12 Flow diagram of F/T controller programming

The RT-Linux OS allows a user (logging in as root) to access serial ports, including port 1 and port 2, by defining the device files as /dev/ttyS0 and /dev/ttyS1 respectively. To open the serial port, the commands below have to be initially declared, including `O_RDWR`, `O_NOCTTY` and `O_NDELAY`. The command which enables the read and write modes of the serial port is `O_RDWR`. Additionally, `O_NOCTTY` indicates that the "controlling terminal" is not required in this program, and `O_NDELAY` functions in the RT-Linux to omit the state checking of the DCD signal line. The file descriptor for accessing the force/torque sensor data can be expressed as follows:

```
File_descriptor = open("/dev/ttyS0", O_RDWR | O_NOCTTY | O_NDELAY);
```

The communication between the ATI F/T sensor and the RT Linux computer was categorized as full-duplex communication, allows the computer to send commands to the ATI F/T sensor and simultaneously receive the force information using two different cables for transmitted and received data. The functional command for sending data over RS-232 is called 'write' as given below. It returns the number of transmitted bytes if it has successfully transmitted the packet; however the function returns -1 if a communication error has occurred.

```
return = write(File_descriptor, "ATZ\r", 4);
if (return < 0)
printf("write function of 4 bytes was failed \n");
```

Reading data through RS-232 is called the 'read' function as expessed below. The `buffer_size` is defined as a pointer array for data capture and `sizeof (read_buffer)` indicates the number.

```
buffer_size = read(File_descriptor, read_buffer,sizeof(read_buffer));
```

The baud rate was set to its highest speed (38,400 bits/s) and the character size was set to 8-bit data using the control option as `options.c_cflag |= CS8`. The serial parity was not required, and so the number of parity bit was selected as `options.c_cflag &=~PARENB`. To disable 2 stop bits and the bit mask for a data bit in serial communication, the instructions, consisting of `options.c_cflag &= ~CSTOPB` and `options.c_cflag &= ~CSIZE`, were applied. The following commands show how to specifically approach the appropriate configuration of the serial port.

```
cfsetispeed(&options, B38400); cfsetospeed(&options, B38400);
options.c_cflag &= ~CSIZE;
options.c_cflag |= CS8;
options.c_cflag &= ~PARENB
options.c_cflag &= ~CSTOPB
options.c_cflag &= ~CSIZE;
```

After serial communication has been successfully established and all data transferred, the communication is then terminated using the 'close' system call to set the DTR (Data Terminal Ready) signal to low, as expressed: `close(File_descriptor);`.

D.2.2 Software Design for Server-Client Communication using TCP/IP Protocol

This section explains how the TCP/IP socket is established in the communication between the external real-time Linux PC and the Stäubli robot controller, CS8C. The fundamental requirement in TCP/IP communication is to effectively provide a reliable data transfer. This communication can be categorized as full-duplex data transmission, i.e. bi-directional communication. First, a server has to be created and bind a socket to a port which is defined before the socket is enabled. In the meantime, the client has to similarly establish a socket to be reserved for the data connection. Afterwards, the server is placed in listening mode and waits until the client acknowledges acceptance of the connection. If the server can detect the *receiver*, then the TCP/IP connection is successfully achieved, and thus the first set of data can be transmitted. An outline of the establishment of server-client-communication is illustrated in Figure D.13.

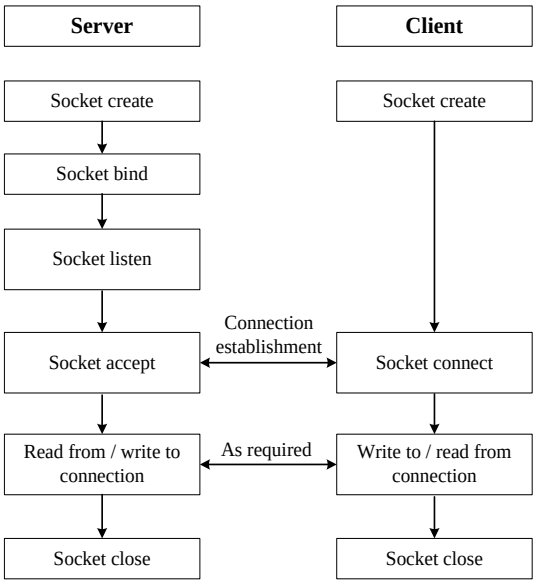

Figure D.13 Client-server programming with TCP/IP sockets [Stevens, 1993]

The TCP socket type was employed to provide communication between the Stäubli robot and the external computer. The CS8C Stäubli robot controller was selected to be the network server and its IP address was manually assigned as 192.168.0.254 with the subnet mask at 255.255.255.0. A port number, which is part of the address information in TCP/IP communication, was used to identify the *handler* and *receiver* of messages and set at 2300. The host PC was adopted as the network client and its fixed IP address was defined at 192.168.0.253. The data transfer speed rate over TCP/IP was initially arranged at 100 Mbit/s, and it can be guaranteed that all data transferred is accurately and reliably delivered due to the extensive error checking mechanisms provided, such as flow control and data acknowledgment.

The crucial steps involved in establishing the communication between the TCP/IP server and client using RT Linux are detailed next. Initially, both server and client have to individually create a socket using the `socket()` system call as expressed below. The socket domain was in `AF_INET` with a 32-bit internet address and the `SOCK_STREAM` type was specified in a byte-steam transfer over TCP/IP communication. The final parameter, `protocol`, indicates the desired communication semantics.

```
int sock = socket(int AF_INET, int SOCK_STREAM, int protocol)
```

The server has to bind the socket to its address by combining its IP address and port number together using the `bind()` system call as illustrated below. The address data has to be initialized and bound to the socket in order to facilitate an effective client connection. The first parameter `sock` is automatically generated following the `socket()` system call, in which `struct sockaddr` has to specify the family, port number and address. The second and third parameters are a pointer of protocol address to bind to the created socket and the number of address bytes respectively. This function returns the values of '0' if it is successful or '-1' if any failure occurs.

```
bind(sock,(struct sockaddr *)&server_addr, sizeof(struct sockaddr))
```

The fixed IP address of the host PC can be specified as `INADDR_ANY` into the declared address structure. Using the `gethostbyname()` system call returns all the information needed, including the IP address. The following command is used to specify the host port number to be directly connected to the socket at port number 2300.

```
server_addr.sin_addr.s_addr = INADDR_ANY;
host = gethostbyname("192.168.0.254");
server_addr.sin_port = htons(2300);
```

The server then waits for the establishment of the TCP/IP connection from the client using the `Listen()` system call. Likewise with the `bind()` system call, the return function value of '0' expresses successful communication or '-1' represents a failure in connection has occurred. Since the TCP/IP socket was already created and bound with the server address structure, the `connect()` function is then called by the client in order to fully connect to the server.

```
listen(sock, int backlog)
connect(sock, (struct sockaddr *)&server_addr
        ,sizeof(struct sockaddr))
```

One last step in the establishment of the server-client connection involves the `accept()` system call from the server side. This function automatically creates another socket file descriptor, which is used for sending and receiving information to the client.

```
accept(sock,(struct sockaddr *)&client_addr, &sin_size);
```

Once the system connection is completely established, the server and client can transfer information until the communication is required to be terminated by the close connection being activated. The instructions used in information transferring between the server and client are `read()` and `write()` system calls or, alternatively, `send()` and `recv()` system calls as follows:

```
write(sock, buffer, sizeof(buffer));
read(sock, buffer, sizeof(buffer)); or
send(sock, buffer, sizeof(buffer),flags);
recv(sock, buffer, sizeof(buffer),flags);
```

Finally, when the TCP/IP communication is required to be terminated, the `close()` system call is utilized, which is expressed as:

```
close(sock);
```

D.2.3 Software Design for Stäubli Robot TX60

The Tx60 Stäubli robot CS8C controller also supports the ALTER real-time path control over a TCP/IP interface via the dedicated robotics language, VAL3, which combines the standard features of a high-level computer language in real-time with functionalities to control the robots. The VAL3 language is made up of key components as follows:

i. a set of user programs or tasks to be executed simultaneously,
ii. a set of global data declared and probably shared over programs under the same application,
iii. a set of libraries used to share programs and/or data, and
iv. a set of user types used to define the structure of data.

As the IP address is needed in TCP/IP communication, the dynamic host configuration protocol (DHCP) was not initially utilized to automatically assign IP addresses to the client and server. Instead, the static IP addresses have been used by selecting the manual IP address configuration. The Stäubli controller was connected to an external PC, in which the controller Ethernet port J205 was defined at IP address 192.168.0.254 (Subnet mask 255.255.255.0) along with the port number of 2300 and the host PC fixed at the IP address 192.168.0.253. Figure D.14 illustrates how the robot static IP address was set using the robot teach pendant (MCP).

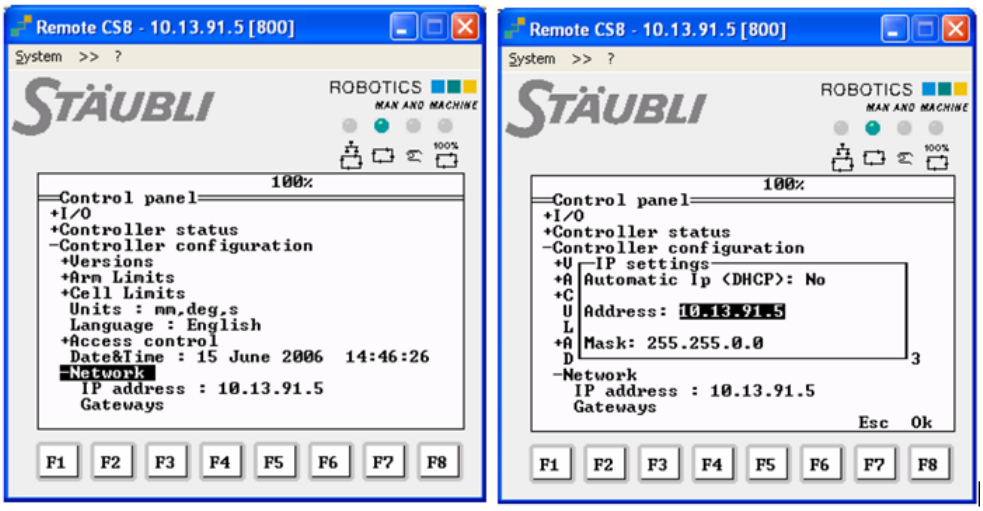

Figure D.14 Stäubli robot IP address configuration

An application may have several task programs running asynchronously or synchronously, depending on task priority and sequence. In this application, the tasks involved can be divided into three main tasks as follows:

5) Task 1 is defined as communication with the RT Linux PC via the TCP/IP connection,
6) Task 2 is developed to control the real-time modification of the robot path using the ALTER motion command, and
7) Task 3 involves the tracking of object velocity

As previously discussed, the data transfer rate between the external RT Linux PC and the Stäubli robot controller, CS8C, was set to 4ms (250Hz). Therefore, to concurrently enable Task 1 execution, the task sampling rate had to be assigned. Tasks 2 and 3 were also required to be synchronized with the first task, using the task-synchronized function and being scheduled at the same period of 4ms. A VAL3 application commences with the *start()* program linked to all inscripted local/global variables, instructions, a number of parameters and inputs/outputs to be executed. A number of tasks or programs can be added into the application. As mentioned above, three tasks were synchronously associated in this application. The first task called 'TCP/IP data acquisition' was utilized to handle the collection of TCP/IP. Task 2, the 'ALTER motion task', was used to generate real-time robot path control, in which the robot's movement can be modified according to the external force assigned. Finally, Task 3, the 'object velocity tracking task', was used to compute the object position and speed whilst performing a human-to-robot handover task. These tasks have to be strictly enforced with the synchronized communication rate at 4ms. Eventually, the *stop()* program is activated when the VAL 3 application is required to be terminated.

The Flow diagram shows that the Ethernet TCP/IP socket communication is first activated using standard instructions – including `socket()`, `bind()`, `listen()` and `accept()` respectively. Once the TCP connection has been completed, the robot is commanded to move to a pre-defined position (specified as the home position), and then the ALTER command is activated, during which time, the object position and its velocity are sensed using the synchronized task of object velocity tracking. The next step involves the real-time modification of the robot path using the ALTER instruction. Once the ALTER function has been enabled (by obtaining the acknowledgment of ALTER activation), the data transfer of the full–duplex TCP/IP communication

immediately starts. A sequence of incremental displacements from the external PC with a cycle time of 4ms is carried out using the external force control. Data is packed into a global-type buffer and accessed by the ALTER function to modify the robot trajectory in real-time. When the HRI task is required to be terminated, then the Ethernet TCP/IP socket, object velocity tracking and ALTER functions have to be deactivated before closing the program.

The following paragraphs present how the VAL3 software was developed for the TCP/IP data acquisition. The type of variables employed to link between a VAL3 parameter to an Ethernet TCP/IP socket connection is the `sio` type. The syntax of `sioGet` function is used to read and store the ASCII number(s) of a single character (or an array of characters) from the `io:sock1` to `num1`, until `nData1` is full. The function of `sioSet` is utilized to write the ASCII number(s) of a single character (or an array of characters) to `io:sock1` from `num`, until all `nData2` is sent. The key function used to adjust the Ethernet communication specification is `sioCtrl`. These commands allow a human user to modify the TCP/IP configurations, such as the TCP/IP port, IP address, maximum response time in the communication and maximum number of clients obtained as follows:

```
num sioGet(<io:sock1>,<num1& nData1>)
num sioSet(<io:sock1>,<num1& nData2>)
num sioCtrl(<io:sock1>,”port” nPort)
num sioCtrl(<io:sock1>,”clients” nClients)
num sioCtrl(<io:sock1>,”timeout” ntimeout)
num sioCtrl(<io:sock1>,”target” nAddress)
```

In order to execute multi-tasking, the `taskCreateSync` instruction is applied for synchronously communication for the three tasks (TCP/IP data acquisition, object velocity tracking and ALTER motion). Their respective flowchart diagrams are illustrated in Figures D.15 - D.17. The function syntax shown below consists of the string name of the task to be generated (`ALTER motion`), the task-interrupt time period (`nPeriod = 4ms`), a boolean variable indicating when overrun errors occur (`bool`), and the name of the synchronized task to be synchronized (`ALTER motion()`). The minimization of each task update time is rounded down to a multiple of 4ms.

```
Void taskCreateSync <”ALTER motion”, nPeriod, bool, ALTER motion()>
```

The Figure D.17 illustrates the flow chart diagram of the ALTER motion task assigned as the synchronized task. The ALTER function allows the robot geometrical transformation, including translation and rotation, to be controlled using the external signal from the force sensor. The first step in using the ALTER instruction involves ALTER initialization, in which all ALTER parameters of the 3-axis transformations, including `trsf_alter.x`, `trsf_alter.y` and `trsf_alter.z`, are set to default values. Several alterable movements are required to begin with the `alterEnd()` instruction, and the `alterBegin()` function is used to terminated the ALTER function. The `alterBegin()` is initially called when the ALTER mode for the robot's path is executed. Its syntax, as demonstrated below, is made up of a robot reference frame for the ALTER deviation and a robot speed. The function returns the value of '1' if it is successfully activated. The `alter()` is the instruction specifying a deviation to a normal path in order to achieve real-time path control, where the transformation (`trsf`) defines the alteration to apply to the robot's movements. The alteration continues to operate unless `alterEnd()` is fetched and executed. The `alterEnd()` function returns the value to '1' if the ALTER is successfully terminated.

```
trsf_alter.x = 0
trsf_alter.y = 0
trsf_alter.z = 0
num alterBegin(frame, mdesc)
num alter(trsf)
num alterEnd()
```

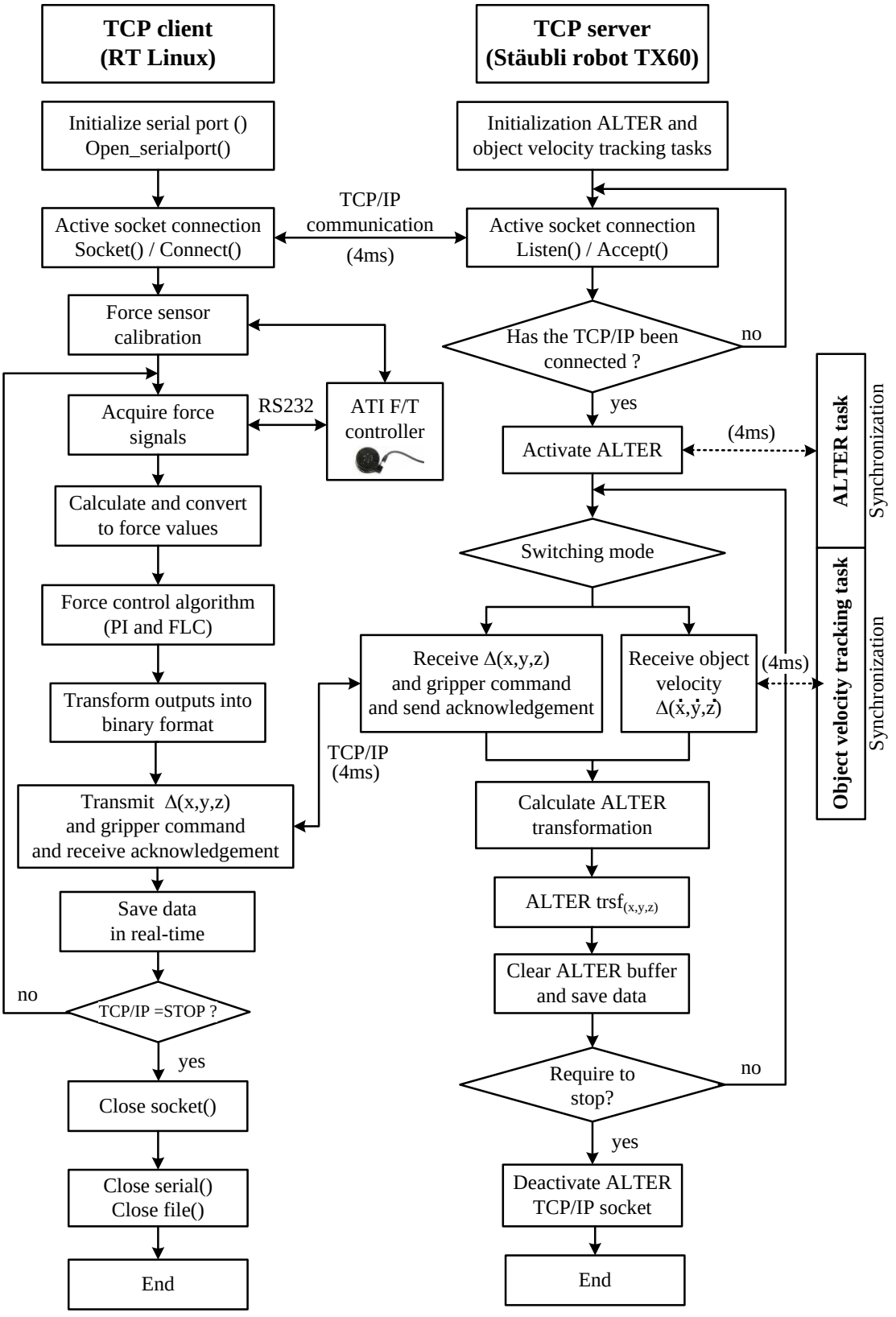

Figure D.15 Flow diagram of the Stäubli robot programming

in the TCP/IP communication task

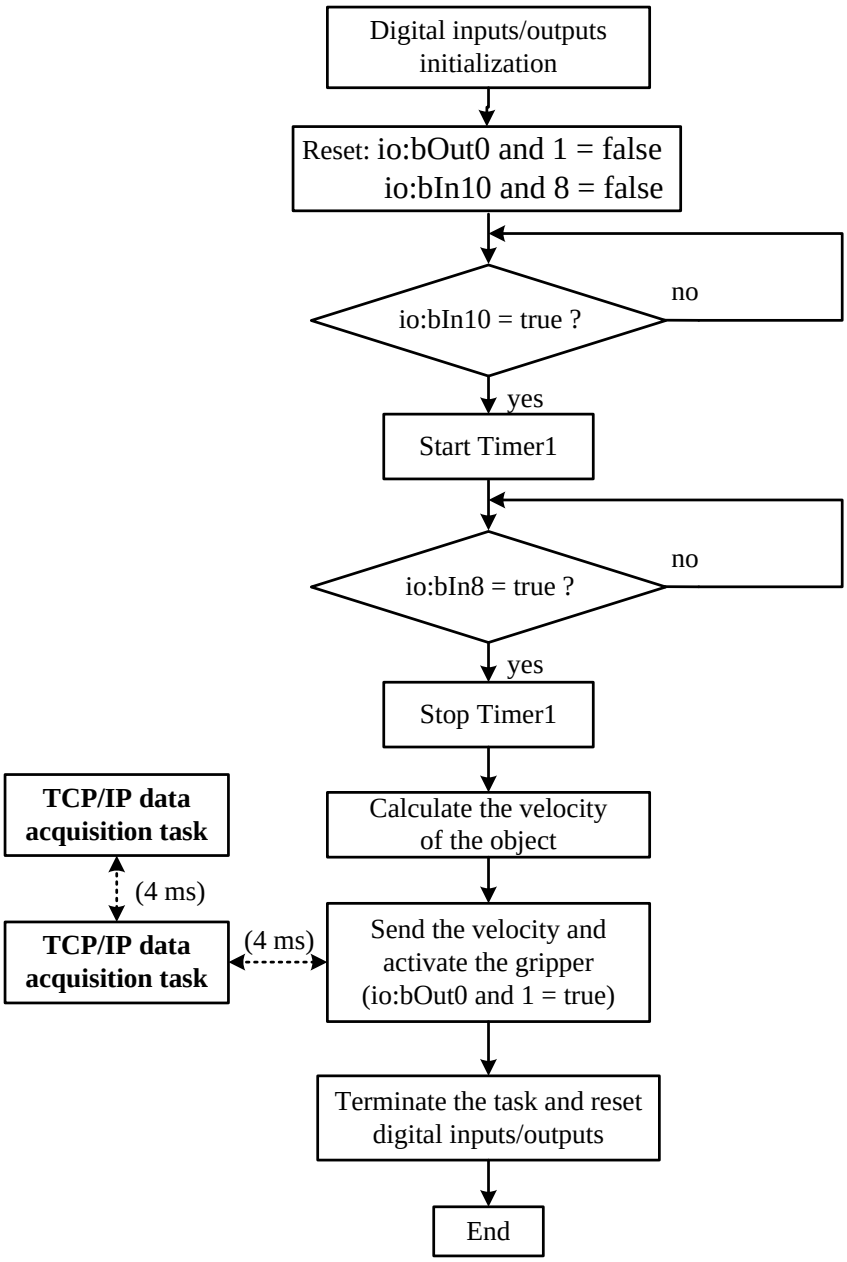

Figure D.16 Flow diagram of the Stäubli robot programming in the object velocity tracking task

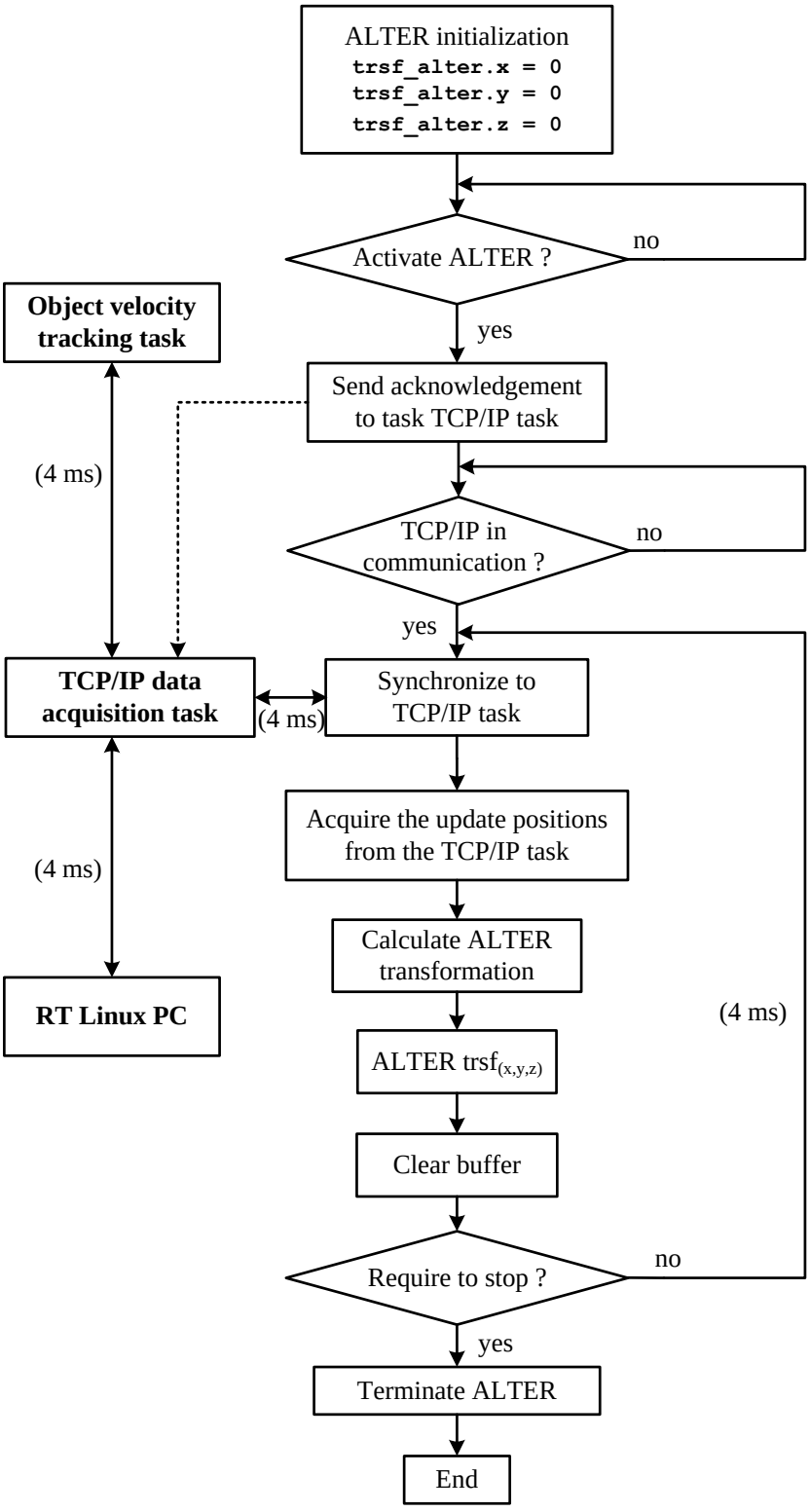

Figure D.17 Flow diagram of the Stäubli robot programming in the ALTER real-time motion task

D.3 Implementation and Evaluation of Force and Velocity Robot Control

D.3.1 Robotic Control Implementation for HRI

The conceptual design of the HRI experiment was based on the goal objective of allowing a robot to transfer an object to a human in a reliable manner, i.e. without dropping or damaging the object. A block diagram of human-robot interaction system is shown schematically in Figure D.18. It is made up of: external force control loop and object tracking loop. In the case of the robot passing the object to the human *receiver*, the interactive force physically occurring during the test was measured by the force sensor, and used as an input to the robot force control algorithm developed based on either a simple proportional integral (PI) control or fuzzy logic control (FLC). The control outputs were produced as incremental displacements Δx, Δy and Δz and transmitted to the robot's ALTER function to modify the robot's trajectory in real-time through TCP/IP communication.

In the case of the human *handler* transferring the object to the robot (*receiver*), the velocity of the object held by the human was first detected by the set of infrared sensors attached to the robot gripper. Once an estimated velocity value was computed, the robot moves along the object's direction at the computed speed using ALTER, and then the robot gripper was activated in order to grasp the object. The PI velocity control applied to the robot was then enabled. After the object transfer phase was executed, the object was individually manipulated to a final position by the robot, where the physical interactive force which occurred was simultaneously monitored and captured by the RT Linux PC. Furthermore, to filter out undesirable signal and facilitate more stability, digital finite impulse (FIR) was applied, where a 4-tap FIR filter was introduced, which is made up of 4 delay elements, 4 multipliers, 3 accumulators and the tap coefficients of h_0=0.1508, h_1=0.2230, h_2=0.2523, h_3=0.2230 and h_4=0.15080 respectively.

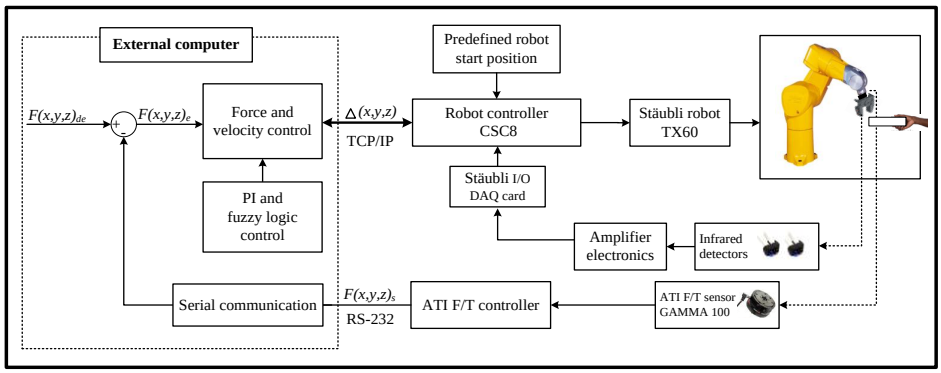

Figure D.18 Overall schematic block diagram of Human-Robot Interaction

D.3.2 Evaluation of ATI *Gamma* Multi-Axis Force/Torque Sensor

Robotic force control was required to ensure safe human-robot interaction. The experimental set-up is shown in Figure D.18. The system should function reliably under different conditions in the human to robot or robot to human object handover tasks. To ensure the reliability of force data acquisition in performing effective and accurate HRI tasks under varying conditions, the force sensor output was monitored and captured in real-time using of RT Linux. Four different modes were selected in order to investigate the robot's dynamic behaviour influencing the force sensing as follows:

- Mode 1: Robot controller power off
- Mode 2: Robot controller power on and arm power on
- Mode 3: Robot controller power on, arm power on and robot moving in the x, y and z axes with a standard moving command, and
- Mode 4: Robot controller power on, arm power on and robot moving in the x, y and z axes under ALTER real-time path control.

The robot arm's configuration was first located in the home position before starting each test in order to minimize the effect of other variables. To collect statistically sufficient volumes of data, 2,000 data were captured every 4ms whilst executing the modes 1 and 2, whereas modes 3 and 4 allowed the robot to move 200 mm in the x-y-z plane at a velocity of 50 mm/s. Additionally, each mode was undertaken for 5 repetition sets, and the overall mean and standard deviation (SD) of the force reading errors were calculated. Table D.1 presents the results obtained with the four modes, in which there was no significant difference between the force values recorded along the x, y and z axes. The 3-axis force values fluctuated between ±0.1N in the different modes. The maximum standard deviation for the z-axis is approximately double the x and y values at ±0.11 N, while the maximum SD values for x and y were around ±0.056 and ±0.054 N respectively.

Table D.1 Means and standard deviations of 3-axis force sensor readings

Mode	Fx (N)		Fy (N)		Fz (N)	
	Mean	*SD*	*Mean*	*SD*	*Mean*	*SD*
1	-0.088	0.032	-0.005	0.022	-0.068	0.065
2	-0.053	0.052	-0.049	0.054	-0.019	0.092
3	-0.006	0.032	-0.101	0.029	-0.025	0.105
4	-0.006	0.056	-0.098	0.048	0.024	0.108

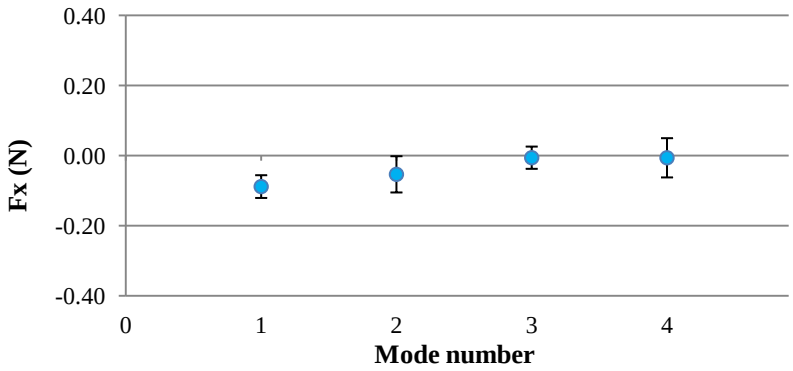

(a) Force/torque sensor readings in x axis

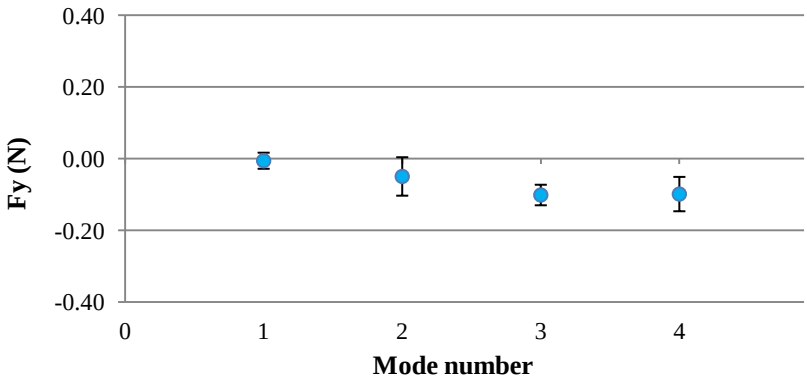

(b) s Force/torque sensor readings in y axis

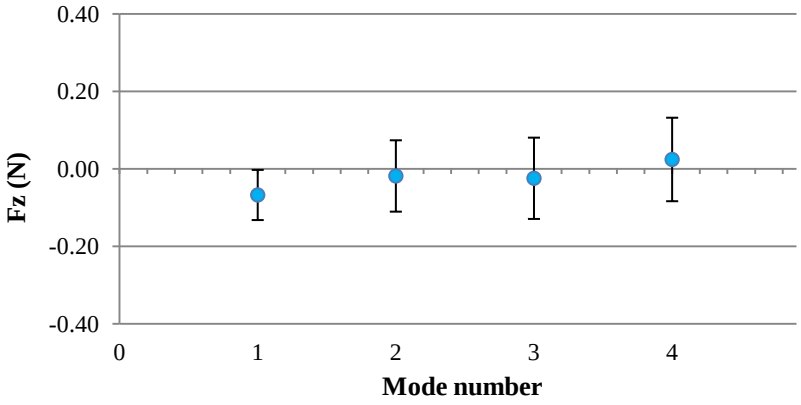

(c) Force/torque sensor readings in z axis

Figure D.19 Means and standard deviations of 3-axis force/torque sensor readings

D.3.3 Evaluation of ALTER Real-Time Control Path

It was necessary to evaluate the robot's ALTER control system in order to ensure effective HRI performance, thus a set of experiments were carried out in which the main objective was to assess the performance of the robot real-time path control in terms of its reliability and accuracy. The robot was required to move along circular paths of 100, 150 and 200mm in diameter in a fixed time period, whereas its motion was simulated and drawn using 1500 points (N) in which the step size is defined by $2\pi/N$. To evaluate the quantitative performance of the ALTER function, the robot's actual positions whilst moving was compared to the desired values, and the following data recorded and compared, namely demanded, received (through TCP/IP) and actual values, as shown in Figure D.20. Demanded values of incremental position were used to modify the robot's path and were generated in the external real-time Linux PC and transmitted to the Stäubli CS8C controller via an Ethernet port using the TCP/IP protocol with a 4ms cycle interrupt. Subsequently, received data, which represent the information acquired by the controller, were computed to establish an ALTER 3-axis transformation matrix in order to enable the changes in actual robotic movements.

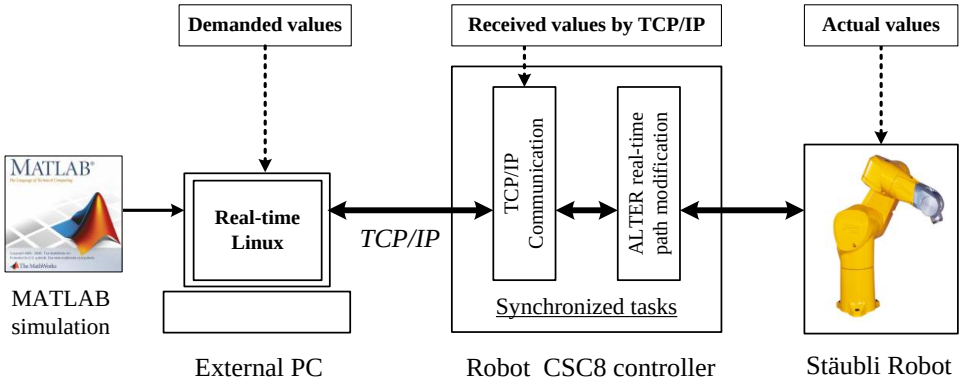

Figure D.20 Schematic diagram of ALTER real-time path control tests

The circular paths were executed in a counter-clockwise direction, with the home position defined to allow the robot to start at the same location. The robot's actual positions during moving along the path were concurrently stored and compared with the desired positions in real-time whilst performing the test in order to calculate the overall mean and standard deviation of position errors.

Matlab (Matrix Laboratory) software was used to simulate x-y world coordinate algorithms and equations in the cycle-path moving test as guidelines for the robot movement. These equations were implemented in real-time Linux to generate an array of x-y world coordinates to modify the trajectory of the robot. The following example demonstrates how a set of x and y position data transferred to the robot controller via the TCP/IP communication is computed, where the robot has to move around a circle of a diameter of 200mm.

```
R=100;
N=1500;
stepsize=2*pi/N;
x(1)=R*cos(stepsize);
y(1)=R*sin(stepsize);

 for i=1:N
      x(i)=R*cos(stepsize*i);
      delx(i)=x(i)-x(i-1);
      y(i)=R*sin(stepsize*i);
      dely(i)=y(i)-y(i-1);
      t(i)=i;
 end
figure(1);
plot(x, y, 'r*')
figure(2);
plot(t, x, 'b*',t, y, 'r-')
figure(3);
plot(t, delx, 'b*',t, dely, 'r-')
```

The results consist of x-y world coordinates and incremental displacements as shown in Figures D.21(a) and (b).

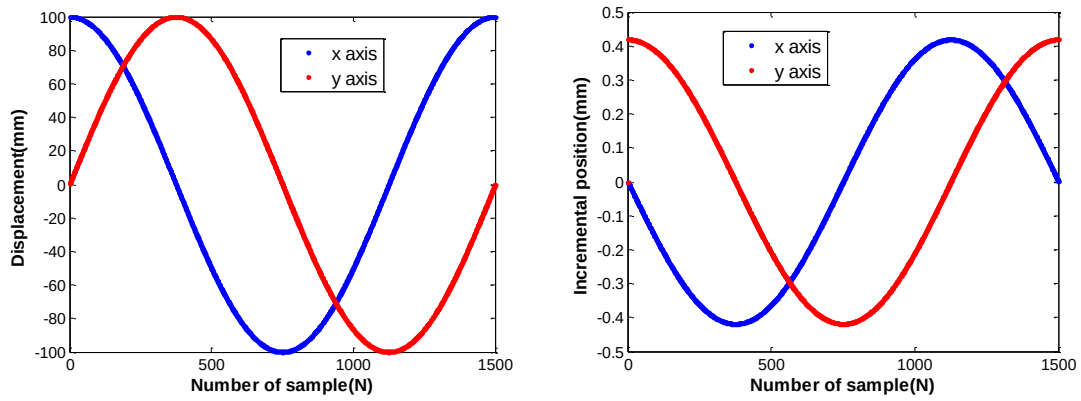

(a) x and y actual positions (b) x and y incremental displacements

Figure D.21 Results of x-y world coordinates and incremental displacements while moving along a 100mm-diameter circular path using Matlab

Figure D.22 illustrates the demanded (simulated), received (by TCP/IP) and actual incremental displacement values, whilst generating three circular paths (diameters of 100, 150 and 200mm) in the x-y plane, and it is evident that the desired values transmitted to the robot controller via the TCP/IP were fully achieved with a delay of 4ms (as shown in Figures D.23 and D.24 representing the zoomed area). The time lag of 4ms was attributed to the data transfer time between the RT Linux and the Stäubli robot controller using TCP/IP communication.

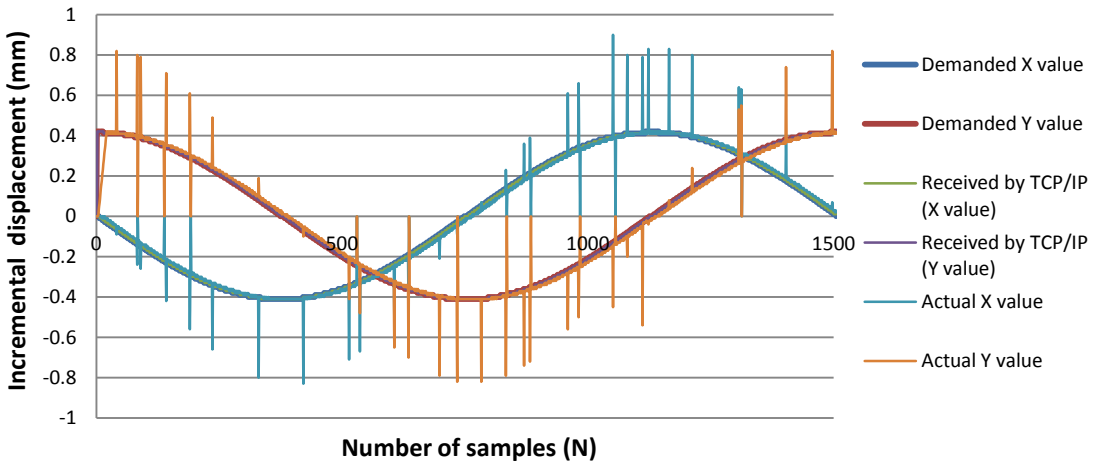

Figure D.22 Results for a 100mm-diameter circular path using ALTER real-time control

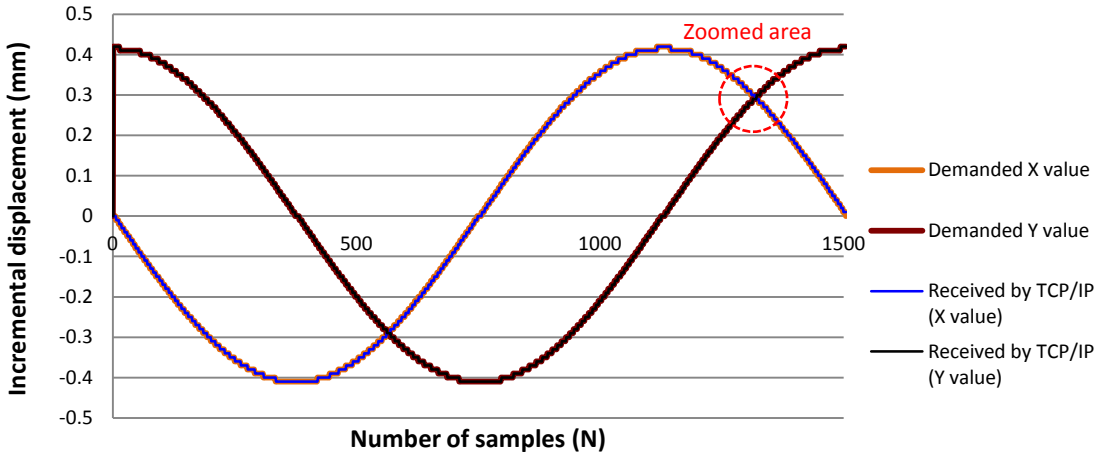

Figure D.23 Results for a 100mm-diameter circular path using ALTER real-time control (comparison of values demanded and received by TCP/IP)

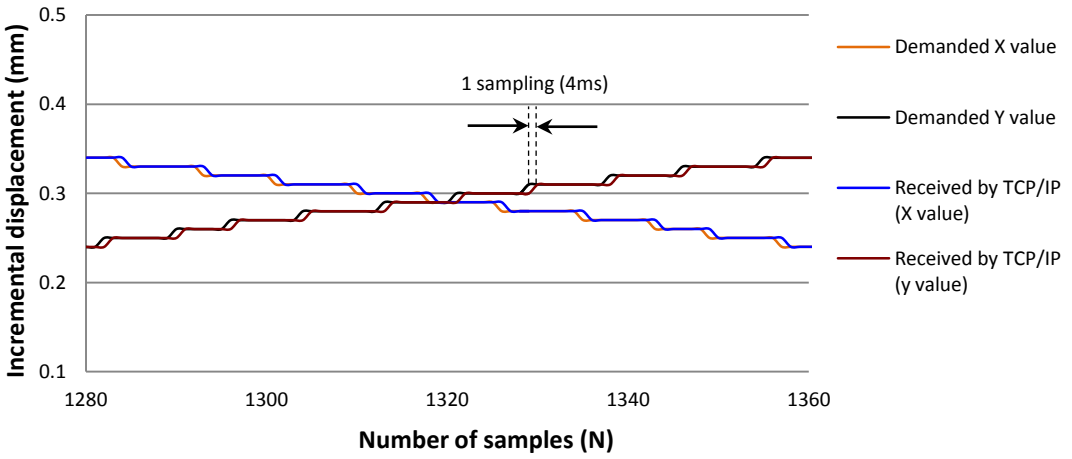

Figure D.24 Results for a 100mm-diameter circular path using ALTER real-time control (comparison of values demanded and received by TCP/IP)

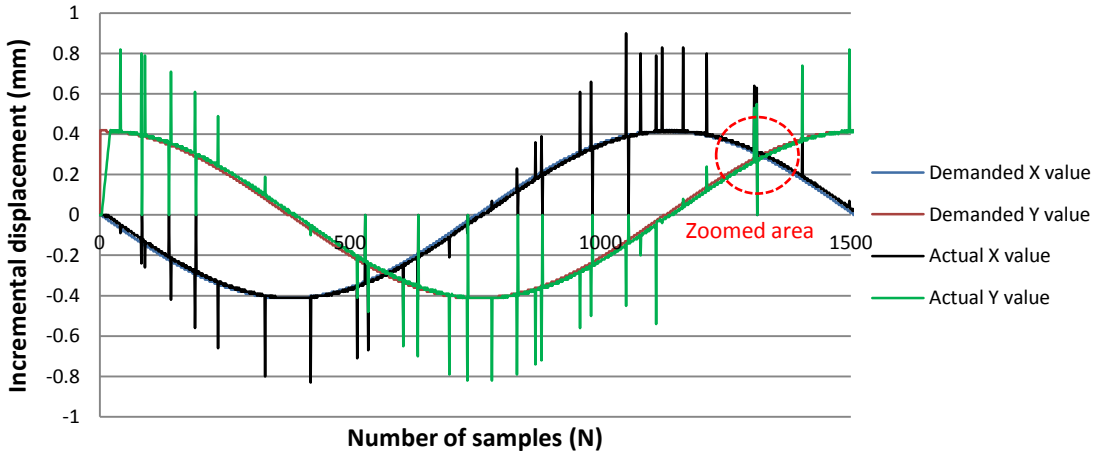

Figure D.25 Results for a 100mm-diameter circular path using ALTER real-time control (comparison of demanded and actual values)

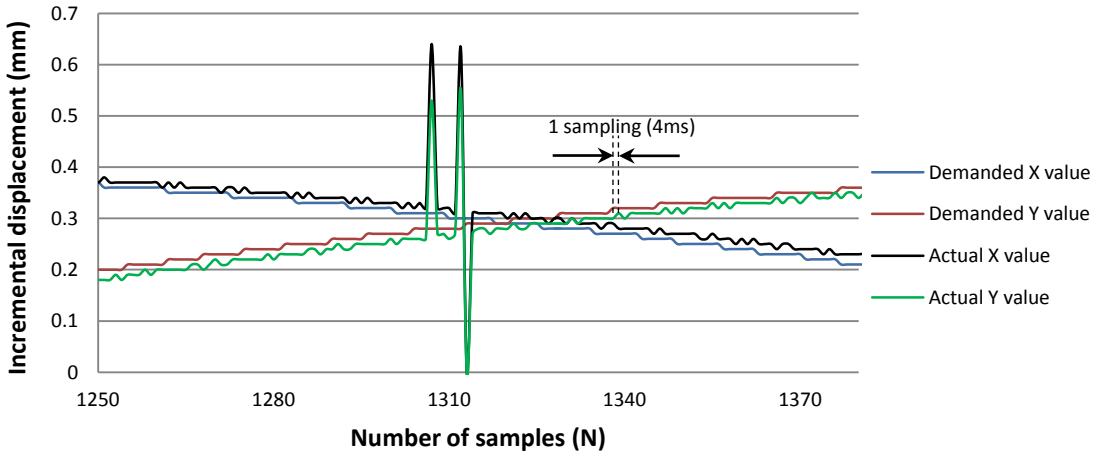

Figure D.26 Results for a 100mm-diameter circular path using ALTER real-time control (comparison of demanded and actual values)

The experimental results show the presence of spikes in the profiles of the x and y coordinates of the robot, as shown in Figures D.25 and D.26 (representing the zoomed area). Whilst the desired x and y path values were smooth the actual x and y values showed pronounced spikes on the trajectories, but for only 1 sample period. These have been attributed to momentary errors occurring during executing of the ALTER command to initiate the incremental transition from one location to the next, largely as a result of attempting to run at 4ms update rate. Zakaria [2012] also found that the ALTER performance of a Stäubli robot deteriorated at higher velocities of greater than 50mm/s, where recorded position errors indicated larger variations. A careful observation of the system revealed that any attempt to further increase the sampling rate of the ALTER real-time path control system does lead to an enhanced performance however, this resulted in a much higher frequency of these errors, and therefore in this application it was decided to maintain the data sampling rate at 4ms.

Table D.2 Means and standard deviations percentage error for x-y axes

Circle of 50mm diameter		
Test	Mean (%)	Standard deviation (%)
x-axis	0.46	0.44
y-axis	1.57	0.47
Circle of 75mm diameter		
Test	Mean (%)	Standard deviation (%)
x-axis	0.84	0.43
y-axis	1.70	0.35
Circle of 100mm diameter		
Test	Mean (%)	Standard deviation (%)
x-axis	2.82	0.39
y-axis	2.95	0.53

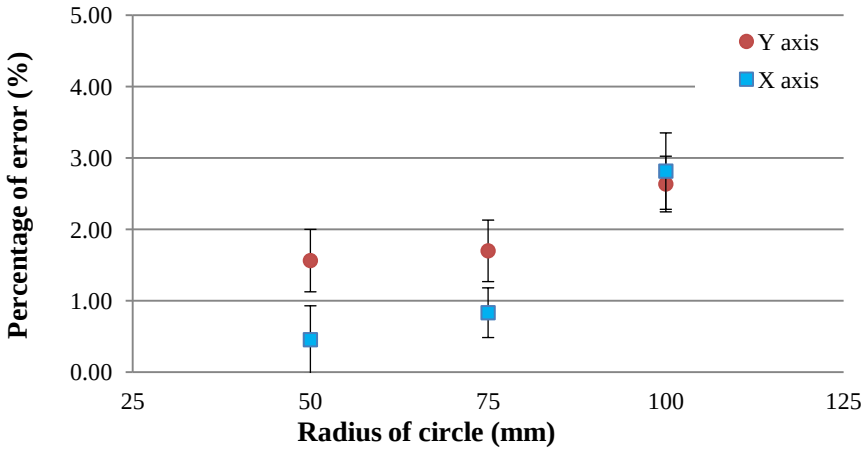

Figure D.27 Means and standard deviations of percentage of error for x-y axes for x and y axes whilst drawing circular paths 100, 150 and 200mm in diameter

The results indicating the overall average and corresponding standard deviations of the x-y position errors whilst drawing the circular paths 100, 150 and 200mm in diameter are summarized in Table D.2. The mean errors of the x and y axes slightly increased and varied from minimum of 0.46% and 1.57% up to maximum of 2.82% and 2.64% respectively, as also shown in Figure D.27. Additionally, the standard deviations of the two dimensions were in the range of 0.35-0.53mm. According to the results, it can be concluded that the performance of ALTER real-time control in path modification can be improved by decreasing the robot's velocity.

D.4 Proportional Integral and Derivative (PID) Control Theory and Proportional Integral (PI) Implementation

D.4.1 Proportional Integral and Derivative (PID) Control

The structure of PID control consists of three key behavioural aspects comprising of a proportional (P) control, an integral (I) control and a derivative (D) control. Equations D.1 – D.3 express the relevant continuous-time equations [Visioli, 2006].

Proportional (P) control:

$$U_P(t) = k_P[y_{de}(t) - y(t)] \tag{D.1}$$

Integral (I) control:

$$U_I(t) = k_i \int_0^t [y_{de}(\tau) - y(\tau)]\, d\tau \tag{D.2}$$

Derivative (D) control:

$$U_D(t) = k_d \frac{d[y_{de}(t) - y(t)]}{dt} \quad \text{(D.3)}$$

Therefore the overall output of PID control can be calculated by summing Equations D.1 to D.3; which gives:

$$U(t) = U_P(t) + U_I(t) + U_D(t) \quad \text{(D.4)}$$

$$U(t) = k_P[y_{de}(t) - y(t)] + k_I \int_0^t [y_{de}(\tau) - y(\tau)]\, d\tau + k_D \frac{d[y_{de}(t) - y(t)]}{dt} \quad \text{(D.5)}$$

$$U(t) = K_P e(t) + K_I \int_0^t e(\tau)\, d\tau + K_D \frac{de(t)}{dt} \quad \text{(D.6)}$$

where $y_{de}(t)$ is the desired process output,

$y(t)$ is the actual process output,

e(t) is the difference between the desired and actual values,

$U(t)$ is the PID control output,

K_P is proportional gain,

K_I is integral gain,

K_D is derivative gain, and

t, τ are continuous time and a sampling time respectively.

D.4.2 Implementation of Proportional Integral Control

Proportional integral (PI) control was adopted and implemented for robot force and velocity control in the human-robot object handover study. However, there is one nonlinear effect, namely integral windup, which has to be considered in the control algorithm. This occurs when there is a large change in set point, and the integral term responds to accumulated errors, and can result in excessive overshoot from the set point value. To overcome this problem, the integral anti-windup was implemented using a discrete-time PI control with sampling time period τ and the discrete time interval k which is transformed in Equation D.12. The proportional and integral terms are represented in Equations D.10 and D.11 respectively [Glattfelder and Schaufelberger, 1986].

Discrete-time proportional (P) control:

$$U_P(k) = k_P \times e(k) \tag{D.10}$$

Discrete-time integral (I) control:

$$U_I(k) = k_I \sum_{j=0}^{k} e(j) \tag{D.11}$$

The discrete-time PI control output:

$$U(k) = k_P e(k) + k_I \sum_{j=0}^{k} e(j) \tag{D.12}$$

Taking into consideration the shifted sampling time at the (k-1) interval gives:

$$U(k-1) = k_P e(k-1) + k_I \sum_{j=0}^{k-1} e(j) \tag{D.13}$$

The incremental PI control value represented by $\Delta u(k)$ can be calculated by applying the following formula:

$$u(k) = u(k-1) + \Delta u(k) \tag{D.14}$$

Substitution Equations D.12 and D.13 into Equation D.14 gives:

$$\Delta u(k) = k_P e(k) + k_I \sum_{j=0}^{k} e(j) - k_P e(k-1) + k_I \sum_{j=0}^{k-1} e(j) \tag{D.15}$$

$$\Delta u(k) = k_P [e(k) - e(k-1)] + k_I e(k) \tag{D.16}$$

Therefore, the incremental PI algorithm is defined by substitution Equation D.16 into Equation D.14 and is given by:

$$u(k) = u(k-1) + k_P [e(k) - e(k-1)] + k_I e(k) \tag{D.17}$$

D.5 Virtual Crank-Turning Tests and Evaluation

D.5.1 Virtual Crank-Turning Preliminary tests

The trial and error method based on virtual crank-turning preliminary tests were carried out to establish appropriate PI control applied to the robot's force and velocity control algorithms. The tests were undertaken by 18 participants as recommended from the pilot study results, and they were first instructed to perform the tasks with the best of their ability and to attempt to minimize the radial forces during task execution. In addition, only one hand was allowed to manipulate the robot end effector to move along the constrained circular path, in which twisting or bending of the gripper were not allowed. The procedure of the virtual crank-turning task permitted the robot to move with a constrained trajectory around the virtual crank radius, at a diameter of 200 mm, in a clockwise direction. The task was required to commence at the proposed home position, and the participant was required to manipulate the robot gripper around the circular path, whilst attempting to minimize the radial force (F_R).

The performance of the system response can be evaluated in terms of the variation in the radial forces, in which the lower the variation in radial force, the better the performance of the system. The constrained circular path of the virtual crank was designed by assuming that the directions of radial force (F_R) and tangential force (F_T) are as expressed in Figure D.28.

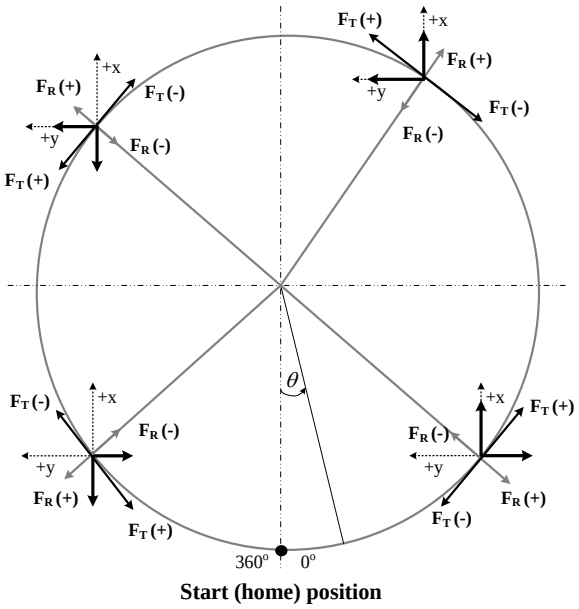

Figure D.28 Force analysis of the virtual crank turning test

The external force exerted by the participant was measured as forces in the x and y directions, represented as F_x and F_y respectively; however these were subsequently transformed into tangential and radial forces using Equations D.18 and D.19:

$$F_T = F_{Tx} + F_{Ty} \tag{D.18}$$

$$F_R = F_{Rx} - F_{Ry} \tag{D.19}$$

where, $F_{Tx} = F_x \cos\theta$, $F_{Ty} = F_y \sin\theta$, $F_{Rx} = F_x \sin\theta$, $F_{Ry} = F_y \cos\theta$,

where, the angle θ of the 'crank' based on the world coordinates can be expressed as:

$$\theta = \arctan2\left(\frac{y_{cur}-y_0}{x_{cur}-x_0}\right) \tag{D.20}$$

where (x_0, y_0) is the world coordinates of the home position,

(x_{cur}, y_{cur}) is the world coordinates of the current position of the robot end effector based on (x_0, y_0),

(x_{new}, y_{new}) is the world coordinates of the updated position of the robot end effector,

θ is the current angle of the robot end effector,

δ is an incremental angle of the robot end effector,

r is the radius of a circle (100 mm), and

θ^* is an updated angle of the robot end effector.

To calculate the incremental change in displacement (ΔU) based on PI control, Equation D.21 is used, and by using the ALTER command, an ALTER transformation matrix ($ALTER_{trsf}$) is represented as:

$$ALTER_{trsf}\begin{bmatrix} ALTER_{trsf}.x \\ ALTER_{trsf}.y \\ ALTER_{trsf}.z \end{bmatrix} \tag{D.21}$$

The virtual-crank turning test was defined as two-dimensional movement control and therefore $ALTER_{trsf}.z = 0$.

$$ALTER.x = (r\sin\theta^* - r\sin\theta) \tag{D.22}$$

$$ALTER.y = (r\cos\theta^* - r\cos\theta) \tag{D.23}$$

The performance was analyzed based on the root mean square error (*E_RMS*) of the radial forces [Kilgus and Gore, 1972; Soroka, 2002; Bruckner et al., 2012]. The equation used to calculate the magnitude of error deviations of *E_RMS* is expressed as:

$$E\_RMS = \sqrt{\frac{\sum_{i=1}^{n}(F_R - F_{De})^2}{n}} \quad \text{(D.24)}$$

where, n is the number of evaluated values,

F_R is the radial forces exerted by a participant and

F_{De} is the demanded radial force (0).

D.5.2 Evaluation of Virtual Crank-Turning Experimental Results

The experimental virtual crank test was undertaken to examine the relationship between the root mean square error (*E_RMS*) of the radial force (F_R) and the tangential force (F_T) applied to the virtual crank. Figure D.29 shows a representative of results of the measured force magnitude profiles of one of the participants. By excluding the transient at the beginning, the analysed results were between 90°-450°, where the tangential force remained reasonably constant at 7.20N to facilitate a constant turning velocity with some fluctuation of ±1.9N. However, the radial force was normally increasing/ decreasing as the participant pushed/pulled in each equivalent and varying by ±2.5N. The results of the preliminary virtual crank-turning tests are illustrated the Table D.3.

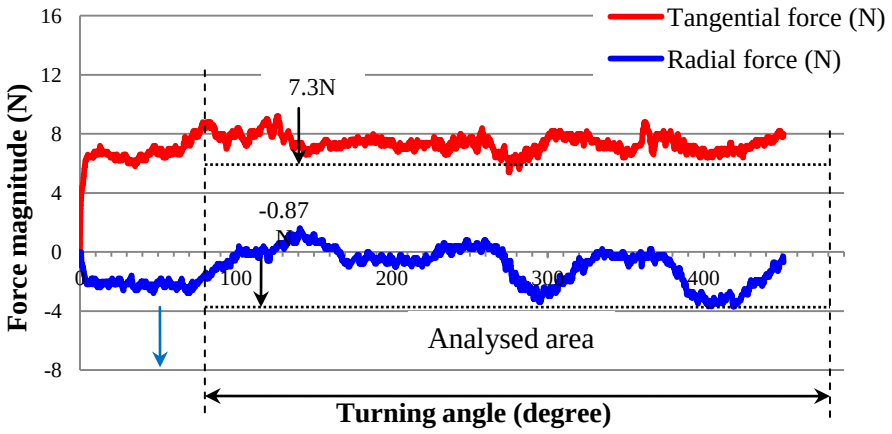

Figure D.29 Actual tangential and radial forces on a virtual crank turning test

Table D.3 Results of virtual crank-turning preliminary tests to evaluate the gain K_P

K_P	***E_RMS* of radial force (N)**		**Tangential force (N)**	
	Average	***Standard deviation***	***Average***	***Standard deviation***
0.025	2.34	0.13	8.37	0.34
0.050	1.21	0.11	4.24	0.23
0.075	0.77	0.09	2.78	0.15
0.100	0.53	0.08	2.14	0.12
0.125	0.65	0.08	1.69	0.10
0.150	0.92	0.12	1.39	0.13

Figure D.30 presents the performance results of the virtual crank test for different values of the proportional gain K_P ranging between 0.025–0.15 with 0.025N resolution. The system performance can be identified based on the *E_RMS* of the radial force. The best performance of this test is represented by the minimum *E_RMS* of (F_R), and was achieved at a gain K_P of 0.100, where the minimum *E_RMS* value is 0.53N with the minimum standard deviation of 0.08N. As expected, the tangential force (F_T), as shown in Figure D.31, decreases when the gain K_P increases, and is approximately inversely proportional to the K_P gain value. It can be noted that at a value of K_P of 0.025, F_T has the largest value of 8.37N with a standard deviation of 0.34N and at K_P of 0.150 the F_T has the smallest value of 1.39N with 0.13N standard deviation. To sum up, it can be concluded that the optimized proportional gain of 0.100 shows the highest performance due to the lowest tracking error represented by the *E_RMS* of F_R.

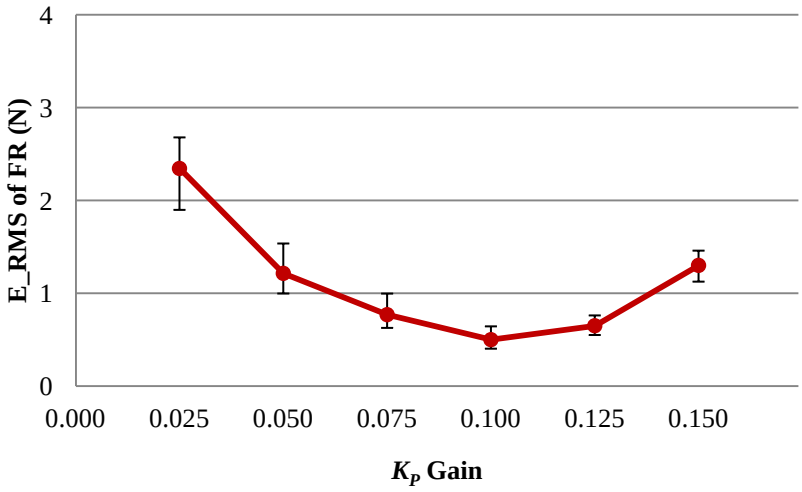

Figure D.30 *E_RMS* of radial forces with various proportional (K_P) gains applied

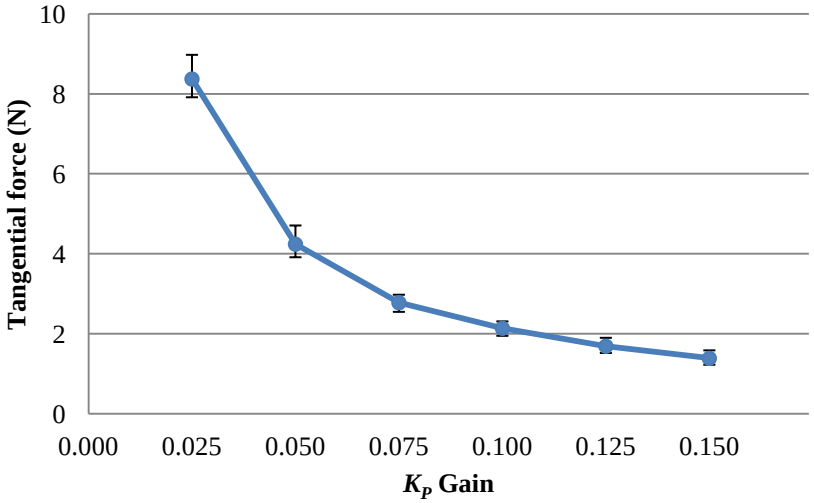

Figure D.31 Effect of tangential forces from different K_P gains at various speed conditions

From the experimental results showing the force profiles, it was indicated that there was small oscillation moderating in the signal; therefore the frequency domain evaluation of the force in the virtual crank tests at the six different K_P gains was determined using fast Fourier transform (FFT) [Cooley and Tukey, 1965]. To suitably identify the noise signal, a high-pass filter with a cut-off frequency at 10Hz was used. Figure D.32 illustrates the results of the FFT analysis over the range of K_P (0.025-0.150), the dominant frequency is in the range between 17-20Hz with the density power spectrum is varied approximately between 450-1050N^2, and the higher frequency (28-30Hz) was clearly seen at the highest K_P, as shown is Figure D.32(f). It can be highlighted that an increase in a K_P gain gives an increase in higher frequency of the system response; however, if the $K_P \geq 0.175$, the robot system has very high unstable oscillation which could damage the robot.

To optimize the integral gain (K_I), the gain K_P was set at 0.100, and then tuning of the integral gain mark by increasing K_I until the best *E_RMS* of F_R is achieved. The same procedure for the virtual crank test developed for evaluating the performance of the gain K_P was used. The same group of the participants was used to perform the assigned tests. A range of integral gains varying from 0.0025 to 0.0175 with 0.0025N resolution was selected.

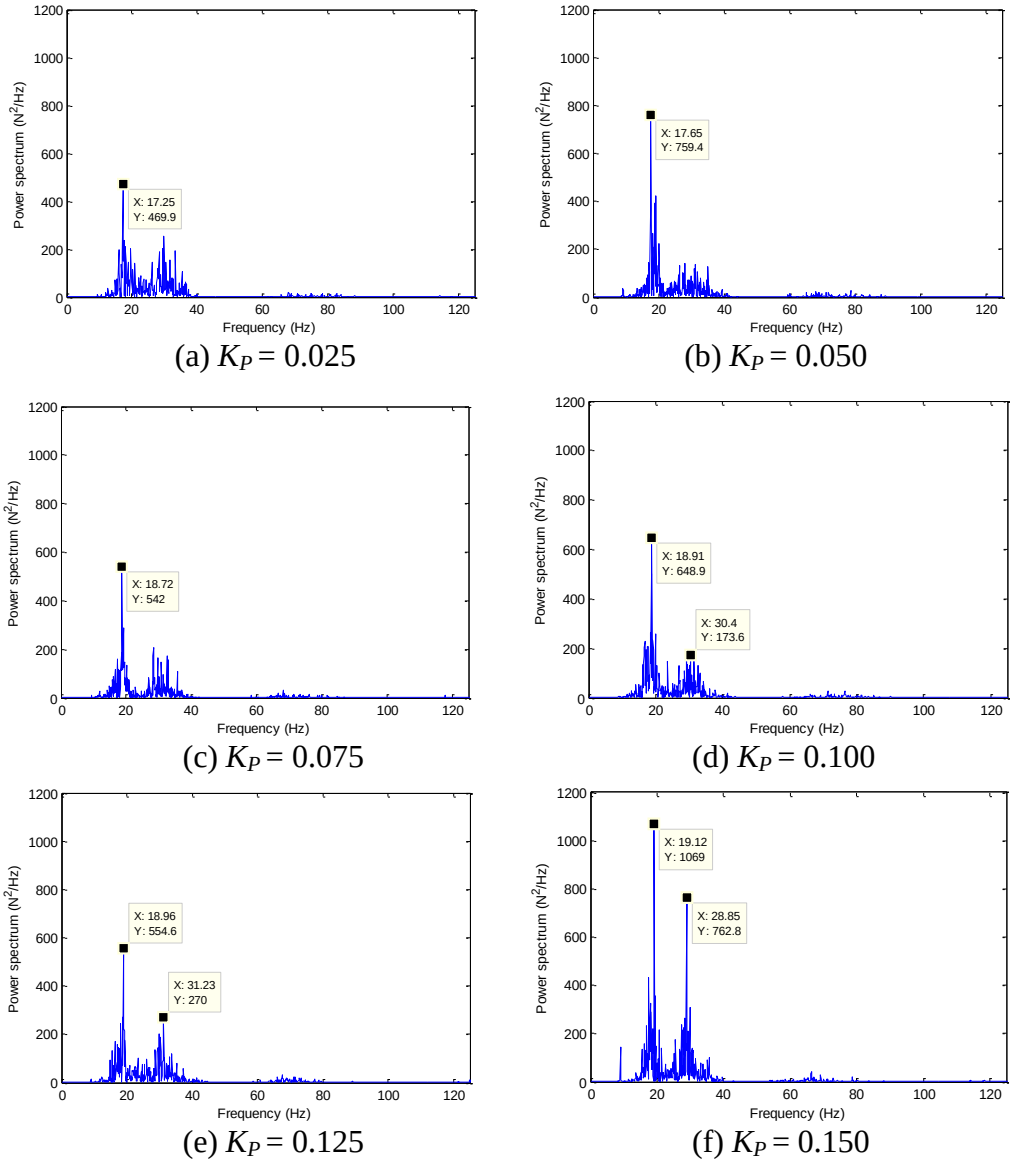

(a) $K_P = 0.025$ (b) $K_P = 0.050$

(c) $K_P = 0.075$ (d) $K_P = 0.100$

(e) $K_P = 0.125$ (f) $K_P = 0.150$

Figure D.32 FFT analysis for virtual crank test

Table D.4 Results of virtual crank-turning preliminary tests to evaluate the gain K_I

K_I	***E_RMS* of radial force (N)**		**Tangential force (N)**	
	Average	***Standard deviation***	***Average***	***Standard deviation***
0.0025	0.53	0.40	2.19	0.49
0.0050	0.44	0.34	1.91	0.42
0.0075	0.45	0.34	1.79	0.45
0.0100	0.46	0.42	1.59	0.47
0.0125	0.53	0.70	1.52	0.61
0.0150	0.71	0.94	1.51	0.96
0.0175	0.92	1.36	1.49	1.50

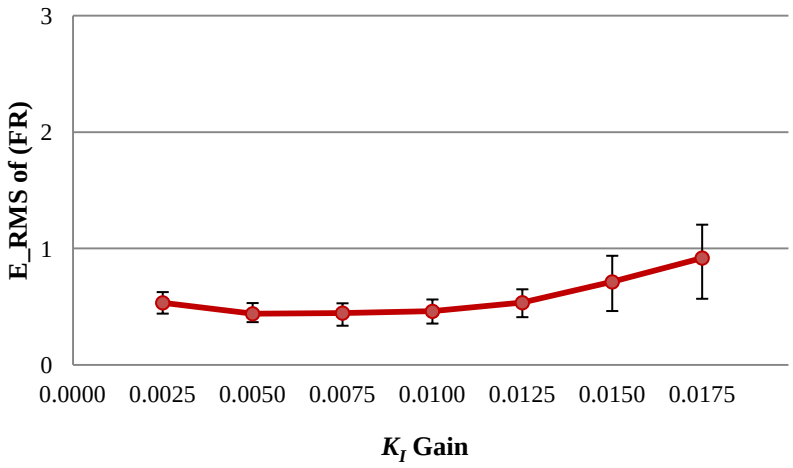

Figure D.33 *E_RMS* of radial forces (F_R) with various integral (K_I) gains applied

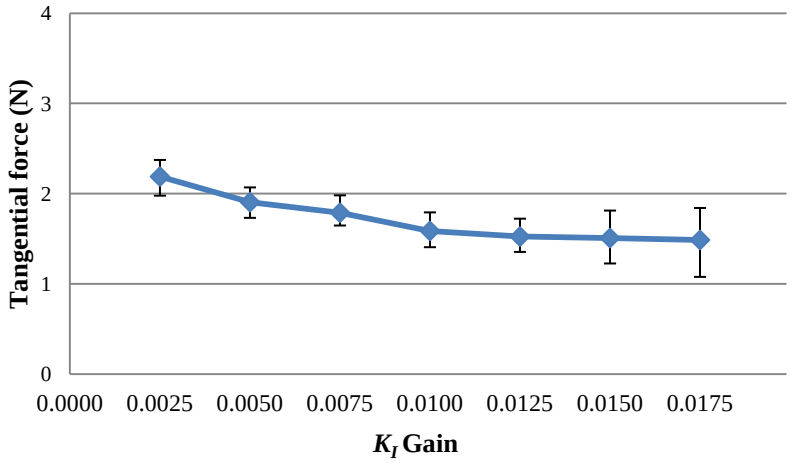

Figure D.34 Effect of tangential forces (F_T) from different K_I gains at various speed conditions

The performance of the virtual crank test for different values of integral gain (K_I) is illustrated in Figure D.33. It can be noted that the best performance of the K_I tuning test is defined as the gain K_I of 0.0050, in which the *E_RMS* value is 0.44N with a standard deviation of 0.34N. The results when the K_I was adjusted between 0.0025 and 0.0125 give low values of the *E_RMS* of F_R, which vary in the range of 0.44–0.53N with standard deviations between 0.34 and 0.70. Once the K_I was set from 0.0150 to 0.0175, the *E_RMS* of F_R significantly increased from 0.71 to 0.94N along with the standard deviations of 0.94 and 1.36N respectively. Increasing the gain K_I is accompanied by a decrease in the tangential force (F_T), as shown in Figure D.34. As demonstrated in the graph, the largest and smallest F_T values are 2.19N and 1.49N respectively. The radial forces start to increase when K_I was set from 0.00125 to 0.00175, in which the standard

deviations are from 0.42 to 1.50N. In summary, the gain tuning for PI control applied to the robot's velocity and force control was implemented. It can be concluded that the best performance as specified by the *E_RMS* of the radial force is observed with proportional and integral gains of K_P = 0.10 and K_I = 0.005 respectively.

D.6 Summary

Appendix D describes the implementation of the real-time force and velocity control systems for the Stäubli TX60 robot. The hardware and software architectures have been discussed, including those for gripper and ATI *Gamma* multi-axis force/torque sensor. The real-time Linux operating system, transmit control protocol and internet protocol (TCP/IP) communication, and the multi-tasking software designed for the robot was also outlined. Outputs from the external force control system were transmitted as incremental displacements transferred to the robot CS8C controller using TCP/IP communication to modify the robot's trajectory in real-time.

The proposed HRI system has been evaluated and the criteria used for the evaluation of the real-time force sensor and real-time control path of the Stäubli robot systems have been also discussed. In particular, proportional plus integral (PI) control was applied to the robot's velocity and force control algorithms, and the gains (K_P and K_I) were experimentally tuned using a trial and error method based on a virtual crank-turning test. Based on the results of these tests, it was established that the best performance (as specified by the *E_RMS* of the radial force) is observed with proportional and integral gains of K_P = 0.10 and K_I = 0.005 respectively.